

# **Cermet based solar selective absorbers; further selectivity improvement and developing new fabrication technique**

Dissertation  
zur Erlangung des Grades  
des Doktors der Ingenieurwissenschaften  
der Naturwissenschaftlich-Technischen Fakultät III  
Chemie, Pharmazie, Bio- und Werkstoffwissenschaften  
der Universität des Saarlandes

von  
Mohammadreza Nejati

durchgeführt am  
Lehrstuhl für Pulvertechnologie von Glas und Keramik

Saarbrücken  
2008

---

---

Eingereicht am:	23.09.2008
Tag des Kolloquiums:	09.02.2009
Dekan:	Prof. Dr. H Vehoff
1. Berichterstatter:	Prof. Dr. R. Clasen
2. Berichterstatter:	Prof. Dr. W. Arnold
Akad. Mitarbeiter:	Dr. G. Falk

---

---

## **Abstract**

Spectral selectivity of cermet based selective absorbers were increased by inducing surface roughness on the surface of the cermet layer using a roughening technique (deposition on hot substrates) or by micro-structuring the metallic substrates before deposition of the absorber coating using laser and imprint structuring techniques. Cu-Al<sub>2</sub>O<sub>3</sub> cermet absorbers with very rough surfaces and excellent selectivity were obtained by employing a roughness template layer under the infrared reflective layer and deposition of the cermet layer at elevated substrate temperatures. Copper and stainless steel plates were laser structured. Through direct laser structuring, solar absorptance of a smooth copper sample increased about 36%, while the increase in thermal emittance was insignificant. To study the optical effect of the imprint surface structuring, a high thixotropic transparent sol-gel layer was micro-structured by a silicon stamp and then a tungsten thin film was deposited. Compared to unstructured tungsten thin film, an increase of 15% in solar absorptance was observed. In addition to selectivity improvement techniques, along of this study a novel economical fabrication method was developed for cermet based solar selective absorbers. Using this new technique, different Ni-Al<sub>2</sub>O<sub>3</sub> cermet selective absorbers were prepared. The best sample showed solar absorptance value of 0.94 and thermal emittance value of 0.11. These Ni-Al<sub>2</sub>O<sub>3</sub> absorber surfaces passed accelerated aging tests.

---

---

## Zusammenfassung

Die Spektralselektivität von Cermet basierten Selektivabsorbern wurde durch Erhöhung der Oberflächenrauigkeit mittels einer Aufrauhtechnik (Abscheidung auf heißen Substraten) oder, vor Abscheidung der Cermet-Schicht, durch Mikrostrukturierung der metallischen Substrate (mittels direkter Laser- und Prägestrukturierungstechniken) erhöht. Durch Abscheidung einer Cu-Al<sub>2</sub>O<sub>3</sub> Cermet-Schicht auf eine IR-Reflektorschicht bei hohen Substrattemperaturen und der Verwendung einer rauhen Templatschicht unter der IR-Reflektorschicht erhält man einen Absorber mit einer sehr rauhen Oberfläche und ausgezeichneter Selektivität. Durch direkte Laserstrukturierung einer glatten Kupferplatte wurde der Absorptionsgrad um über 36 % verbessert, während die Zunahme des thermischen Emissionsgrades geringfügig war. Um optische Effekte der geprägten strukturierten Oberflächen zu untersuchen, wurde durch Prägeverfahren mittels eines Silikonstempels eine Sol-Gel Schicht mikrostrukturiert. Danach wurde eine Dünnschicht aus Wolfram aufgesputtert. Gegenüber einer unstrukturierten Wolframdünnschicht wurde eine Zunahme des Solarabsorptionsgrades um 15 % beobachtet. Zusätzlich zu den Selektivitätsverbesserungstechniken wurde im Rahmen der Untersuchungen eine neue ökonomische Herstellungsmethode der Cermet basierten Solarabsorber entwickelt. Mittels dieser neuen Technik wurden verschiedene Ni-Al<sub>2</sub>O<sub>3</sub> Cermets vorbereitet. Die beste Probe zeigte einen absorptionsgrad von 0.94 und einen Emissionsgrad von 0.11. Diese entwickelten Ni-Al<sub>2</sub>O<sub>3</sub> Absorber bestanden die relevanten Alterungstests.

---

For her devotion, to my wife “Bahareh” and my family  
who supported and encouraged me.

**Contents**

	<b>Acknowledgment</b> .....	10
	<b>List of abbreviations</b> .....	11
<b>1.</b>	<b>Introduction</b> .....	13
<b>2.</b>	<b>Objectives</b> .....	17
<b>3.</b>	<b>Theoretical background</b> .....	19
3.1	Solar thermal collectors.....	19
3.2	Thermal Radiation.....	21
3.3	Solar radiation.....	22
3.4	Selective absorber.....	24
3.5	Selectivity mechanisms.....	25
3.6	Deposition techniques.....	28
3.6.1	Vapor deposition techniques.....	29
3.6.1.1	Sputtering.....	29
3.6.1.2	Ion-Surface interactions.....	32
3.6.1.3	Processes at the substrate surface.....	33
3.6.2	Wet Chemical deposition techniques.....	33
3.6.2.1	Dip-coating method.....	34
3.6.2.2	Spin coating.....	35
3.6.2.3	Suspension characterization.....	35
3.7	Different techniques of surface structuring.....	40
3.8	Best structuring techniques for solar absorbers.....	42
3.9	Optical characterization of selective surfaces.....	43
3.9.1	Total solar absorptance and thermal emittance.....	44
3.10	Degradation of selective absorbers and the stability tests.....	45
3.11	State of the art of selective absorber design.....	46
3.10	Material selection and experiment design.....	52
<b>4.</b>	<b>Theoretical modeling</b> .....	55
4.1	Snell's equation and Fresnel's law.....	55
4.2	Optical properties of metals and dielectrics.....	56
4.3	Optical properties of inhomogeneous media.....	56
4.3.1	Lorenz-Mie scattering theory.....	56
4.3.2	Effective medium theories.....	57

4.4	Optical simulation.....	57
4.5	Selectivity calculator.....	60
4.6	Multilayer optimization.....	61
4.7	Optical simulation of regular gratings.....	62
4.8	Interaction of light with periodical surface structures.....	65
4.8.1	Integral method.....	66
4.9	PCGrate simulation.....	67
4.9.1	Setup of numerical simulation.....	68
4.9.2	Effect of structure shape on the spectral selectivity of copper.....	69
4.9.3	Effect of structure shape on the spectral selectivity of tungsten.....	71
4.9.4	Difference behavior of gratings for TE and TM polarizations.....	72
4.10	Conclusions.....	74
<b>5.</b>	<b>Experimental setup.....</b>	<b>75</b>
5.1	Substrate cleaning.....	75
5.2	Increasing the selectivity by surface texturing.....	76
5.2.A	Sample preparation - Sputter deposition.....	76
5.2.B	Sample preparation - Direct laser structuring.....	78
5.2.C	Sample preparation - Embossing technique.....	79
5.3	Wet chemical deposition technique.....	82
5.3.1	Physical properties of used materials.....	82
5.3.2	Suspension characterization.....	83
5.3.3	Substrates.....	83
5.3.4	Sample preparation.....	84
5.4	Characterization of the prepared samples.....	86
5.4.1	Optical characterization.....	86
5.4.2	Non-optical characterization.....	87
5.5	Durability test procedure .....	89
<b>6.</b>	<b>Results and discussion.....</b>	<b>90</b>
<b>6A</b>	<b>Effect of surface roughening on spectral selectivity of Cu-Al<sub>2</sub>O<sub>3</sub> ..</b>	<b>90</b>
6A.1	Numerical calculations and cermet structure optimization.....	90
6A.2	Effect of substrate heating on selectivity of double cermet structure.....	92
6A.3	Structure characterization of the prepared samples.....	93
6A.4	Role of roughness template layer - single cermet structure.....	97

6A.5	Conclusions.....	102
<b>6B</b>	<b>Selectivity enhancement by laser structuring</b> .....	104
6B.1	Structuring of metallic samples.....	104
6B.2	Optical properties of structured materials.....	106
6B.3	Effect of higher structure periods.....	110
6B.4	Comparing simulation and experiment results.....	112
6B.5	Conclusions.....	114
<b>6C.</b>	<b>Selectivity enhancement by embossing technique</b> .....	116
6C.1	Structure parameters of the embossed layer.....	116
6C.2	Enhancement in solar absorption.....	118
6C.3	Conclusions.....	119
<b>6D.</b>	<b>Suspension derived Ni-Al<sub>2</sub>O<sub>3</sub> cermet selective absorber</b> .....	120
6D.1	Structural and physical properties of Alu C powders.....	120
6D.1.1	Powder characterization.....	120
6D.1.2	Zeta potential and conductivity of Alu C suspension.....	122
6D.1.3	Maximum solid load for Alu C suspension.....	123
6D.2	Characterization of the coating suspension.....	125
6D.2.1	<i>Nickel nitrate-AluC</i> suspension.....	125
6D.2.2	Effect of ultrasound dispersion.....	127
6D.2.3	Dispersion of non-aqueous suspension and effect of TEOS binder.....	128
6D.2.4	ATR spectroscopy of <i>nickel nitrate-Alu C</i> suspension.....	130
6D.2.5	Suspensions with different nickel contents.....	131
6D.2.6	pH and conductivity.....	132
6D.2.7	Conclusions.....	136
6D.3	Heat treatment in H <sub>2</sub> atmosphere.....	136
6D.4	Non-optical characterization of the prepared samples.....	138
6D.4.1	Phase identification and crystal size determination by XRD.....	138
6D.4.2	SEM Characterization.....	139
6D.4.3	EDX analysis.....	142
6D.4.4	Adhesion test.....	143
6D.4.5	Conclusions.....	145
6D.5	Optical characterization of the prepared samples.....	145
6D.5.1	Effect of nickel volume fraction on spectral selectivity.....	146



## Contents

---

6D.5.2	Thickness of the deposited cermets.....	152
6D.5.3	Conclusions and discussions.....	154
6D.6	Stability Test.....	154
6D.6.1	Effect of anti-reflection (protective) SiO <sub>2</sub> layer .....	156
6D.6.2	Effect of humidity test on the optical properties.....	156
6D.6.3	Effect of thermal aging test on the optical properties.....	161
6D.6.4	Conclusions and discussion.....	166
<b>7.</b>	<b>Conclusion remarks and summary.....</b>	<b>167</b>
<b>8.</b>	<b>Future outlook.....</b>	<b>172</b>
<b>9.</b>	<b>References.....</b>	<b>174</b>
<b>10.</b>	<b>Appendix.....</b>	<b>184</b>

### **Acknowledgment**

I want to express my gratitude to all people who supported me during my PhD work. First of all, my supervisor Prof. Dr. Rolf Clasen who continuously encouraged and supported me with his invaluable suggestions and supervisions. He gave me the chance of being his postgraduate student and he kindly supported me along of my research, scientifically and financially.

I am most grateful to the DFG for a part of the financial support of my study under the awarded Graduiertenkolleg scholarship (GRK 232/3-2). I also thank Prof. Dr. Walter Arnold who agreed to participate in the examining committee.

I want to express my deepest and special thanks to Dr. G. Falk (Dept. of powder technology, University of Saarland) for stimulating suggestions and encouragement helped me in all the time of research.

I would like to appreciate Dr. H. Schmidt (Engineering Physics Dept., University of Saarland) for his valuable guidance and assistance in the sputtering laboratory.

Dr. P. Oliveria and Dr. M. H. Jilavi, from “Institute for New Material (INM)” are acknowledged greatly for providing some analysis and required software and also Dipl.-Ing. B. Schäffer from the same institute is acknowledged as well for his help in providing requirements of embossing technique.

I would like to thank Dr. A. Djahanbakhsh from “Bundesanstalt für Materialforschung” for his help in simulation programming.

Prof. Dr. F. Mücklich, Dr. A. Lasagnie and Dipl. Ing. I. Lopez are gratefully acknowledged for providing laser structured samples.

I would like to acknowledge Daniel Pontasch, as well as my other colleagues in the department of powder technology of glass and ceramic. The friendly atmosphere of our group provided a perfect source of motivation for me.

Finally, I want to express my deepest and special thanks to my family, without whom I would never have been able to achieve so much.

I dedicate this thesis to Bahareh, because of her patience, understanding and continuous support during all these years. I thank for her endless love, patience, and understanding.

**Saarbrücken, September 2008**

**Mohammadreza Nejati**

## List of abbreviations

Abs.	Absorptance
a. u.	arbitrary units
AC	Alternative Current
AFM	Atomic Force Microscopy
AIBN	Azoisobutyronitril
Al	Aluminum
AM	Air Mass
anti-ref.	Anti-reflection
AR	Aspect Ratio
Aq.	Aqueous
ATR	Attenuated Total Reflection
BR	Bruggeman
CSP	Concentrating Solar Power
CVD	Chemical Vapor Deposition
DC	Direct Current
DRA	Diffuse Reflectance Accessory
EDX	Energy Dispersive X-ray
Eq.	Equation
ESA	Electrokinetic Sonic Amplitude
et al.	et alia (and others)
etc.	et cetera
EMT	Effective Medium Theory
FAB	Fast Atomic Beam
Fig.	Figure
FTIR	Fourier Transform Infrared
FWHM	Full Width at Half Maximum
GW <sub>th</sub>	Gigawatt Thermal
GRG	Generalized Reduced Gradient
h	hour
HCE	Heat Collection Element
HMFV	High Metal Volume Fraction
HT	High Temperature
i.e.	Idest
ITO	Indium tin oxide
IR	Infrared
ITO	Indium tin oxide
LMVF	Low Metal Volume Fraction
LT	Low Temperature
MA	Methacrylic Acid
MG	Maxwell-Garnet
min.	minute
MIM	Modified Integral Method
MPTS	Methacryloxypropyltrimethoxysilan
MT	Medium Temperature
NIR	Near-infrared wavelength range

## List of abbreviations

---

Pa	Pascal
PC	Performance Criterion
PEO	Polyethylen oxide
pm	Picometer
PS	Ping-Sheng
PSD	Particle Size Distribution
PTFE	Polytetrafluoroethylene
PVD	Physical Vapor Deposition
QSE	Quantum Size Effect
RD	Roughness Depth
Re	Real
Ref.	Reference
RF	Radio Frequency
RP	Roughness Period
RUC	Random Unit Cell
SEM	Scanning Electron Microscopy
SID	Strong Ion Difference
SRA	Specular Reflectance Accessory
SS	Stainless Steel
Sputt.	Sputtering
ST	Segment Thickness
TE	Transverse Electric
TEM	Transmission Electron Microscope
Tech.	Technique
TEOS	Tetraethoxysilane
Temp.	Temperature
TM	Transverse Magnetic
TMAH	Tetramethylammonium hydroxide
us	unstructured
US	Ultra-Sound
UV	Ultra Violet
UV-VIS- NIR	Ultra Violet-Visible-Near Infrared
vol. %	volume percent
WLI	White Light Interferometry
wt. %	weight percent
XRD	X-Ray Diffraction
ZR	Zirconium isopropylate

### **1. Introduction**

The fossil fuel prices still grow progressively. The importance of overcoming our dependence on fossil fuels is becoming more and more evident. Due to human activities, developments and industrialization processes the composition of our atmosphere is changing rapidly by creation of gases such as carbon monoxide, carbon dioxide and ozone. The enhancement of the environmental problems on the one hand and increasing need of the energy from time to time on the other, motivated people to look for alternative energy resources. This has stimulated the utilization of solar, wind, geothermal, biomass and other renewable energy technologies.

The sun is the source of the vast majority of the energy we use on the earth. Most of the energy we use has undergone various transformations before it is finally utilized, but it is also possible to tap the solar energy as it arrives on the earth's surface. The solar energy is inexhaustible in quantity and environmentally friendly and can be converted to thermal and electricity energy. Therefore, public expectations for its successful development and early commercialization have been high. The gap between public expectation and technological reality has been of particular consequence for the potential role of material science in the development of solar energy. An effort to improve the performance of existing devices, and to lower their cost, encounters problems that involve materials and manufacturing processes. Economically attractive conversion of solar radiation into useful heat involves the optical properties of solids, modification of micro- or nano-structures and optimization of material characteristics and preparation techniques.

The modern solar industry began with the oil embargo of 1973-1974 and was strengthened with the second embargo in 1979. With so extreme growth of fossil fuel prices during the years 2005-2008, it is expected that using solar devices comes to people's attention and the solar market reaches again to its splendid situation.

Solar thermal devices use direct heat from the sun, concentrating it in some manner to produce heat at useful temperatures. Although solar thermal energy is mostly used for space and water heating, it can also be used to turn water into steam and produce electricity. First appearing in the early 1980's, currently 400 peak megawatts of solar thermal electricity are available in the United States. Worldwide, around 105 GW<sub>th</sub>, corresponding to 150 million square meters of solar thermal collectors were installed by the year 2004 [1]

## 1. Introduction

---

Solar absorber surfaces are the most important part of thermal collectors. Most absorbers are constructed of a metal that has good heat conductivity and coated with a thin absorbing layer. Depending on the spectral selectivity (different surface reflectivity behavior for solar spectrum wavelengths and thermal radiation wavelengths), solar absorbers are classified as non-selective, moderately selective and selective. In order to compare the performance of different absorber surfaces, the parameters solar absorptance (absorbed fraction of the incoming solar radiation) and thermal emittance (emitted fraction of the absorbed energy through infrared radiation) have been defined.

It is essential for an absorber to absorb the incoming solar radiation as much as possible and at the same time keep the collected heat. Selective absorbers can accomplish this requirement by having high solar absorptivity and high thermal reflectivity simultaneously.

There are different mechanisms for achieving spectral selectivity like; using semiconductors with suitable band gaps, using optical interference effect of a multilayer stack of thin films and using materials which are black for solar wavelengths but transparent for the heat like metal-ceramic nano-composites (called cermet). It is also possible to increase the solar absorptivity of a metallic surface by roughening of its surface. In this method, higher solar absorptivity is obtained by multiple absorption-reflection of the light inside the surface grooves. Among these mechanisms, having a cermet layer deposited on a highly infrared-reflective metal is the most flexible method, which leads to a good selectivity. In a simpler manner, having a textured infrared-reflector metal with surface feature periodicity in the size of incoming solar wavelengths is another method of achieving moderate spectral selectivity.

The commercialized solar selective absorbers were fabricated by electroplating, anodization-coloration and chemical conversions-oxidations techniques. Black chrome, black zinc, copper oxide, black cobalt, black nickel, iron oxide and pigmented aluminum oxide are the most common electrochemically produced selective absorber coating. Inal and Scherer have reviewed these kinds of absorbers in [2]. All prepared absorbers by such processes had solar absorptance of about 0.9 and thermal emittance of about 0.1-0.3.

## 1. Introduction

---

Many fabrication methods need poisonous acid baths, complex metal salt combinations and present a non-flexible solar absorber design. In these methods, changing the optical properties of the absorber to the desired characteristics is very difficult or in some cases, it is impossible. Moreover, wastes of these deposition techniques are very dangerous for the environment and they have to be disposed in a proper and expensive manner.

It is about two decades that, nano-composite thin films have been intensively studied as solar selective absorbers, due to their suitable and flexible optical properties. Optical properties of a composite layer can be easily modified by changing the thickness, metal volume fraction, and the shape of metal nano particles.

Nowadays, the most common commercial type of selective absorbers are composed of two [3] to four [4] homogenous cermet layers with different metal contents or one cermet layer with a graded refractive index [5], deposited on reflector substrates like bulk copper, aluminum plate or glass tubes coated with thin films of Al or Cu. In some configurations, an anti-reflective or protective coating can be deposited on the cermet stack to reduce the light reflection of the air-absorber interface.

Using cylindrical or rolling sputtering techniques, different metal-dielectric selective coatings like SS-C [6], SS-AIN [7, 8] (SS stands for Stainless Steel), Al-N [9], TiNO<sub>x</sub> [10, 11] have been produced commercially. The industrial sputtering systems for mass production of such selective absorbers are high-tech devices and very expensive because of the need of the large vacuum chamber, expensive vacuum pumps, clean rooms, high purity gas, strict pressure, plasma and thickness controlling systems and high-tech power supplies for establishing stable plasma by thousands of volts. These all make the preparation process complex and costly. Only companies which invest a huge capital cost (in the range of millions Euro) will be able to produce such kind of absorbers in large scales. In addition, with the momentary solar market, which is still at the beginning of its growth and the fact that the absorber surface is still the most expensive part of the collector, sputtering process would not be an economical mass production option for producing cheap collectors.

In contrast to the sputtering, painted solar absorber coatings are a cheaper option but they suffer from a very high thermal emittance close to 80-90 % due to the vibrational modes of incorporated organic polymer binders and a poor long-term stability [12]. Orel et al. increased the stability of such paints using an organo-modified silicon resin

[13, 14]. The poor optical properties of such thick paint coatings (100-200  $\mu\text{m}$ ) made them practically useless so that these surfaces are categorized under non-selective black absorbers [15].

P. Konttinen has developed also a low cost solar absorber by chemical reaction of a graphite layer with an aluminum sheet during mechanical grinding. Such coatings are very sensitive to grinding parameters and have solar absorptance of 0.9 but thermal emittance as high as 0.22 [16, 17]. Besides high emittance value, this kind of absorbers suffer from degradation at high humidity and water condensation condition [18].

The actual selectivity of the selective absorbers can be still improved by different ways like using multiple anti-reflection layers or cermets composed of different metals and ceramics [19] but adding any new layer or having many coatings make the absorber system more complex and expensive. In addition, the sensitivity to degradation increases rapidly with complexity of a thin film system. A photo-thermal converter consisting of a small number of layers, preferably only one, will be more durable than a system composed of several layers [20].

Current research topics on solar absorbers include further improvement of the microstructure, modeling and manufacturing of the sputtered surfaces [21]. Therefore, any feasible methods than can facilitate the fabrication process and improve the optical properties of the selective absorbers are of the actual interest of the market. Moreover, in comparison with expensive methods like sputtering, developing absorbers with comparable optical properties through a cheaper manufacturing method is the actual need of the solar industry.



### **2. Objectives**

None of the various selectivity mechanisms can individually generate a good approximation to the desired spectral profile. It takes the tandem action of two or more processes to produce sufficient selectivity. Until now, little effort has been invested to carry different selectivity mechanisms in one process to further increase the solar absorptance. Most studies were product-oriented, and carried an empirical note. As a result, the designer of solar absorbers has a number of choices to choose from fabrication method and combination of various mechanisms to control and improve the optical property of an absorber.

Textured surfaces with required spectral selectivity have not been realized until now [22] but they could increase the selectivity of pure metals significantly. In contrast, graded cermet or double cermet structures equipped with an anti-reflection layer show reasonable spectral selectivity [23] but these structures are still complicated and thickness sensitive. If the thickness of each optical layer is not controlled precisely during the deposition, the interference effect can create some undesired reflection peaks, which can lay in high intensity solar energy wavelengths and lead to the absorption loss.

The thesis work consists of optimization and further selectivity improvement of the existing cermet based solar absorbers by combining the surface roughness effect with the absorption effect of cermet composite layer. Combination of surface roughness and composite absorber will lead to a higher solar absorption but keeping the emittance value unchanged needs special attentions. In this thesis, it is tried to study theoretically and experimentally, the geometrical effect of thin film and substrate surfaces on enhancement of optical absorption. Increase of solar absorption in rough surfaces is due to the multiple reflections and partial absorptions of the trapped light between the surface features. Having effective surface roughness at the interface of air-absorber would even eliminate the need of an anti-reflection layer because rough interface brings the required refractive index graduation.

In addition to improving the selectivity of the sputtered cermet coatings using roughness effect, another important objective of this thesis is developing a novel environmental friendly fabrication method of cermet based selective absorbers in a cheaper and easier manner.

## 2. Objectives

---

### **The goals of this study are:**

1- Further improving of the selectivity of cermet-based absorbers by applying three different surface roughening and structuring techniques as follows:

A- Inducing surface roughness on the absorber/air interface by heating the substrate during deposition of the absorber coatings and by adding a roughness template layer between the cermet layer and the substrate.

B- Direct laser structuring of the metallic substrates before deposition of the absorber layer.

C- Applying a thixotropic sol-gel film on the substrate and quick structuring of this layer by embossing technique.

Embossing, laser structuring and substrate heating during sputter deposition are three feasible and simple surface texturing methods. Depending on a given fabrication process, one of these new alternatives can be selected and employed as a new step in the fabrication process (pre-structuring of the substrate by laser or embossing technique) or as a process modification (substrate heating during thin film deposition). These structuring and surface roughening techniques have not been applied for solar absorbers before.

2- Developing a novel cost-effective deposition method of cermet composite absorbers using stable colloidal suspensions of nano-powders. According to this technique a stable suspension, which contains both precursors of metal and ceramic parts of the final cermet, is developed and applied on the substrates. The deposited cermet thin films are then characterized and studied. Effect of thickness and metallic content of the cermet layer on the optical property of the developed absorber is investigated. Finally, by conducting thermal and humidity stability tests the durability of the prepared coating with and without anti-reflection layer is examined. The aim of this study is only developing the method and not final optimizing the optical property of the prepared samples.

### 3. Theoretical background

#### 3.1 Solar thermal collectors

There are different kinds of solar thermal collectors like parabolic trough systems, evacuated solar tubes and normal flat plate collectors which through efficient photo-thermal conversion of their absorber surfaces, transform solar energy to the heat.

Regarding to the temperature levels needed, three main categories of application can be identified for photo-thermal conversion of solar radiation:

- 1- Low temperature applications ( $T < 60\text{ }^{\circ}\text{C}$ ) like heating of swimming pools and water heating.
- 2- Medium temperature applications ( $60\text{ }^{\circ}\text{C} < T < 150\text{ }^{\circ}\text{C}$ ) like space heating or cooling and water desalination.
- 3- High temperature applications ( $150\text{ }^{\circ}\text{C} < T < 800\text{ }^{\circ}\text{C}$ ) like mechanical energy production and catalytic dissociation of water.

In Fig. 3-1, different kinds of solar collectors are shown. A flat-plate collector is the simplest of all devices used for solar energy utilization. It consists of an absorber panel, which may be spectrally selective, or in the chipper manner, non-selective. In efficient collectors, the space between the absorber and the cover plates is evacuated. Solar radiation passes through the cover plate (usually low-iron glass) and is converted by the absorber into thermal energy, which is then transferred to a heat transfer fluid.

A parabolic trough system (see Fig. 3-1 right) is made of long rows of concentrators only curved in one direction. Focus line of such collector called Heat Collection Element (HCE) and have been composed of a stainless steel pipe coated with an efficient selective absorber and protected with a glass tube against thermal losses. A heat transfer fluid is run through the pipe that located at the focus point of the reflective troughs. The heat is then transferred to a working fluid (usually water) that can be used to derive super heated steam for running a turbine.

Evacuated solar collectors (Fig. 3-1, middle) can be equipped with individual planar absorber surfaces protected in an evacuated glass tube or it can be made completely

### 3. Theoretical background

of two glass tubes. Here the absorber surface is coated on the interior glass tube and the space between the glass tubes is evacuated.



Fig. 3-1: Different kinds of solar thermal collectors (upper row) and their components (lower row). From left to right: Flat-plate collector, evacuated absorber tube and parabolic concentrated collector

The simplified heat balance of a solar collector is given by the following expression:

$$Q_{\text{out}} = S_C \alpha \phi_0 - S_A (HT + \epsilon_{\text{th}} T^4) \quad (3.1)$$

where  $Q_{\text{out}}$  is the collector thermal output,  $\alpha$  is the solar absorptance,  $S_C$  is the collector area,  $S_A$  is the absorber surface area.  $\phi_0$  is the total solar energy flux onto

### 3. Theoretical background

---

the collector plane,  $H$  is the coefficient of thermal losses by convection and conduction,  $\varepsilon_{th}$  the coefficient of radiation losses and  $T$  the temperature of the absorber.

At high temperatures, conductive and convective heat losses are negligible with respect to the radiation losses. In addition, the convection and conduction losses can be minimized with proper collector design and sufficient insulation or using vacuum but radiation loss is dominated by the absorber plate characteristics. Therefore, the heat balance of the collector is then reduced to:

$$Q_{out} = S_C \alpha \varphi_0 - S_A \varepsilon_{th} T^4 \quad (3.2)$$

Under these conditions, the photo-thermal conversion efficiency of a solar collector is given by:

$$\eta = \frac{Q_{out}}{\varphi_0 S_C} = \alpha - \frac{\varepsilon_{th} T^4}{C \varphi_0} \quad (3.3)$$

where  $C$  represents the concentration coefficient.

As can be seen in Eq. 3.3, the collector efficiency is directly proportional to the solar absorptance ( $\alpha$ ) and to the thermal emittance coefficient ( $\varepsilon_{th}$ ) of the absorber plate. The solar absorbing surface is one of the key components of a solar collector and its quality and optical properties influence both the heat losses and gains. In order to utilize the solar energy effectively, absorption of incident solar radiation should be maximized and thermal losses from the collector minimized. This thesis aimed to develop solar absorbers, which provide such kind of characteristics called selective absorbers.

#### 3.2 Thermal Radiation

All heated objects emit thermal electromagnetic radiation whose wavelength and intensity are dependent on the temperature of the body and its optical characteristics. A blackbody is one that absorbs all wavelengths of the incident radiation and emits the maximum amount of energy for a given body temperature ( $T$ ). It is an ideal

### 3. Theoretical background

---

surface whose emissive power, given by Planck's law Eq. 3.4, is used as a reference to compare with the properties of the real surfaces. The spectral blackbody radiation is given by:

$$E_{b\lambda} = \frac{C_1}{\lambda^5 (e^{C_2/\lambda T} - 1)} \quad (3.4)$$

where  $C_1 = 3.74 \times 10^8 \text{ W} \cdot \mu\text{m}^4 \text{m}^{-2}$  and  $C_2 = 1.44 \times 10^4 \mu\text{m}^\circ\text{K}$  are the first and second Planck's radiation constants, respectively. The wavelength  $\lambda$  is given in  $\mu\text{m}$  and  $E_{b\lambda}$  in  $\text{W}/\text{m}^2 \mu\text{m}$ .

The total emitted energy is obtained by integrating the Planck's spectrum over the whole wavelength range. Stephan-Boltzmann law gives the hemispherical total emitted energy for an ideal blackbody as follows:

$$E_b = \int_0^{\infty} E_{b\lambda}(\lambda, T) d\lambda = \sigma T^4 \quad (3.5)$$

where  $\sigma = 5.671 \times 10^{-8} \text{ W} / \text{m}^2 \text{K}^4$  is the Stephan-Boltzmann constant.

#### 3.3 Solar radiation

The solar energy striking the earth's surface at any one time depends on weather conditions, as well as location and orientation of the surface. Outside the earth's atmosphere, solar radiation has an intensity of approximately  $1370 \text{ W}/\text{m}^2$ . This is the value at mean earth-sun distance at the top of the atmosphere and is referred to as the solar constant. On the surface of the earth on a clear day, at noon, the direct beam radiation will be approximately  $1000 \text{ W}/\text{m}^2$  for many locations. Approximately 99 % of solar, or short-wave, radiation at the earth's surface is contained in the region from  $0.3$  to  $3.0 \mu\text{m}$ . Solar radiation is an electromagnetic wave which 6.4 % of it lying in the ultraviolet, 48 % in the visible and 45.6 % in the near-infrared wavelengths.

**Air Mass (AM):** The intensity of the terrestrial spectrum depends on the distance traveled through the atmosphere. The air mass is defined as the ratio of the mass of

### 3. Theoretical background

---

the atmosphere through which beam radiation passes to the mass it would pass through, if the sun were at the zenith (i.e., directly overhead). Air mass is 1 at the zenith and about 2 at an altitude of  $60^\circ$ .

In Fig. 3-2, the distribution of the energy from the sun as a function of wavelength at AM0 and AM1 has been indicated. The differences between two curves come from the atmospheric attenuation of solar radiation due to (1) atmospheric scattering by air molecules, water, and dust and (2) atmospheric absorption by  $O_3$ ,  $H_2O$ , and  $CO_2$ . The extraterrestrial radiation of the sun can be approximated with a blackbody radiation at  $5800^\circ C$ . As shown in Fig. 3-2, in comparison with solar spectrum the blackbody radiation of a surface at  $300^\circ C$  lies far from it between 2-30  $\mu m$  wavelengths. As there is no important overlapping between these two curves, therefore it would be possible to prepare surfaces, which absorb the solar wavelengths and which emit poorly at thermal infrared wavelengths. "Bandpass reflection filters", "black infrared mirrors" and "spectrally selective absorber" are descriptive names sometimes used in literature for such surfaces.

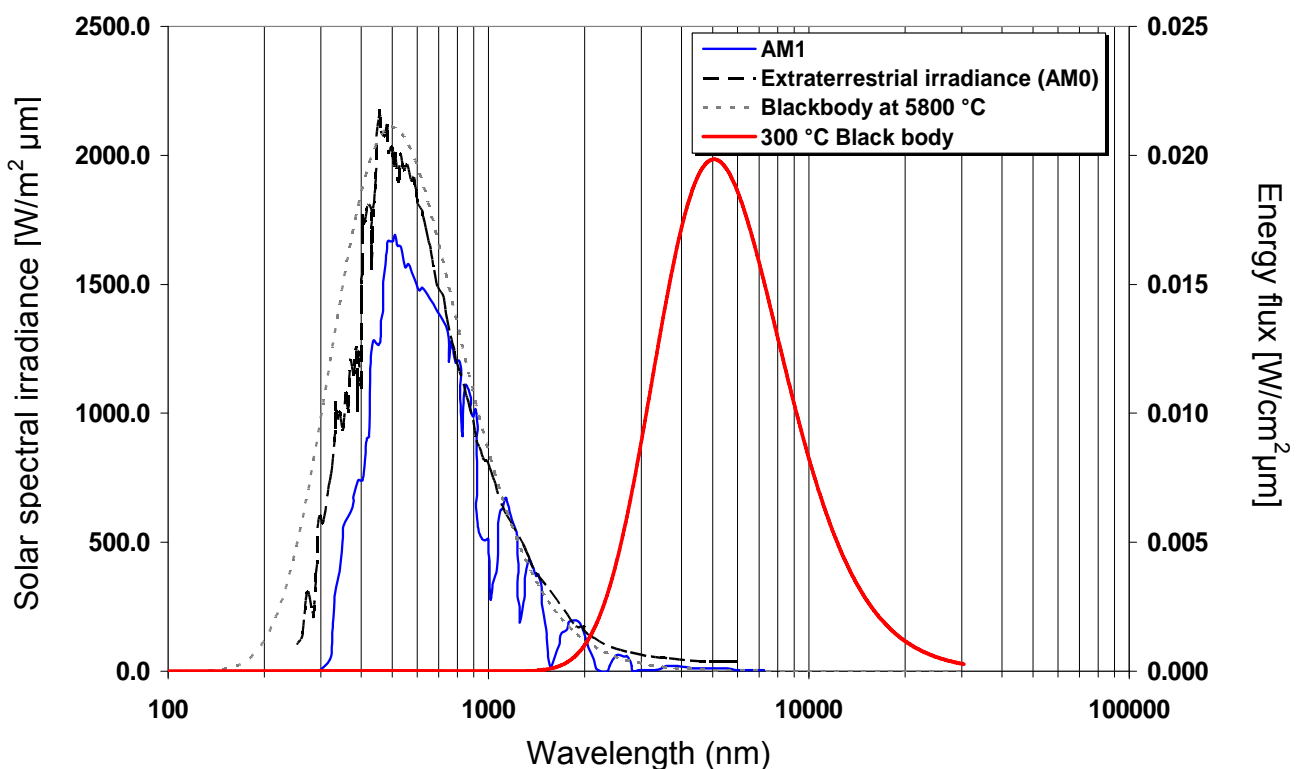


Fig. 3-2: Left: Solar irradiance at AM0 (extraterrestrial) and AM1 (on the earth's surface) and normalized energy distribution of a blackbody at  $5800^\circ C$ ; Right: Thermal radiation spectrum of a blackbody at  $300^\circ C$

#### 3.4 Selective absorber

The most critical part of an energy efficient solar collector is the absorber surface which should be spectrally selective and exhibit high absorptance (low reflectance for wavelengths  $< 2.5 \mu\text{m}$ ) in the solar spectrum that is incident on the surface of absorber and low thermal emittance (high reflectance for wavelengths  $> 2.5 \mu\text{m}$ ) in thermal infrared wavelengths. Fig. 3-3 shows the reflectance curve of an ideal selective absorber.

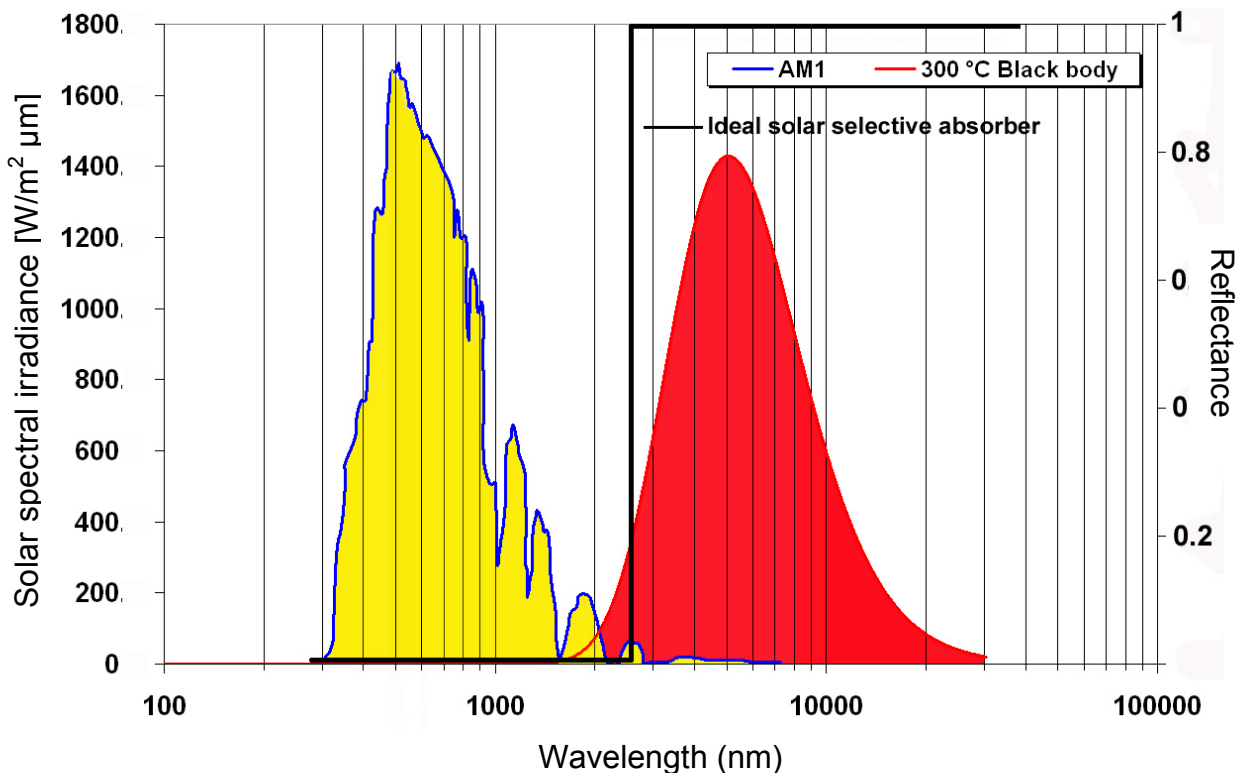


Fig. 3-3: Reflectance curve of an ideal solar selective absorber in comparison with solar irradiance at AM1 and blackbody radiation at 300 °C

Ideal spectral selective coatings should be low-cost and easy to manufacture and of course, they need to be thermally and chemically stable in air at elevated temperatures at least for 25 years and high thermal cycles.

In high operating temperature applications like concentrating solar power (CSP) systems, for reducing the cost of parabolic trough solar power technology, one of the approaches is to increase the operating temperatures of the solar field from approximately 400 °C to 500 °C (or higher). To accomplish this, highly selective coatings that are stable at high temperatures are needed. Such coatings must have high solar absorptance and low thermal emittance at 500 °C. As the losses



associated with thermal emission increase proportionally by the fourth power of temperature, therefore having an absorber surface whose thermal emittance as low as possible, is the great necessity for CSPs.

In low- and mid-temperature applications like glass evacuated tube collectors or flat plate collectors, absorber coatings do not suffer from high temperature degradation and therefore can be designed with cheaper materials.

#### **3.5 Selectivity mechanisms**

There are different design principles for achieving spectral selectivity. They can be categorized into six distinct types: (1) intrinsic, (2) multilayer absorber, (3) quantum size effect, (4) textured surfaces (light trapping), (5) Absorber-reflector tandem, (6) heat mirrors (is not the case here and is not explained). Brief descriptions of different selectivity mechanisms are presented here but detailed information can be found elsewhere [2, 15, 24, 25].

**1) Intrinsic selective absorber:** It is the simplest type of design which can be carried using substances that have the desired selectivity naturally (Fig. 3-4 a). Unfortunately, in the nature there are no materials that have satisfactory optical selectivity. Carbides and nitrides of the transition metals have been shown experimentally to possess semi-selectivity [26]. Another kind of intrinsic selective absorbers like metallic W, MoO<sub>3</sub>-doped Mo, Si doped with B, CaF<sub>2</sub>, HfC, SnO<sub>2</sub>, ZrB<sub>2</sub>, have been also developed [15] but they were not optically effective and some of them require structure and compositional changes. Research in intrinsic absorbers has not been very fruitful because there are no ideal intrinsic materials.

**2) Multilayer absorber:** multilayer absorbers use multiple reflections and destructive optical interferences of the light between alternating layers (with a well-controlled thickness) of metal and dielectric. The desired absorption effect in the interference stack is resulted from multiplicity of passes of light through the dielectric portion of the stack lying between the two reflective metal layers. The upper metal layer is semitransparent and very thin (about 5 nm). The basic design for a 4-layer interference stack is shown in Fig. 3-4 c. The sandwiched dielectric layer has not any

### 3. Theoretical background

---

intrinsic absorptance in the solar spectrum but could fruitfully have some to complete the natural properties of metal films.

The main problem of such absorber design is multilayer deterioration at elevated temperatures because of inter-diffusion between the layers. In addition, this design of solar absorber is very sensitive to the thickness of layers. Extra precautions for exact controlling the thickness of each layer make this kind of absorbers very expensive.  $\text{Al}_2\text{O}_3/\text{Mo}/\text{Al}_2\text{O}_3$  multilayer selective absorber [27] is an example of such kind of multilayer absorbers designed for high temperature applications.

**3) Quantum size effect (QSE):** QSE in ultra thin films produces selectivity with high solar absorptance. The critical thickness for appearing the QSE for a metal is in the order of 2-3 nm. This thickness for semiconductors is higher (in the range of 10-50 nm) because of their lower free carrier concentration [28]. Such effect is also observable in the multilayer interference stack, which is equipped with a very thin semitransparent metal layer as mentioned in the previous section. The ultra-thin metal layer provides the major absorption effect for the stack.

**4) Surface texturing:** Solar selectivity can also be created by geometrically changes of surface, like dendrite, needle-like, or porous microstructures on the same scale as the wavelength of the incident radiation. The rough surface absorbs solar energy by trapping the light through the surface features of a roughened surface by multiple reflection and partial absorptions after each light-surface geometry incident. For long wavelength radiation, the surface looks fairly smooth and acts like a mirror because the thermal infrared wavelengths are greater than the dimension of the surface features. According to the Mie theory [29], the surface features scatter the light strongly at short wavelengths and weakly at long. This geometrical selectivity is not very sensitive to severe environmental effects but may be damaged by surface contact or abrasion. It is possible to protect such surfaces from abrasion damage by a sol-gel protective coating. Roughening the surface of a single material can be done through chemical or sputtering etching, ion bombardment and sandblasting.

**5) Absorber-reflector tandem:** The most common type of absorber is the absorber-reflector tandem. It is obtained by the combination of two surfaces, one that is highly

### 3. Theoretical background

---

absorbing in the solar wavelengths and another, highly reflecting in the thermal infrared. Coating a good IR reflector base metal with a highly solar absorbing thin film, which should be also transparent for thermal infrared wavelengths, is called dark-mirror configuration. An alternative way for achieving the absorber-reflector tandem is covering a thick absorbing material by a solar transparent but IR-reflecting coating, which is normally called a heat mirror (category 6). Dark-mirror tandem stacks cover a wide range of selective coatings, ranging from very simple ones to very complex ones including multilayer but acts like a tandem layer. For achieving a quite good selectivity for dark-mirror configuration, there are varieties of designs with their own advantages and disadvantages, which can be categorized into the following subcategories:

**5-1) Semiconductor-metal tandem:** It is limited to semiconductors with band gaps from  $\sim 0.5$  eV ( $2.5 \mu\text{m}$ ) to  $1.26$  eV ( $1.0 \mu\text{m}$ ) like Si [30], Ge [31], and PbS [32], in thin and thick film coatings. As shown in Fig. 3-4 b, the selectivity is obtained by placing such low band gap semiconductors on highly IR reflecting metal substrate. The semiconductor layer absorbs photons having energies greater than the band gap as a result of raising the material's valence electrons into the conduction band. Photons with energies less than the band gap energy are transmitted through the coating unchanged. As the semiconductor coatings have high refractive indices, for obtaining high solar absorptance, using an anti-reflection layer for reducing the air/semiconductor interface reflection is necessary.

The semiconductor selective absorbers can be useful in low- and mid- temperature applications. The other form of semiconductor-metal tandem is semiconductor-pigmented paint mixed with silicon binder coated on metal. It is low cost design with good thermal stability but it suffers from high thermal emittance of binder around 0.7 [33].

**5-2) Composite Coatings:** Composite coatings are surfaces usually consisting of small transition metal particles embedded in a dielectric matrix (also called cermet) deposited on a highly infrared reflecting metal substrate. These coatings absorb solar radiation strongly due to inter-band transitions in the metal in combination with small particle resonance, while they are almost transparent in the infrared region. Hence,

### 3. Theoretical background

---

the base metal dominates the infrared properties (the low thermal emission) of the absorber.

Spectral selectivity and characteristic cut-off wavelength (transition wavelength from low to high reflection) of composite absorbers depend on the volume fraction, shape of the particles, optical constants of the constituents and thickness of the composite coating. This offers a high degree of flexibility to solar selectivity. The optical properties of composite coatings can be understood from effective medium theories (see chapter 4). Fig. 3-4 d and 3-4 e show schematic view of two selective composite coatings, one with metal particles uniformly distributed in the ceramic matrix and the other one with graded distribution.

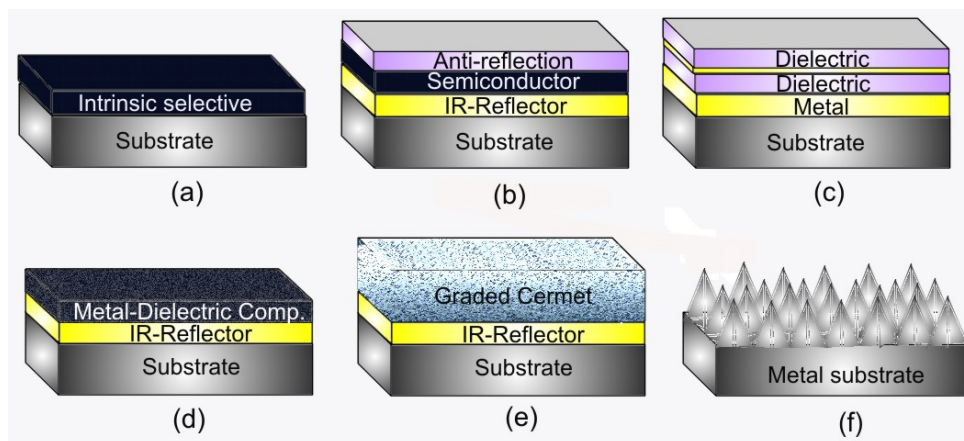


Fig. 3-4: Different configurations for achieving the spectral selectivity: (a) intrinsic selective material, (b) semiconductor-metal tandems, (c) multilayer absorber, (d) homogenous metal-ceramic composite coatings, (e) graded metal-dielectric composite (f) textured surfaces (light trapping)

#### 3.6 Deposition techniques

The deposition techniques, which have been used in this study, can be generally classified under two main categories:

- 1- Vapor deposition
- 2- Wet chemical deposition

Each process has its own parameters to control the growth and formation of the films. For a given material, the microstructure and the morphology depend on the kinetics

### 3. Theoretical background

---

of the growth, the deposition rate, the deposition atmosphere and the substrate temperature. These parameters can be optimized according to the required film property. The deposition techniques play a very important role to achieve desired film properties since the deposition of the same material by different deposition methods usually lead to different coating properties. Each method has its own advantages and disadvantages. In engineering studies always, the economical parameters of the deposition technique should be considered and regarded. With such an outlook, choosing a suitable technique is more limited.

As in this work only thin films but not thick coatings bring the desired optical properties, here only the most commonly used techniques for deposition of thin films are described.

#### **3.6.1 Vapor deposition techniques**

Vapor deposition techniques can be classified into two main classes: (1) Physical vapor deposition (PVD) and (2) Chemical vapor deposition (CVD).

PVD based on the deposition of a vapor from a source onto a substrate in a chamber and under vacuum. The creation of the vapor from a source can be achieved by thermal evaporation (vacuum evaporation) or by bombarding (sputtering) the surface of a target by high energetic particles, usually  $\text{Ar}^+$ . Here only sputtering process is described. More information on the CVD and evaporation techniques are available in different handbooks like [34] .

##### **3.6.1.1 Sputtering**

Sputtering is a non-thermal vaporization process, in which surface atoms are physically ejected from a surface by momentum transfer from an energetic bombarding species of atomic/molecular size. Typically, sputtering uses glow discharge or an ion beam to generate ions incident on the target surface. These ions cause atoms and occasionally cluster of atoms to be knocked free from the target surface by impact transfer or sputtering. There are different kinds of sputtering; Direct-Current (DC) diode, Radio Frequency (RF) diode, triode and magnetron sputtering.

Sputter deposition techniques have several distinct advantages:

### 3. Theoretical background

---

- Deposition from unlimited range of source and film materials (i.e. metals, semiconductors, insulators, alloys, and compounds)
- Small sputtering-yield variations from one material to another as compared to the relative variation in the evaporation rates at a given temperature
- Ease of low temperature deposition of refractory materials
- Absence of droplets, which are common in arc or thermal evaporation deposited films
- Ease of forming multi-components films
- Uniformity of film thickness over large areas
- High degree of film adhesion
- Environmentally friendly processing

Sputter deposition processes have several limitations as well as:

- Target (source) materials must ordinarily be in sheet or tube form
- Deposition rates are typically less than 300 nm/min
- Setup costs are high because of the required vacuum environment
- Energy efficiency is low (70 % or more of the input energy is expended in target heating)

#### **Glow discharge sputtering**

DC diode discharge is the simplest case of glow discharge. As shown in Fig. 3-5, the discharge has five rather distinct regions: cathode glow, cathode dark space, negative glow, Faraday dark space, and positive column. Adjacent to the cathode is cathode glow region, which is luminous because of the decay of excitation energy of the positive ions during neutralization with electrons at the cathode surface. Next to it is the cathode dark-space across which most of the voltage is dropped, providing the accelerating force driving the ions into the target. In the plasma, the potential varies slowly and changes again close to anode. When an ion strikes the cathode, in addition to the generation of the heat and removal of neutral atoms and ions, there is about 5-10 % probability of secondary electron emission. These secondary electrons are then accelerated back across the dark space into negative glow region where they expend most of their energy creating additional ions (approximately, 10-20 ions/electron). The secondary electrons will transfer energy, leave by diffusion and

### 3. Theoretical background

---

recombination, slow by the anode and are transferred into the outside circuit. These secondary electrons are primarily responsible for sustaining the discharge. The luminous glow is produced because the electrons have enough energy to generate visible light by excitation collisions. Simplistically, the electrons absorb energy from the field, accelerate, ionize some atoms, and the process becomes continuous.

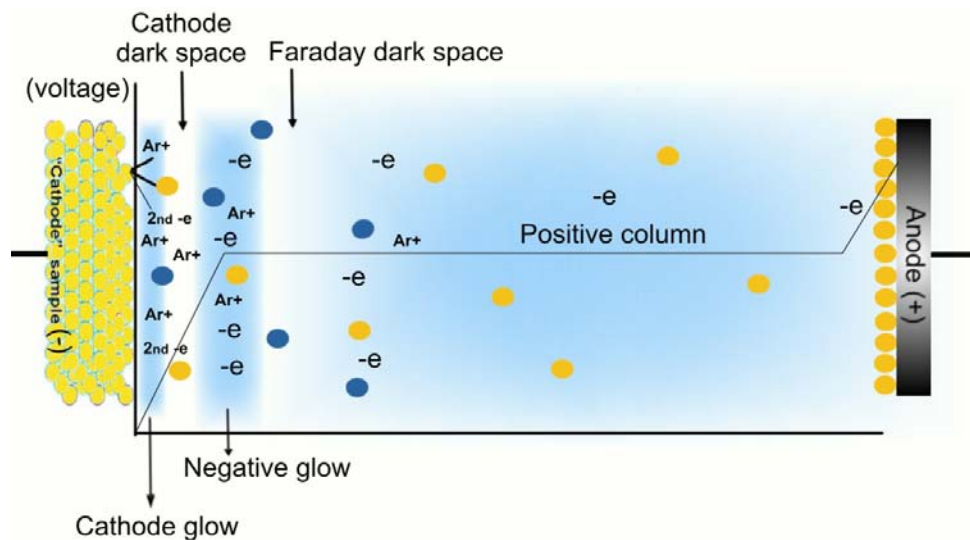


Fig. 3-5: Glow discharge regions and voltage along the discharge zones

#### DC (Direct Current) Sputtering

Diode DC sputtering uses a plate of the material to be deposited as the cathode electrode (target) in a glow discharge. Material can thus be transported from the target to a substrate to form a film. Films of pure metals or alloys can be deposited when using noble gas discharges (typically Ar) with metal targets.

#### RF (Radio Frequency) Sputtering

A high frequency alternating voltage applied between the electrodes is adequate to sputter conducting as well as insulating materials. In RF sputtering, the application of a high frequency (13.56 MHz) alternating field causes the electrons to oscillate in the negative glow region. In this way, they acquire enough energy to cause ionizing collisions to sustain a discharge without necessitating secondary electron emissions. Therefore, RF voltage can also be coupled through any kind of impedance, which eliminates this restriction that the electrode must be a conductor. RF discharge can be maintained at considerably lower pressures, 0.13-2 Pa, than pressures required

### 3. Theoretical background

---

for sustaining a DC glow discharge. It is because of the increased collisions of the electrons with the sputtering gas which resulting enhanced ionization.

#### **Reactive Sputtering**

Compounds can be synthesized by reactive sputtering, that is, sputtering elemental or alloy targets in reactive gases; alternatively, they can be deposited directly from compound targets.

#### **Magnetron Sputtering**

Another variant in sputtering sources uses magnetic fields transverse to the electric fields at sputtering-target surfaces. This class of processes is known as magnetron sputtering. Target-generated secondary electrons do not bombard substrates because they are trapped in cycloidal trajectories near the target, and thus do not contribute to increased substrate temperature and radiation damage. This allows the use of substrates that are temperature-sensitive (for example, plastic materials) and surface sensitive (for example, metal-oxides-semiconductor devices) with minimal unfavorable effects. In addition, this class of sputtering sources produces higher deposition rates than conventional sources and lends itself to economic, large-area industrial application. There are cylindrical, conical, and planar magnetron sources, all with particular advantages and disadvantages for specific applications. As with other forms of sputtering, magnetron sources can be used in a reactive sputtering mode.

#### **3.6.1.2 Ion-surface interactions**

The sputtered material is primarily in the atomic form but there are other species that come off a target, when an energetic ion hits the target. These processes are shown in the Fig. 3-6. The incidence ion itself can be reflected back after being neutralized. In addition to the sputtered atomic flux, the target material can also be ejected as clusters and negative ions although they constitute only a fraction of the total flux. X-ray, photon, and secondary electrons are other probable emissions off the target material.



### 3. Theoretical background

---

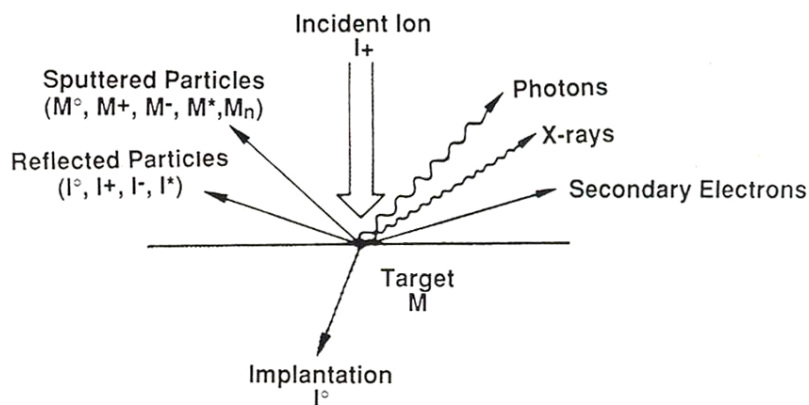


Fig. 3-6: Interaction of incident ion with the surface of the target material

#### 3.6.1.3 Processes at the substrate surface

Main processes occurring at the substrate surface are shown in Fig. 3-7. The arriving atoms diffuse around the substrate and their diffusivities are dependent on the interaction between the arrived atoms, substrate and temperature of the substrate. In randomly diffusing, they come across other atoms and join them to form doubles, which have lower diffusivities. As more flux arrives at the surface, the nuclei sizes grow and eventually islands are formed.

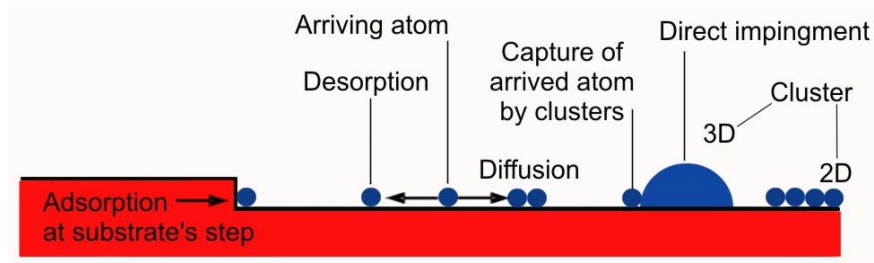


Fig. 3-7: Thin-film formation in sputtering deposition

#### 3.6.2 Wet chemical deposition techniques

Wet chemical deposition are techniques, in which the material species to be deposited are dispersed in a liquid medium. The resulting coatings should be usually heated at high temperatures but curing at low temperatures is possible and depends on the coating solution. To obtain high quality coatings the solution must have special physical and chemical characteristics like follows:

### 3. Theoretical background

---

- The solution must have a sufficiently small contact angle with the substrate. The smaller the contact angle is, the higher is wettability of the solution. Wettability can be improved in some cases by the addition of the wetting agent to the coating solution or by an appropriate pretreatment of the substrate.
- The solution must have an adequate durability under certain conditions. The colloidal stability is an important factor affecting the coating quality. The durability of the coating solution could be enhanced by using stabilizers.
- The drying and heating process must be carried out carefully in order to obtain reproducible solid and homogeneous coatings.

There are different wet-deposition methods like: spray pyrolysis, dip coating and spin coating methods but here only the applied dip and spin coating methods are described.

#### 3.6.2.1 Dip-coating method

The dip-coating is a good technique for preparation optical coatings with high quality and homogeneity. It is simple, cheap and allows coating complex shapes. No need to vacuum and no complicated instrumentation are required. In dip-coating, both sides of the substrate at one run are coated. In dip-coating, the substrate is immersed into the suspension or solution and normally withdrawn vertically from the coating bath at a constant speed under controlled temperature and atmospheric conditions. Dip coating process consists of 3 stages: 1-immersion, 2- formation of the wet layer and 3- drainage and evaporation. The thickness of the coating depends on the viscosity of the solution, the rate of solvent evaporation, and the angle at which the substrate is taken out. It can be determined using the Landau-Levich equation [35]:

$$h = 0.94 \frac{(\eta v)^{2/3}}{\gamma_{LV}^{1/6} (\rho g)^{1/2}} \quad (3-6)$$

### 3. Theoretical background

---

where  $h$  is the film thickness,  $\eta$  is the sol or suspension viscosity,  $v$  is the withdraw speed,  $\gamma_{VL}$  is the liquid-vapor surface tension,  $\rho$  is the density, and  $g$  is the earth gravity acceleration.

#### 3.6.2.2 Spin Coating

Spin coating is the preferred method for application of thin, uniform films to flat substrates. An excess amount of solution is placed on the substrate. The substrate is then rotated at high speed in order to spread the fluid by centrifugal force. Rotation is continued for some time, with fluid being spun off the edges of the substrate, until the desired film thickness is achieved. The solvent is usually volatile, providing for its simultaneous evaporation. Edge effects are often a problem in spin coating because the fluid flows uniformly outward and it forms droplets at the edge to be flung off.

After spinning, the coating may be sintered at high temperatures or it may be cured using UV or infrared radiation depending on the desired application. The film thickness in spin coating method depends on the rotation speed, time of spinning, viscosity and liquid concentration. The final thickness of the coating can be estimated using Meyerhofer formula [35]:

$$h_{\text{final}} = c_0 \left[ \frac{C\sqrt{\omega}}{2(1-c_0)\left(\frac{\rho\omega^2}{3\eta}\right)} \right]^{1/3} \quad (3-7)$$

where  $h_{\text{final}}$  is the final film thickness,  $c_0$  is the solid concentration in the solution,  $\rho$  is the liquid density,  $\omega$  is the rotation rate,  $\eta$  is the viscosity of the solution and  $C$  is the proportionality constant which depends on the experiment conditions.

#### 3.6.2.3 Suspension characterization

For preparing a stable suspension, the solid particles (here ceramic nano-particles) are dispersed throughout water or alcohol based solvent medium through mechanical agitation. For successful dispersion of powders in a liquid, knowledge of wetting of the powder into the liquid, breaking of aggregates and agglomerates, and stabilization of the resulting dispersion is required.

#### **Dispersion**

Nano-materials, such as metal oxides tend to be agglomerated when being mixed into a liquid. Therefore, effective means of deagglomeration and dispersing are required to overcome the bonding forces after wetting the micron or nano-powders. Dispersion can be accomplished with different techniques like ultrasonic, ball-milling, bead-mill, or dissolver. High rotation speed of dissolver applies high shearing forces to the suspension to break the agglomerates. For dispersing nano-powders, ultrasound dispersion has proven to be more effective than many other devices. It would be useful for breakage of both agglomerates and aggregates. Thin film deposited from a well-dispersed suspension would have less porosity, better homogeneity and film quality.

#### **Stabilisation**

Stabilization serves to prevent colloids from renewed association (flocculation) and its consequence sedimentation due to the relatively high strength of the inter-particle van der Waals attractive forces between particles. The goal of stabilization is maximizing the repulsive forces between particles in order to keep each particle discrete and prevent them from gathering into larger, faster settling agglomerates. The dispersion quality is highly dependent on the surface chemistry of the dispersed particles. Three different surface modification methods can prevent particles aggregating:

- Electrostatic stabilization: By adjusting the pH value of the suspension, an electrostatic barrier avoids possible flocculation. This kind of stabilization is only possible in polar liquids.
  
- Steric stabilization: Adsorption of a polymer with high molecular weight on the particle surface creates a physical barrier that hinders aggregation.
  
- Electrosteric Stabilization: Electrosteric stabilization is obtained by combination of both steric and electrostatic stabilizations. i.e., a charged polymer is adsorbed on the surface of particle.

#### **Electrostatic stabilization**

Electrostatic stabilization is based on the common electrostatic repulsion of particles with similar electrical charges. There are two inter-particle forces; Van der Waals attraction forces and repulsive forces due to charge double layers around the particles. Van der Waals attraction is the result of forces between individual molecules in each colloid. Such attraction between one molecule of one colloid to each molecule in the second colloid is repeated for each molecule so that an attraction force is created between the colloidal particles. In contrast, interaction between molecular dipoles on the particle surface with the surrounding counter ions produces a long-range attractive force from particle surface to the liquid. As different phases, generally have different charge affinities therefore a charge double-layer forms at any interfaces.

DLVO theory, which named after Derjaguin, Landau, Verwey and Overbeek, explains the stability of the colloids in the suspensions by considering the balance between electrostatic repulsion and van der Waals attraction forces. When two particles approach each other, their double layers interfere and an electrostatic repulsion becomes significant, while the van der Waals forces between particles attract colloids to each other. If the repulsion force between particles is large enough, they will bounce away from each other and that keeps the particles in a dispersion state. Otherwise, the particles may stick together and grow aggregates that make the suspension unstable and the aggregates will quickly settle out from the surrounding medium. In a stable colloid, the mass of a dispersed phase is so low that its buoyancy is too small to overcome the electrostatic repulsion between charged layers of the dispersed particles.

#### **Dispersion of Al<sub>2</sub>O<sub>3</sub> powders**

By mixing and wetting alumina powder with distilled water, surface hydroxyl groups of oxide surfaces (e.g.  $\text{-AlOH}$  on alumina) adsorb or desorb  $\text{H}^+$  ions at low and high pH respectively, creating either a positively ( $\text{AlOH}_2^+$ ) or negatively ( $\text{AlO}^-$ ) charged surface [36].

#### **Double layer and zeta potential**

The potential at the particle surface of a negatively charged colloidal in an ionic solution attracts ions in solution of opposite charge (counter-ions). The attracted positive ions form a firmly attached layer around the surface of the colloids. This layer is called Stern layer. After creation of such counter-ion layer, additional positive ions are repelled. The concentration of positive ions near the solid surface is high but it is decreased gradually with distance until it reaches equilibrium with the ion concentration in the solution. This results in a formation of a Guoy or diffuse layer of counter-ions. The attached counter-ions in the Stern layer and the charged atmosphere in the diffuse layer is called double layer. The double layer causes an electro-kinetic potential difference (in the order of millivolts) between the surface of colloid and any point in the suspending liquid.

The particle mobility with a fixed velocity in a voltage field is related to the dielectric constant, viscosity of the suspending liquid and to the electrical potential at the particle-liquid boundary. The slip plane at particle-liquid boundary is defined as the plane where Stern layer and diffuse layer meet each other. The electrical potential at this junction is called zeta ( $\zeta$ ) potential. As the electrical potential at this shear plane related to the particle's mobility, the  $\zeta$ -potential can be calculated by measuring the velocity of a particle subjected to a DC electric field. It can be also related to the energy needed to shear the particle and its inner layer of counter-ions away from the outer layer / bulk medium.

For keeping the system in a well-dispersed state only with electrical charge, the zeta potential needs to be kept above 25 mV. Particle size, density and viscosity of the fluid are other parameters, which affect the settling behavior of the suspended particles. These parameters are studied in the next sections.

#### **Nano-powders**

In comparison with micro-powders, nano-powders have higher specific surface area and therefore, lower sintering temperatures. Dispersion of nano-powders is more difficult because with the rising curvature of small particles, the agglomeration is increased and inter-particle forces grow. There are different methods for synthesizing nano-powders like flame hydrolysis, gas condensation, laser ablation, PVD, thermal synthesis, microwave-plasma synthesis and sol-gel method.

#### **Particle Size Distribution (PSD)**

The particles in a colloidal suspension are not all of the same size and may vary over a wide range. There are different PSD measuring methods based on sedimentation rate, light scattering patterns and projected image size. Mastersizer and Acoustosizer are well-known devices for measuring the particle size distribution. Mastersizer uses laser diffraction principle for measuring the particle sizes according to the fact that large particles scatter laser light at narrow angles with high intensity, whereas small particles scatter at wider angles but with low intensity. The measured size range is directly related to the angular range of the scattering measurement.

Acoustosizer is an instrument, which calculates the zeta potential and the size of the particles by measuring the dynamic mobility of the particle over a wide frequency range (from 0.2 to 20 MHz). In this method, an alternating electric field forces the particles in the colloid to move back and forth in a high-frequency oscillation. This particle movement results in sound waves, which are analyzed to determine particle size and zeta potential. This effect of sound waves generated by an applied electric field is called the Electrokinetic Sonic Amplitude effect or ESA for short. This frequency range is not suitable for oscillating nano-particles. There are also methods, in which sound energy is applied directly to the system and the resulted electric field created by the vibration of the colloid double layer is measured.

Most measurement techniques assume that the particles are spherical and the particle sizes are reported as the diameter of the “equivalent sphere”. For example in Mastersizer the diameter of the sphere that yields an equivalent light scattering pattern to the particle being measured, is reported. Therefore, because of the different equivalent sphere approximations and employed physical properties of the particles, different techniques would measure different size distributions.

#### **Viscosity**

Viscosity is another property that can be modified by varying the balance between repulsion and attraction forces. In dip- or spin-coating depositions, viscosity of the suspension is one of the key parameter, which dominates the final thickness of the deposited thin film.

#### **Suspension conductivity and pH**

Electrical conductivity is a measure of a suspension's ability to conduct an electric current and has the SI units of Siemens per meter (S/m). It can be an indirect measurement of the concentration of ions. Consequently, conductivity can be used to estimate levels of total dissolved solids.

#### **3.7 Different techniques of surface structuring**

The most common micro patterning methods are: optical photolithography, e-beam lithography, imprint lithography, replica molding, micro contact printing, laser writing, holographic patterning and direct laser interference patterning. Existing micro-structuring techniques can be categorized into two main groups depending on their processing; on one hand, the methods, which require a mechanical process such as printing, molding or embossing and on the other hand, those process that are activated by light, ions or electrons such as optical lithography, laser writing, holographic patterning and direct laser interference patterning [37]. In general, a lithographic technique is built upon following key elements: A pre-designed set of patterns in the form of a mask or a master, a means to mediate the transfer or replication patterns, a responsive medium, which is usually a functional material capable of serving as the resist for subsequent steps. The main interest of this section is quick reviewing the available structuring methods and introducing the most applicable ones for solar industry.

#### **Optical lithography**

In optical lithography, printing is done by projection the image of the pattern onto the substrate using a light source, photo-mask and negative or positive photo-resist.

#### **E-beam lithography**

Electron beam lithography is a method with higher resolution than optical lithography, which removes the resist film by its focused electron beam. It is not suitable for large patterning area and needs expensive apparatus but it has the advantage that no mask is required. For detailed information regarding lithography techniques see [38].



#### **Laser structuring**

##### **- Laser structuring using photo-resist**

A focused laser beam scans a substrate coated with a polymer resin containing a unique dye to create a desired hardened polymer structure according to the preprogrammed pattern. For getting 2D structures a photo-resist layer is exposed twice against of focal point of laser pattern [39]. In comparison to that, holographic method is faster and is done by interfering two or more laser beams. The resulted pattern is then recorded in an exposed photo-resist film.

##### **- Direct laser structuring**

This technique uses interference of 2 or more laser-beams, like in holographic laser patterning but no photo-resist or special active medium is required. Compared to the more common lithography methods for surface roughening of solar absorbers, the novelty of laser interference micro patterning lies in the fact that only one processing step is required. It enables direct processing of the probe itself rather than the exposure of the photo resist film. Using laser micro-structuring, surface micro-patterns from 2 up to 20  $\mu\text{m}$  can easily be created in only one simple step by femto- or nano-second laser pulses. The method is based on the formation of interference patterns, which are produced when two or more coherent laser beams are overlapped on the surface of a material. The only requirement is the absorption ability of the material at wavelength of the incoming laser beam.

Micro-structuring characteristics like pattern period and pattern depth can be controlled by the laser parameters like wavelengths, pulse width, pulse number and the power. In direct structuring of metal substrates the periodical heat source produces the local heating of the metal through photo-thermal interaction at the interference maxima positions [40]. Different metallurgical effects such as melting, resolidification and phase formation are also happening in this point. These effects permit the texturing of the metallic surfaces, which can be exploited to produce structured solar-absorbers.

#### **Imprint structuring**

Instead of direct structuring of the substrate material, which is difficult and highly melting temperature and material flow dependent, it is possible to structure an organic-inorganic sol-gel film deposited on the substrate [41].

In imprint (embossing) technology, a structured elastomeric mold is used to deform an active material deposited on a substrate. The active layer can be UV- or thermally curable material or a deformable material with high thixotropic characteristic. The elasticity and low surface energy of the mold allows it to be released easily. After thermal curing of embossed resist layer, a glassy layer is obtained. Now, the structure is ready and the desired material can be deposited on it.

Thermal curing of imprint micro-structured inorganic sol-gel materials would lead to 70 % shrinkage [41]. Therefore structure heights of only few nanometers are obtainable. The shrinkage rate of such materials can be reduced by adding organic components, like Polyethylen oxide (PEO). However using that reduces shrinkage rate but not less than 30 % with final film thickness of 200 nm [41].

Mennig described a method using phenyl- and methyl-triethoxysilane modified nanoparticulate sols, which after thermal treatment leads to only 25 % shrinkage in the structure height [42]. The shrinkage rate is limited due to the high solid content of the sol and the high green density. Using his route, the structure height up to 25  $\mu\text{m}$  can be prepared. In his developed sol,  $\text{SiO}_2$  nano-particles with particle size of about 10 nm with different surface modifications are dispersed in a polymethacrylat matrix. Sol coatings with thicknesses up to 15 micrometer can be obtained by dipping of a flat substrate into the sol.

This method realized high structure heights in a structured glass like material with high durability. Because of the organic part, these materials are in gel state flexible and the imprint takes place in a low viscose sol, so that just small pressure (2.5  $\text{mN/mm}^2$ ) is necessary to structure the layer. This allows the employment of flexible stamps [42], which is intended for large area structuring.

#### **3.8 Best structuring techniques for solar absorbers**

In Table 3-1, a summary of advantages and disadvantages of different described structuring techniques is shown. It is clear that for mass production and structuring of large surfaces, direct laser structuring and imprint technologies are more suitable

### 3. Theoretical background

---

than the other methods. Embossing can rapidly pattern large areas with feature sizes that are more costly and time consuming with electron-beam or ion-beam patterning. In comparison, direct laser structuring is a robust and simple patterning way but is more expensive than embossing. Therefore, in this study these methods are preferred and selected for structuring of the substrates prior to the deposition of the absorber layer.

Table 3-1: Comparison of different structuring techniques

("\*" means; not good, not bad)

Structuring	Different structures	Mass production	Process time	Simplicity
Holography	+	-	-	-
Direct laser structuring	-	+	*	+
Imprinting (embossing)	+	+	+	+
Lithography	*	+	*	-

#### 3.9 Optical characterization of selective surfaces

The reflectance, transmittance and absorptance are three parameters, which describe characteristics of an optical surface. For a given incident angle of  $\theta$ , reflectance  $R(\theta, \lambda)$  is the fraction of incident light at specific wavelengths  $\lambda$  that is reflected. The absorptance  $\alpha(\theta, \lambda)$  of a plane is the fraction of incident radiation at a given wavelength, which is absorbed by the surface and  $T(\theta, \lambda)$  is the fraction that is transmitted. Energy conservation gives:

$$\alpha(\theta, \lambda) + R(\theta, \lambda) + T(\theta, \lambda) = 1 \quad (3-8)$$

If the surface is opaque to the radiation then the angular solar absorptance can be expressed in terms of the angular total reflectance

$$\alpha(\theta, \lambda) = 1 - R(\lambda, \theta) \quad (3-9)$$

The emittance ( $\varepsilon_{th}$ ) is described as the ability of a surface to radiate thermal power. It is the ratio of the radiancy of the surface to the radiancy (or monochromatic radiancy

### 3. Theoretical background

---

at a given wavelength) of the blackbody at the same temperature and under the same condition. According to Kirchhoff's law stating that the absorptance is equal to the emittance, for an opaque object, it can be concluded that:

$$\varepsilon_{th}(\theta, \lambda) = 1 - R(\lambda, \theta) \quad (3-10)$$

#### 3.9.1 Total solar absorptance and thermal emittance

Total solar absorptance for a given angle of incidence  $\theta$  is obtained by weighting the spectral absorptance with the spectral solar irradiance and integrating over the wavelengths, in which solar radiation reaches the absorber surface. In the same way, total thermal emittance is obtained by integrating the weighted spectral emittance of the surface over all wavelengths in which thermal energy is emitted.

Eqs. (3-11) and (3-12) describe the total hemispherical solar absorptance and total normal emittance of an absorber for an incident angle of  $\theta$ , respectively.

$$\alpha(\theta) = \frac{\int_{\lambda_1}^{\lambda_2} A(\lambda) [1 - R_{total}(\theta, \lambda)] d\lambda}{\int_0^{\infty} A(\lambda) d\lambda} \quad (3-11)$$

where  $\lambda_1$ ,  $\lambda_2$  are then 0.2  $\mu\text{m}$  and 3  $\mu\text{m}$ , respectively, and  $\theta$  is the angle of incidence of light measured from the surface normal of the absorber.  $A(\lambda)$  is the wavelength dependent solar spectral radiance.

$$\varepsilon_{th_n}(\theta, T) = \frac{\int_{\lambda_1}^{\lambda_2} E(T, \lambda) [1 - R_s(\theta, \lambda)] d\lambda}{\int_0^{\infty} E(T, \lambda) d\lambda} \quad (3-12)$$

where  $\lambda_1$ ,  $\lambda_2$  are then 2.5  $\mu\text{m}$  and 50  $\mu\text{m}$ , respectively and  $\theta$  angle of incidence of light measured from the surface normal of the absorber.  $E(T, \lambda)$  the emitted spectral power of a blackbody at temperature  $T$  and wavelength  $\lambda$ .

### 3. Theoretical background

---

$R_{\text{total}}(\theta, \lambda)$  and  $R_s(\theta, \lambda)$  are the angular total and specular components of reflected light at wavelength  $\lambda$ . Solar reflectance measurements are usually performed in the wavelength range 0.3-2.5  $\mu\text{m}$  at near normal ( $\theta \approx 2^\circ$ ) angle of incidence using standard spectrophotometers. This means the solar absorptance is characterized at near normal incidence for which the sun is at the zenith angle relative to the absorber. For oblique incidence, where the sun is at other elevations than the zenith, the near normal solar absorptance must be modified when characterizing solar thermal collector systems. This is usually done by using the angle of incidence modifier (optical efficiency),  $K_{\tau\alpha}(\theta)$  which is a function of  $\theta$  given by [43]:

$$K_{\tau\alpha}(\theta) = \frac{(\tau\alpha)}{(\tau\alpha)_0} = 1 - b_0 \left( \frac{1}{\cos\theta} - 1 \right) \quad (3-13)$$

where the subscript "0" represents values at normal (zero) angle of incident. The constant  $b_0$  is called an incidence angle modifier coefficient and its value can be different for different collectors.

#### **3.10 Degradation of selective absorbers and the stability tests**

In order to use a material in a given application effectively, its degradation under service conditions must be tested or predicted. For validation of our new kind of absorber surface, conducting durability qualification test is necessary. Series of accelerated aging tests are normally carried out to determine the estimated service lifetime of an absorber surface. In a standard solar collector, only absorbers with a minimum lifetime of 20-30 years can be qualified. A general methodology for durability test procedures and service life time prediction has been defined in [44]. The standard high temperature and humidity test procedures are shown also in appendix B. A detailed description of the testing procedure can be found in [45]. For evaluating the degradation and estimating the acceptable service life of an absorber coating, a performance criterion function (PC) has been defined in [46].

$$PC = -\Delta\alpha + 0.5\Delta\varepsilon < 0.05 \quad (3-14)$$

### 3. Theoretical background

---

Coefficient of 0.5 is a weighting factor, which expresses the relative importance of the thermal emission compared to the solar absorptance and  $\Delta$  is the difference between optical properties of aged and unaged samples. 5 % is the maximum acceptable reduction of the annual solar fraction of a typical thermal collector. The failure time is defined as the time passing until this value reached.

Among three degradation process of 1) high temperature, 2) high humidity and water condensation and 3) sulphur dioxide corrosion test, only main part of the first two tests is carried in this study. Conducting a full durability test was out of the scope of this study.

#### 3.11 State of the art of selective absorber design

##### Single cermet layer structure

Cermet materials as solar absorbers have attracted interest since 1950s, when Tabor studied practically black nickel selective absorber [47]. Cermet films for solar application have been fabricated by either thermal evaporation or sputtering from separate or composite source or by using anodization-coloration process.

Cermets for solar applications usually consist of nanometer-sized metal particles (1–20 nm) embedded in a ceramic host [48]. The metallic particles could be either homogeneously distributed in the ceramic matrix or graded (from a low metal particle density at the air/cermet interface to a high density at the cermet/substrate interface). Such graded distribution of metal particles improves the spectral selectivity of the coatings by gradually increasing of the refractive index that reduces the reflection loss of the top interface and eases the entering of the light to the cermet layer [5]. Ungraded single cermet layers with uniform metal volume fraction deposited on metal reflectors show a solar absorptance of about 0.8 and low emittance [49].

Cermet layer is deposited over a metallic substrate and may be covered with an anti-reflection coating to reduce the refractive index mismatch between air and the absorbing layer to enhance the solar absorptance. It is convenient to produce the anti-reflection layer from the same oxide layer as used as ceramic part of the cermet. Until now, several selective absorbers with single homogenous and graded cermet structures have been studied and some of them commercialized. In Table 3-2, many of them have been listed. In the past, the most widely used practical cermet absorbers were black chrome (graded Cr-Cr<sub>2</sub>O<sub>3</sub> composite) [50] and nickel-

### 3. Theoretical background

pigmented  $\text{Al}_2\text{O}_3$  [51]. Surfaces such as these yield a high solar absorptance of 0.92 to 0.96. The production costs of these two kinds of solar coatings are low, so they are widely used in flat plate collectors. However the emittance of both coatings is high around 0.09-0.20 at 100 °C [9].

Table 3-2: Solar absorptance and thermal emittance values of some developed and commercialized selective absorbers with single cermet structure

Cermet	Deposition tech.	$\alpha$	$\epsilon_{th}$	Commercial name	Reference
Ni- $\text{Al}_2\text{O}_3$	Electroplating	0.93	0.13	Showa Aluminium Co.	[52]
Ni- $\text{Al}_2\text{O}_3$	Electroplating	0.96	0.2		[51]
Ni- $\text{Al}_2\text{O}_3$	RF sputtering	0.94	0.07		[53]
Ni- $\text{Al}_2\text{O}_3$	Electroplating	0.85	0.08	Tekno Term Energi	[54]
graded Ni- $\text{Al}_2\text{O}_3$	Co-evaporation	0.94	0.1		[55]
graded Ni-NiOx	Reactive sputtering	0.96	0.1 (100°C)	Sunstrip	[56]
Black Nickel	Sputtering	0.95	0.13	Tekno Term	[57]
Ag- $\text{Al}_2\text{O}_3$	Evaporation	0.7	0.1		[15]
Cu- $\text{Al}_2\text{O}_3$	Sputtering	0.9	0.045		[58]
Au- $\text{Al}_2\text{O}_3$	Sputtering	0.95	0.025		[58]
graded Ni-MgF <sub>2</sub>	e-beam evaporation	0.96	0.13		[59]
W- $\text{Al}_2\text{O}_3$	RF sputtering	0.96	0.16 (350 °C)	Solel	[25]
Mo- $\text{Al}_2\text{O}_3$	RF-sputtering	0.96	0.1	Luz	[60]
CrN-CrxOy	DC magnetron sputtering	0.93	0.07 (100 °C)	Sunselect (Interpane)	[61]
Cr-Cr <sub>2</sub> O <sub>3</sub>	RF-sputtering	0.92	0.08		[62]
Cr-Cr <sub>2</sub> O <sub>3</sub> (black chrome)	Electroplating	0.97	0.12	MTI/ChromeCoat e/Energie Solaire	[2]
Au-MgO	RF-sputtering	0.93	0.09		[62]
TiN <sub>x</sub> O <sub>y</sub>	Reactive evaporation	0.85	0.05	TiNOx (Thermomax)	[63]
Pt- $\text{Al}_2\text{O}_3$	RF sputtering	0.95	0.10		[64]
graded SS-C	Sputtering	0.92	0.04 (100 °C)	Shiroki (Japan)	[65]

Graded Mo- $\text{Al}_2\text{O}_3$  cermet solar collector tubes that were manufactured by Luz Co. Israel, were used for solar thermal power plants constructed in southern California

### 3. Theoretical background

during 1984 -1990. Seven planar targets (3 Mo and 4 Al<sub>2</sub>O<sub>3</sub> sputtering targets) were used to produce Mo-Al<sub>2</sub>O<sub>3</sub> cermet solar collector tubes [60]. In Fig. 3-8, the layer configuration of single cermet absorbers is shown.

#### Double and multiple cermet layer structures

New cermet film structure composed of two cermet sub-layers has been investigated and proposed by Q. Zahng [3, 23, 66, 67]. These two cermet layers must have different metal volume fractions. The one with high metal volume fraction is called HMFV and another one with lower metal volume fraction is called LMVF cermet layer. The cermet layers are located between a conventional metal reflector and a ceramic anti-reflection layer. Fig. 3-8 shows layers configuration of this double cermet structure. This new cermet structure design has photo-thermal efficiency higher than that of single graded cermet layer [49, 68]. In Table 3-3, optical properties of some promising selective absorbers with double and triple cermet structures have been listed.

Table 3-3: Solar absorptance and thermal emittance values of some developed and commercialized selective absorbers with double and triple cermet structures

Cermet	Deposition tech.	$\alpha$	$\epsilon_{th}$	Structure name	Reference
Mo-AlN	Reactive DC Sputt.	0.94	0.11(350 °C)	2 Cermets	[67, 69]
SS-AlN	Reactive DC Sputt.	0.95	0.05	2 Cermets (Turbo Sun)	[67], [7]
W-AlN	Reactive DC Sputt.	0.92	0.08	2 Cermets	[67]
Al-N	Reactive DC Sputt.	0.96	0.08	2 Cermets	[9]
Cr-Cr <sub>2</sub> O <sub>3</sub>	Reactive DC Sputt.	0.94	0.06	3 Cermets	[70]
Ti-TiN <sub>x</sub> O <sub>y</sub>	Reactive DC Sputt.	0.91	0.04	3 Cermets	[70]

Turbo Sun in China produced 3.5 million commercial U-shaped all-glass evacuated solar collector tubes in 1997 for low-temperature hot-water collectors using SS-AlN double cermet layer [25]. Farooq & Hutchins [4] developed a new 4-layer cermet destructive interference coating system with non-linear metal gradation, which enabled maximum interference in the multilayer. Compared to single cermet layer with uniform metal concentration, they observed 3 % increase in solar absorptance



### 3. Theoretical background

---

and 2 % reduction in emittance value. They have not compared their structure with double structure explained above.

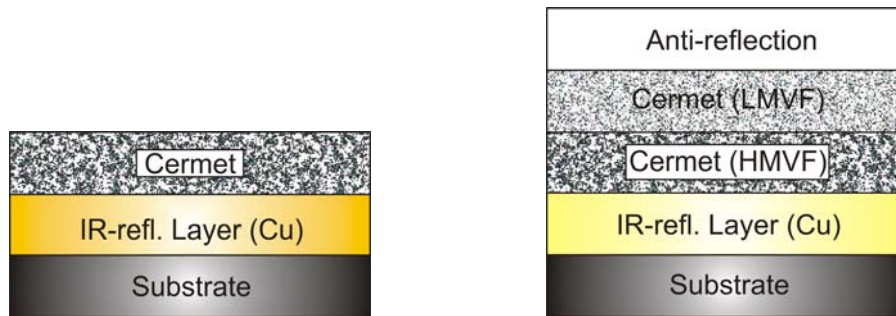


Fig. 3-8: Left: Single cermet structure; right: double cermet structure with anti-reflection

#### **Optical trapping surfaces (wave-front discriminators):**

As described in selectivity mechanisms, moderate spectral selectivity can be obtained for metals only by geometrical effect of their top surface. By choosing and structuring a high temperature stable metal, which has low thermal emission, a moderate selective but stable absorber can be obtained. For example thermally stable metals include molybdenum, rhodium, platinum, tungsten and hafnium carbide are good candidates for making high thermally stable absorbers in this way. Textured copper is suitable for high temperature only in an evacuated tube, but attempts to texture aluminum failed because of sample overheating [25].

The structuring method should be simple and inexpensive. In solar energy industry, surface roughening of a single material has been done mostly through chemical etching [31, 71], reactive ion etching [72], thermal evaporation onto heated substrate [73, 74], sputter etching [75], and unidirectional solidification [76]. G. Pettit et al. developed dendritic tungsten surfaces on electro-polished tungsten wafers by CVD process. The prepared rough tungsten surface was then anodized in phosphoric acid. They reached  $\alpha/\varepsilon$  (100 °C)=0.99/0.55 [77]. In such roughening methods, it is very difficult to create the desired pattern shape and control the aspect ratio of the surface feature.

Photo-thermal conversion using just morphology effects of metal substrates without any extra absorber layer has been investigated in [78] for Cr and Ni. There, periodic surfaces were produced by holographic technique on photo-resist film and then coated with a metallic layer of nickel or chrome by evaporation. Unfortunately, these

### 3. Theoretical background

---

surfaces are not suitable for high temperature applications due to the deterioration of the polymer which constitutes the under layer.

Sai et al. have introduced a sequential method called fast atomic beam (FAB) to structure a tungsten surface in 2 dimensions for developing a solar absorber based on the light trapping phenomena [22]. A porous alumina-etching mask is needed to produce such periodical structures. Such technique is not applicable for industrial applications because of its very complicated mask preparation procedure, limited micro-structured area and high expenses. In his method, the desired microstructure is copied using X-ray and an X-ray sensitive resist. Structuring using FAB or lithography methods gives more flexibility to produce desired patterns but unfortunately they are sequential structuring methods and many steps are needed to achieve the final desired patterned surface. Having many steps in the fabrication process in addition to the high costs may impose the possibility of losing information or pattern distortion during different steps.

#### **Wet-chemically derived cermet absorbers:**

Known to author, there are numerous chemical ways for preparation bulk pieces of nano-composite cermets or cermet powders but no important work has been done to apply these methods in making solar cermet absorbers or even cermet thin films for other applications. Previous studies were mainly focused on the microstructure and improved physical and mechanical properties of metal-ceramic nano-composites due to the micro-structural modification by nano-dispersion and their plasticity [79]. Especially Sekino et al. investigated the mechanical properties of different metal-ceramic nano-composites prepared by conventional powder metallurgical method and reduction and sintering of ceramic and metal oxide powders like W-Al<sub>2</sub>O<sub>3</sub> [80, 81] or through a chemical process like sol-gel and preparation of metal-ceramic composite powders like Ni-Al<sub>2</sub>O<sub>3</sub> [82, 83]. Such preparation methods were applied for making bulk composite samples with limited metal volume fraction of about 5-30 % in the final composite and metallic particle sizes of about 40-150 nm.

In 1995 Eisenhammer et al. granted patents in Germany [84] and the USA [85] claiming a sol-gel technique by dispersing conductive metal particles in an initial solution (Sol) or admixing them to a gel forming during a sol-gel process. In this technique, the conductive particles must be protected against chemical reaction and

### 3. Theoretical background

---

diffusion with a dielectric coating. The metallic particle sizes must be less than 70 nm and may be produced by spraying or evaporation in an inert gas atmosphere or a reactive atmosphere like oxygen or nitrogen at high pressures (10 Pa to 1000 Pa). Larger particles must be grinded and separated using different sieving techniques. In this method, the high surface area of the fabricated metal nano-particles and their high tendency for agglomeration would be the main challenges for avoiding any oxidation and homogeneous dispersion of metal particles in the dielectric medium. Surface modification of metallic nano powders, grinding and sieving are additional and complex processes, which make this production technique very expensive.

#### **Ni-Al<sub>2</sub>O<sub>3</sub> composite absorber:**

In the last decades, different spectrally selective Ni-Al<sub>2</sub>O<sub>3</sub> composite films were prepared by different methods. Sathiaraj et al. [53] prepared them by RF planar magnetron sputtering in laboratory scale using hot-pressed targets of Ni and Al<sub>2</sub>O<sub>3</sub>. In his method, changing the nickel content in the composite layer was not easy and he had to place additional Ni pellets on the composite target with a special geometry to reach higher metal volume fractions. He achieved for a single Ni-Al<sub>2</sub>O<sub>3</sub> cermet coated with 78 nm SiO<sub>2</sub> anti-reflective layer, solar absorptance of about 0.94 and thermal emittance of 0.07 coating.

Andersson et al. anodized the aluminum substrates using acid phosphoric and then colored the anodized aluminum via AC electrolysis in a bath containing NiSO<sub>4</sub>. He achieved solar absorptance of 0.93-0.96 and thermal emittance of 0.1-0.2 [51]. Salmi et al. have used the same fabrication method and investigated the effect of impregnation parameters on the optical properties. They obtained solar absorptance higher than 0.9 and thermal emittance of 0.14 [54]. Although pigmented aluminum oxide coatings are commercially used as solar collectors, they are generally not considered to be very selective [2]. Bostrom et al. according to their previous work on sol-gel derived anti-reflection coating [86] and carbon-silica composite films [87], prepared Ni-Alumina coatings from a chemical sol of Ni-Al<sub>2</sub>O<sub>3</sub> [88, 89]. They achieved solar absorptance of 0.83 and normal thermal emittance of 0.03 with a cermet layer which had a nickel content of 65 %.

#### **3.10 Material selection and experiment design**

##### **1- Enhancing the selectivity by surface roughness**

Combining the enhanced optical absorption effect of a rough surface or structured metallic substrate with good selectivity of a simple single cermet layer is an effective way for further improving the spectral selectivity of the conventional absorber coatings without the difficulty of exact controlling both thickness and composition. An effective rough air/absorber interface facilitates entering of the light into the absorber layer and increases the light absorption by light trapping effect. Moreover, surface roughness diminishes undesired interference reflection peaks at short wavelengths.

As explained in section 3-8, the methods of "Direct Laser Interference Patterning" and embossing are the most suitable candidates for structuring the substrates, which are used in solar absorber industry. Any large surfaces can be quickly structured in a simple manner and with least processing steps. In this thesis, these two patterning techniques are used and their robustness and capabilities in creation or transferring any structure shapes is investigated. The weakness and effectiveness of these methods in increasing the spectral selectivity of the absorber layer are also studied.

In this study, bulk copper and stainless steel substrates are structured with laser. Copper was selected because of its availability, very low thermal emittance and price. Moreover, Cu is the most used substrate material for solar absorbers. Stainless steel is more stable than copper at higher temperatures but it has higher thermal emissivity.

For embossing, a sol-gel layer is first structured on a glass substrate and then for simplicity instead of deposition of a cermet absorber only a tungsten thin film is deposited on it. Tungsten was selected because of its good intrinsic selectivity.

It is known that the deposited coating on an already structured substrate keeps the same structure shape in its interface with air. In case of depositing of thin coatings on the structured substrate with moderate sputtering rates, surface profile of the substrate is effectively duplicated on the surface of the thin film. Therefore, it is preferred to compare the optical properties of laser structured and embossed samples without deposition of cermet layer. In this case, inhomogeneity in the thickness of the cermet layer does not exist to change the optical properties of the samples.

### 3. Theoretical background

---

These kinds of substrate structuring prior to deposition of absorber coating despite of their simplicity impose a new step in the fabrication process. In contrast to this process, a textured selective surface can be created by oriented growth structures during film deposition.

The substrate temperature is a parameter which can change the microstructure and surface morphology of the growing film. The effect of this temperature is first studied on the double Cu-Al<sub>2</sub>O<sub>3</sub> cermet structure deposited on a copper reflective layer. Thereafter to obtain a higher roughness aspect ratio a thick roughness template layer is deposited between the IR-reflector layer and the substrate. The effect of substrate heating on this new structure is also studied. Among the variety of cermet-based absorbers, Cu cermets like Cu-Al<sub>2</sub>O<sub>3</sub> combinations have not been studied in detail despite of their very good selectivity which were predicted by simulations [49]. In addition, copper (or copper sputtered or plated substrates) is usually used in the solar absorber industry as substrate material because of its very low thermal emittance and low price. Therefore, selection of Cu for both reflective and cermet layer facilitates the fabrication process and provides a very low thermal emittance.

#### **2- Developing a novel cost-effective deposition method of cermet absorbers**

In this study a low-cost and novel production method of composite selective absorbers, which is based on powder technique, is developed. This fabrication method is very simple, reliable and economic. In addition, the consumed materials are very cheap and easily available and applicable for industrial mass productions on the large surfaces. Beside that, any surfaces not necessarily flat with desirable shape can be coated with a cermet layer by immersion them easily into the prepared suspension. In this procedure, no poisonous chemicals are used and the process is completely environment-friendly. This method is also very flexible in the mixing fraction of metal-part inside the ceramic part and vice versa. It also easily supports a multilayer deposition of cermet layers after quickly drying the foregoing layers.

In sol-gel technique, ceramic films or bulk composite materials are derived from expensive metal alkoxides precursors. Moreover all possible reactions of sol-gel process (hydrolysis, re-esterification, alcohol and water condensations) are highly dynamic and are not easily controllable. Sol lifetime is another problem in sol-gel route, which limits the stability and usability of the hydrolyzed alkoxides. In the course

### 3. Theoretical background

---

of time, because of the condensation process, sol particles aggregate and cause linking of particles into chains and create a network that is called gel. In fact, early gelation of the sol makes the sol useless and the created high viscosity gel is not more suitable for applying on the substrate. Adding metallic ions or powders in high quantity, accelerates the thickening and networking processes and prevents addition of desired amount of metal ions into the sol. sol-gel prepared thin films with a thicknesses of 1  $\mu\text{m}$  or higher suffer from many cracks formation after drying process [87, 90].

As described above, difficulties in controlling the hydrolysis process, the complexity of the chemical reactions, short lifetime of the sol, and usual crack development after heat treatment are the main problems of the sol-gel technique. In comparison, the developed powder suspension in this study has not such problems so that the prepared suspension can be used as long as it is stirred. Also without stirring a well dispersed and stabilized suspension does not show any significant sedimentation for hours. In addition, the stored or aged suspension kept in a closed container can be easily dispersed and reused. In this study, Ni-Al<sub>2</sub>O<sub>3</sub> cermet is fabricated by this method. Nickel was selected because of its thermal stability, low price and the fact that nickel oxide is readily reduced at low temperatures under H<sub>2</sub> atmosphere. Al<sub>2</sub>O<sub>3</sub> was selected because of its low price and availability of its nano-powder in our laboratory. Instead of that other ceramic nano powders like SiO<sub>2</sub>, ZrO<sub>2</sub>.... could also be used.

After preparation and stabilization of the suspension, different polished substrates like glass, copper and aluminum are coated with a thin film of Ni-Al<sub>2</sub>O<sub>3</sub> absorber material using dip coating deposition methods. The final dense absorber layer is obtained after special heat-treatment of the wet film. In chapter 6, the variation of optical properties of single cermet layer on the copper substrate for a constant metal volume fraction are studied. Using some commercial additives, the wetting and adhesion properties of the coating are remarkably improved. Finally, the optimum metal fraction is obtained, through the variation of metal content of the cermet for a constant thickness. X-Ray Diffraction analysis (XRD), Scanning Electron Microscopy (SEM), and Energy Dispersive X-ray Spectroscopy (EDX) analyses are also conducted on the samples to investigate the microstructure and film composition. The effect of binder and protective coating on the optical properties of single cermet

### 3. Theoretical background

---

absorber is also studied. Finally, to investigate the stability of the coatings, some samples are aged at elevated temperatures under vacuum and air. The stability of the coating under high humidity conditions is also tested. The optical properties of the samples before and after aging tests are compared and according to the obtained PC value, the stability is evaluated.

### 4. Theoretical modelling

#### 4.1 Snell's equation and Fresnel's law

Fresnel's equations describe the reflection and transmission of electromagnetic waves at an interface. That is, they give the reflection and transmission coefficients for waves parallel and perpendicular to the plane of incidence. Fresnel's equations can be stated in terms of the angles of incidence  $\theta$  and the relative refractive index of  $n$ :

$$r_p = \frac{-n^2 \cos\theta + \sqrt{n^2 - \sin^2\theta}}{n^2 \cos\theta + \sqrt{n^2 - \sin^2\theta}} \quad (4-1)$$

$$r_s = \frac{\cos\theta - \sqrt{n^2 - \sin^2\theta}}{\cos\theta + \sqrt{n^2 - \sin^2\theta}} \quad (4-2)$$

where  $r_s$  is the complex reflection ratio or relative amplitude of the reflected light having its electric vector perpendicular to the plane of the incidence (TE) and  $r_p$  is the reflection ratio or relative amplitude of the reflected light polarized parallel to that plane of incidence (TM). Light reflectance for p and s polarization is obtained from square of relative amplitudes of reflected light:

$$\begin{aligned} R_s &= |r_s|^2 \\ R_p &= |r_p|^2 \end{aligned} \quad (4-3)$$

Reflection of unpolarized radiation is defined as the average of the two polarisation components:

$$r = \frac{I_r}{I_i} = \frac{1}{2}(r_p + r_s) \quad (4-4)$$

When the light is at near-normal incidence to the interface of mediums 1 and 2, the reflection coefficients are given by:

$$R = R_s = R_p = \left(\frac{n_1 - n_2}{n_1 + n_2}\right)^2 \quad (4-5)$$



### **4.2 Optical properties of metals and dielectrics**

The classical theory of absorption in dielectrics is due to H. A. Lorentz and in metals to P. K. L. Drude [91]. Both models treat the optically active electrons in a material as classical oscillators. In the Lorentz model, the electron is bounded to the nucleus by a harmonic restoring force, just as for the non-conductive dielectric. Drude theory, however, considers the electrons free.

### **4.3 Optical properties of inhomogeneous media**

The metal-dielectric composites (cermets), composed of metal particles embedded in a dielectric medium host, are considered as inhomogeneous materials. Light propagating in a medium is scattered only when the medium has inhomogeneities. Optical properties of disordered mediums are derived from optical measurements combined with modeling of the experimental results using appropriate theoretical considerations. In this section the optical properties of the metal particles embedded in a non-absorbing medium, is studied. For particles that have a size much smaller than the wavelength of the incident light, effective medium theories can be applied. If the particles are of the order or larger than the incident wavelength, scattering become important in addition to absorption and Lorenz-Mie theory provides a solution to the single scattering problem [92].

#### **4.3.1 Lorenz-Mie scattering theory**

In contrast to Rayleigh scattering, Mie solutions to scattering takes account of all possible scatterer diameter/wavelength ratios. Therefore for a particle smaller or larger than the incoming wavelength the Lorenz-Mie scattering theory can generally be applied for calculation of scattering and absorption cross sections [93]. When a single particle is illuminated by an incident electromagnetic radiation, part of the incident energy is absorbed and the rest is scattered out. Lorenz-Mie theory is very complex and involves spherical Bessel functions, size of the particle, and refractive indices of the particle and host medium.

Scatterings by small and large particles haven been summarized by van de Hulst [93]. Using the boundary conditions and series expansions of the electric field of the scattering amplitude in the forward direction,  $S(0)$ , the light scattering by a particle

## 4. Theoretical modelling

---

can be characterized. The optical theorem for absorbing media relates the extinction cross-section ( $C_{\text{ext}}$ ) to the real,  $\text{Re}$ , part of the forward scattering amplitude,  $S(0)$  by:

$$C_{\text{ext}} = \frac{4\pi}{K^2} \text{Re}\{S(0)\} \quad (4-6)$$

where  $S(0) = (1/2) \sum_{n=1}^{\infty} (2n+1)(b_n + c_n)$  and  $K = \frac{2\pi}{\lambda}$  is the wave vector amplitude in the effective medium.  $b_n$  and  $c_n$  indicate scattering coefficients containing Bessel functions and their derivatives.

In case of spherical particles by enforcing the boundary condition on the spherical surface, the expansion coefficients of the scattered field can be computed.

### 4.3.2 Effective medium theories

The microstructure of inhomogeneous materials is represented with Random Unit Cell (RUC) models. The basic definition of an effective medium is that the RUC, when embedded in the effective medium, should not be detectable in an experiment using electromagnetic radiation confined to a specific wavelength range [52]. According to this definition for an effective medium,  $C_{\text{ext}}$  must be equal to zero which leads to  $S(0) = 0$ . Now, according to the structure of composite materials like separated grain or aggregate structures, different RUCs are defined like coated or uncoated spherical or non-spherical particle in a continuous host, so as the defined RUCs account for the major features of the microstructures. Now,  $S(0)$  can easily be obtained for defined RUCs through Lorenz-Mie theory and then by equaling it to zero the related dielectric function of considered structure is obtained.

### 4.4 Optical simulation

If the refractive indices of the metal, ceramic and cermet materials are known, one can calculate the reflectance, then the solar absorptance, emittance and photo-thermal efficiency of the solar selective coatings. The refractive index of cermet materials can be calculated from the refractive indices of metal and ceramic components using a physical model. The most widely physical models used for the

#### 4. Theoretical modelling

---

dielectric function of a composite have been proposed by “Maxwell-Garnet, 1904”, “Bruggeman, 1935”, “Ping Sheng, 1980” [52, 94].

For identical spherical grains with sizes much less than the wavelength of light, the average dielectric function of a composite in the Maxwell-Garnet (MG), Bruggeman (BR) approximations, is given by the following formulas:

$$\epsilon^{MG} = \epsilon_B \frac{\epsilon_A + 2\epsilon_B + 2f_A(\epsilon_A - \epsilon_B)}{\epsilon_A + 2\epsilon_B - f_A(\epsilon_A - \epsilon_B)} \quad (4-7)$$

$$f_A \frac{\epsilon_A - \epsilon_{-Br}}{\epsilon_A + 2\epsilon_{-Br}} + (1 - f_A) \frac{\epsilon_B - \epsilon_{-Br}}{\epsilon_B + 2\epsilon_{-Br}} = 0 \quad (4-8)$$

$\epsilon^{MG}$  and  $\epsilon^{BR}$  are the average dielectric functions of a composite in Maxwell-Garnet (MG) and Bruggeman (BR) approximations. Where  $\epsilon_A$  and  $\epsilon_B$  are the dielectric functions of metal (A) and ceramic (B), respectively. The filling factor  $f_A$  represents the volume fraction occupied by the metal spheres having  $\epsilon_A$ .

For the separated grain-structure with particles of A, embedded in a continuous host of B, the RUC is a core of A surrounded by a concentric shell of B. For the aggregate structure in which A and B enter on equal footing to form a space-filling random mixture, the RUC is a core of A with probability  $f_A$  of being A and a probability  $f_B$  of being B. As explained in the last section, these equations were derived from equaling the forward scattering amplitude,  $S(0)$  to zero.

According to the Ping-Sheng (PS) model that supposes a composite film as a mixture of two types coated oblate spheroid units, dielectric-coated metal spheroids described as type-a units and metal-coated dielectric spheroids described as type-b units, estimates the average dielectric function of a cermet as follows:

$$v_2 \frac{\zeta_1 - \epsilon^{PS}}{\zeta_1 + 2\epsilon^{PS}} + (1 - v_2) \frac{\zeta_2 - \epsilon^{PS}}{\zeta_2 + 2\epsilon^{PS}} = 0 \quad (4-9)$$

While:

$$\zeta_1 = \epsilon_A \frac{(2\epsilon_A + \epsilon_B) - 2(1 - f_A)(\epsilon_A - \epsilon_B)}{(2\epsilon_A + \epsilon_B) + (1 - f_A)(\epsilon_A - \epsilon_B)} \quad \zeta_2 = \epsilon_B \frac{(\epsilon_A + 2\epsilon_B) + 2f_A(\epsilon_A - \epsilon_B)}{(\epsilon_A + 2\epsilon_B) - f_A(\epsilon_A - \epsilon_B)} \quad (4-10)$$

#### 4. Theoretical modelling

---

where:

$$v_1 = \frac{(1 - f_A^{1/3})^3}{(1 - f_A^{1/3})^3 + [1 - (1 - f_A)^{1/3}]^3} \quad v_2 = (1 - v_1) \quad (4-11)$$

$v_1$  and  $v_2$  are the relative probabilities of the occurrence for type-a and type-b units, respectively, at any metal volume fraction. Also  $\xi_1$  and  $\xi_2$  are defined just for simplifying the Eq. 4-9 to make it similar to Bruggeman formula.

These theoretical approximations are often in good agreement with experiment results. For composites consisting of metal particles in an amorphous insulator matrix, the MG theory is usually in good agreement just for low filling factors ( $f_A > 0.2-0.3$ ) [95] but the Bruggeman theory works quit good up to filling factors of 0.3 to 0.4 [52].

#### Matrix formulation:

Now by having the obtained optical constants of cermet material, the optical properties of the cermet solar selective absorber coatings can be calculated according to the following Matrix formulation.

$$\begin{bmatrix} 1 \\ n_0 \end{bmatrix} + \begin{bmatrix} 1 \\ -n_0 \end{bmatrix} r = M \begin{bmatrix} 1 \\ n_T \end{bmatrix} t \quad (4-12)$$

where  $n_0$  and  $n_T$  represent refractive index of air and substrate, respectively and  $M$  denotes the characteristic transfer matrix. In addition,  $r$  and  $t$  are amplitude of reflectance and transmittance of one layer thin film sandwiched between air and substrate.

$$M = \begin{bmatrix} \cos kl & -\frac{i}{n_1} \sin kl \\ -in_1 \sin kl & \cos kl \end{bmatrix} \quad K = \frac{2\pi}{\lambda} = \frac{2\pi n_1}{\lambda_0} \quad (4-13)$$

#### 4. Theoretical modelling

---

where  $l$  and  $n_1$  are the thickness and refractive index of the thin film respectively. If there is a multilayer, the characteristic matrix and reflectance amplitude are calculated as follows:

$$M = M_1 M_2 M_3 \dots M_N = \begin{bmatrix} A & B \\ C & D \end{bmatrix} \quad (4-14)$$

$$r = \frac{An_0 + Bn_T n_0 - C - Dn_T}{An_0 + Bn_T n_0 + C + Dn_T} \quad (4-15)$$

$$R = |r|^2 \quad (4-16)$$

where  $R$  is the reflectance of the multilayer.

#### 4.5 Selectivity calculator

Using Visual Basic programming language a user-friendly calculator was written to calculate the solar absorptance and thermal emittance from wavelength-reflectance data (see appendix A for visual basic code details). Fig. 4-1 shows a picture of the program interface.

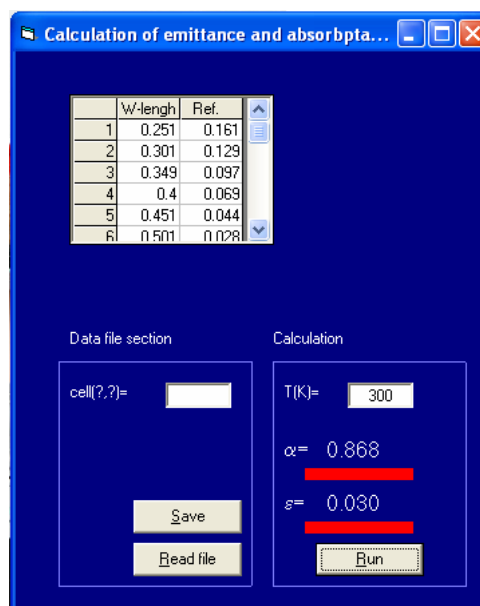


Fig. 4-1: Calculator of solar absorptance and thermal emittance from reflectance data

## 4. Theoretical modelling

---

By measuring the monochromatic reflectance at each wavelengths ( $\rho_\lambda$ ), the related  $\alpha_\lambda$  and  $\varepsilon_\lambda$  are obtained from equation 4-17 and 4-18.

$$\varepsilon = 1 - \frac{1}{n} \sum_{j=1}^n \rho_{\lambda,j} \quad (4-17)$$

$$\alpha = 1 - \frac{1}{n} \sum_{j=1}^n \rho_{\lambda,j} \quad (4-18)$$

The summation is calculated on special wavelengths, which are called mid-point wavelengths. Actually, the blackbody and the solar incident energy spectrums are divided into segments with equal energies but different widths. For example, an energy increment located in the wavelengths range, in which the maximum thermal emission or solar radiation exists, is the increment with the lowest width. Regarding to the solar radiation or thermal radiation in a given temperature, the midpoint wavelength of these energy increments have been tabulated in [43]. The program compares the measured wavelengths with the mid-point wavelengths of each segment located in the program library. In case of agreement between these two wavelengths, the related reflectance at the mid-point wavelength is considered. This process is continued for all energy segments. After selection of all required reflectance data, solar absorptance and thermal emittance are calculated using Eqs. 4-17 and 4-18.

### 4.6 Multilayer optimization

In order to achieve an optimum spectral selectivity, it is necessary to optimize the thin film parameters, after reflectance simulation of a multilayer stack. For example thickness of each layer, metal content of the cermet layers, number and order of layers can be optimized to maximize or minimize the reflectance spectrum for a specific wavelength range.

In this study, the simulation program was written using Visual Basic editor of the Microsoft Excel. Excel provides an environment, in which data can be inserted easily. In this way, changing the active parameters of each layer like layer thickness and metal volume fraction or studying the effect of new layers are done simply. For optimization of film thicknesses and metal volume fractions, Downhill-simplex and Generalized Reduced Gradient (GRG2) nonlinear optimization codes were used. To

## 4. Theoretical modelling

---

have a near ideal solar selective absorber coating, one should optimize the optical response of the absorber so that the reflectance of the multilayer should be minimized in the solar region of the spectrum and maximized in the IR region. To achieve this goal, the difference between summations of all reflectance values of solar wavelengths and thermal radiation wavelengths was defined as the optimization target. To reach logical values, constraints like positive volume fractions and thicknesses were considered.

### 4.7 Optical simulation of regular gratings

In interaction of light with a rough and matt surface, a part of the incoming energy is absorbed and the rest is reflected or scattered. A regular textured surface can scatter the light in preferential directions while a surface with random roughness can scatter the light in all directions. In this section, we are interested to study the interaction of light with a regularly textured surface without considering the scattering issue. The reflectance of light by such surfaces can be simulated by considering the roughness as a series of composite layers composed of air and material.

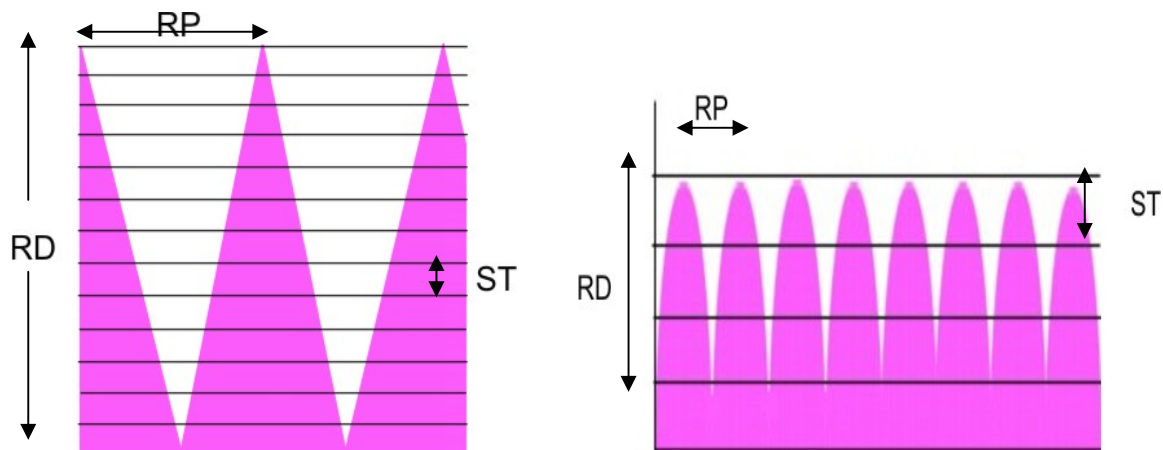


Fig. 4-2: Left: Triangle model; Right: Spheroid model

RP: Roughness Period; RD: Roughness Depth; ST: Segment Thickness

Roughness between air and substrate is divided in sub-layers, whereas for each sub-layer a thickness and volume fraction can be allocated. The material volume fraction in each sub-layer can be calculated by considering air as matrix and material as the dispersed element. Therefore, the roughness can be considered easily as many

#### 4. Theoretical modelling

---

composite layers, whose constituents are air and material. Now the dielectric function of each layer, dependent to its position, can be estimated with the same effective medium theories explained for cermets. Interaction of normal incident light with such surfaces can be simulated mathematically using following equations:

$$\text{Spheroid-Model [71]} \quad F = 1 - \left[ \frac{(i \times TD) - RD}{RD} \right]^2 \quad (4-19)$$

$$\text{Triangle-Model} \quad F = \frac{ST \times (2i - 1)}{2RD} \quad (4-20)$$

where F is the material fill factor and i is a counting parameter. ST, RP, RD stand for “Sub-layer Thickness”, “Roughness Period” and “Roughness Depth”, respectively.

These equations obtained by calculation the fraction of area occupied by material to the whole area of the first sub-layer and extending the formula to the further layers. The Bruggeman theory can be used to estimate the refractive indices of an air-graded composite layer. The spheroid graded refractive index model has been used by Niklasson to simulate the optical behavior of chemically etched Al-Si selective absorber [71] but the triangle model developed in this study.

Fig. 4-3 and 4-4 show the effect of roughness depth on the reflective properties of a textured copper with a roughness period of 4  $\mu\text{m}$ , using triangle and spheroid models, respectively. The ratio of the roughness depth to the roughness period is called roughness aspect ratio and here is simply called AR. Increasing the roughness aspect ratio (AR) leads to reflectance-edge shift toward higher wavelengths resulting in a gradual refractive index increase and higher solar absorption. These models do not consider the diffracted orders and scattered light and therefore cannot simulate the real cases but they are useful to show the effect of surface roughness and fine graduation of refractive index on increasing of spectral selectivity. In section 4-6, a more realistic model (PCGrate) will be used to simulate the selectivity improvement resulted from surface texturing effect.



#### 4. Theoretical modelling

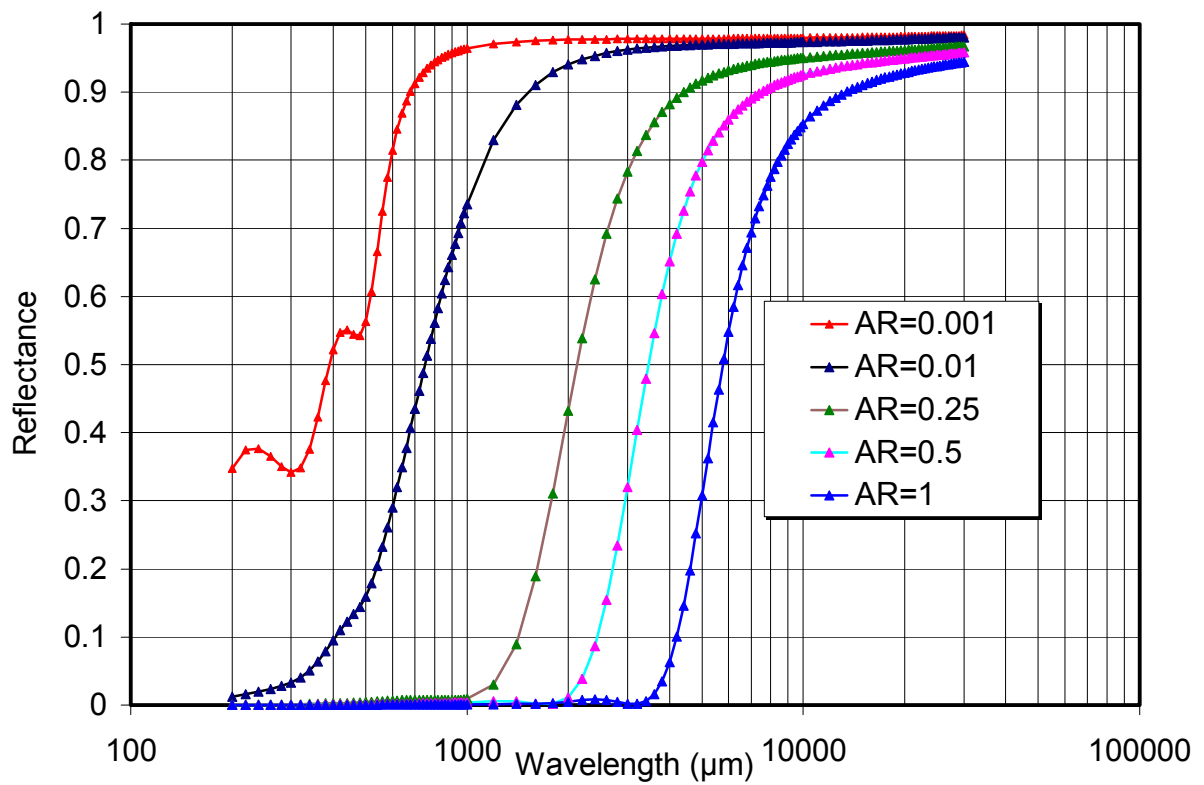


Fig. 4-3: Triangle model; effect of roughness depth on the reflectance curve of a textured bulk copper with a roughness period of 4000 nm

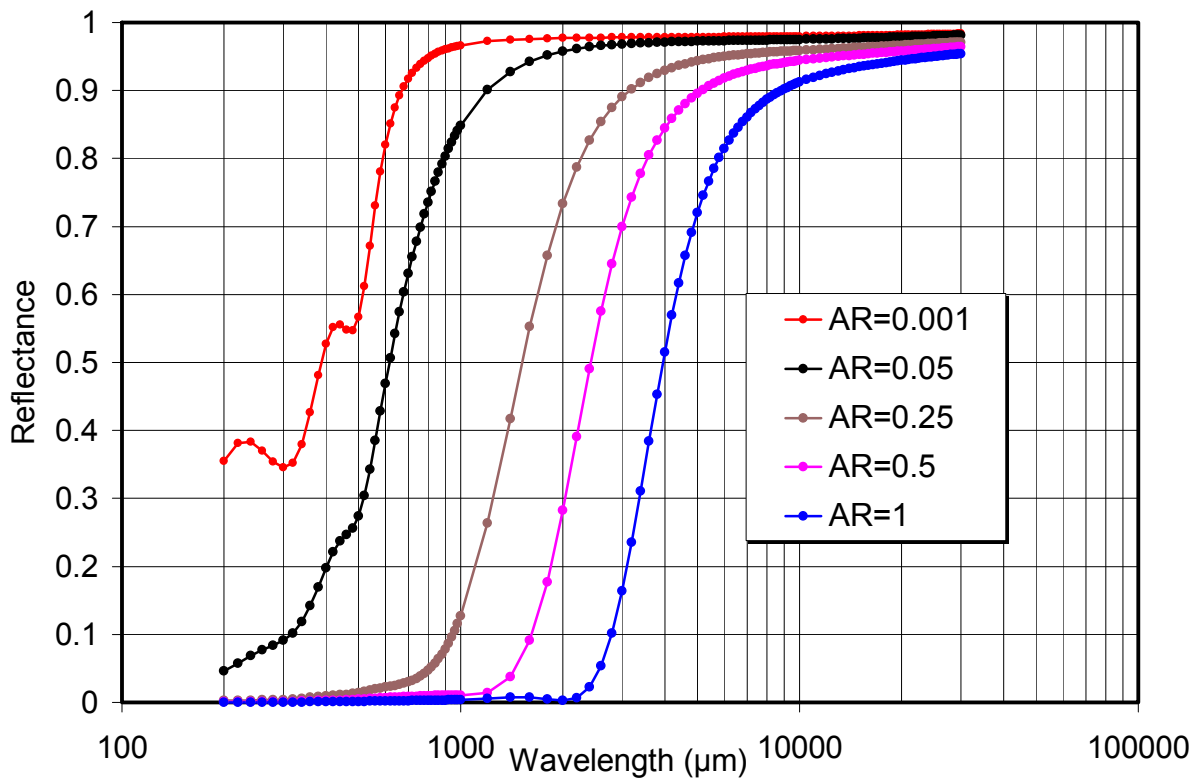


Fig. 4-4: Spheroid model; effect of roughness depth on the reflectance curve of a textured bulk copper with a roughness period of 4000 nm

Fig. 4-5 shows the effect of roughness shape on the reflectance spectrum. It can be seen that for a textured surface with a given roughness height and period, the triangular model is more effective in absorbing solar wavelengths than spheroid model. For comparison, reflectance curve of smooth copper sample has been shown together with simulation results of an almost smooth copper surface with feature heights of about 1 nm.

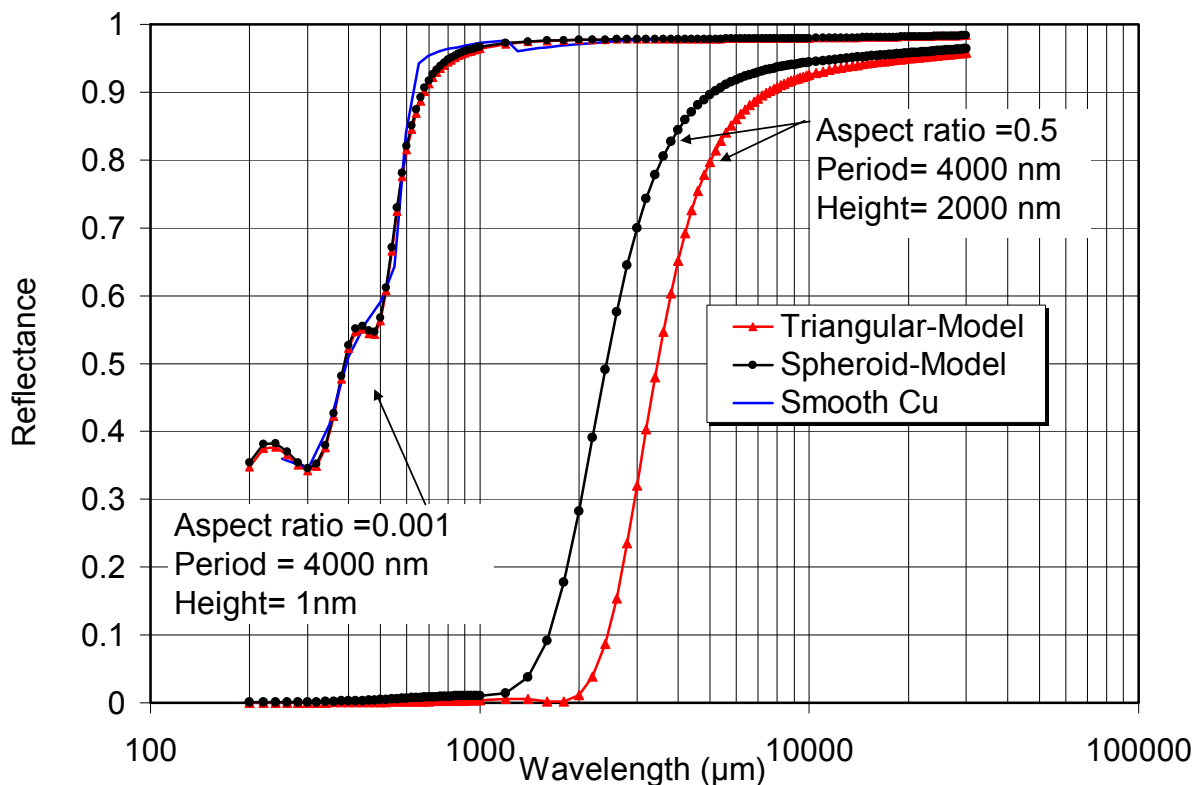


Fig. 4-5: comparison of triangle and spheroid models for a textured copper with similar roughness depth and period

#### 4.8 Interaction of light with periodical surface structures

The effective use of regular textured surfaces in optical selectivity calls for an understanding of how grating parameters affect the system range and performance. Periodic gratings behave differently from rough surfaces in the sense that they diffract an incident plane wave into preferential directions called spectral orders instead of scattering it over the entire space.

Light behavior in periodic media is subject to Maxwell equations. There are some numerical treatments for modeling and optimization of light propagation in periodic

media developed since 1960 that are considered as “rigorous” ones, in the sense that they provide numerical solutions of the Maxwell equations and boundary conditions without any theoretical approximation. There are several rigorous theories: the integral method, the classical differential method, the finite-element method, the modal methods, the method of Green functions, etc [96]. The methods start with integral or differential form of Maxwell equations, developing them to some set of functions and simplify the equations to obtain a linear algebraic system of equations for the diffraction order amplitudes.

For obtaining an optimized grating design for solar application, variations of the appropriate parameters such as geometry of the surface feature, light incident angle, grating depth, grating period and grating aspect ratio can be scanned.

### 4.8.1 Integral method

The integral method was the first rigorous grating theory. The basic principle of the integral method can be understood more easily for a perfectly conducting substrate. When an incident plane wave falls on the grating surface, it induces a surface current  $j_s(M')$  at each point  $M'$  of the surface. When propagating along the grating, the surface current radiates a diffracted field  $E(P)$  at a given point  $P$  above the surface, which is related to  $j_s$  by the Kirchhoff-Huygens formula using the Green function  $G$  technique [97]:

$$E(P) = \int_{\text{One grating Period}} G(P, M') \varphi(M') ds' \quad (4-21)$$

where  $\varphi(M')$  is proportional to  $J_s(M')$ .

The integration can be carried over the curvilinear of  $s'$  coordinate along the grating profile because the path of integration for  $j_s(M')$  is coincident with real surfaces of the grating layer boundaries. However, the problem is more complex than just a single integration, because the surface current is not produced only by the incident wave  $E^{(i)}$ , but also resulted from the diffracted field, radiated from the other points of grating surface. Thus  $j_s(M')$  depends both on  $E^{(i)}$  and on the current  $j_s(M'')$  at each other

point  $M''$  on the profile. Therefore, the above equation is then transformed into an integral equation for  $\varphi(M')$ . The situation becomes even more complicated for finitely conducting gratings. When the points  $M'$  and  $M''$  on the profile become too close to each other, this theory finds the numerical solution for an integral equation because of the divergence of the Green functions. Fortunately, the singularities can be eliminated analytically and the integral equation is reduced to a linear set of algebraic equations by discretization along the profile [96].

### 4.9 PCGrate simulation

In this study, PCGrate-S Version 6.1 program (International Intellectual Group, Inc.) was used for simulation the interaction of the light with different periodic surfaces. It is based on the modified method of integral equations (MIM), which enables the user to solve accurately a linear boundary integral equation or a system of such equations, which describes the incidence of a light beam on a rough surface. In MIM method, the groove profiles are represented not in a distorted form in terms of the Fourier expansions, but in a more correct form by means of collocation points which coincide with points of the real groove profile [98].

The most general integral theory used in the calculations enables one to deal with almost all kinds of gratings problems and very deep gratings with arbitrary profiles. The calculated output parameters of this program are physical quantities that characterize how power of incident field is distributed among different diffraction orders and what percentage of it is absorbed in the grooves by rigorous calculations of electromagnetic theory of diffraction.

An accurate knowledge of the total reflected energy over the entire wavelength range is necessary for designing an effective textured selective surface. Following parameters are the most interesting output parameters of this simulation for investigation of spectral selectivity of an ordered rough surface:

**Reflected energy** is the sum of absolute diffraction efficiencies of all reflected orders.

**Relative (groove) diffraction efficiency of the m-th order** is the ratio of the intensity of the radiation diffracted into the m-th order to the reflectivity of a plane mirror of the same material for the same conditions.

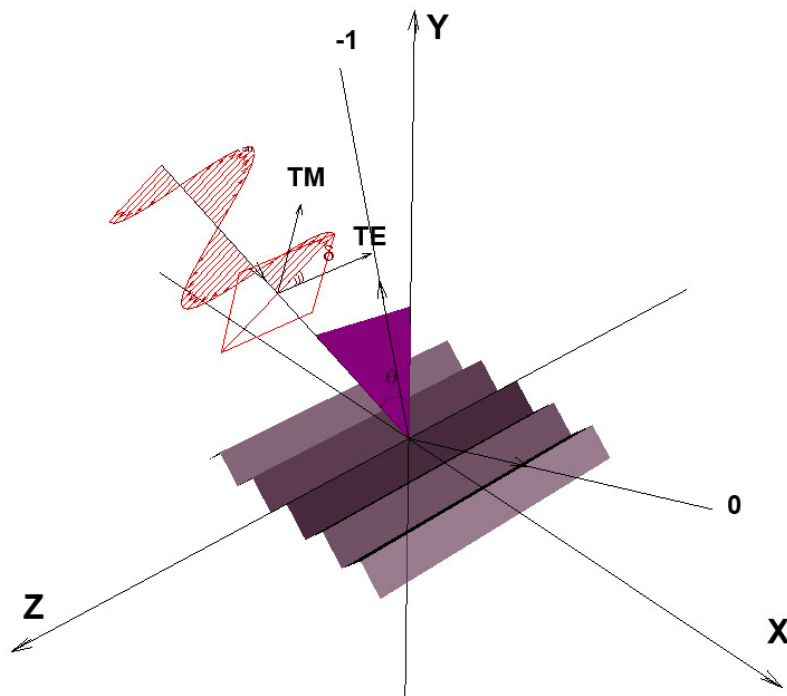


Fig. 4-6: Refraction orders of an incident beam with wavelength of 1200 nm and incident angle of  $70^\circ$  caused by a grating with a period of 1000 nm

As the solar absorptance is calculated from total reflectance data, the reflected energy is the most important output parameter of PCGrate simulation for comparing the effectiveness of different gratings in absorbing solar energy. In Fig. 4-6, refracted orders of an incident unpolarized beam with wavelength of 1200 nm and an incident angle of  $70^\circ$  are shown. Using the PCGrate program, diffraction efficiency of each order and the total reflected energy are easily calculable.

### 4.9.1 Setup of numerical simulation

In this section, light interaction with grating metal surfaces with, triangular, lamellar and sinusoidal border profiles are investigated. For numerical calculations, the following setup was considered:

Grating period = 3000 nm

Light incident angle: 5 degree

Wave front type: Plane

Type of polarization: Non-polarized

Sample size: 100 mm X 100 mm

Grating shape: plane

Wavelengths: 300-15000 nm step 40 nm

Structured copper and tungsten are our two candidates for investigation of the grating parameters on their spectral selectivity. Copper as a metal with very low thermal emittance and tungsten as an interesting element with intrinsic semi-selectivity characteristic.

### 4.9.2 Effect of structure shape on the spectral selectivity of copper

Figures 4-7, 4-8 and 4-9 demonstrate the effect of structure aspect ratio (AR) on the total reflectance of unpolarized light by the structured copper with lamellar, triangular and sinusoidal profiles, respectively. Structure period is considered 3000 nm and constant.

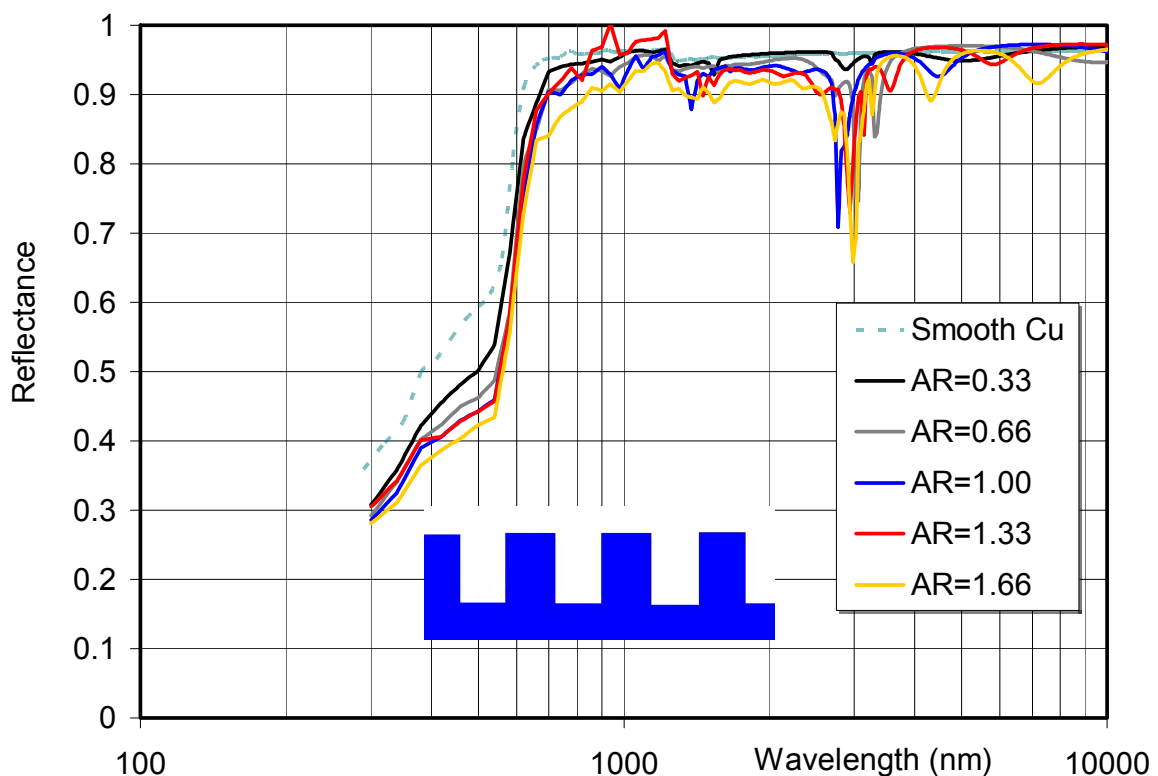


Fig. 4-7: Effect of structure aspect ratio (AR) on the total reflectance of unpolarized light by the structured copper with lamellar profile and structure period of 3000 nm

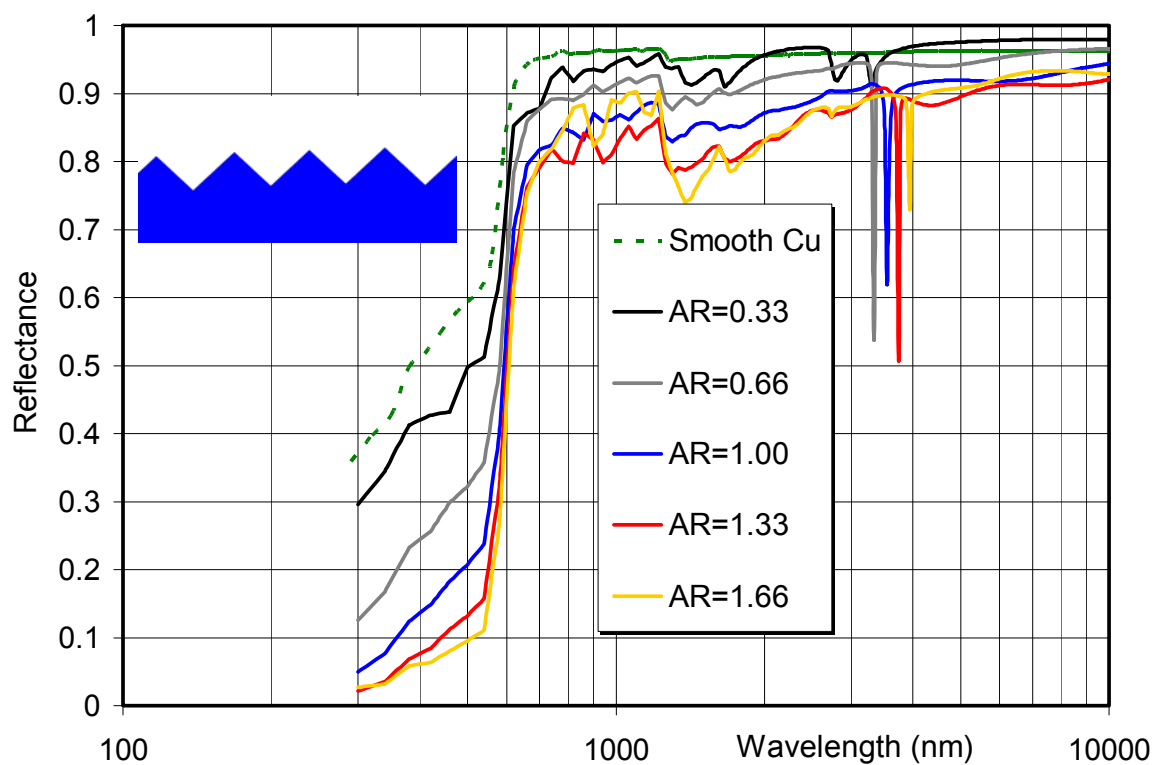


Fig. 4-8: Effect of structure aspect ratio (AR) on the total reflectance of unpolarized light by the structured copper with triangular profile and structure period of 3000 nm

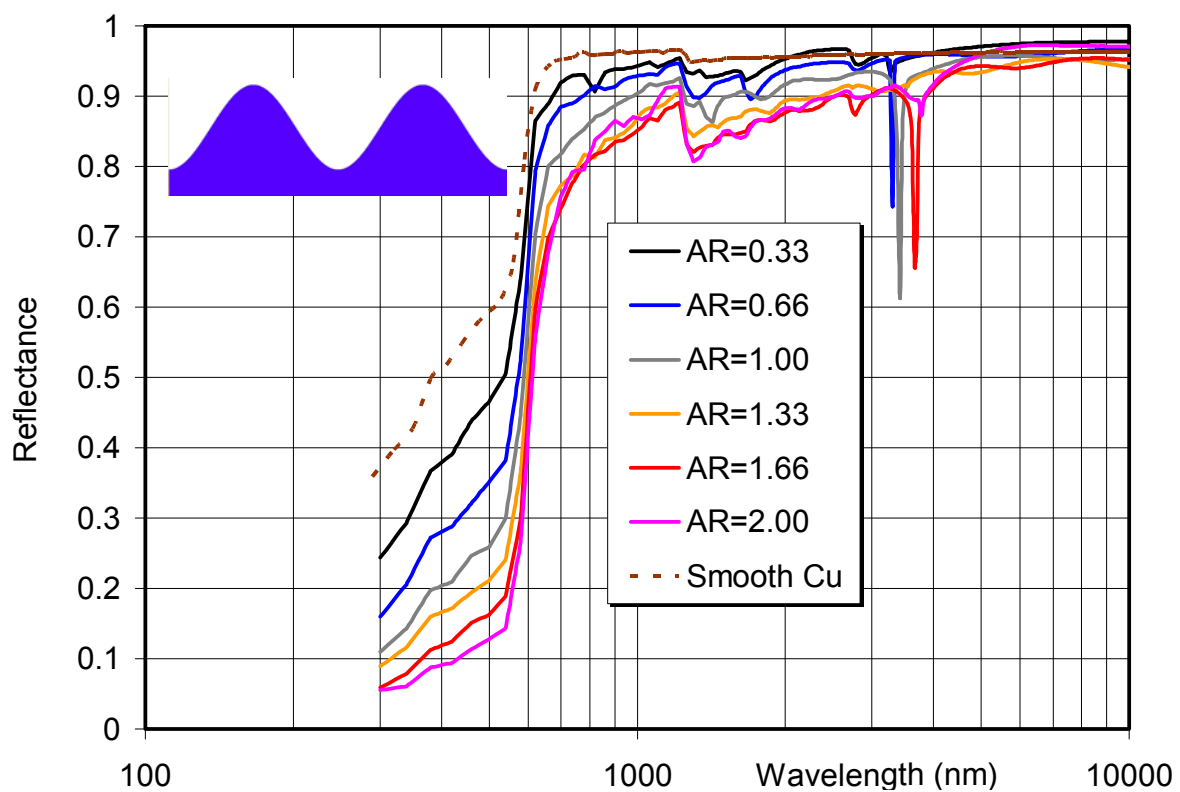


Fig. 4-9: Effect of structure aspect ratio (AR) on the total reflectance of unpolarized light by the structured copper with sinusoidal profile and structure period of 3000 nm

Period of 3000 nm was selected to make the structures indistinguishable for wavelengths higher than 3000 nm. Therefore, IR wavelengths see the surface mirror like and are reflected. In this case, solar radiation can be well absorbed without significant increase in the thermal emittance value of the used material.

From these simulation studies, it can be concluded that the reflectance curve of the lamellar profile (Fig. 4-7) is not sensitive to the profile depth and there is no significant enhancement in solar absorptivity by increasing the aspect ratio. In addition, reflectance in infrared wavelengths is kept almost unchanged. As can be seen from Figs. 4-8 and 4-9, sinusoidal and triangular profiles both show enhanced solar absorption (low reflection of solar spectrum) at higher aspect ratios but in triangular structure, the IR-reflectivity of the structured surface has been reduced as well. This would lead to a higher emittance value at higher profile's depth in comparison with almost unchanged IR-reflection of the triangular model. Finally, it can be fairly concluded that the most efficient structure profile in increasing the spectral selectivity of copper is sinusoidal.

### **4.9.3 Effect of structure shape on the spectral selectivity of tungsten**

The same behavior observed for structured tungsten substrate. That means the sinusoidal profile is the most effective structure shape in increasing the spectral selectivity of tungsten by increasing the absorption of solar spectrum and keeping the IR-reflectivity unchanged. Reflectance curves of Fig. 4-10 show that increasing the profile's depth results high selectivity for tungsten. For high aspect ratios, few absorbing peaks in infrared wavelengths and unusual increase in reflectance of 300-600 nm wavelengths are observed. As, these anomalies are seen only at high aspect ratios and many difficulties were experienced during reflectance calculation at high profile's depths, it is supposed that a part of the reflection anomalies is program related. But it has been stated in [99] that in diffraction of TM polarized light by metallic gratings, strong threshold and resonance anomalies may exist. Resonance anomalies depend strongly on polarization, while threshold phenomena appear in both polarizations. For verifying that, reflectance of TM and TE polarized lights are investigated.



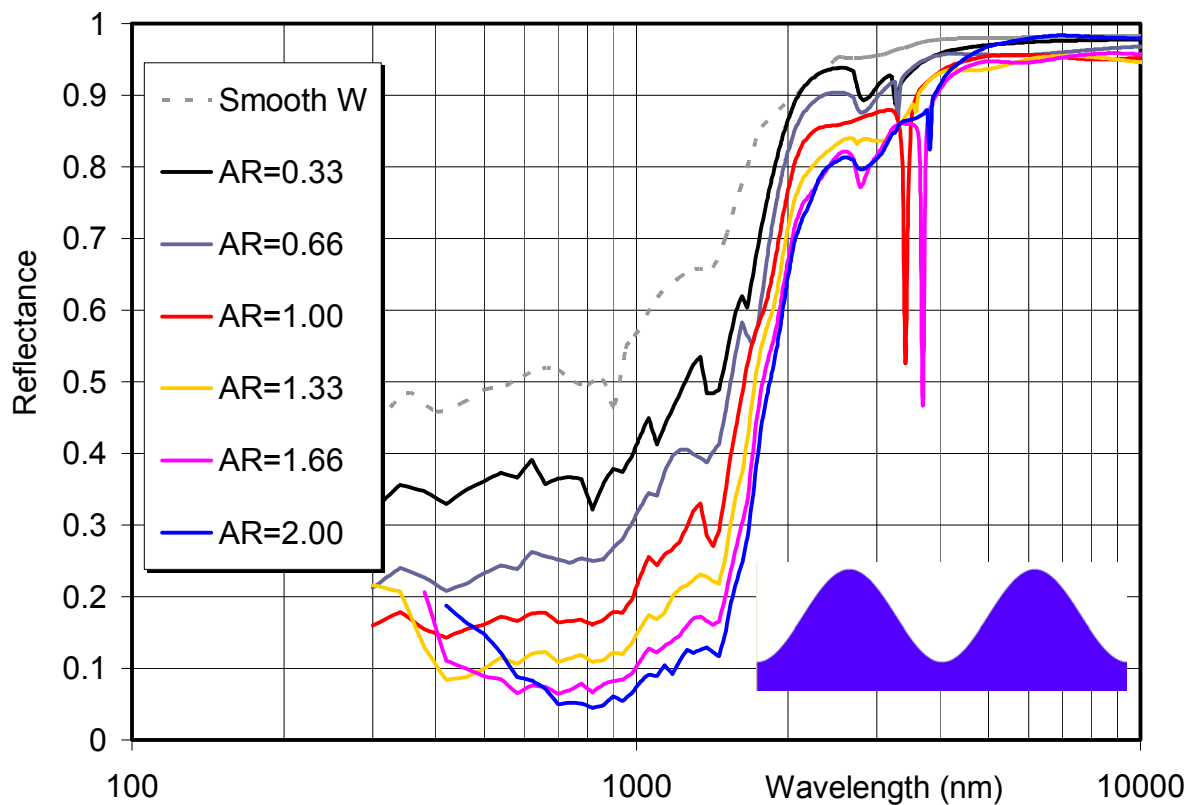


Fig. 4-10: Effect of structure aspect ratio on the total reflectance of unpolarized light by the structured tungsten with sinusoidal profile and structure period of 3000 nm

#### 4.9.4 Difference behavior of gratings for TE and TM polarizations

In Figs. 4-11 and 4-12 reflections of TE and TM polarized light by the structured tungsten is studied. Again, sinusoidal grating is considered due to its interesting selectivity. Because diffraction efficiency is different in the two planes of polarization [99], reflections of TM and TE differ from each other too. In Fig. 4-11, which shows the reflectance of TE polarized light, no sharp peaks (resonance anomalies) are seen but in TM polarization two narrow peaks located between 3000-4000 nm. Resonance domain includes wavelengths, which are in the same order of magnitude as the structure period. Resonance anomalies at such wavelengths are due to the guided wave excitations (plasmon wave along the metallic surface), or to a resonance inside the groove [99].

#### 4. Theoretical modelling

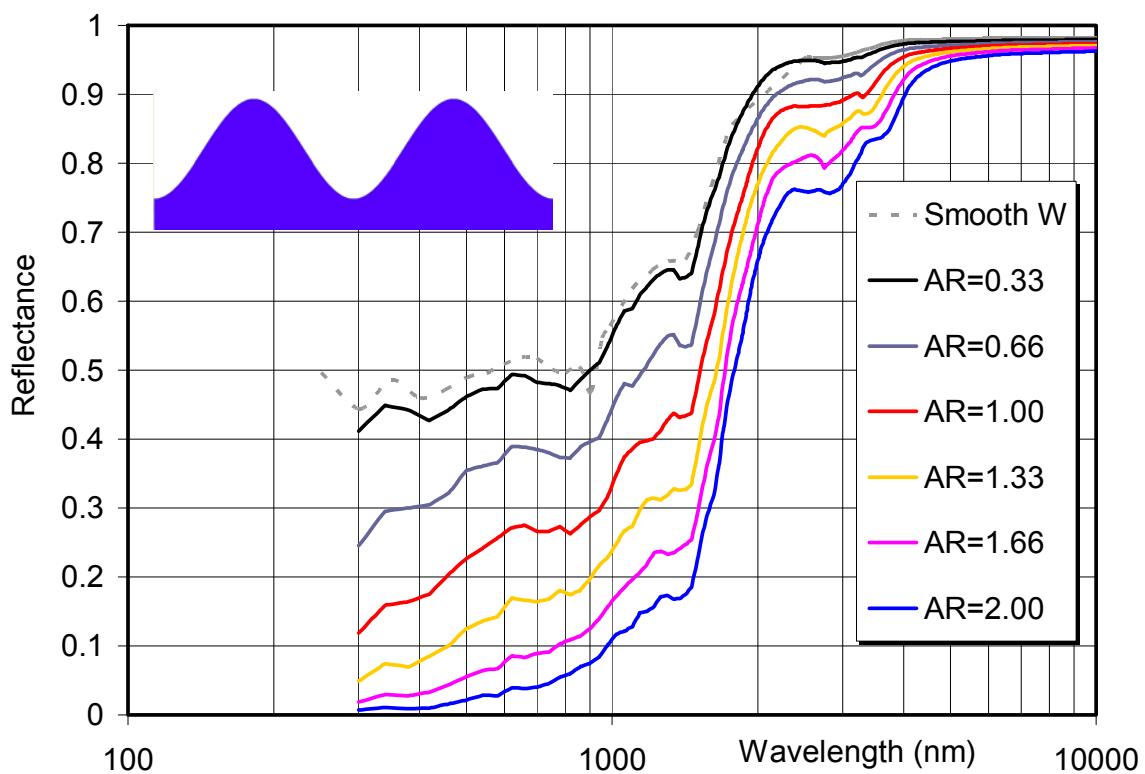


Fig. 4-11: Effect of structure aspect ratio on the total reflectance of TE polarized light by the structured tungsten with sinusoidal profile and structure period of 3000 nm

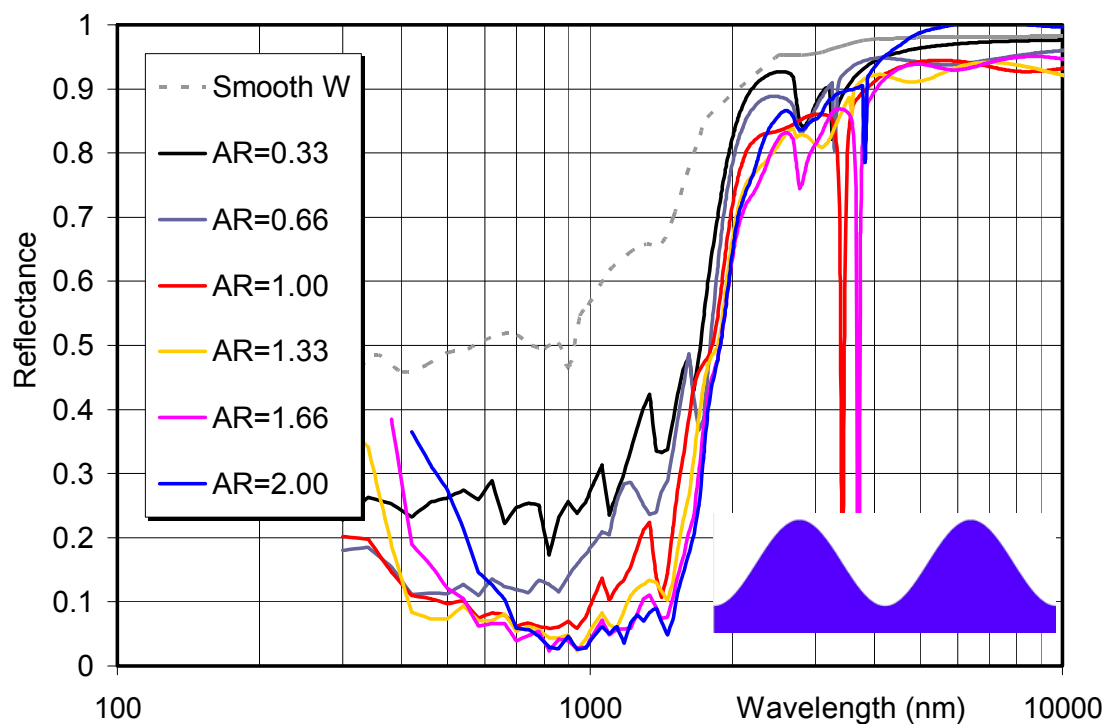


Fig. 4-12: Effect of structure aspect ratio on the total reflectance of TM polarized light by the structured tungsten with sinusoidal profile and structure period of 3000 nm

### 4.10 Conclusions

- Simple gradual refractive index models (triangle and spheroid) were able to simulate the interaction of light with the structured metal surfaces by ignoring the diffuse scattering. It was shown that in case of having deep structures and effective light trapping between the surface features, significant increase in solar absorption can be obtained.
- If scattering (diffuse reflection) could be ignored, then increasing the roughness aspect ratio could lead to significant reflectance-edge shift toward higher wavelengths, resulting gradual increase in refractive index and higher solar absorption. By considering the scattered light in the theoretical calculation (PCGrate simulation), similar shift of cut-off wavelength toward higher values was observed but not as much as what simple simulation predicted.
- Structure shape and structure aspect ratio both had large influence on the spectral selectivity of pure metals like copper and tungsten, which both have low thermal emittance. The higher the aspect ratio, the higher solar absorption is obtained.
- For both copper and tungsten, deep sinusoidal structure was the most effective surface profile that created the highest spectral selectivity. Optical property of lamellar structure was not sensitive to different aspect ratios and no significant increase in selectivity observed. Sinusoidal and triangular profiles both shown enhanced solar absorption at higher aspect ratios but in triangular structure the reflectivity of near-infrared wavelengths has been reduced as well. This would lead to a higher emittance value at higher profile's depth, in comparison with almost unchanged infrared reflectivity of the triangular model.
- Structured tungsten behaved differently in interaction with TM and TE polarized lights. Reflection of TE polarized light was more sensitive to aspect ratio of the sinusoidal structure than TM polarization. In addition, smooth reflectance curves obtained for TE polarization while few sharp absorption peaks were observed in reflectance curve of TM polarization. Such sharp absorption peaks in the reflectance curve maybe related to the resonance anomalies of TM polarization. Theses anomalies were excited and appeared only at deep structures.

### 5. Experimental setup

This chapter describes how the absorber samples were prepared and characterized. Samples prepared for increasing the spectral selectivity using the effect of surface structure and surface roughness are explained in one section. This section is divided to three sub-sections of A, B and C, which explain experimental procedure of sample preparation by sputtering, laser and embossing structuring techniques, respectively. Thereafter, wet chemical route developed for making Ni-Al<sub>2</sub>O<sub>3</sub> selective absorber out of powder suspension is explained. Finally, this chapter is completed with describing characterization method of selective absorbers.

#### 5.1 Substrate cleaning

In thin film deposition technology, proper cleaning of the substrate surface is an important issue. If a surface is contaminated with foreign substances like oil or grease, the adhesion of the film will be degraded and there will be a tendency for the coating material to be cracked or peeled off. It is also possible that the desired film properties are affected by the impurities on the surface of the substrate. In addition, In order to achieve a good vacuum in vacuum deposition techniques, it is imperative to clean thoroughly all surfaces that are exposed to vacuum.

In this study the glass or metallic substrates, which were used in different deposition or structuring processes were cleaned using the following procedure:

First, substrates were cleaned with a mixture of dishwashing liquid detergent and lukewarm water and rinsed in a bowl of water. Pure ethanol was then used to dissolve the rest of oil and fatty contaminations from the surface. A soft towel dipped in ethanol was then rubbed on the substrate surface to remove the residuals better by applying a mechanical force. Then samples rinsed with distilled water and dried with pressurized air. The extremely low surface tension of a solvent permits it to penetrate fine cracks or blind holes and dissolve organic oils and other contaminants. The solvents penetrating action as well as its chemical action clean the surface. Bulk copper, aluminum or stainless steel plates were pre-cleaned before solvent cleaning step by immersing into a diluted HCl to remove any oxide layer from their surfaces. Finally, ultrasonic cleaning was utilized to further cleaning the surface. In an ultrasonic bath, high-frequency sound cavitates a liquid medium. This cavitation forms small micro bubbles that burst on the surface of the metal being cleaned,

## 5. Experimental setup

---

providing mechanical action as well as the chemical cleaning action of the liquid medium.

### 5.2 Increasing the selectivity by surface texturing

#### 5.2.A Sample preparation - Sputter deposition

A planar sputtering system as shown in Fig. 5-1 was used in this work. The system could accommodate two targets (one Cu and the other  $\text{Al}_2\text{O}_3$ ), mounted on a horizontal upper plate in the vacuum chamber. The substrate holder could be rotated around the central axis of the system. Thus, the substrate could be placed under the desired target. A heater also was installed under the rotatable substrate holder, enabling increase of the substrate temperature up to 500 °C during deposition. The temperatures were obtained from voltages measurement by a mounted J (Iron-Constantan) thermocouple. The base substrate temperature as measured in the sputtering chamber was about 100 °C. The substrates were then heated to three different temperature levels between 100 and 400 °C. The targets were being cooled through a closed silicon oil cooling system, which was connected to a thermal heat exchanger and cold water.

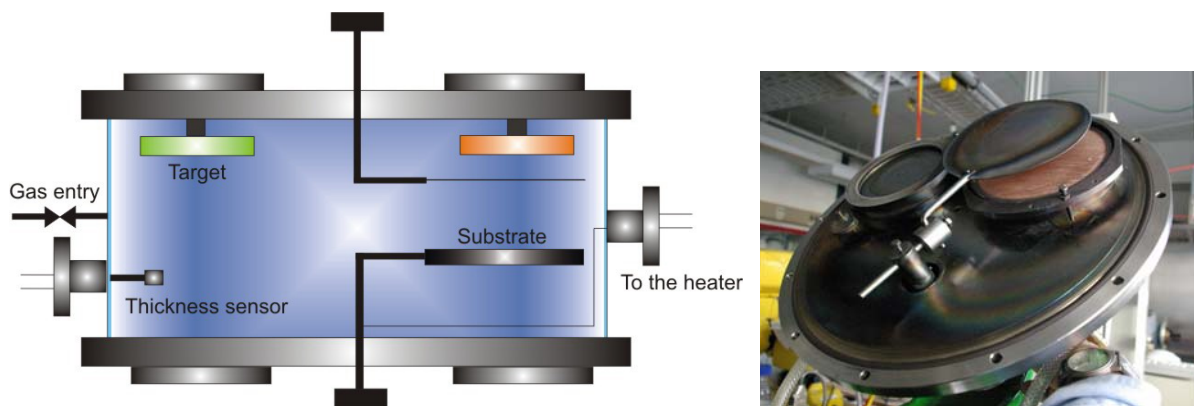


Fig. 5-1: Left: Schematic of the sputtering chamber; right: installed targets

For avoiding any contaminations during thin film deposition, all depositions were carried out after letting the chamber to reach to the vacuum of about  $1 \times 10^{-4}$  Pa. After introducing argon gas to the chamber, both materials were sputtered at a total pressure of about 7 Pa. The Cu films were deposited by a DC (Direct Current) power supply at 2.3 kV from a pure (99.999 %) copper target and  $\text{Al}_2\text{O}_3$  was deposited at 100 W RF (Radio Frequency) power directly from an  $\text{Al}_2\text{O}_3$  target (99.99 % purity).

## 5. Experimental setup

---

During the deposition, the thickness and deposition rates were monitored with a quartz crystal oscillator and a quartz crystal growth rate monitor model IL150 with thickness resolution of 0.1 nm. The thickness of the film was measured again after deposition by a surface profilometer Tencor P-10 (KLA Tencor, USA). According to the position of the thickness sensor in the chamber, the thickness monitor device had to be calibrated for each material to show the correct thickness. The real thicknesses measured by profilometer were used for calibration of thickness monitor.

### **Fabrication of the cermet layer**

An alternating deposition of very thin layers of  $\text{Al}_2\text{O}_3$  and Cu was used to obtain the composite layer of Cu- $\text{Al}_2\text{O}_3$ . In this method, the substrate is first located under ceramic target for a while to deposit a 3-5 nm thin film, and then substrate holder is turned to place the substrate under the metallic target until 3-5 nm metallic thin film is deposited. This procedure is repeated until the desired cermet thickness is reached. As shown in Fig. 5-2, this method offers independent control of the volume fraction and the size of the nano-particles. In this way, Cu particle sizes are limited by the nominal thickness of the thin layers.

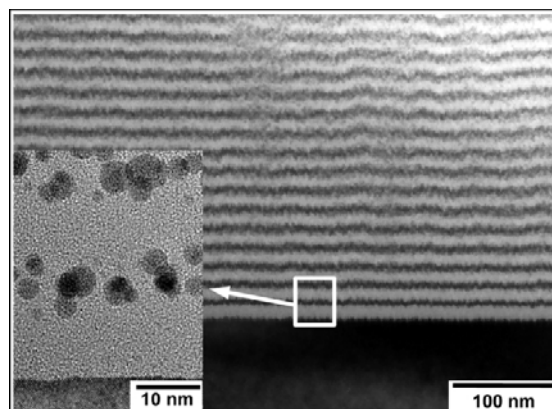


Fig. 5-2: TEM picture of an Au-SiO<sub>2</sub> nano-composite layer produced by alternating deposition of metal and ceramic thin films [100]

### **Substrate**

For low substrate temperatures, plain microscopic slides were used as substrate. These standard glass slides are 1" x 3" and 1 to 1.2 mm thick. For samples prepared at high substrate temperatures, borosilicate glasses were used. For measuring thickness of the deposited film using a profilometer, small cover glasses 0.13-0.17 mm thick were placed on the substrate to make sharp steps.

### 5.2.B Sample preparation - Direct laser structuring

A high power pulsed Nd:YAG laser (Quanta-Ray PRO 290, Spectra Physics) was used for the laser interference structuring. The primary wavelength of the Nd:YAG laser was 1064 nm from which shorter wavelengths (532, 355 and 266 nm) can be generated by means of frequency doubling (also called second-harmonic generation). The samples were irradiated with a wavelength of 355 nm. The repetition frequency of the laser was 10 Hz and the pulse duration 10 ns.

The experimental setup of direct laser structuring is shown in Fig. 5-3. A circularly polarized laser beam is splitted into two beams with a beam splitter. Both splitted rays will interfere on the sample surface. The material is just ablated at the interference maxima. A square-shape mask was used to obtain a final beam with dimensions of 1.5 x 1.5 mm<sup>2</sup>.

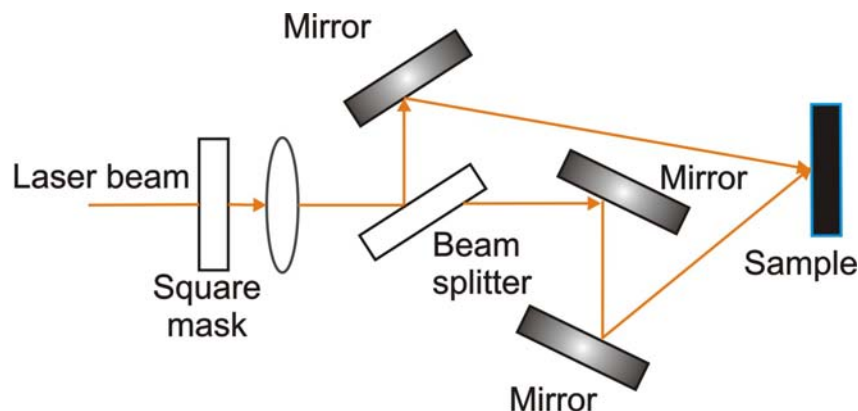


Fig. 5-3: Experimental set-up of laser beam and optical devices for a direct laser interference structuring system

Commercial copper and stainless steel foils 3 mm thick were used as samples for structuring. As the amount of laser light absorbed by a metal strongly depends on its surface morphology, thus, before structuring all samples were grinded and polished with diamond suspension. Whereby, the final stage of polishing was carried out using diamond particle size of 0.05  $\mu\text{m}$ .

20 x 20 mm<sup>2</sup> metallic samples were structured by using a sample positioning equipment (Kleindiek) and computer-controlled micro-positioning stages. For adjusting the energy level incident on the sample, a mechanical shutter (Uniblitz

## 5. Experimental setup

---

Electronic) was used to control the number of laser pulses hitting the sample. The energy of each partial beam was measured by using a power meter (Power Max® model PM30V1).

The grating period (or grating spacing) was varied by changing the intersecting angle of the beams; and different structure heights were obtained by varying the number of pulses utilized in each experiment.

The topography of the structures (period and structure height) was measured by using a white light interference (WLI) microscope model (Zygo- New View 5000) equipped with 3D Imaging Surface Structure Analyzer.

### **5.2.C Sample preparation - Embossing technique**

An e-beam structured metallic mold made by AMO GmbH was utilized to create a flexible rubber silicon stamp for replicating the surface patterns onto the substrate. Many master copies can also be made from this resulting negative mould. The master can be prepared and structured by holography or lithography methods using electron or laser beams.

The transparent silicone rubber material (Elastosil RT 604 from Wacker company) comes in two components A and B was used and the two components were mix by a volume ratio of 9(A):1(B). The master was enclosing in a retaining frame and the prepared silicon rubber was poured into the frame. After 30 minutes drying at 70 °C, the silicon stamp was detached from the master. Then the prepared sol was flooded on a glass substrate and silicon stamp was placed on it for 30 minutes at room temperature. After removing the silicon, the structured sol-gel layer was cured at 450 °C for 1 hour. The ramping and cooling time was around 4 hours. The silicone rubber mold and its polyurethane parts could replicate exactly the surface of the original master. After that, a tungsten layer with thickness of 100 to 200 nm was sputtered on this structured substrate.

Fig. 5-4 shows a schematic view of surface structuring using an imprint process. After applying the mould onto the resist, the mold is pressed, then the mold is removed and pattern is transferred onto the substrate. Moreover, the rubber silicon die copied from structured metallic master has been shown in this picture. This silicon mould was used in this study for transferring a given surface pattern onto the substrate.



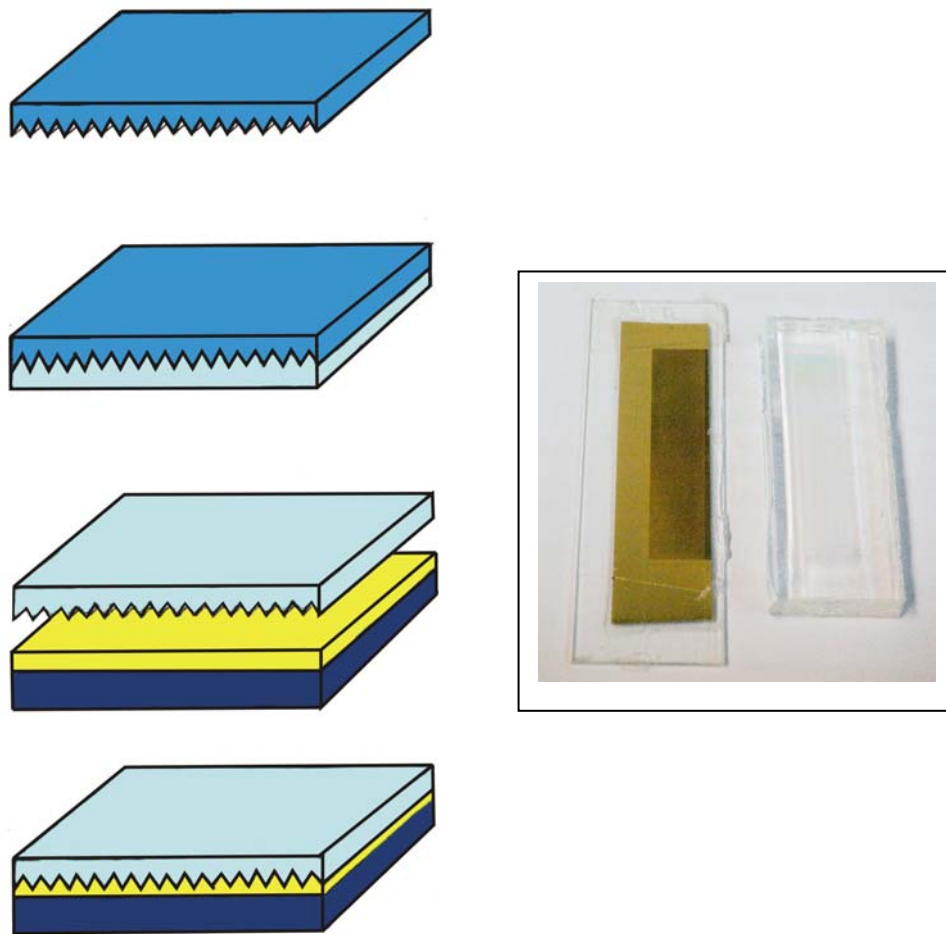
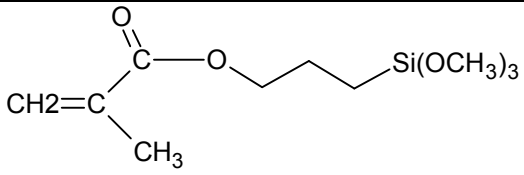
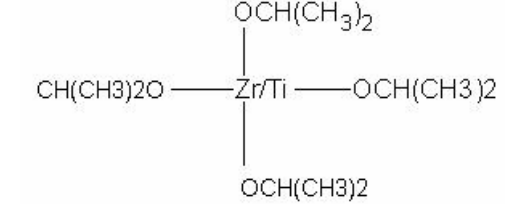
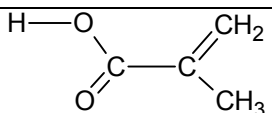


Fig. 5-4: Schematic view of imprint structuring process (left), Master and silicone rubber mold with replicated surface pattern (right)

### **MPTS/ZR/MA sol preparation for structuring by imprint technique**

Along of this study, special nano-composite sol prepared by Bruno Schäfer and developed in INM GmbH was used. This sol applied on a surface as an active medium for transferring the master structure onto a given substrate. This sol had high thixotropy and could keep the deformation shape after removing the mold and drying. The applied sol was prepared in a way that a dense, transparent and thermally stable gel layer to be obtained. Organic-inorganic nano-composite layer derived from the prepared nano-composite sol is synthesized from the following precursors:

## 5. Experimental setup

Methacryloxypropyltrimethoxysilan		MPTS
Zirconium or titanium-isopropylate		ZR
Methacrylic acid		MA

### ZR/MA sol

At room temperature, 8.59 g (0.1 mol) methacryl acid (MA) is added to 0.1 Mol. zirconium-n-propylate. The mixture is stirred at least for 30 minutes.

### Prehydrolyzed-MPTS

At room temperature, 23.01 g H<sub>2</sub>O and 4 g 0.1 n HCl are added to 248.11 g (1 Mol) MPTS. The mixture is stirred for 15 minutes. 30 minutes after complete reaction of HCl, under ice cooling the ZR/MA solution is added gradually. Finally, after 80 minutes 5.37 g H<sub>2</sub>O is added. The final mixture is stirred continuously for 4 hours to bind completely the zirconium component to silicate network by condensation reaction between alkoxide groups of zirconium and Si-OH groups. For thermally polymerization, 1 wt. %  $\alpha, \alpha'$  Azoisobutyronitril (AIBN) is added to the final solution. Before pouring the sol onto the substrate, it is stirred for 1 hour.

### Synthesis Summary

An organic-inorganic composite system based on MPTS and ZR was developed. MPTS was used for making an inorganic network. On this network an organic network is created through polymerization of methacrylgroup with MA.

### 5.3 Wet chemical deposition technique

#### 5.3.1 Physical properties of the used materials

**Al<sub>2</sub>O<sub>3</sub>:** High purity nano-powder of fumed Al<sub>2</sub>O<sub>3</sub> from Evonik Degussa, Germany (called AEROXIDE® or Alu C) produced by flame hydrolysis was used to prepare colloidal suspension of aluminum oxide. This powder consists of meta-stable gamma (γ, cubic spinel) and delta (δ, tetragonal) Al<sub>2</sub>O<sub>3</sub>. Other physical specifications of Alu C are as follows:

Al<sub>2</sub>O<sub>3</sub> content based on ignited material: > 99.8 %

95 % of particle sizes are smaller than 20 nm (TEM and X-ray)

Average primary particle size: 13 nm

Specific surface area: 100 ± 15 m<sup>2</sup>/g

Porousless surface

Tapped density: 50 g/l

Density γ structure: 3.67 g/cm<sup>3</sup>

Density δ Structure: 3.988 g/cm<sup>3</sup>

pH (in 4 % dispersion): 4.5-5.5

pH = 4 for well-dispersed suspension

pH =9 for flocculated Suspension:

#### **Nickel nitrate**

To have nano nickel crystalline embedded in an alumina matrix in the final cermet thin film, dispersion of metal ions in the suspension is preferred to the dispersion of solid metal particles because of disadvantages of nano metallic particles like high reactivity with the surrounded medium, oxidation and high tendency of agglomeration. Salts of metals, which have high solubility in water and alcohol systems, are more suitable sources for nickel ions in the suspension. One of the highly soluble salts of nickel is the nickel nitrate. When green clusters of this salt are dissolved in the water or alcohol, a clear green ionic solution full of nitrate and nickel ions is obtained. Nickel nitrate has physical properties as follows:

## 5. Experimental setup

---

Decomposition temperature: 200 °C

pH: 4 (aqueous solution)

Solubility: 238.5 g/100 cm<sup>3</sup> water at 20 °C

Nickel (II) nitrate-hexahydrate Ni (NO<sub>3</sub>)<sub>2</sub>·6H<sub>2</sub>O from Alfa Aesar

Color: green

Density: 2.05 g/cm<sup>3</sup>

Molar mass: 290,810 g/mol

Purity: 99.98 %

### 5.3.2 Suspension characterization

In this study for determining the particle size distributions of dispersed powders at different conditions, Mastersizer 2000 (Malvern) and Acoustosizer II (Colloidal Dynamics Inc.) were used. In addition to particle size measurements, Acoustosizer measured the Zeta potential of the suspension at different pH values .

Viscosity, pH and conductivity are three important parameters for characterizing a powder suspension. In this study, a rotational RheoStress 1 Rheometer of Thermo Haake GmbH was used for measuring shear stress as a function of shear rate. The slope of the obtained flow curves at corresponding shear rate is equal to the apparent viscosity at that rate. The conductivity of the suspensions was measured with a conductivity meter of the type LF340-A of WTW. The pH value of the suspension was determined with a pH meter of the type CG 843 with an electrode of the type Blue Line 12 (both from Schott Instrument).

### 5.3.3 Substrates

Thin films of Ni-Al<sub>2</sub>O<sub>3</sub> and SiO<sub>2</sub> anti-reflection layer were deposited on three different substrates as follows:

- Borosilicate glass (3 mm thick), cut manually in different sizes, was used for optimizing the rheology of the suspension and thickness measurement.
- Unpolished commercial copper plate cut in larger sizes and polished by 9, 6, 3, 1 μm diamond suspensions, respectively. Such fine polishing was done to eliminate the contribution of surface roughness of the substrate on the optical properties of the absorber.

## 5. Experimental setup

---

-Polished Aluminum plate 430 EN with 99.5 % purity (Alcan-Singen GmbH) and thickness of 0.5 mm cut into pieces with the size of 3 X 10 cm. Already polished aluminum substrates were very useful especially for conducting aging tests and other optical characterizations, because the quality and surface roughness of the substrates were the same for all the prepared samples.

### 5.3.4 Sample preparation

Depending on the desired nickel to  $\text{Al}_2\text{O}_3$  ratio, nickel nitrate was first dissolved in distilled water or ethanol; then under stirring, Alu C powder was added gradually. The prepared mixture was dispersed mechanically for 15 minutes with 60 % power (12000 rpm) using a dissolver of the type Dispermat® N1-SIP of VMA-Getzmann Company. In order to achieve an improved dispersion, suspensions were ultrasonicated with Branson Sonifier W 450 (Branson Scientific, Inc., Plainview, NY) for 4 minutes. Ultrasonic amplitude was adjusted on 50 % and applied every half a second. It means there was a pause for 0.5 second between each sonification pulses with duration of 0.5 second. This was done to avoid any temperature increase during ultrasonic treatment. Again, the ultrasonicated suspension was dispersed mechanically for 15 minutes to deagglomerate any agglomerations left in the suspension.

At all dispersing stages, the temperature was controlled and kept between 5 °C and 12 °C. Different additives like wetting agents (like BYK 348 for aqueous or BYK 341 non-aqueous coatings), coupling agents (like hydrolyzed TEOS) and dispersing agents were added to the suspension before dispersion, because adding any new modifier could change the electrostatic balance between the particle and could lead to new agglomerations. Suspensions were characterized by measuring pH, conductivity, zeta potential and viscosity measurements. Stability and sedimentation of the suspensions were controlled using ATR spectroscopy and by visual monitoring.

Fig. 5-5 shows the procedure, which was used for preparing Ni- $\text{Al}_2\text{O}_3$  cermet selective absorbers. After preparing *nickel nitrate-Alu C* suspensions, cleaned substrates were dipped into the coating suspension using a dip coater (see Fig. 5-6) and withdrawn at different speeds. The higher the speed, the thicker layer is obtained

## 5. Experimental setup

(see equation 3-6). The wet films were dried for 30 minutes at 120 °C and then quickly annealed for 1 hour at 450 °C in H<sub>2</sub> atmosphere.

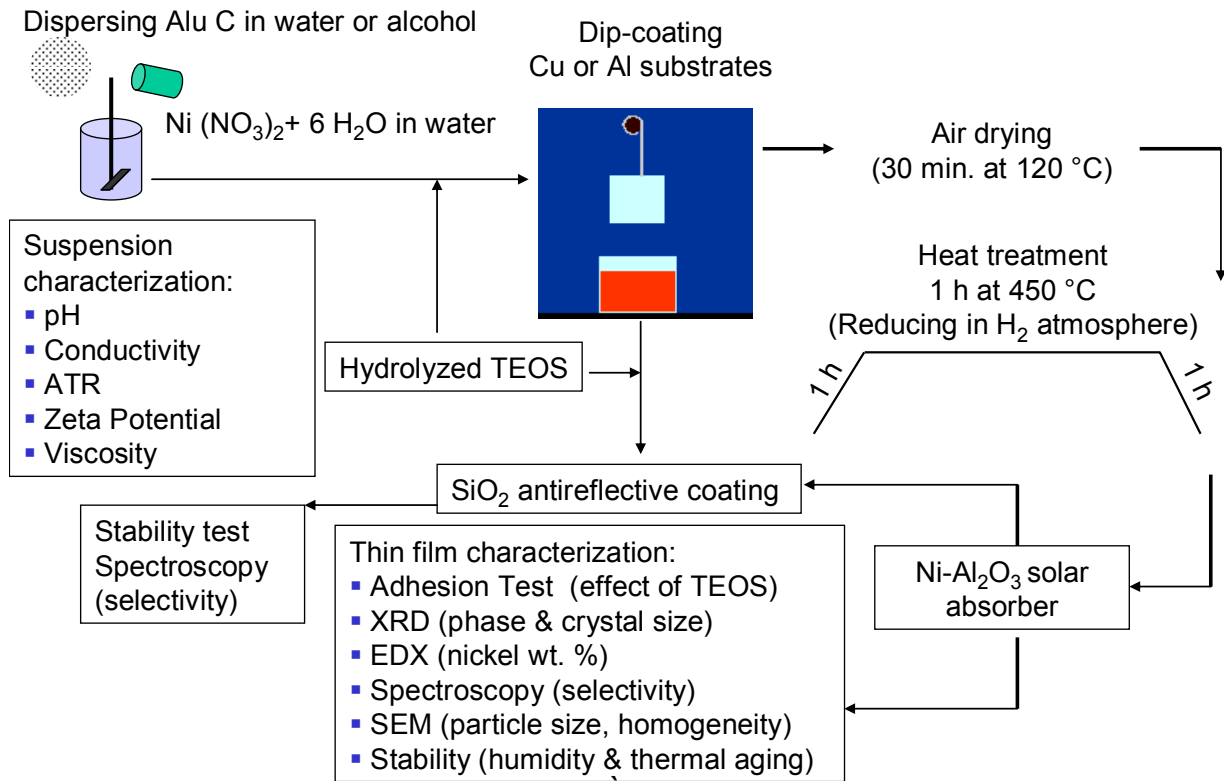


Fig. 5-5: Schematic diagram illustrating the different production and characterization stages of cermet nano-composite selective absorbers by wet chemical deposition technique

A one-meter long tube furnace consisting of a sealed transparent quartz glass, heating element and protective clamps (shown in Fig. 5-6) was used for annealing the deposited samples. A hydrogen generator CFH200 from Peak Scientific Instruments was used as hydrogen source. Generated hydrogen passed the furnace tube continuously so that, always fresh hydrogen was in contact with the sintering object. For safety reasons three hydrogen sensors placed along the tube furnace in different positions.

Different thin film characterizations like XRD, SEM and EDX were done on the prepared coatings. Spectral selectivity of the coatings was investigated using reflectance curves.

## 5. Experimental setup

---

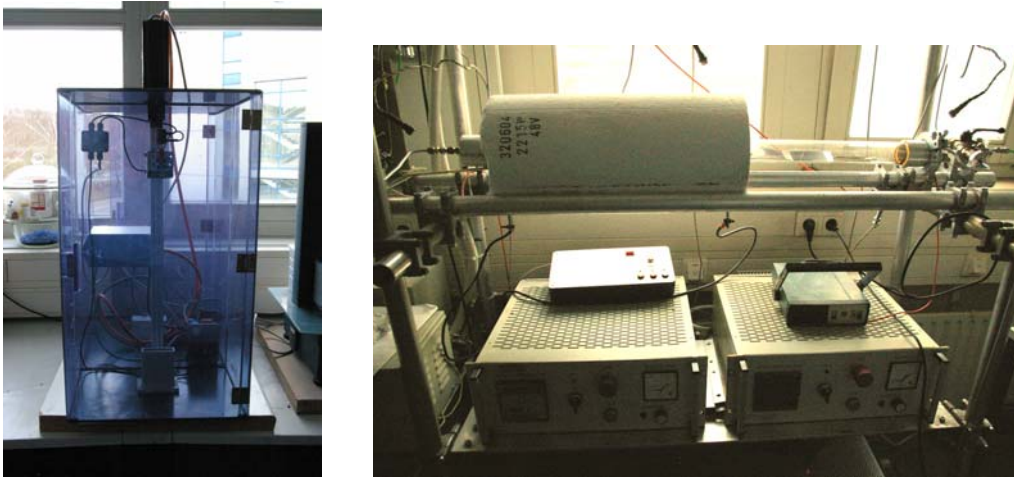


Fig. 5-6: Dip coater that was used for coating the substrates (Left), sealed tube furnace for annealing the cermet layers (right)

For improving the thin film adhesion, hydrolyzed TEOS was added to the suspension. The diluted TEOS sol was also used for deposition of  $\text{SiO}_2$  anti-reflection (protective) layer on the cermet coatings to protect the absorber layer against environmental degradations and increase the solar absorption. Finally, stability tests were performed to investigate the durability of the prepared absorber samples.

### 5.4 Characterization of the prepared samples

#### 5.4.1 Optical characterization

After making the samples, optical reflectance at each wavelengths of 0.3 to 3  $\mu\text{m}$  were measured using ultraviolet/visible/near infrared (UV-Vis-NIR Varian Carry 5E) spectrophotometer. Reflectance of wavelengths between 1.7 and 25  $\mu\text{m}$  was measured using a Fourier Transform Infrared (FTIR-Bruker IFS 66v) spectrophotometer. In UV-Vis-NIR spectrophotometer, the specular reflectance of the samples was measured using VW technique. The 'VW' absolute specular reflectance accessory (SRA) has been designed to measure absolute 'mirror-like' reflectance by a pair of matched mirrors to perform the calibration and measurement. This has the advantage that the same optical components are in the light path during both calibration and measurement and when a sample is mounted; the only change in the system is due to the reflectivity of the sample. Therefore, an absolute value of the

## 5. Experimental setup

---

reflectance is obtained. This technique of reflectance measurement is more robust and accurate than normal measuring methods.

Rough surfaces scatter light in all directions and have so-called diffuse reflectance. For structured samples or coatings with rough surfaces, the total reflectance (diffuse + specular) of the samples must be considered. In this study, measuring the total reflectance of structured or rough surfaces was done using DRA-900 (PMT) internal diffuse reflectance accessory and an integrated sphere coated with PTFE (Polytetrafluoroethylene). The same material (PTFE- Labsphere plate) has been used as reference. For rough samples only from total reflection, total solar absorptance is obtainable. Because the utilized FT-IR spectrophotometer was not equipped with gold integrated sphere for measuring the total hemispherical emittance, only normal emittance values were considered. Using selectivity calculator, solar absorptance and thermal emittance values were calculated from the measured reflectance. The calculation procedure was described in chapter 4.

### 5.4.2 Non-optical characterization

#### **X-Ray Diffraction (XRD)**

The X-ray diffraction (XRD) is a useful tool for investigating phase and structural properties of materials from studying the interaction of monochromatic X-rays with a periodic crystal lattice. X-ray diffraction measurements are made by causing a beam of X-radiation to fall onto a sample surface and measuring the angles at which the specific characteristic X-ray wavelength is diffracted. In this study D-500, BRUKER AXS X-ray diffractometer was employed to characterize the phase and crystal size of the absorber samples. For the analysis a monochromatized Cu  $K_{\alpha}$  -1 line with a wavelength of 154.05 pm was used. Crystal sizes were determined by TOPAS V3 software (BRUKER AXS), which uses Double-Voigt approach for calculation the crystallite size broadening.

#### **Scanning Electron Microscopy (SEM)**

The interaction of well-focused electron beam and the matter gives the emission of X-rays, auger electrons, backscattered as well as secondary electrons. In SEM, the most important signals are the secondary electrons, which have low energy and the



## 5. Experimental setup

---

reflected (backscattered) electrons. Both give information about sample topography. Using appropriate detectors, the signals from the surface of the sample can be detected and then focused on a screen using cathode ray tube (CRT) to reproduce the image. In general, SEM requires a conducting sample in a low vacuum chamber but for non-conducting samples a very thin gold film is applied to reduce charging effects. In this study a high-resolution scanning electron microscope (HR-SEM) JSM-6400F (Jeol, Tokyo, Japan) was used for particle size, surface and microstructure studies. To avoid electrostatic charge, the samples were previously sputtered with 5 nm gold layer before putting them in the SEM chamber.

### **Energy Dispersive X-ray spectroscopy (EDX)**

EDX or EDS is a method used to determine the energy spectrum of X-ray radiation using a semiconductor detector. SEMs often have a microprobe for energy dispersive analysis by studying the characteristic X-ray lines for rapid evaluation of elemental constituents. The same SEM system was used for EDX analysis.

### **Surface roughness analysis by Atomic Force Microscopy (AFM)**

As in this study the surface roughness has an important contribution in increasing the selectivity, therefore it should be analyzed properly. AFM is a technique for studying the surface morphology. The system operates by scanning a tip across the sample surface while monitoring the change in cantilever deflection with a split photodiode detector. A feedback loop maintains a constant deflection between the cantilever and the sample by vertical moving the scanner at each (x,y) data point to maintain a “set point” deflection. The distance the scanner moves vertically at each (x,y) data point is stored by computer to form the topographic image of the sample surface. Digital Instrument Dimension 3000 AFM with a resolution of 10 pm in accompany with Nanoscope software used for recording the surface topography and analyzing the recorded image.

### **White light Interferometer (WLI)**

White Light Interferometry (WLI) is a powerful technique for non-contact measurement of surface topography and for measuring height, depth and other roughness parameters of a textured surface. A 3D image of the surface is computed

## 5. Experimental setup

---

by frequency domain analysis, allowing a maximal vertical resolution of 0.1 nm when keeping a lateral resolution between 0.64 nm and few mm depending on the magnification of the used lens. Along of this study a Zygo-New View 5000 interferometer was used. This tool has been equipped with MetroPro™ software for data analysis and profile demonstration in three dimensions.

### 5.5 Durability test procedure

For thermal stability test, a normal static oven with high accuracy and temperature uniformity was used. A climate chamber PR-15 (Thermo TEC GmbHEY-101) with a temperature range of 0-70 °C and maximum humidity of 100 % was used for humidity test. The durability test was carried out only for solar absorber prepared by wet-chemical method. Table 5-1 shows duration, temperature and humidity conditions, which were applied in this study for thermal, and humidity aging tests.

Table 5-1: Adjustments for Thermal and humidity aging test

	Temperature	Humidity	Period
Non-condensing high humidity test	60 °C	60 %	144 h
Thermal test	300 °C	--	200 h

## 6. Results and discussion

### 6A. Effect of surface roughening on spectral selectivity of Cu-Al<sub>2</sub>O<sub>3</sub>

#### 6A.1 Numerical calculations and cermet structure optimization

As mentioned in the state of the art, the graded cermet is more efficient than non-graded single cermet. Moreover double cermet structure shows better selectivity and is simpler than graded structure. Here, the effect of additional cermet and anti-reflection layers on improving the selectivity is investigated. For doing that different structures are defined in the simulation program and the GRG-2 optimization is run for each of them. For comparison, the resulted optimum volume fraction and layer thicknesses are plotted in one graph. For calculation refractive indices of Cu-Al<sub>2</sub>O<sub>3</sub> cermet layers, bulk refractive indices of Cu and Al<sub>2</sub>O<sub>3</sub> from handbook of optical constants [101] and Bruggeman model were used. Fig. 6-1 shows the optimized thickness and volume fractions for single, double, triple and quintuple cermets and graded cermet structures.

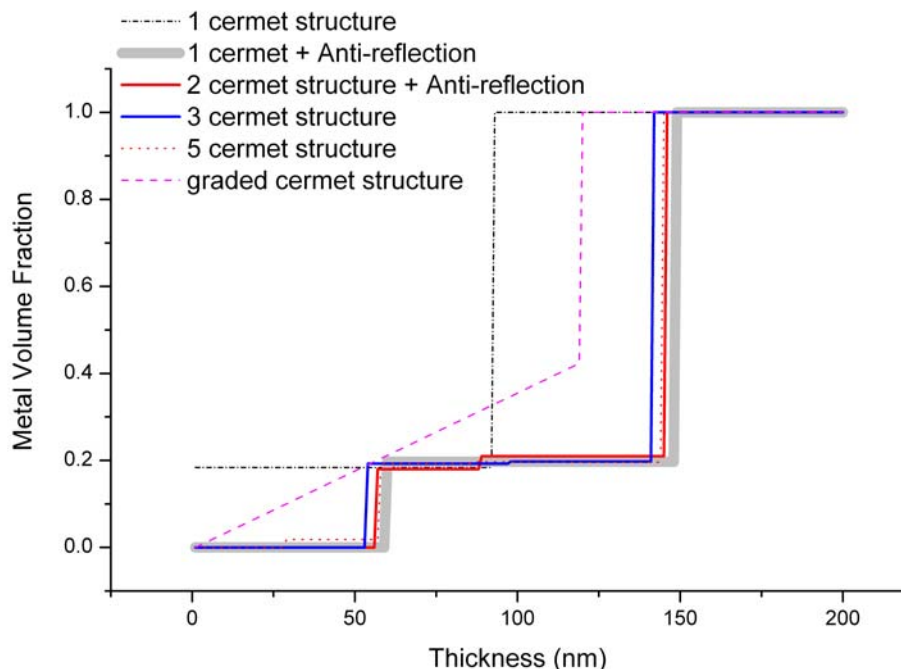


Fig. 6-1: Optimized thickness and metal volume fraction for the different cermet structures considered

## 6. Results and discussion

---

The calculated solar absorptance and thermal emittance values, listed in Table 6-1, show that increasing the number of cermet layers will not improve the spectral selectivity.

According to Fig. 6-1, the optimum volume fractions and thicknesses of different considered structures are equal to thickness and metal content of a single cermet structure, which is equipped with a 58 nm anti-reflection layer of  $\text{Al}_2\text{O}_3$ . The graded structure also shows slightly better optical properties than the simple single cermet structure without any anti-reflection layer.

Table 6-1: Solar absorptance ( $\alpha$ ) and thermal emittance ( $\varepsilon$ ) calculated for different cermet structures

	1 cermet	1 cermet + anti-ref.	2 cermet + anti-ref.	3 cermet	5 cermet	graded
$\alpha$	0.88	0.96	0.96	0.96	0.96	0.93
$\varepsilon (RT)$	0.02	0.02	0.02	0.02	0.02	0.02

From these predicted optical results, it can be concluded that a single cermet structure including an anti-reflection layer is the most efficient and simplest model among those studied, especially for Cu and  $\text{Al}_2\text{O}_3$ . The proposed optimum thickness and metal volume fractions are:

59 nm  $\text{Al}_2\text{O}_3$  (anti-reflection) / 89 nm Cu- $\text{Al}_2\text{O}_3$  cermet (metal content = 19.7 %) / Cu (IR- reflector)

As this optimum configuration has low thickness and the experiment conditions do not give sufficient time for reaching the desired roughness, the following layer parameters were chosen:

39 nm  $\text{Al}_2\text{O}_3$  (anti-reflection) / 48 nm Cu- $\text{Al}_2\text{O}_3$  cermet (metal content = 14 %) / 102 nm Cu- $\text{Al}_2\text{O}_3$  (metal content = 43 %) / Cu (IR-reflector)

In this choice, we sacrificed some of the emittance but sufficient time and thickness for creating the desired roughness will be given to the layers. It is important to note

that the optical properties, which were theoretically calculated here, can differ from experimentally measured ones because in practice the porosity of thin films changes the actual metal volume fraction. Furthermore, the size, shape and direction of embedded metal particles play an important role in the modification of cermet refractive indices.

### 6A.2 Effect of substrate heating on selectivity of double cermet structure

Figure 6-2 shows the measured and simulated reflectance curves of Cu-Al<sub>2</sub>O<sub>3</sub> absorbers which were prepared at different substrate temperatures of 176 °C (low temperature, LT), 236 °C (medium temperature, MT) and 320 °C (high temperature, HT).

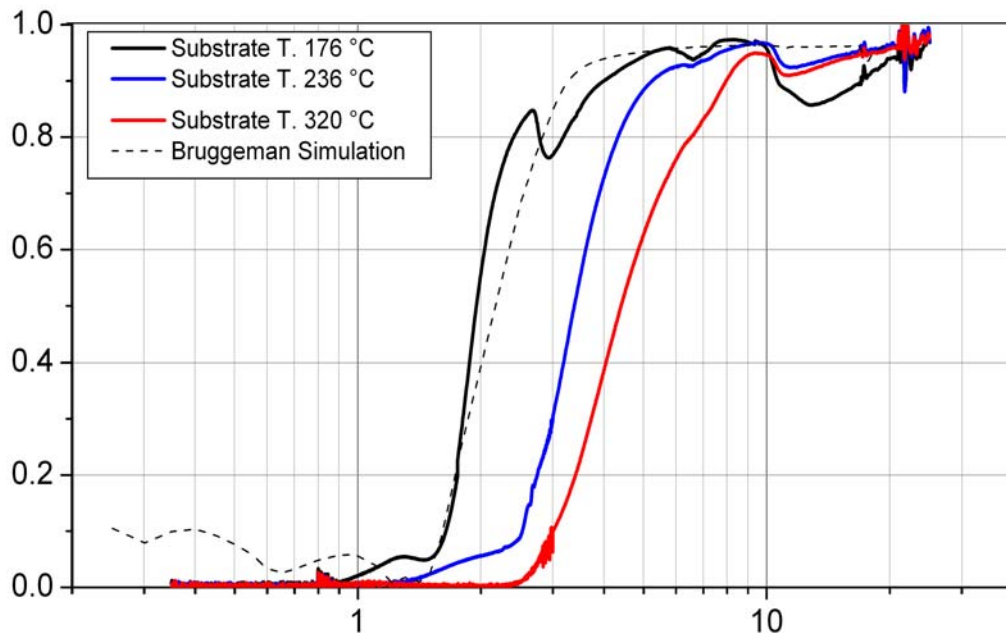


Fig. 6-2: Specular reflectance curves of double cermet structure of Cu-Al<sub>2</sub>O<sub>3</sub> solar selective absorbers prepared at 3 different temperatures

Small deviations between simulated and experimental curves arise from the difference between bulk and thin film refractive indices of the materials and from errors in the thickness measurement during deposition. From Table 6-2, it is obvious that increasing the substrate temperature during the film deposition can strongly improve the solar absorptance values, which were calculated from total reflectance data. The advantage is that the change in the emittance value is not significant while the absorptance increases to 0.96.

## 6. Results and discussion

Table 6-2: Solar absorptance ( $\alpha$ ) and thermal emittance ( $\varepsilon$ ) for the double cermet solar absorbers deposited at substrate temperatures of 176 °C, 236 °C and 320 °C

	Bruggeman approximation	Sample prepared at 176 °C (LT)	Sample prepared at 236 °C (MT)	Sample prepared at 320 °C (HT)
$\alpha$	0.94	0.90	0.95	0.96
$\varepsilon(100^\circ\text{C})$	0.04	0.083	0.05	0.08

Higher emittance values come from inaccuracy in film thicknesses and the high total thickness of the anti-reflection and absorber layers. Another interesting effect, which resulted from heating the substrate, is the shift of reflectance edge to longer wavelengths thereby increasing the solar absorptance. Such effect enables the designer of the selective absorber to adjust the cut-off wavelength to the desired wavelength by changing the substrate temperature. Such effect also observed by heating the substrate during deposition of SnO<sub>2</sub> layer which sprayed pyrolytically on anodized Ni-Al<sub>2</sub>O<sub>3</sub> [102].

### 6A.3 Structure characterization of the prepared samples

In Fig. 6-3, the cross-section and surface SEM view of these LT, MT and HT Cu-Al<sub>2</sub>O<sub>3</sub> samples are shown. As can be seen, continuous growth occurred at the lower temperature with particle sizes in the region of 50 nm, but at the higher temperature, the particle size is about 10 times larger. In addition, in medium and high temperature deposition, the cermet particles have a columnar structure and they have not grown in the same way as the metal particles of the IR-reflector layer. Their surfaces also look rougher, with many grooves. At 320 °C growth of copper and cermet are completely different and copper particles made a dense layer on the glass substrate. It can be resulted from a reduced rate of deposition at higher temperatures

XRD analysis was used for phase and crystal size investigation. Using a diffractometer the diffraction patterns of 150-200 nm Cu-Al<sub>2</sub>O<sub>3</sub> cermets deposited on glass substrate at different temperatures, were recorded. As shown in Fig. 6-4, the Cu in the matrix of dielectric and the IR-reflector have a crystalline phase. In addition, Al<sub>2</sub>O<sub>3</sub> is deposited amorphously and shows no crystal diffraction peaks.

## 6. Results and discussion

---

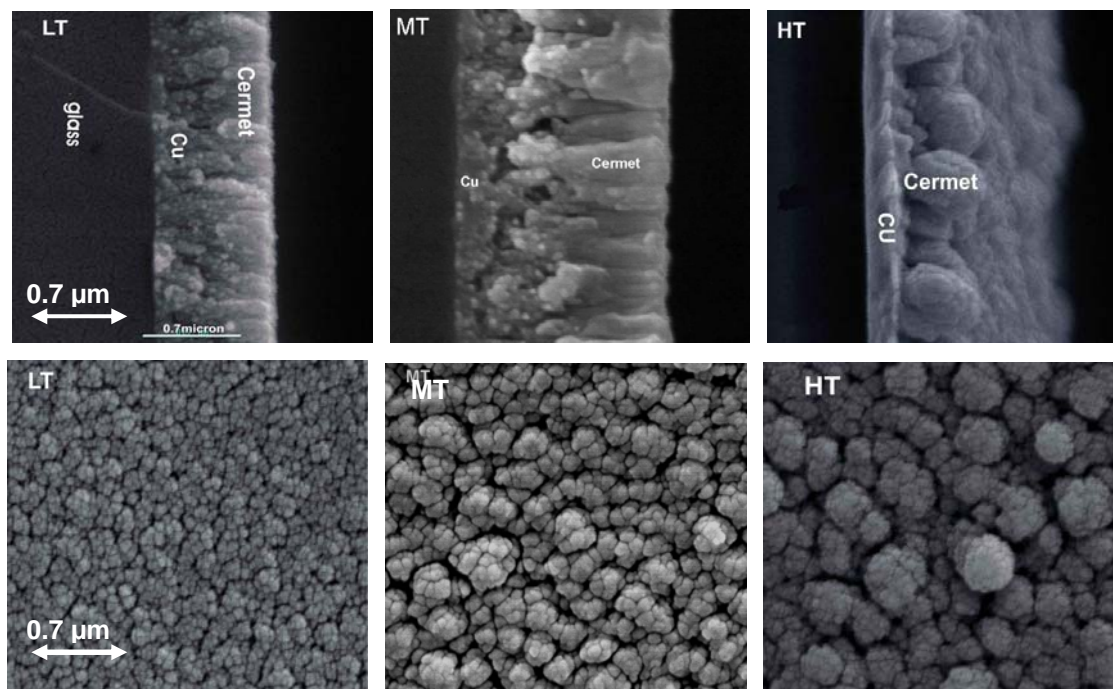


Fig. 6-3: Cross-section and surface view of LT, MT and HT Cu–Al<sub>2</sub>O<sub>3</sub> solar absorbers, fabricated at 176 °C, 236 °C and 320 °C substrate temperatures

Similar structures (crystalline phase of metallic part and amorphous phase of sputtered ceramic part) reported in [52] for sputtered cermet thin films. In Table 6-3 positions of diffraction peak of copper powder have been listed which are in good agreement with our measured peaks at double Bragg-angles.

The crystal sizes of Cu in the composite were calculated using different fitting functions and were about 5 nm for LT sample and 7 nm for HT. Therefore, no significant crystal growth occurred in the copper at higher temperatures. At high temperature (HT sample), a weak diffraction peak is observed around 67°. It should be noted that no Cu<sub>2</sub>O or CuO peaks correlated with this observed diffraction peaks. The samples prepared at substrate temperatures higher than 400 °C were not suitable for use as selective absorbers. At such high deposition temperatures, stress inside the film causes small cracks in the as-deposited samples. One explanation for these cracks may come from the formation of Cu<sub>2</sub>O. The formation of Cu<sub>2</sub>O islands induces tensile stress in the Cu film due to the large lattice mismatch. The difference between the thermal expansion coefficient of Cu and that of the glass substrate is another cause of stress in deposited films at high substrate temperature.

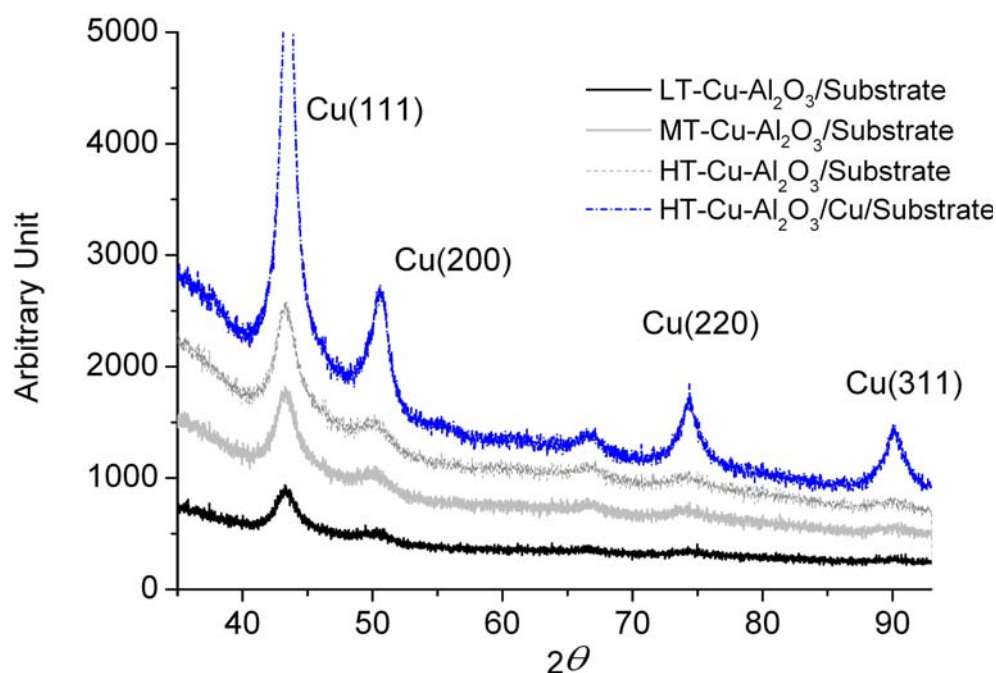


Fig. 6-4: XRD analysis of HT, MT and LT samples

Table 6-3: Diffraction peak positions of copper powder

Lattice parameter (d)	$I/I_1$ (normalised intensity)	hkl (miller indices)	$2\theta$
2.088	100	111	43.29
1.808	46	200	50.43
1.278	20	220	74.13
1.090	17	311	89.93

Zhou and Yang have shown that, with oxygen in the chamber, no oxidation takes place until 150 °C for Cu thin [103]. Also, the most likely oxide at higher temperatures in air or in oxygen during deposition will be  $\text{Cu}_2\text{O}$  [104].  $\text{Cu}_2\text{O}$  thin film has high optical transmittance of about 40-75 % for the wavelengths between 500-700 nm [105]. The existence of this oxide would lead to poor absorption in this range of wavelengths, which is not seen in reflectance spectrum of the samples. In addition, the existence of copper oxides could have caused high absorptions at wavelengths of 16.260, 20.833, 18.903  $\mu\text{m}$  [106] which are not observed in FTIR spectrums illustrated in Fig. 6-2 and 6-9. EDX and XRD analysis of the samples showed also no oxidation of the deposited copper thin films prepared at substrate temperatures up to 320 °C in the presence of argon gas.



## 6. Results and discussion

---

The Argon gas, which was used during the sputtering, had purity of 4.6 (99.996 %) and the sputtering chamber had a base vacuum of about  $1 \times 10^{-4}$  Pa. Therefore, the partial pressure of oxygen in the chamber could not be so high to cause any oxidation during the deposition of thin films for temperatures less than 400 °C. In addition, heating the substrate helps to remove any small amount of water vapor, which normally exists in the chamber.

AFM surface analysis was carried out to see how high-temperature deposition results in better optical properties. Fig. 6-5 shows micro-scanning of the surface and its related section analysis.

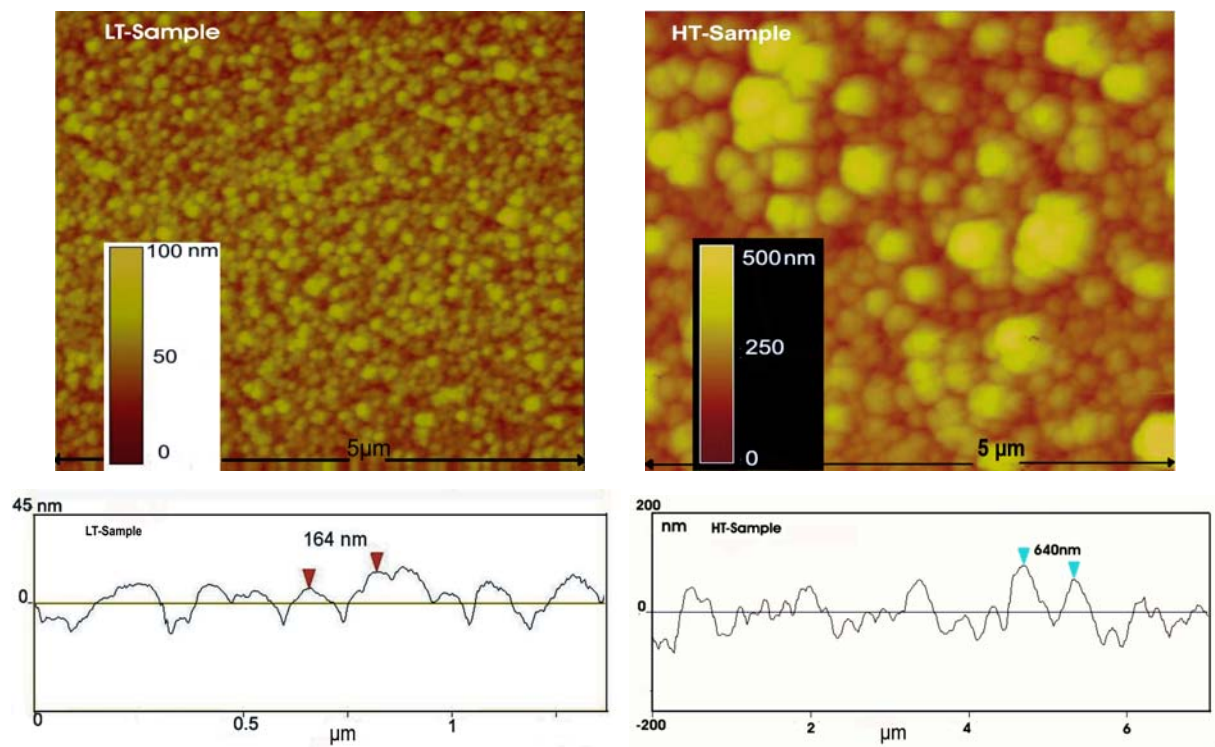


Fig. 6-5: AFM image and cross section profile of the surface roughness of LT (left) and HT (right) samples

For the high-temperature deposited sample, the size of the peaks is in the region of 640 nm, but for the lower temperature prepared sample, it is about 164 nm. Therefore, the high-temperature prepared sample can better absorb the higher-energy wavelengths of the solar spectrum by multiple reflections inside of the grooves.

The optical properties and surface morphology analyses showed that heating the substrate greatly helped in forming the desired roughness and reasonably increased the absorptance values. The obtained emittance values are a little bit high. It is due to high thicknesses, which were selected for the cermet layers. The double cermet structure, in conjunction with an anti-reflection layer needs very careful thickness control, which is not desired in mass-production. Instead of fine selection and controlling of thicknesses, an equivalent structure of a single cermet with anti-reflection, i.e. a single cermet with an effective rough interface, is proposed. In the next section, this structure will be studied.

### 6A.4 Role of roughness template layer - single cermet structure

For better adhesion of the IR-reflector layer to the substrate and avoiding any diffusion from substrate to multilayer, an  $\text{Al}_2\text{O}_3$  coating about 200 nm thick, as shown in Fig. 6-6, was deposited on the substrate first. Such a layer in conjunction with a thicker copper reflector layer helps the formation of roughness with a larger aspect ratio, and therefore increases the selectivity of the absorber.

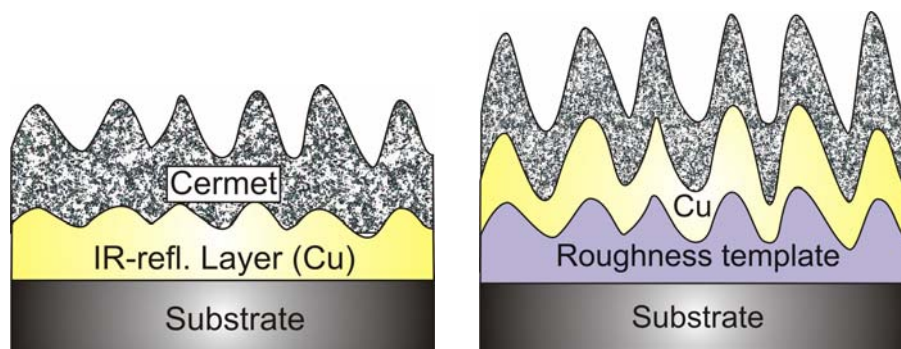


Fig. 6-6: Single cermet structure but with random roughness (left), single cermet structure with larger roughness aspect ratio using roughness template layer (right)

### Optimum thickness and metal volume fraction - single cermet structure

The optical properties of a single cermet solar absorber deposited on copper substrate or thick copper-deposited substrates are easily obtained from simulation and selectivity calculator programs, which were described in chapter 4. To use efficiently the selectivity of a single cermet layer, its metal volume fraction and thickness must be optimized.

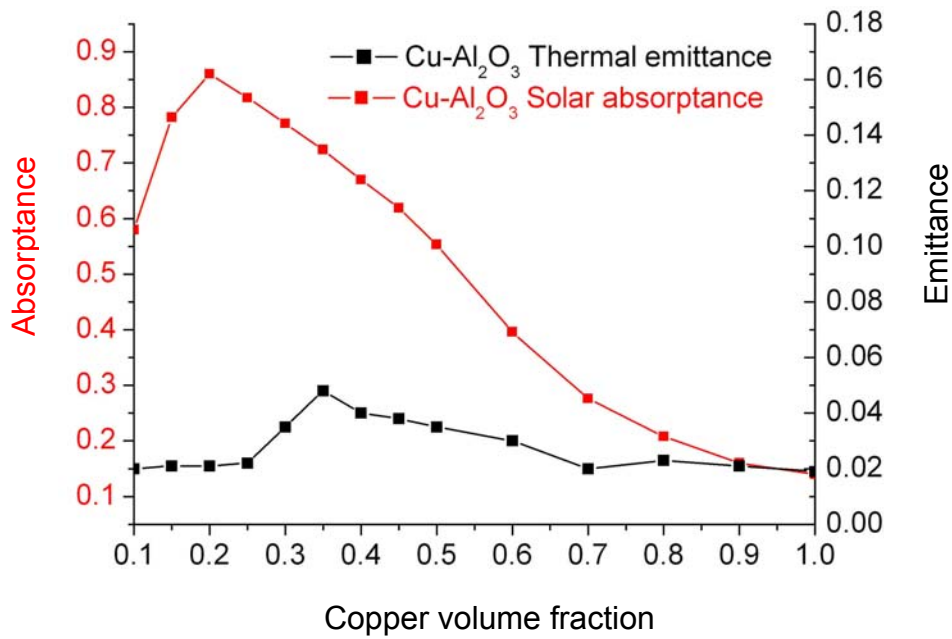


Fig. 6-7: Solar absorptance and thermal emittance at various metal volume fractions of a Cu-Al<sub>2</sub>O<sub>3</sub> cermet layer with a thickness of 100 nm.

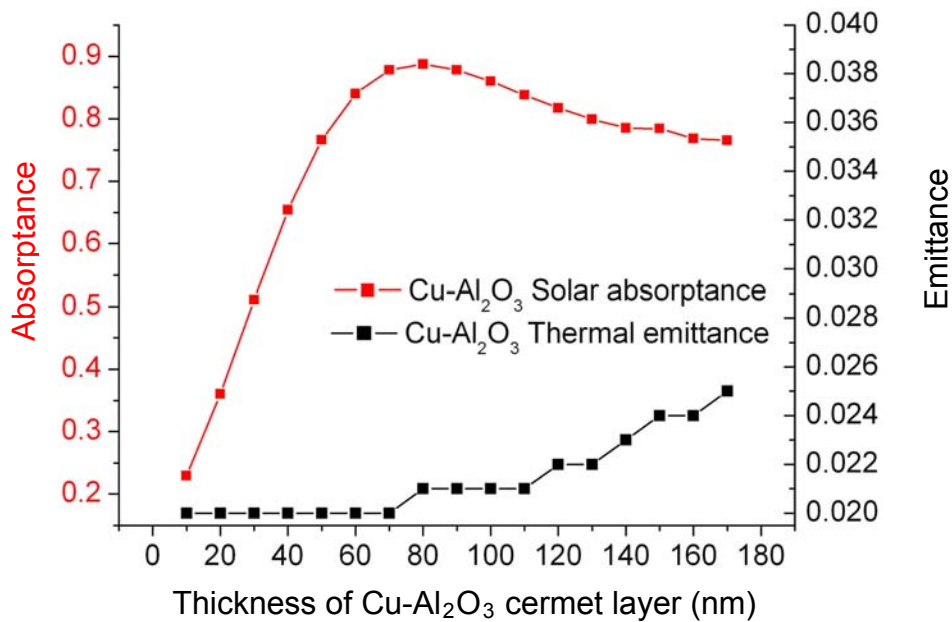


Fig. 6-8: Solar absorptance and thermal emittance at various thicknesses of a Cu-Al<sub>2</sub>O<sub>3</sub> cermet absorber with metal volume fraction valuation of 0.2

To find the optimum copper volume fraction, which leads to the highest solar absorptance and lowest thermal emittance, a Cu-Al<sub>2</sub>O<sub>3</sub> cermet layer with a thickness of 100 nm is considered and the effect of different metal filling factors is examined. Resulted absorptance and emittance values shown in Fig. 6-7 propose an optimum volume fraction of around 0.2 for copper. Similar study was done for evaluation of

optimum thickness for a cermet with metal volume fraction of 0.2. From Fig. 6-8 the optimum thickness would be around 80-90 nm.

Using non-linear GRG optimization program an optimum cermet thickness of 92 nm and optimum volume fraction of 0.2 were obtained for such single cermet structure which are in good agreement with the optimum values obtained above.

### **Effect of substrate temperature**

Different samples with single cermet structure were prepared at different substrate temperatures. According to the optimum thickness and metal volume fraction obtained in the previous section, the following thin film setup was considered:

92 nm Cu-Al<sub>2</sub>O<sub>3</sub> Cermet (metal content = 20 %) / 400nm Cu (IR-reflector) / 200 nm Al<sub>2</sub>O<sub>3</sub> (Roughness template) / Substrate

A 200 nm thick Al<sub>2</sub>O<sub>3</sub> layer was deposited between the substrate and IR-reflector layer. To obtain surface roughness with higher aspect ratio compared to the previous samples, thicker copper layer was deposited. Fig. 6-9 shows the effect of substrate temperature and roughness template layer on specular and total reflectance curves of a single cermet structure. No interference peaks are observable in the solar spectrum. Moreover, zero reflection at 550 nm where the highest power of solar radiation is located, led to a high solar absorptivity. Very sharp transition from low reflectivity region to high reflectivity is very close to that of an ideal selective absorber. It is even impossible to achieve so sharp transition by using a highly graded cermet layer because any graded selective surface with a solar absorptance high enough to be a useful absorber must also have a relatively large emittance, particularly at high temperatures. The reflectance edge between low solar reflectance and high thermal infrared reflectance for graded films is not sharp enough, causing the emittance to increase steeply with temperature [69].

Measuring the total reflection of the absorbers at wavelengths higher than 2500 nm due to the lack of a gold integrating sphere in FTIR spectrophotometer was not possible. As the difference between specular and total reflectance in solar spectrum is not too much and periodicities of the induced roughness features are only few

## 6. Results and discussion

microns, therefore with a good approximation the total hemispherical emittance value would be very close to the normal emittance value.

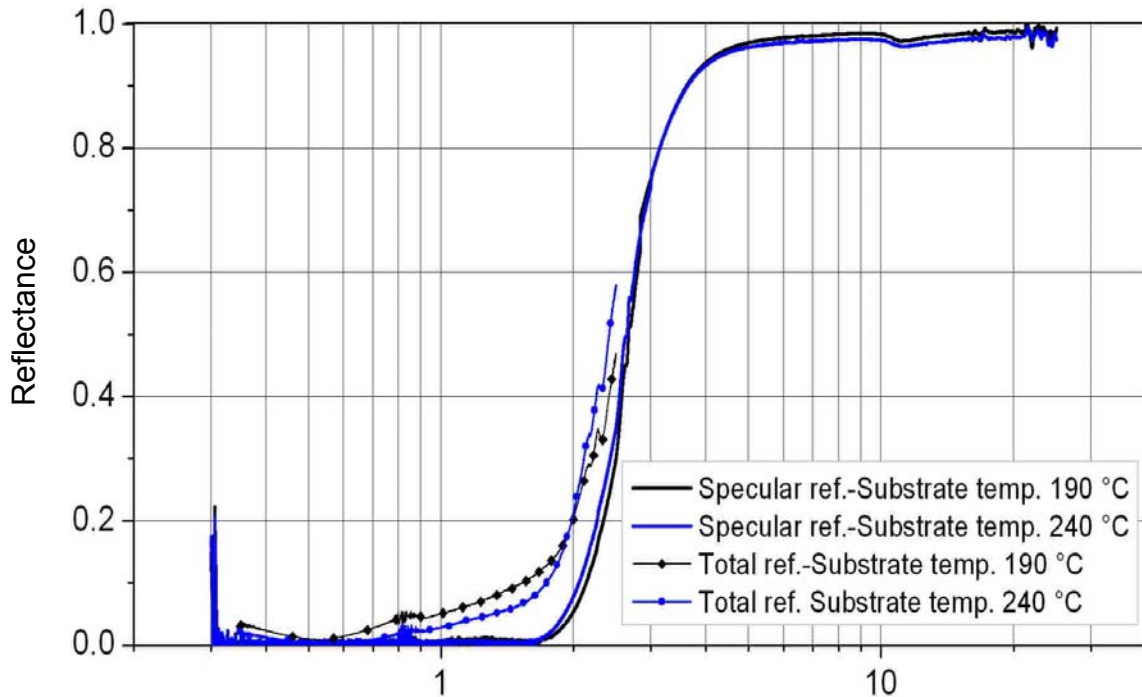


Fig. 6-9: Specular and total reflectance curves of single Cu–Al<sub>2</sub>O<sub>3</sub> cermet structure equipped with roughness template layer and prepared at 190 °C and 240 °C substrate temperatures

The developed structure is simpler than the double cermet structure and led to the highest absorptance and lowest possible emittance. In Table 6-4, the measured solar absorptance and thermal emittance values of the developed single cermet absorbers with and without rough template layer have been listed. Emittance values have been presented for two working temperatures of 100 °C and 200 °C.

Table 6-4: Solar absorptance ( $\alpha$ ) and thermal emittance ( $\varepsilon$ ) of single cermet absorbers with and without roughness template layer and in different substrate temperatures

	Unheated substrate without template layer	Substrate temp. 190 °C with template layer	Substrate temp. 240 °C with template layer
$\alpha$	0.840	0.942	0.956
$\varepsilon$ (100 °C)	0.019	0.019	0.028
$\varepsilon$ (200 °C)	0.026	0.026	0.034

## 6. Results and discussion

---

For investigation the effect of substrate temperature on surface morphology of the deposited sample, AFM scans of three samples with the new structure, deposited at temperatures 120 °C, 190 °C and 240 °C, were recorded and are shown in Fig. 6-10. Their related roughness height distributions illustrated in Fig 6-11. It is obvious that the higher substrate temperature increased the roughness aspect ratio and led to higher selectivity.

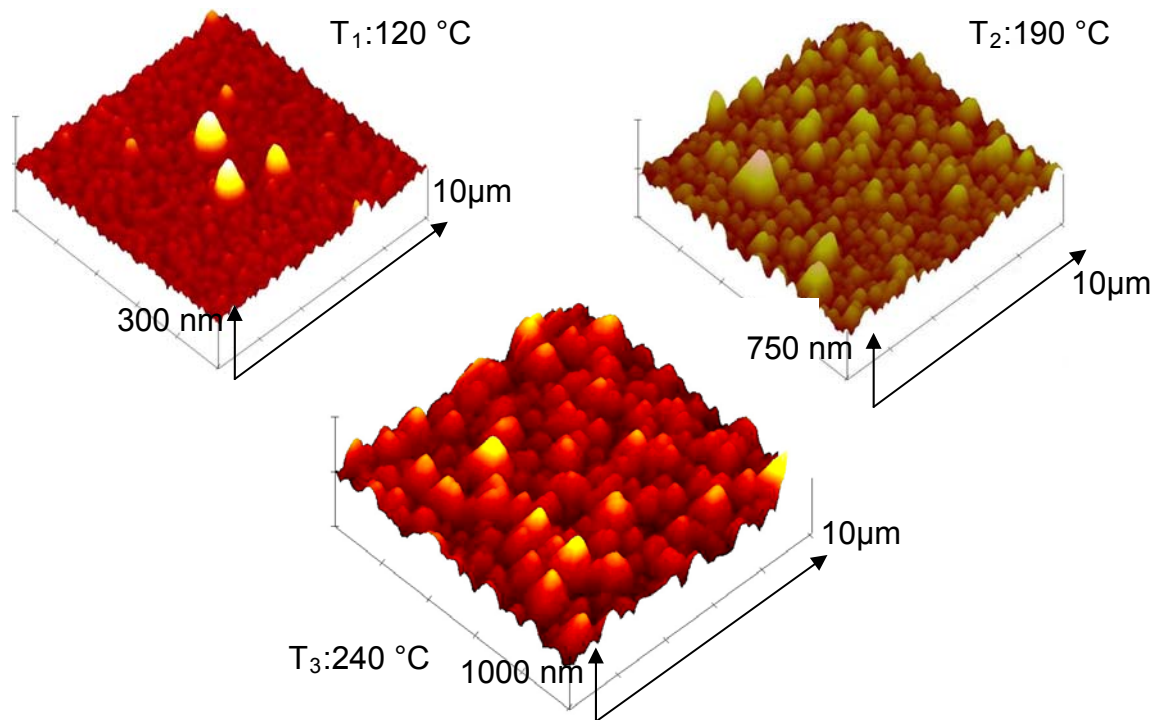


Fig. 6-10: AFM surface scanning of samples prepared at 120 °C (without template layer), 190 °C and 240 °C substrate temperatures

The distribution of relative frequency of the roughness heights along the surface normal (Fig. 6-11) shows that deposition at higher substrate temperatures increased the roughness heights. Moreover, the size of roughness heights of the sample prepared at 240 °C ranges from 100 to 600 nm. Compared to the sample prepared at 120 °C with average roughness height of about 70 nm, this sample has the possibility to trap more effectively the incoming light at higher wavelengths. For example the reflectance curve for the sample prepared at 240 °C shows zero reflection for the fraction of solar spectrum which has the highest solar power (from 400-600 nm).

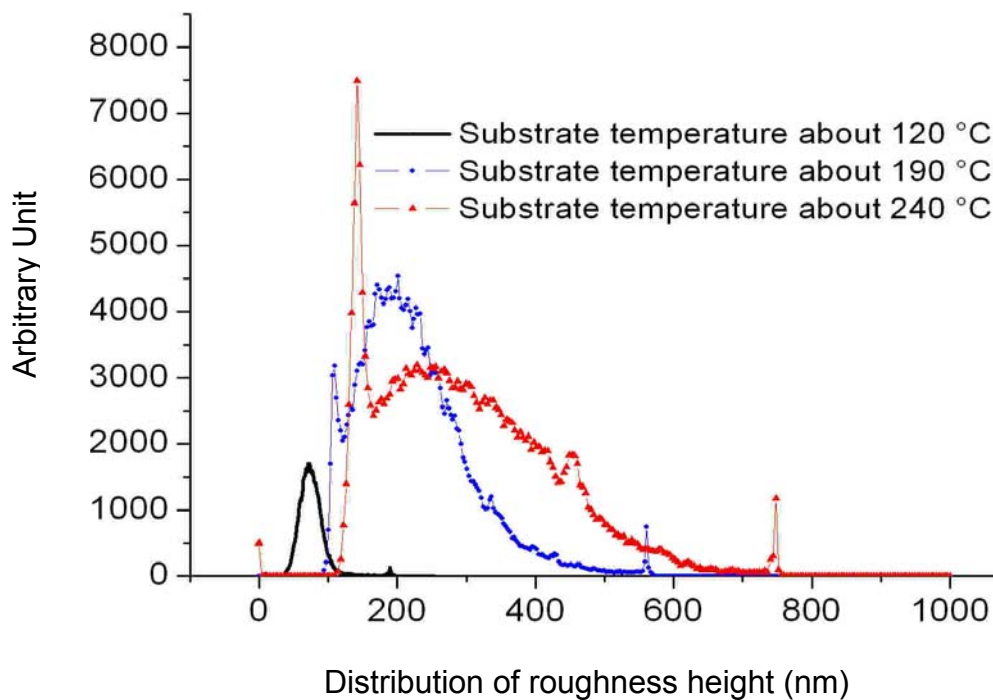


Fig. 6-11: Distribution of roughness height for three samples prepared at 120 °C (without template layer), 190 °C and 240 °C

Finally, successful Cu-Al<sub>2</sub>O<sub>3</sub> cermet based absorbers with an excellent spectral selectivity and a simplified structure were prepared and tested. With the help of roughness template layer and deposition at high substrate temperatures, desired selectivity with the least absorber thickness and without any needs to an anti-reflection layer or precise thickness controlling obtained.

### 6A.5 Conclusions

- The optical simulation showed that increasing the number of cermet layers would not improve the spectral selectivity. After layers optimization of different structures, optical simulation proposed single-cermet structure equipped with an Al<sub>2</sub>O<sub>3</sub> anti-reflection layer, as the simplest optimum structure for Cu-Al<sub>2</sub>O<sub>3</sub> composite absorbers.
- The graded structure also showed slightly better optical properties than the simple single cermet structure without anti-reflection layer.
- It was found that heating the substrate during thin film deposition changes the structure and morphology of the deposited films, i.e. at high substrate temperatures; copper, which has high sputtering rate, creates a denser layer but cermet and Al<sub>2</sub>O<sub>3</sub> layers are grown totally different. The increased thermal energy gives the arriving

atoms of such materials with lower sputtering yield, enough energy to diffuse around the substrate, form larger irregular islands, and induce roughness on the surface of the film. In addition, heating the substrate removes the water vapor and other volatiles, which exist in the chamber and on the substrate, and consequently improves the adhesion of the deposited films to the substrate.

- To absorb more light, deeper surface roughness is required. Increasing the thicknesses of the cermet or anti-reflective coating could increase the depth of the induced roughness but thicker layers would lead to higher thermal emittance. For avoiding that, a rough template layer (here  $\text{Al}_2\text{O}_3$ ) was deposited under the IR-reflector layer. The thickness of the rough template layer could be as high as desired because it would not affect the thermal emittance. Therefore forming a cermet layer with very rough surface morphology was easily achieved by applying a rough template layer.

- The optical property of a multilayer with smooth thin films is very sensitive to the thickness of each layer. Therefore, fabrications of the single- or double-cermet structures, in conjunction with an anti-reflection layer are still complicated and need accurate controlling of the deposition parameters. The developed structure along of this study because of its high surface roughness is less thickness-sensitive and has only one effective layer (cermet layer). Using such simple layer configuration is easier for fabrication and can reduce the production costs.

- Rough surfaces increase the solar absorption by multiple reflections and partial absorptions of the light between the surface features. Moreover, due to the gradual increase of the refractive index of a rough interface and lower surface reflection, more light can be entered into the active absorber layer. Therefore, rough absorbers do not need essentially an anti-reflection layer.

- The new developed structure increased the solar absorptance ( $\alpha$ ) of the smooth  $\text{Cu-Al}_2\text{O}_3$  from 0.840 to 0.965, while the emittance value was kept as low as the thermal emittance value ( $\varepsilon$ ) of the copper substrate (0.028).

-The  $\text{Cu-Al}_2\text{O}_3$  cermet layer under vacuum is stable only for temperatures less than 200 °C in the long terms [107], therefore the high-efficiency structure developed in this study can be a good candidate for evacuated solar tube collectors or other low temperature applications.



### **6B. Selectivity enhancement by laser structuring**

For investigation of light absorption property of ordered structures, some metallic samples prepared using laser interference system of Functional Materials Institute of Saarland University. Then, surface morphology of samples was analyzed by different methods like White Light Interferometer microscope (WLI) and SEM. The samples were optically characterized using UV/Vis/NIR spectrophotometers. From diffuse and total reflectance data of optical spectroscopy, solar absorptance and thermal emittance values of each sample were calculated using the method described in chapter 4.

#### **6B.1 Structuring of metallic samples**

The variation of parameters such as period, number of laser pulses and laser fluence will determine the aspect ratio and roughness of the resulting micro-patterns. Different conditions i.e. number of pulses and periods were used for the laser interference experiments. These conditions are shown in Table 6-5 together with the characteristic dimensions of the obtained periodical structures in both, copper (Cu) and stainless steel (SS) samples. Structure period, structure height and aspect ratios were measured by analyzing WLI 3D scans of the surface. Laser intensities for structuring copper and stainless steel plates were 2.15 and 3.5 J/cm<sup>2</sup>, respectively. *Cu8* and *SS4* are the structured copper and stainless steel samples with the highest solar absorptance. These two samples have the highest aspect ratios 0.446 and 0.333 for copper and stainless steel, respectively. Both values correspond to the samples structured with wide grating spacing and 10 laser pulses (see Table 6-5).

## 6. Results and discussion

Table 6-5: Laser structuring parameters and measured total solar absorptance and thermal emittance values of copper and stainless steel samples.

“us” stands for unstructured

Sample name	Solar absorptance	Thermal emittance at (300 K)	Structure period ( $\mu\text{m}$ )	Structure height ( $\mu\text{m}$ )	Aspect ratio	Pulse number
<i>Cu1(us)</i>	0.156	0.018	-	0	0.000	0
<i>Cu2</i>	0.150	0.044	2.00	0.282	0.140	1
<i>Cu3</i>	0.250	0.029	2.00	0.490	0.245	10
<i>Cu4</i>	0.223	0.022	2.00	0.442	0.221	4
<i>Cu5</i>	0.242	0.035	3.59	0.627	0.175	1
<i>Cu6</i>	0.261	0.048	3.59	1.030	0.287	3
<i>Cu7</i>	0.288	0.038	3.59	1.307	0.364	6
<i>Cu8</i>	0.352	0.040	3.59	1.601	0.446	10
<i>SS1(us)</i>	0.349	0.076	-	0	0.00	0
<i>SS2</i>	0.410	0.093	4.01	0.593	0.148	1
<i>SS3</i>	0.450	0.111	4.01	0.982	0.245	5
<i>SS4</i>	0.498	0.093	4.01	1.335	0.333	10
<i>SS5</i>	0.343	0.107	2.00	0.078	0.039	1
<i>SS6</i>	0.411	0.087	2.00	0.344	0.172	5
<i>SS7</i>	0.451	0.097	2.00	0.410	0.205	10

In general, few laser pulses and large periods produce more homogeneous structures with characteristic sinus-shape topography (Fig. 6-12a). For small periods, due to the large thermal conductivity of metals, the heat is easier evacuated from the interference maxima toward the interference minima and thus the difference in temperature between this both regions is smaller. This effect makes it difficult to melt the metal only at the interference maxima [108]. Consequently, smaller aspect ratios (quotient between structure height and period) can be achieved (Fig. 6-12b). However, if metals with a lower melting point and surface tension are structured, rougher surfaces can be obtained (see Fig. 6-12d) but also in this case with a low aspect ratio. By increasing the number of pulses, higher aspect ratios are achieved but in a similar way as explained in [109] the structures are less homogenous (Fig. 6-12c).

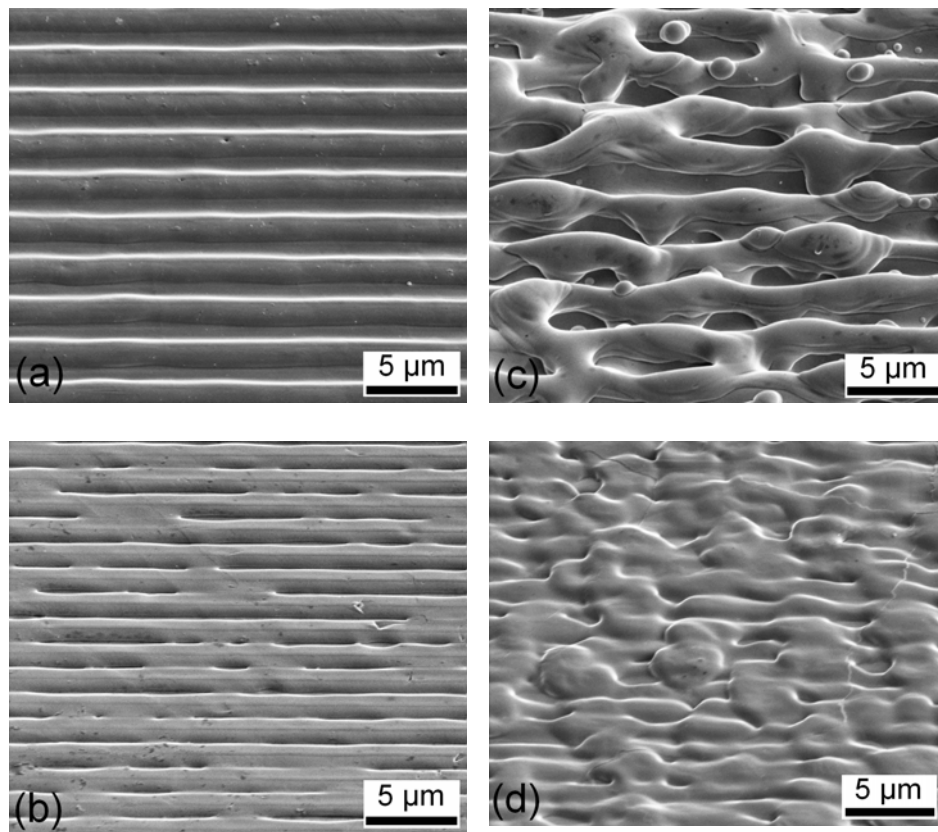


Fig. 6-12: Periodical structured surfaces on: (a) stainless steel, period = 4.01  $\mu\text{m}$ , 1 laser pulse (sample SS2); (b) stainless steel, period = 2  $\mu\text{m}$ , 1 laser pulse (sample SS5); (c) stainless steel, period = 4.01  $\mu\text{m}$ , 10 laser pulses (sample SS4); (d) copper, period = 2  $\mu\text{m}$ , 1 laser pulse (sample Cu2)

### 6B.2 Optical properties of structured materials

Measurements carried out on different metals show that the solar absorptance depends on the structure height, period and optical properties of the metal. Fig. 6-13 and 6-14 show the total reflection of the structured and unstructured stainless steel and copper surfaces. The curves indicate how the total reflection of the metallic surfaces can be changed depending on the different period and structure height of the samples. For example, in Fig. 6-13 it can be seen that the sample Cu2 with a low structure height (282 nm) practically does not increase the total solar absorptance. Cu8 shows a good decrease in reflectivity while the reflectance for wavelengths higher than 2.5 is still very close to that of unstructured copper. Similar behavior is seen for stainless steel sample SS4. Moreover, although the sample SS2 has a two times higher structure height than the sample SS6 (593 and 344 nm respectively),

## 6. Results and discussion

the total absorptance is practically the same (see Table 1). It means that the total absorptance of the structured samples does not depend individually upon their periods or structure height at so low structure parameters.

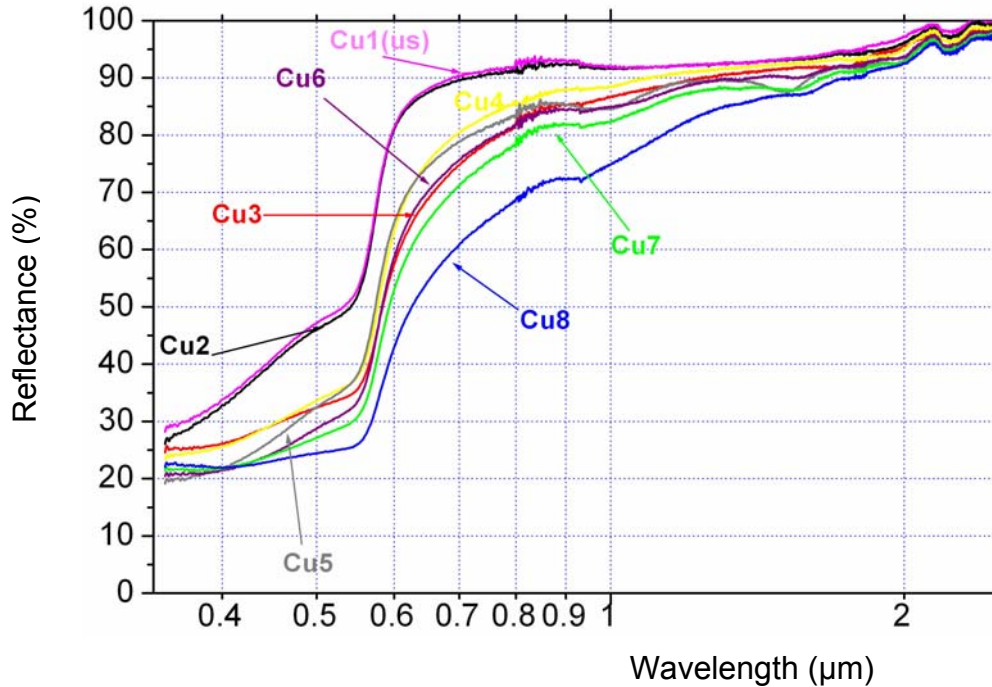


Fig. 6-13: Total spectral reflectance for copper samples structured with different periods and structure heights

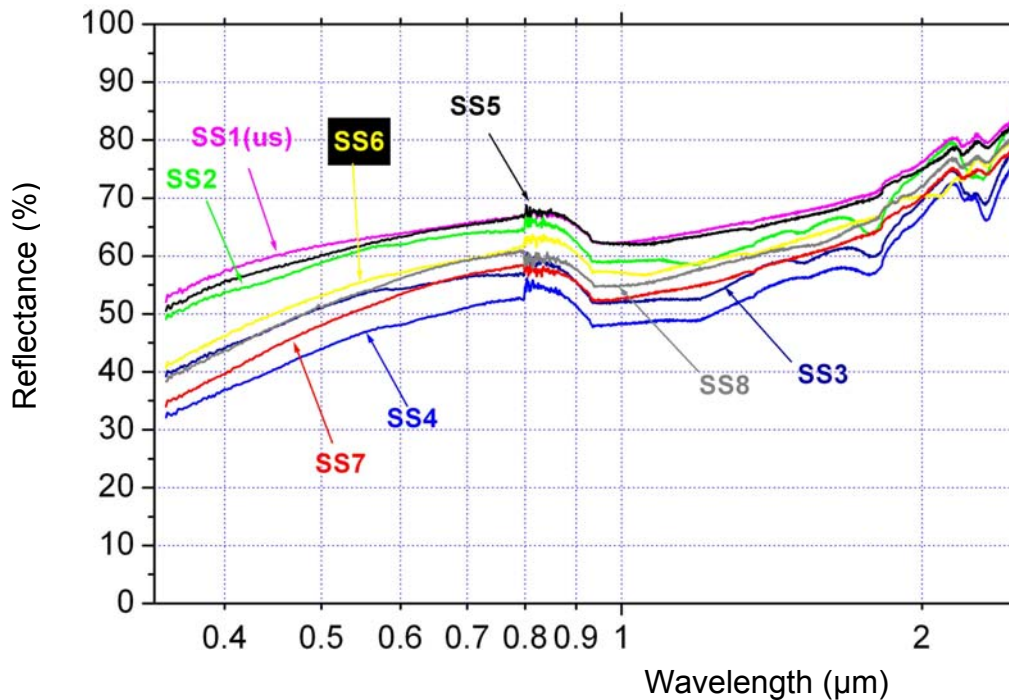


Fig. 6-14: Total spectral reflectance for copper samples structured with different periods and structure heights

## 6. Results and discussion

---

Similar to [78] it is possible to define one parameter which resumes both above mentioned characteristic to describe the structured surfaces: the aspect ratio (this last was defined in section 6.B.2). The dependence of the total absorptance for both stainless steel and copper samples depending on the aspect ratio is shown in Fig. 6-15. From this figure it can be clearly seen that the higher aspect ratio, the better total absorptance. Comparing in both studied metals the total solar absorptance of the unstructured and the structured samples with the largest aspect ratio, an increase of about 20 and 15 % can be observed in copper and stainless steel, respectively.

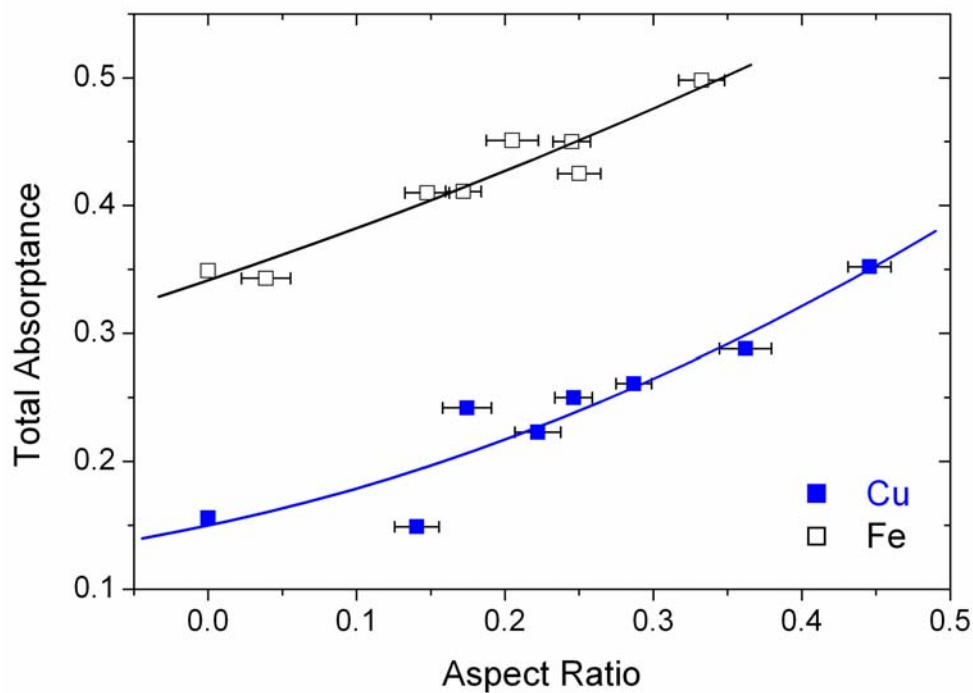


Fig. 6-15: Total solar absorptance as a function of the aspect ratio for structured copper and stainless steel samples

In the case of multi-pulse experiments, for a fixed period the higher the number of laser pulses, the higher the structure height. Consequently larger aspect ratios are obtained and thus the total spectral absorptance is increased (see for example samples *Cu2*, *Cu3* and *Cu4*).

Spectral properties of line-type periodical structures can be explained by the graded refractive index model [110] as discussed in chapter 4. Fresnel reflection is changed mainly by the sharp change of the refractive index at the boundary between the

## 6. Results and discussion

---

material and its surrounding medium. Therefore, the reflectivity becomes low by changing the effective refractive index gradually.

Measured thermal emittance at room temperature, as it can be seen in Fig. 6-16, has not an important dependency on aspect ratio of the structured samples. This different optical behavior is explained by “wave-front discrimination” effect. For visible wavelengths, which are small compare to the actual irregularities, the surface looks rough and radiation may be trapped through multiple forward reflections and partial absorptions in the micro-cavities. For the thermal infrared wavelengths, the surface appears smooth and mirror like, because the incoming wavelength is larger than the dimension of the surface roughness. Therefore, a rough surface with surface features smaller than the incident infrared wavelengths radiates as a flat surface in the long-wave spectrum and the metal will show its bulk properties of low infrared emittance.

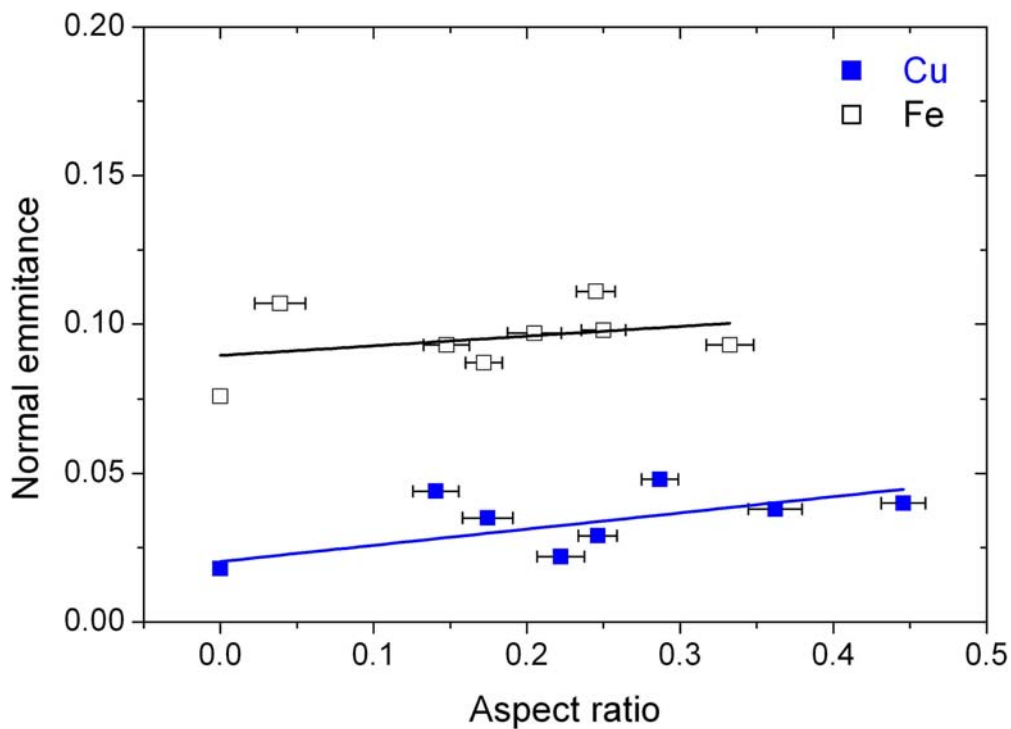


Fig. 6-16: Normal thermal emittance as a function of the aspect ratio for structured copper and stainless steel samples

### 6B.3 Effect of higher structure periods

Again, six different copper samples were structured but this time with larger periods. The goal is absorption of more wavelengths by shifting the cut-off wavelength to higher values. Table 6-6 shows the structuring parameters and optical properties of each sample. WLI surface analyzing shows that surface features are not necessarily equal which means the surface profiles were not symmetric lamellar or sinusoidal but mostly non- symmetric trapezoidal with different lands and ridges (see Fig. 6-17 for example).

*Cu9* was structured two times by rotating the sample 90 degrees after the first laser shot (see [111]). This sample had a net shape structure but the structure height (0.918  $\mu\text{m}$ ) was not sufficient for effective absorption. Comparing that with the absorption and emission properties of *Cu4*, *Cu9* had higher solar absorptance of about 0.07.

The blue line in the Table 6-6 shows the physical and optical properties of the best sample (*Cu10*) with a solar absorptance of 0.508 and thermal emittance of 0.096. This sample has the highest aspect ratio among the other samples and fabricated with 10 laser pulses. The surface profile of this sample is shown in Fig 6-17. 35 % improvement in solar absorptance and 40 % less reflection at 550 nm wavelengths is a promising result, which can increase the selectivity of a flat absorber in the same order.

Table 6-6: Laser structuring parameters and measured total solar absorptance and thermal emittance values of copper samples with large periods

Sample name	$\alpha_{\text{solar}}$	$\varepsilon_{\text{th}}$	Structure period ( $\mu\text{m}$ )	Structure height ( $\mu\text{m}$ )	Aspect ratio	Pulse Nr.	Laser fluence ( $\text{mJ}/\text{cm}^2$ )
Cu9	0.3	0.035	4	0.918	0.23	5	3974
Cu10	0.508	0.096	4	1.442	0.36	10	4575
Cu11	0.298	0.058	6	1.406	0.24	1	3102
Cu12	0.279	0.069	4	1.137	0.28	1	4420
Cu13	0.273	0.07	4	1.274	0.32	1	4110
Cu14	0.305	0.075	5.3	1.86	0.35	1	2714

## 6. Results and discussion

---

*Cu10* and *Cu11* both have similar structure height but because of the influence of more applied energy, lower structure period and higher aspect ratio, *Cu10* shows better selectivity. Fig. 6-17 shows surface profile of both *Cu10* and *Cu11* samples but it must be noted that units of the X and Y-axis are not equal in these images. The surface profile of the *Cu10* sample presents smoothed peaks, which are due to the usage of high number of laser-pulses while structure peaks in *Cu11* are sharper and have semi triangular shape.

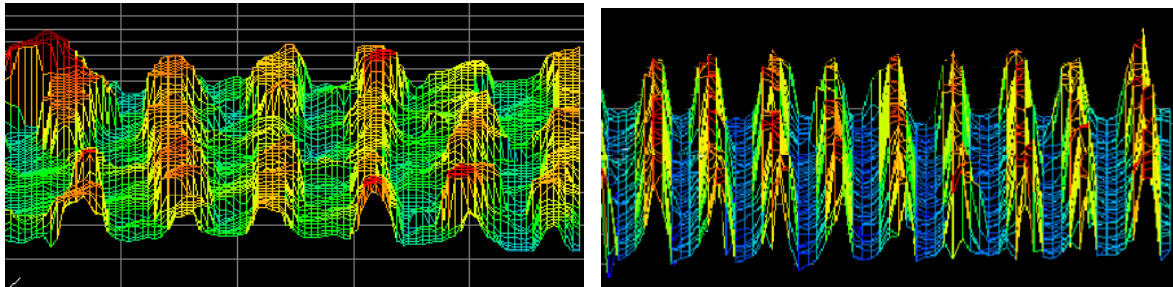


Fig. 6-17: Surface profile of the *Cu10* and *Cu11* copper samples

As can be seen in Fig. 6-18, both *Cu11*, *Cu12* samples show similar reflectivity profiles because of their similar aspect ratios and structure shapes. *Cu9* has three-dimensional structures but its aspect ratio is in the same range of those of *Cu11* and *Cu12* samples. Therefore, its reflectance behavior is very close to the reflectance curves of *Cu11* and *Cu12* samples. In comparison, higher aspect ratio of *Cu14* led to lower reflections of short wavelengths (0.3-0.57  $\mu\text{m}$ ) but similar reflectivity for higher wavelengths. This can be explained by the structure shape of *Cu14* so that this sample has higher peak length (ridge) about 1.4  $\mu\text{m}$  than the other samples, which have ridges of about 0.85  $\mu\text{m}$ . larger peak length means higher unstructured surface, which can reflect more portion of the incoming light. By comparing Tables 6-5 and 6-6, it can be concluded that having a higher structure period for a constant aspect ratio would lead to a higher absorptivity and to some extent higher thermal emittance (see structuring and optical properties of *Cu7* and *Cu10* samples).



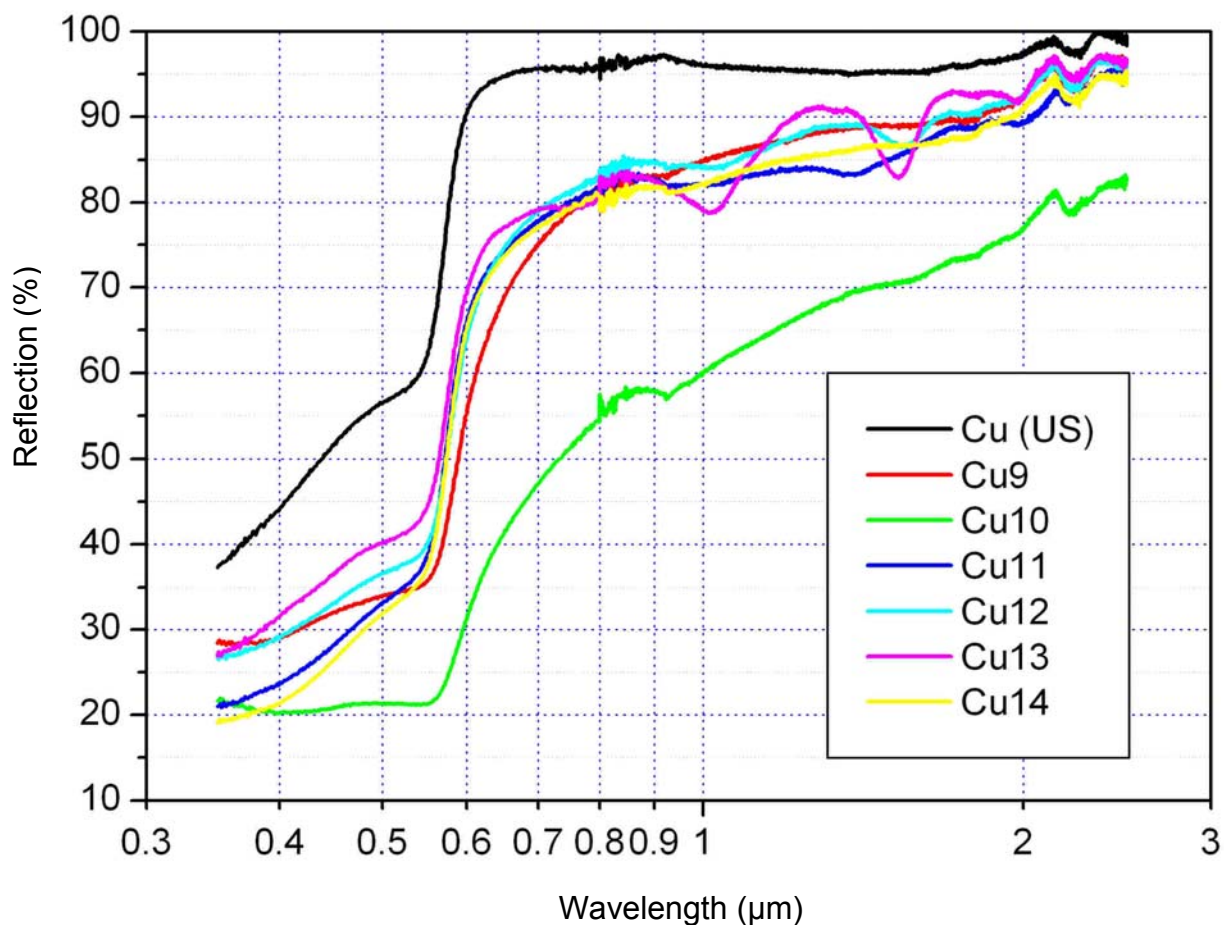


Fig. 6-18: Total spectral reflectance of copper samples structured with different periods and structure heights

#### 6B.4 Comparing simulation and experiment results

In order to check the validity of the optical simulation with experimental results, the wavelength dependent reflections of two laser structured copper samples, *Cu4* and *Cu14*, from both experimental data and those calculated with PCgrate® were compared (see Fig. 6-19 and Fig. 6-20). It is seen that the numerical results are in good agreement with the experiment data. Especially for *Cu4*, theoretical total reflections are found to provide reasonable agreement with the measured reflectance data.

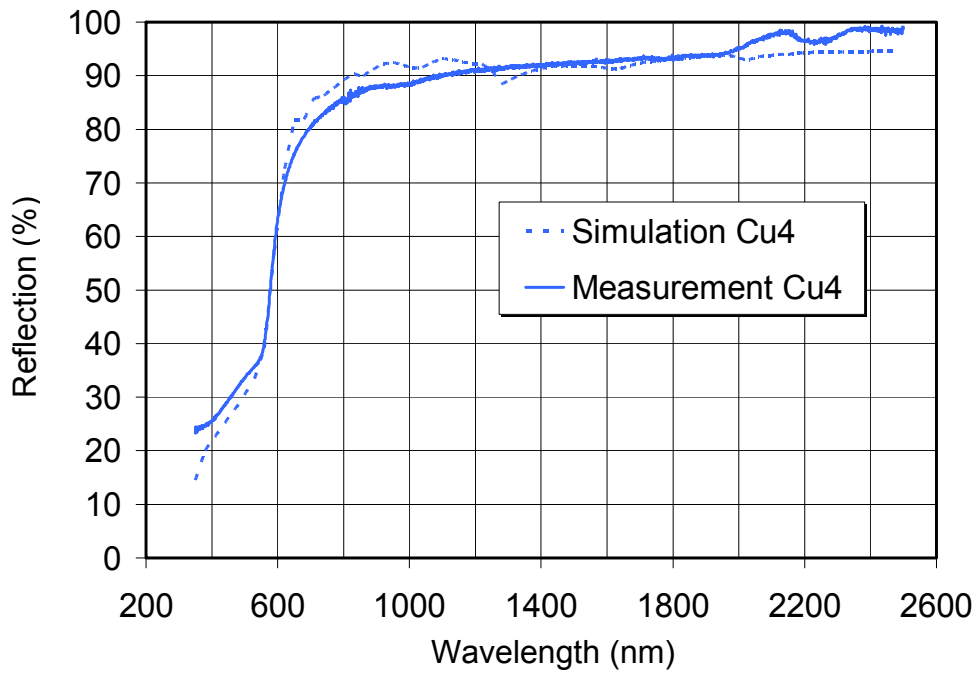


Fig. 6-19: Total spectral reflectance of *Cu4* sample

Small deviation is observed between theoretical and experimental reflectance curves of *Cu14* sample; especially for wavelengths between 0.6 and 2.2  $\mu\text{m}$ . Sample *Cu14* possesses structures with large period of about 5.3  $\mu\text{m}$  and average structure height of about 1.86  $\mu\text{m}$ .

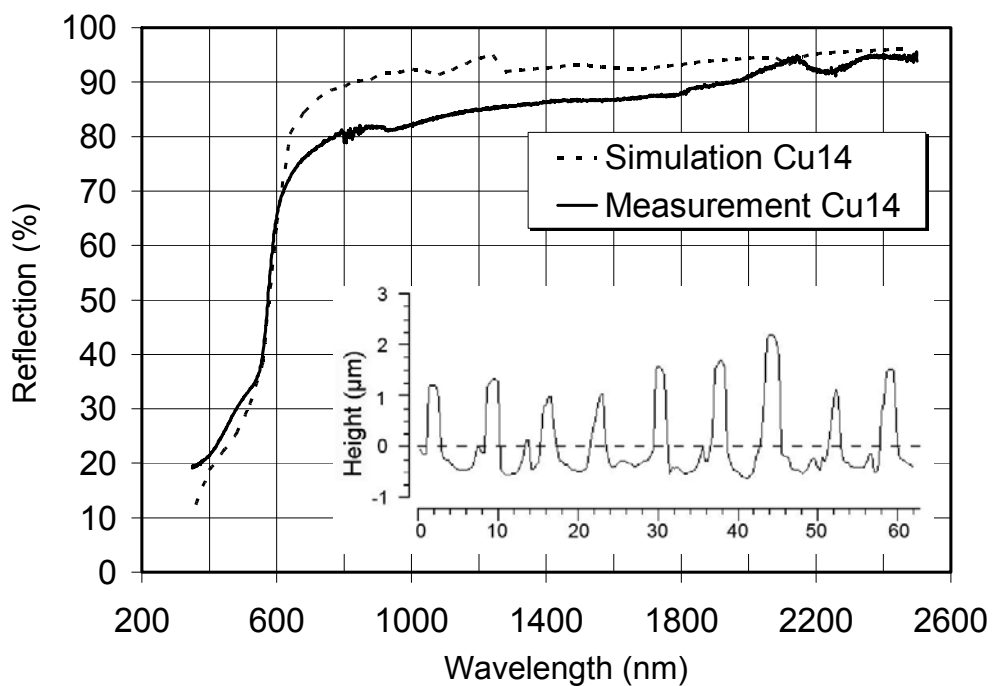


Fig. 6-20: Total spectral reflectance of *Cu14* sample

Cross sectional view of the sample *Cu14* has been depicted in inset of Fig. 6-20. There are few structures heights, which are larger than 1.86  $\mu\text{m}$ . Higher absorption of near-infrared wavelength due to higher local aspect ration can explain the deviation between experiment and theory.

### 6B.5 Conclusions

- The viability of the laser interference structuring method to produce structured surfaces on bulk metals (without masks or any other secondary steps) for photo-thermal solar absorbers was demonstrated.
- Direct laser structuring is a simple fabrication method for preparing semi-selective absorbers by structuring only metallic surfaces which have low thermal emissivity.
- Structuring parameters like structure periods or depths can be modified easily by changing the interference parameters, laser intensity and number of laser pulses.
- Surface micro-structures with a periodicity up to 4  $\mu\text{m}$  enable good spectral selectivity, featuring high absorption in the UV and NIR when keeping low emissivity in the infrared wavelengths.
- Solar absorptance of 0.508 and thermal emittance of 0.096 were obtained for a structured copper sample with structure aspect ratio of 0.36 and period of 4  $\mu\text{m}$ .
- The results indicate that the factors that strongly affect the solar absorption are the aspect ratio and the profile.
- Spectral properties of the structured samples indicates that the larger the aspect ratio, the better the solar absorptance. Moreover, due to the increase of the surface roughness, the diffuse reflectance of both copper and stainless steel samples also increases. It means that the still retained reflectance is much more diffuse than specular.
- Due to the smaller sizes of the prepared structure periods to the thermal infrared wavelengths, thermal emittance values remain almost unchanged at higher aspect ratios.
- Larger obtained aspect ratios correspond to the samples irradiated with periods wider than 3  $\mu\text{m}$  and large number of laser pulses.
- Considering laser parameters, in order to increase absorption, several laser pulses must be used. The larger number of laser pulses (up to 20-30), the higher the aspect

ratio is obtained. However, several laser pulses decrease the homogeneity of the samples and increase the emissivity of the thermal infrared wavelengths.

- Samples, prepared with high number of laser-pulses present smoothed structure peaks while peaks of surface features of the samples prepared with lower pulses are sharper and have well-defined shapes.
- Having a higher structure period for a constant aspect ratio would lead to a higher absorptivity and to some extent higher thermal emittance.
- To increase the solar absorptance to the values higher than 40–50 %, larger aspect ratios must be achieved and also different pattern shapes (i.e. periodical dots arrays or nets) should be evaluated.
- Metals with low melting temperatures like copper are not suitable for structuring with very high number of laser pulses. In this case non-homogenous structured surfaces and distorted structure shapes are obtained.
- Structuring of other low emittance metals like molybdenum or tungsten, which are more stable at higher temperatures and show good intrinsic selectivity is recommended. This would lead to high temperature selective absorbers with high spectral selectivity and durability.
- After calculation total reflectance of the structured sample and comparing that with measured reflectance values, good agreement between simulated and measured data was observed.
- In order to reach the best possible absorption and spectral selectivity, numerical calculations of chapter 4 can be used to structure a surface in accordance to the optimized parameters such as period, structure depth, profile and aspect ratio.

## 6C. Selectivity enhancement by embossing technique

### 6C.1 Structure parameters of the embossed layer

It is important to investigate the structure parameters of the transferred pattern because this can show the ability of the embossing technique in making structures with high depths. Achieving an undamaged surface profile and a low shrinkage in structure depth of the imprinted medium are the main concerns of this study. Here only the embossing results of our best available master are presented.

The used metallic master had trapezoid structures with the period of  $2.8 \mu\text{m}$  and depth of  $1.32 \mu\text{m}$ . According to the simulation results of chapter 4, the resulted aspect ratio of the above structure parameters is not high enough for boosting the solar absorption significantly. Using the above-explained metallic master, a flexible silicon stamp was prepared. Figs. 6-21 and 6-22 show 3D and cross sectional views of this structured silicon rubber, respectively. It can be seen that well-defined structures obtained and without any pattern damage, structures were transferred from metallic master to the silicone. Structure height of  $1.31 \mu\text{m}$  and period of  $2.87 \mu\text{m}$  were measure by analyzing the WLI photos.

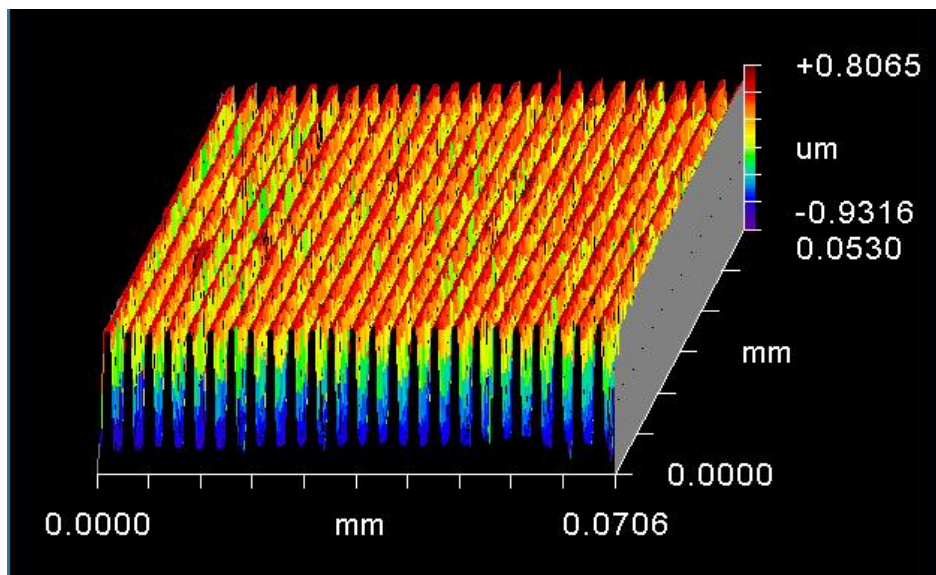


Fig. 6- 21: Three-dimensional WLI image of the structured silicon rubber

## 6. Results and discussion

---

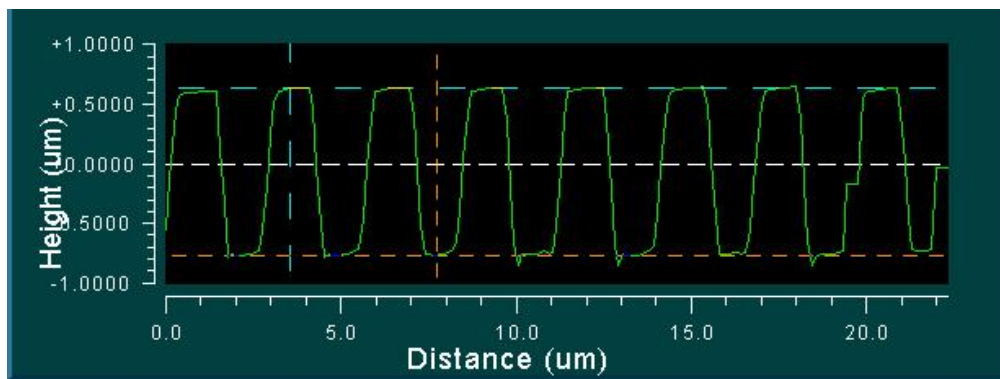


Fig. 6-22: Cross sectional view of the surface profile of the structured silicon rubber

The prepared sol was spread on a glass substrate and was embossed by using the structured silicon rubber. Then substrate and the sol-gel layer were tempered. After tempering, shrinkage of the structure parameters was only 10-15 %. As shown in Fig. 6-23, the sol-gel layer replicated well the structuring pattern of the silicon rubber. Finally, a structured substrate with structure height of 1.20  $\mu\text{m}$  and period of 2.76  $\mu\text{m}$  was ready for optical investigation. For studying the optical effect of the structuring, a tungsten thin film with a thickness of about 200 nm was deposited on the structured sol-gel layer. Similarly, the deposited thin film kept the initial form of the surface profile and replicated that in its interface with air. Deposition of the tungsten layer slightly decreased the depth of the structure but it could be avoided by decreasing the rate of sputtering and decreasing the thickness of the layer.

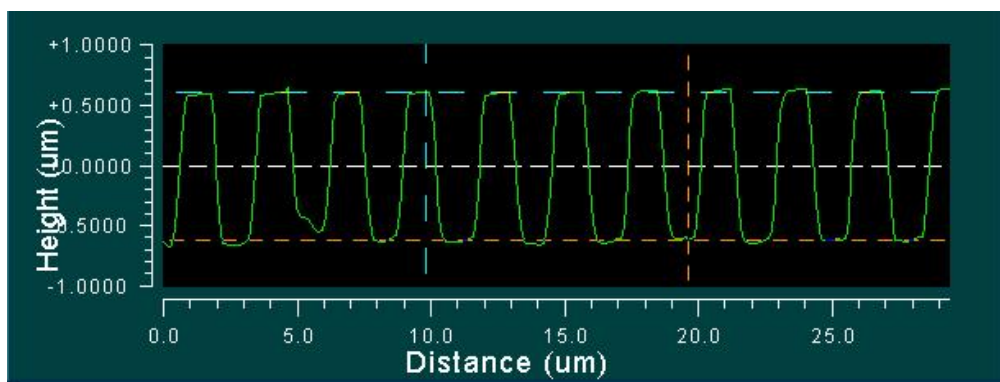


Fig. 6- 23: Cross sectional view of the surface profile of the structures sol-gel layer

Table 6-7 shows the measured structure periods and heights of the metallic master, silicon rubber and patterned sol-gel layer, after creation and after deposition of

## 6. Results and discussion

200 nm tungsten film. In the next section, effect of imprinted structure on enhancement of solar absorption is studied.

Table 6-7: Structure height and period of the master, silicon stamp, structured sol-gel layer and after deposition of 200 nm tungsten

Object	H ( $\mu\text{m}$ )	P ( $\mu\text{m}$ )
Metallic master	1.32	2.87
Flexible silicon stamp	1.31	2.87
Transferred pattern on nano-composite layer	1.20	2.76
After deposition of 200 nm tungsten film	1	2.70

### 6C.2 Enhancement in solar absorption

In Fig. 6-24, reflectance curves of smooth and structured tungsten film are shown. Compared to the unstructured tungsten thin film, decrease of about 16 % in reflectance of solar spectrum is observed which can be translated as 16 % increase in the solar absorptance value.

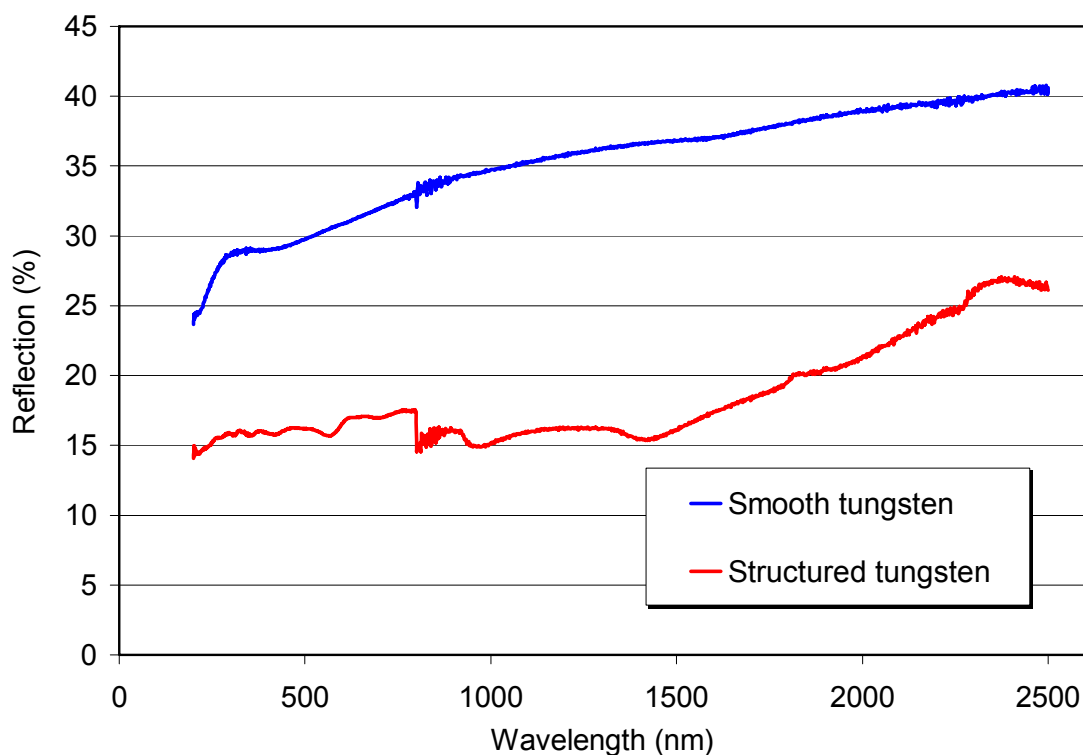


Fig. 6-24: Cross sectional view of the surface profile of the metallic master

Both curves of the Fig. 6-24 were measured using an integrating sphere. As for measuring the total reflectance of rough surfaces, a highly diffuse reference is used; the reflectance values of the unstructured tungsten are not absolute. To eliminate the differences, which can be resulted from having different references, it was preferred to measure the reflectance curves of both structured and unstructured samples in a same way.

### 6C.3 Conclusions

- Using a synthetic sol with an organic-inorganic composite system, a crack free transparent and imprintable layer obtained.
- The pattern of metallic master was transferred exactly to the silicon rubber. No decrease in structure height or period was observed. In addition, after printing the pattern on the sol-gel layer and heat treatment only 10-15 % shrinkage in the dimension of the surface structures was measured. This shows high capability of this structuring technique in making and replicating structures with high depths.
- This method of structuring is simple and has not difficulties of lithographic methods. In this method, the entire surface can be printed at once or in steps. Therefore, using small mold, large areas can be structured by repeating the print procedure or by preparation of a larger mold from initial fabricated small mold. Such flexibility in structuring of the large surfaces is the most important advantage of imprint lithography among other methods. In addition, by bending a thin flat mold around a roller, a roller-imprint can be obtained and therewith, large areas can be printed easier.
- As an example of the potentiality of this structuring method in increasing the solar absorptivity of a surface, metallic tungsten was sputtered on the structured sol-gel layer. Deposited thin film of tungsten replicated the same structuring pattern in its interface with air. Deposition of the tungsten layer slightly decreased the depth of the structure but it could be avoided by decreasing the rate of sputtering and decreasing the thickness of the layer. According to the total reflectance measurements, the solar absorptance of the structured tungsten surface was 16 % higher than that of the smooth tungsten.
- Using imprint technology, creation of three-dimensional features in just one easy step is possible whereas photolithography is not able to produce such patterns.



### 6D. Suspension derived Ni-Al<sub>2</sub>O<sub>3</sub> cermet selective absorber

#### 6D.1 Structural and physical properties of Alu C powders

Alu C powder is the only solid constituent of the final coating suspension. This section reports on Alu C powder characterization by XRD, particle size, and zeta potential measurements. Viscosities of the Alu C suspensions and maximum possible loading of this powder into the water and ethanol mediums are also investigated.

##### 6D.1.1 Powder characterization

The TEM picture of Alu C nano-powder (Fig. 6-25) shows that primary particle size of this powder is about 13-15 nm but inter-particle agglomerations also exist. The observed particle sizes are in good agreement with the powder specification sheet provided by Evonik Degussa.

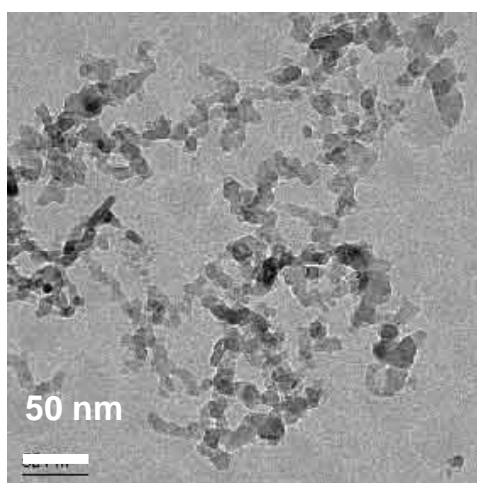


Fig. 6-25: TEM picture of Alu C nano-powder [112]

The particle size distribution (PSD) of Alu C nano-powders in the suspension was measured with both acoustic attenuation (Acoustosizer) and laser diffraction (Mastersizer) techniques. The results are shown in Fig. 6-26. For these PSD measurements, a 5 wt. % suspension was prepared by dispersing Alu C powder in distilled water mechanically for 30 minutes. The rotation speed of the mechanical disperser was 12000 rpm. It can be seen in Fig. 6-26 that the particle size distribution measured using Acoustosizer is narrow and spreads from 43 to 90 nm but Mastersizer measurement shows a broader distribution from 75 nm to 500 nm. It

## 6. Results and discussion

will be shown later that the particle sizes measured by Acoustosizer are closer to the real sizes measured by analyzing SEM images. As explained in chapter 3, measuring absolute particle sizes of nano particles with Mastersizer and Acoustosizer is not possible but they are useful tools for comparing relatively the PSDs measured under different conditions. Light scattering methods are more sensitive to the presence of larger particles because this phenomenon exhibits a stronger dependence on the particle size, such as fifth or sixth power [113]. As a result, light scattering methods tend to overestimate the amount of larger particles and are not able to resolve the presence of small particles [114].

The frequency range of 0.2 to 20 MHz of Acoustosizer is not suitable for oscillating nano-particles (typically  $100\% < 100\text{ nm}$ ). Acoustosizer has been designed actually for conventional large pigments and not for nano-sized materials.

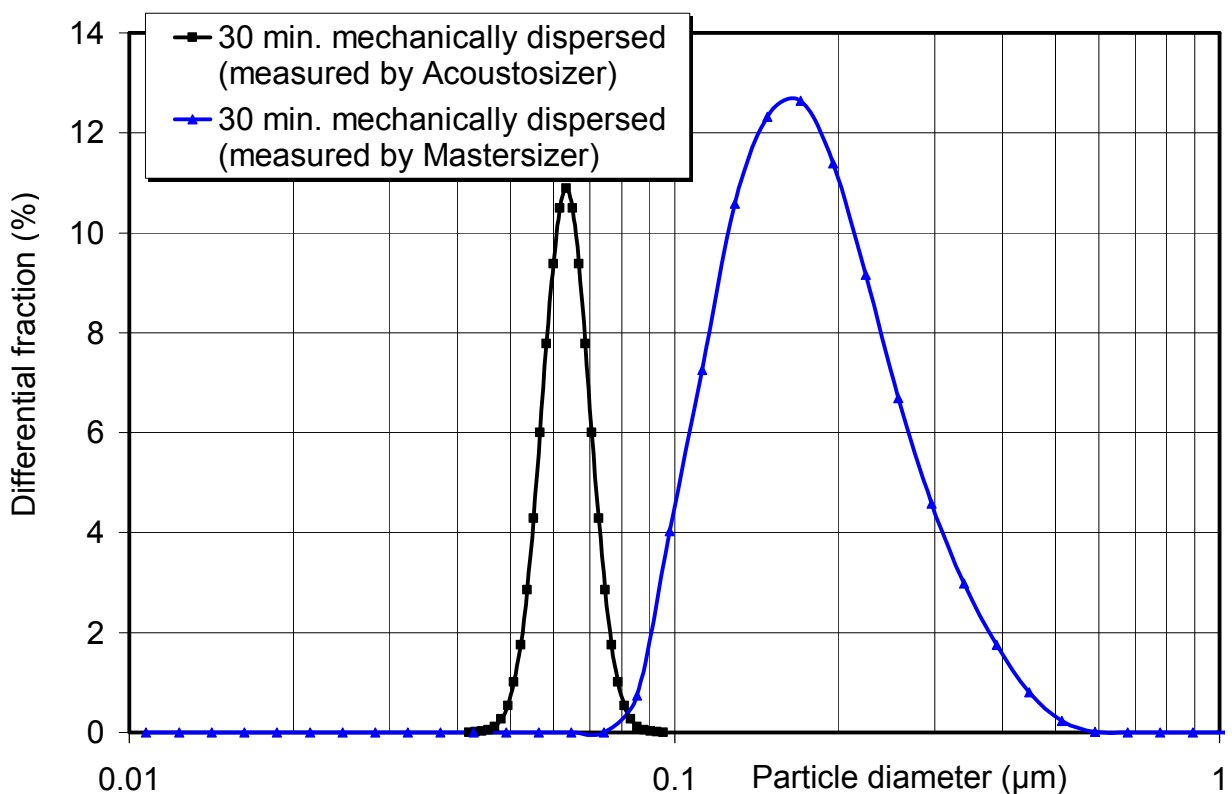


Fig. 6-26: Particle size distribution of Alu C

In terms of phase identification, the XRD-spectrum of the Alu C alumina powder shows the presence of both cubic ( $\gamma$ ) and tetragonal ( $\delta$ ) phases. Fig. 6-27 shows the refracted peaks of Alu C powders (black background) compared with diffraction peaks of delta and gamma phases of pure aluminum oxide.

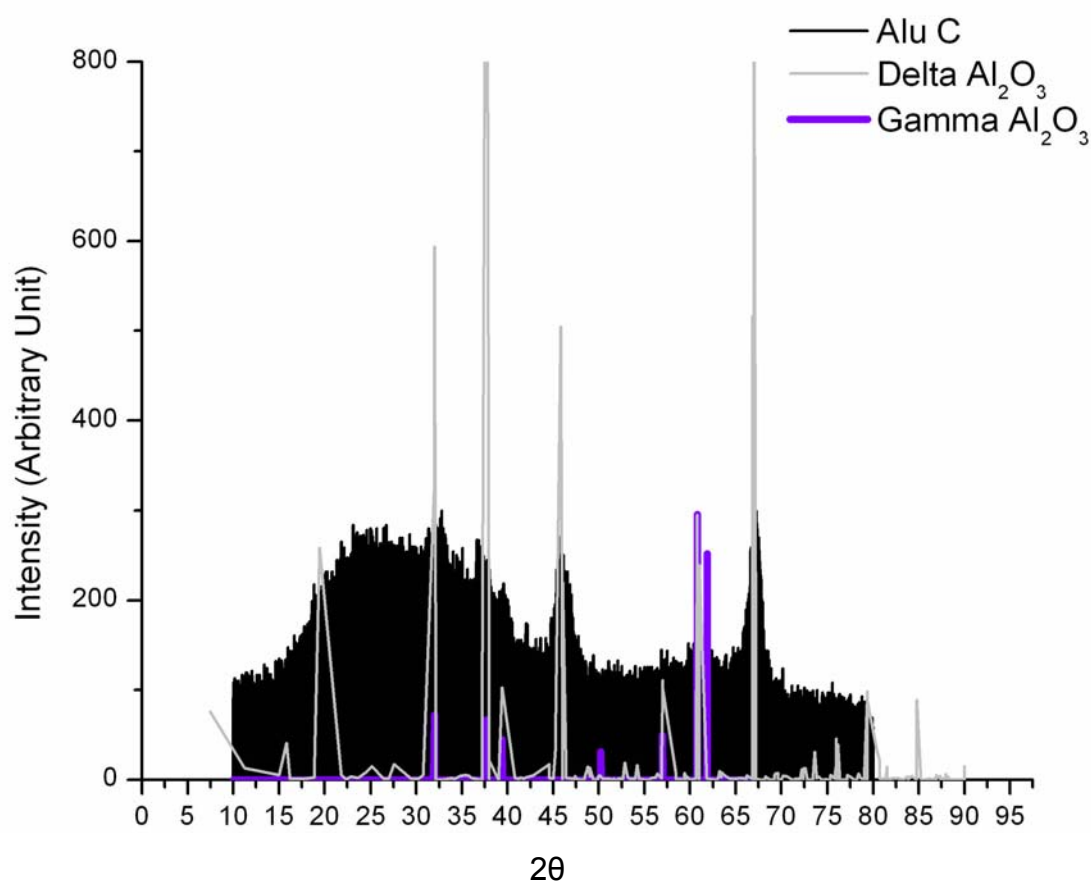


Fig. 6-27: XRD-spectrum of nano-sized alumina powder (Alu C, Evonik Degussa) compared with delta and gamma phases

### 6D.1.2 Zeta potential and conductivity of Alu C suspension

Measurement of zeta potential is used to assess the stability of a colloidal system as a function of the pH. Zeta potential larger than 20 mV is necessary for electrostatically stabilization of alumina powders in the water. Zeta potential and conductivity of an aqueous Alu C suspension with 5 wt. % loading were measured at different pHs via Acoustosizer. For the titration in acidic and basic regions, HCl and TMAH were used, respectively. As shown in Fig. 6-28, the conductivity is slightly increased with increasing pH from 3 to 12. The zeta potential is sensitive to the pH value and by increasing the pH value is decreased dramatically. By adjusting pH value of the suspension between 2 to 6, one can get a well-dispersed colloidal aqueous alumina suspension.

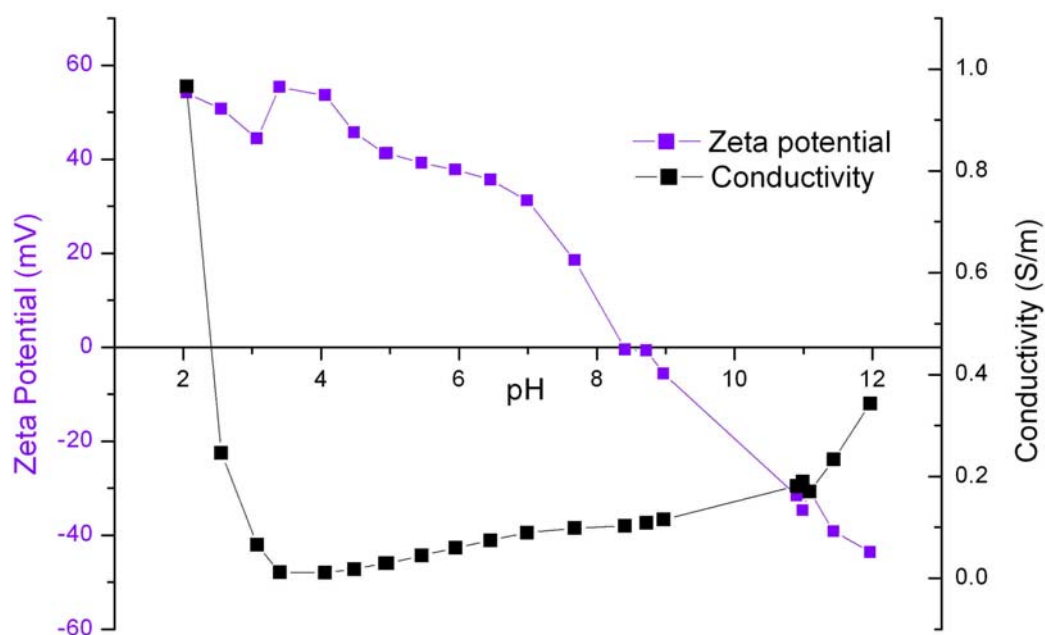


Fig. 6-28: Zeta potential and conductivity of aqueous suspension of Alu C with 5 wt. % solid load

The isoelectric point (where the zeta potential is zero) for alumina is between pH 8 to 9. Isoelectric point (i.e.p) is a good indicator for the cleanliness of the powder's surface. The location of this point, in pH, is a characteristic of the particle surface and depends on the particle crystal structure and level of impurities. By measuring the i.e.p of oxide suspensions prepared from different batches of powders and comparing them with a given isoelectric point, one can readily distinguish the purest one.

Measuring zeta-potential of alcohol based Alu C suspensions by Acoustosizer was not possible because the software of Acoustosizer II has been designed just for aqueous suspensions.

### 6D.1.3 Maximum solid load for Alu C suspension

As the viscosity controls the thickness of the dip-coated layer, rheology of the suspension is an important property that should be determined. The viscosity of a ceramic suspension is influenced by the solution, specific surface area of the powder, acidity and solid loading of the suspension. To determine the most suitable solid content for preparation a practical low viscose and well-dispersed suspension for thin film applications, it is necessary to investigate the effect of the solid load of the suspension on viscosity. For this aim, few aqueous and non-aqueous Alu C

## 6. Results and discussion

suspensions with different solid contents of 5 to 20 wt. % were prepared. The viscosities of these suspensions were measured under controlled temperature at 25 °C. Fig. 6-29 demonstrates measured viscosities of Alu C powder dispersed in distilled water and ethanol at different shear rates.

The maximum possible Alu C load for both water- and ethanol-based suspensions was 17.3 wt. %. Dispersing more than 9.5 wt. % Alu C powder in distilled water changes the viscosity of the suspension in a manner that it can no longer be considered as a Newtonian fluid. The same behavior is observed for ethanol-based suspension with solid contents of around 13.6 wt. %. The viscosity of a Newtonian fluid does not change with the applied strain rate and only such fluids are suitable for thin coating processes.

As the target thickness of the absorber must be less than 1  $\mu\text{m}$ , only diluted suspensions with viscosities less than 10 mPa·s are suitable for deposition of thin films. Therefore, for all experiments only suspension with solid Alu C contents of maximum 5 wt. % solid were prepared and used.

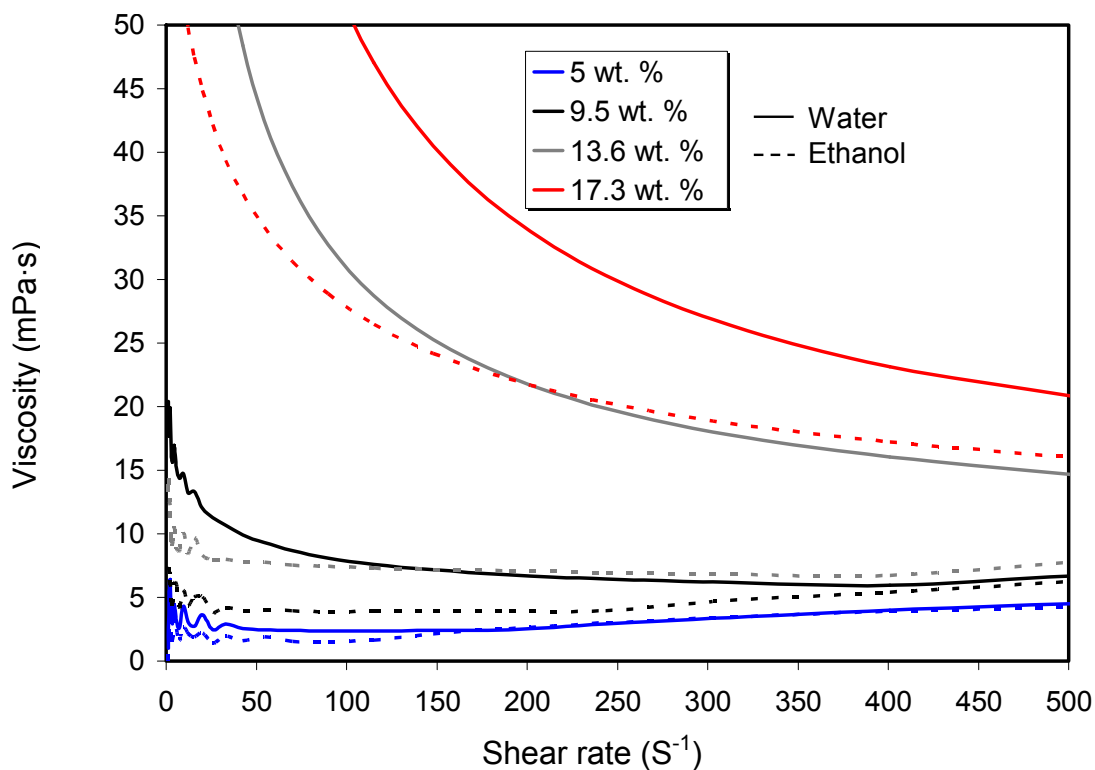


Fig. 6-29: Viscosity of aqueous and non-aqueous alumina suspensions with different solid contents from 5 to 17.3 wt. %

### 6D.2 Characterization of the coating suspension

The coating suspensions consist of Alu C nano-particles dispersed in ethanol or water as disperse medium, in which nickel nitrate has been already dissolved. In this section, the effect of mechanical and ultrasonic dispersions on viscosity and particle size distribution of this coating suspension is investigated. Zeta potential, pH and conductivity of the prepared suspensions are also presented. Stability and sedimentations behavior of the suspensions are monitored using ATR spectroscopy. Finally, effect of a coupling agent like TEOS on the properties of the *nickel nitrate-Alu C* suspension is studied.

#### 6D.2.1 Nickel nitrate-Alu C suspension

After dissolving 13.51 wt. % nickel nitrate into the water, 4.32 wt. %  $\text{Al}_2\text{O}_3$  powder was added gradually and dispersed mechanically for 30 minutes. Zeta potential of this suspension was measured by Acoustosizer and was shown in Fig. 6-30.

According to the zeta potential curve of Fig. 6-30, the prepared suspension would be stable electrostatically for pH values of 2 to 6 and preferably for pH values of 4 to 6. For pH values higher than 6 the zeta potential drops noticeably and the suspension is no longer stable. Similar behavior can also be concluded from Fig. 6-31. As it can be seen, at pH values higher than 6, particles start to agglomerate and enlarge particles. For pH values lower than 6, D15, D50 and D85 are less than 80 nm. It is believed that the zeta potential approaches asymptotically an isoelectric point in the neighbourhood of pH 12. Decreasing pH much below 4 would again result in a decrease in the magnitude of the zeta potential, mainly due to the compression of the electric double layer. This occurs as the ionic strength increases with decreasing pH.

## 6. Results and discussion

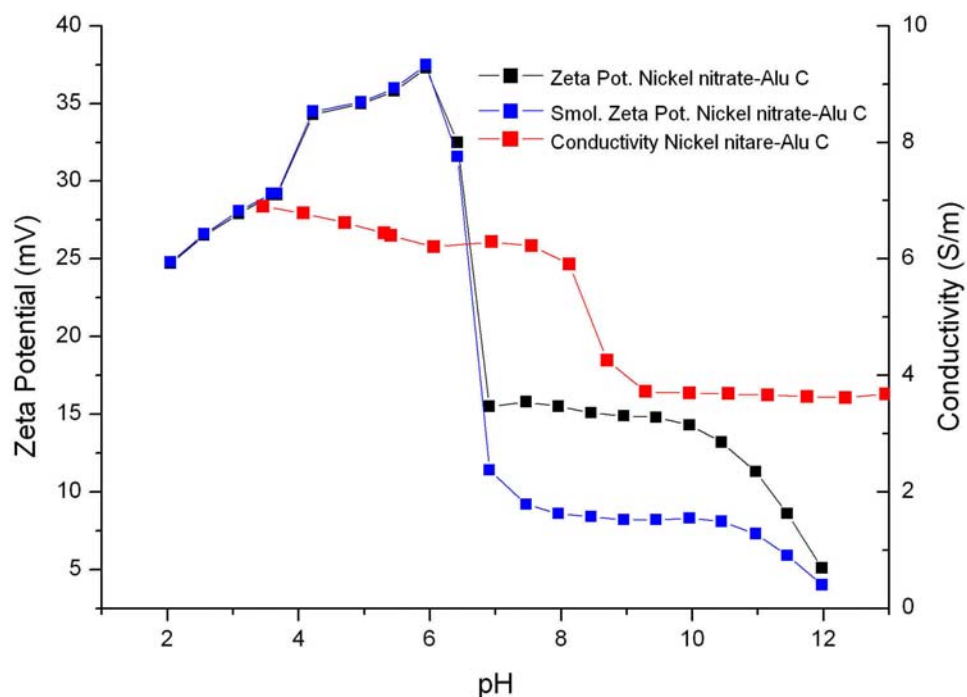


Fig. 6-30: Zeta potential and conductivity of aqueous *nickel nitrate-Alu C* suspension.  
Alu C wt. % = 4.32, Nickel nitrate wt. % = 13.51

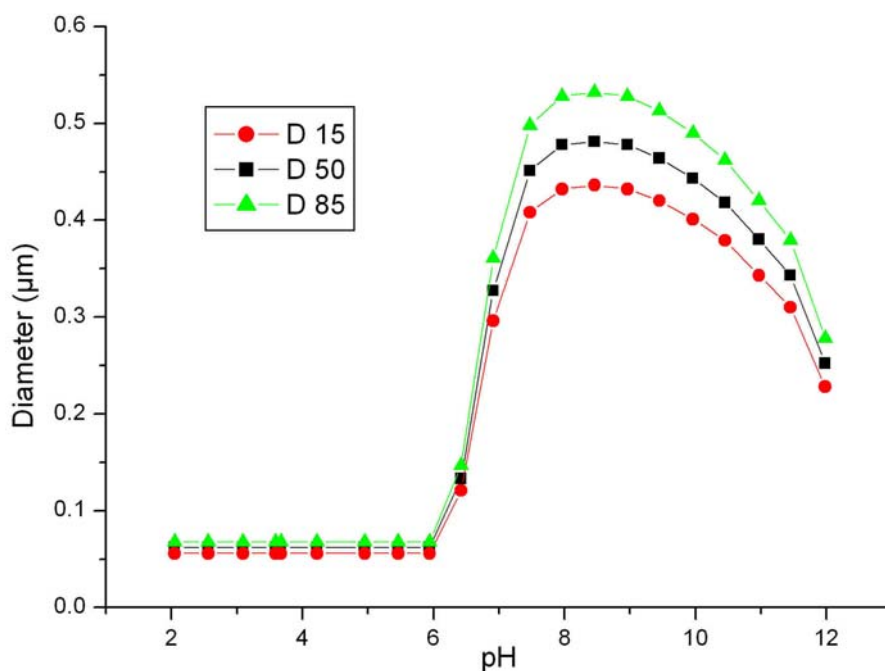


Fig. 6-31: Particle size distribution of aqueous *nickel nitrate-Alu C* suspension.  
Alu C wt. % = 4.32, nickel nitrate wt. % = 13.51

Comparing both suspensions shows that the maximum zeta potential of the *nickel nitrate-Alu C* suspension is about 16 mV less than that of Alu C suspension.

Moreover, in the presence of metallic and nitrate ions no negative potential is created and conductivity is one order of magnitude higher than that of pure alumina suspension.

### 6D.2.2 Effect of ultrasound dispersion

Flocculation of alumina particles in poorly dispersed slurry would influence the rheological properties of the slurry. As explained in chapter 3, it is preferred to disperse nano-powders with an ultrasonicator. In Fig. 6-32, effect of mechanical dispersion, with and without ultrasonification, on viscosities of aqueous and non-aqueous *nickel nitrate-Alu C* suspensions (contained 4.3 wt Alu C. % and 13.51 wt. % nickel nitrate) is shown.

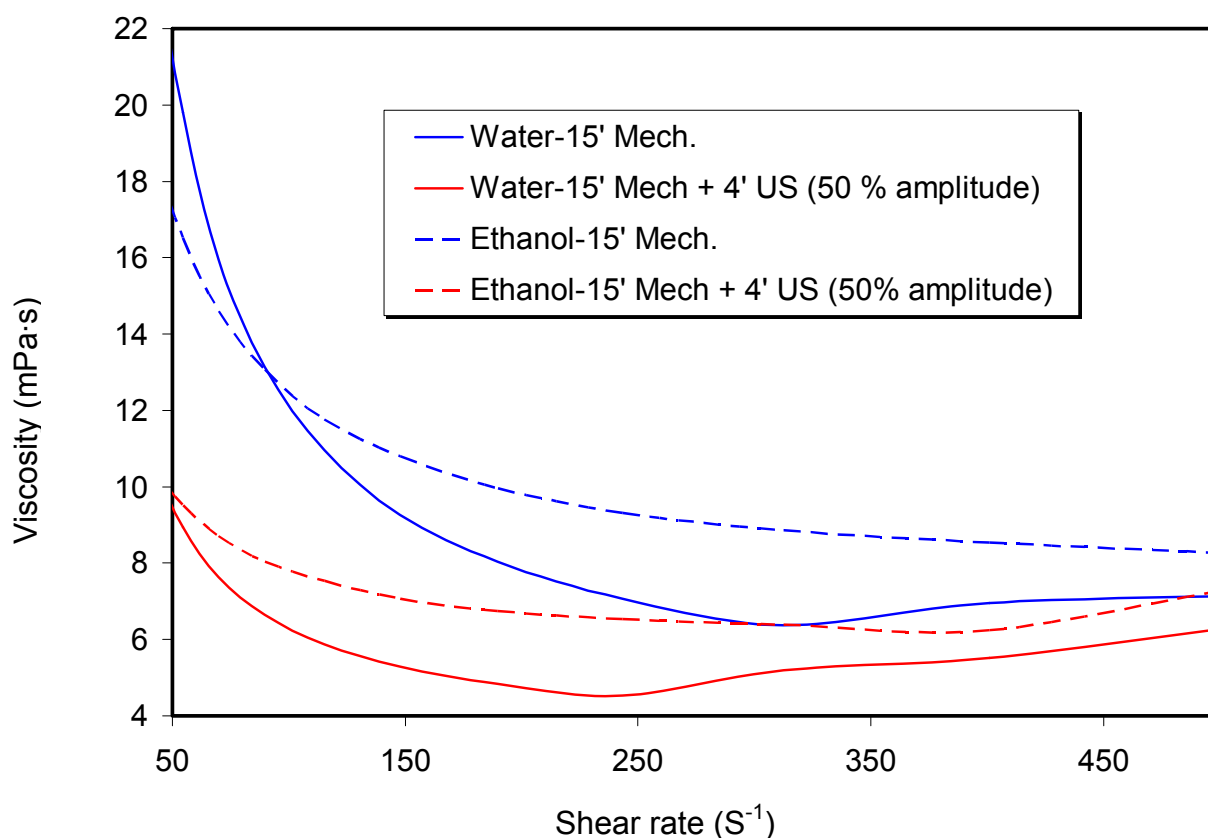


Fig. 6-32: Effect of ultrasound and mechanical dispersion on viscosity of the aqueous and non-aqueous *nickel nitrate-Alu C* suspensions (“US” stands for Ultra-Sound)

It is seen from Fig. 6-32 that mechanical dispersion, which followed by an ultrasonic treatment, resulted in lower viscosities for both ethanol- and water-based suspensions, compared to only mechanically dispersed suspensions. This means,



## 6. Results and discussion

ultrasonification had a positive effect in deagglomeration of large aggregates and it should be applied for making well-dispersed suspensions of nano-powders. The same conclusion can be drawn from Fig 6-33, which shows the effect of ultrasound dispersion on particle size distribution of the powders in an aqueous suspension. Aqueous *nickel nitrate-Alu C* suspension was dispersed in two different ways; first time only through mechanical disperser and second time through combination of ultrasonic and mechanical dispersions. Fig. 6-33 shows a broad particle size distribution from 80 nm to 20 micron for the aqueous *nickel nitrate-Alu C* suspension, which is dispersed only mechanically but narrower mono-modal distribution from 75 nm to 400 nm for the same suspension, which was additionally treated with ultrasound waves.

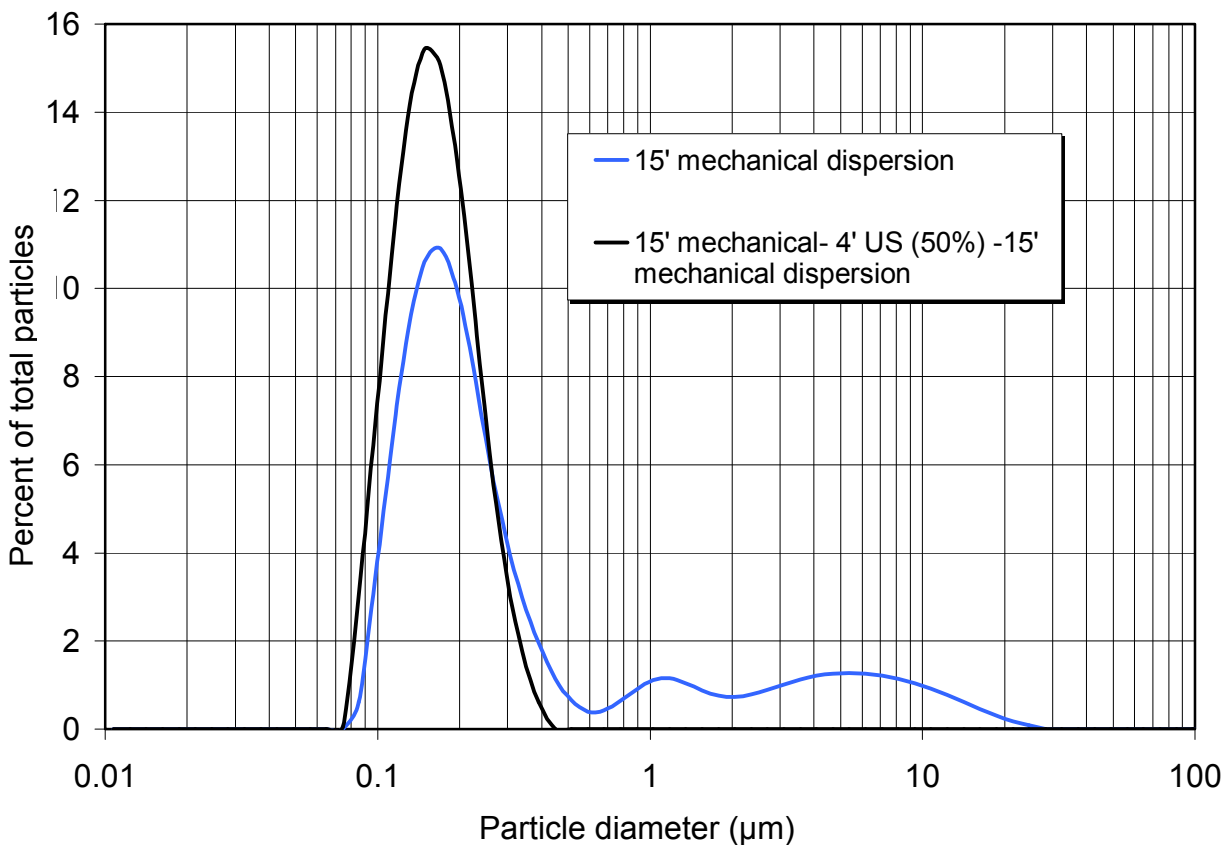


Fig. 6-33: Particle size distributions of aqueous *nickel nitrate-Alu C* suspension (suspension A) under different dispersion conditions (“US” means Ultra-Sound)

### 6D.2.3 Dispersion of non-aqueous suspension and effect of TEOS binder

Adding any additives to a stable suspension would be critical because it can change the double layer of the particles and disorder the electrostatic balance between the

## 6. Results and discussion

particles. Particle size distribution measurement is a useful tool to investigate the effect of adding any additive on stability of the suspensions. In this study using TEOS binder was inevitable because the adhesion and scratch resistance of the cermet coating was not enough good, therefore addition of an adhesion promoter was necessary. Here only ethanol-based suspensions are studied. Fig. 6-34 shows the particle size distributions of non-aqueous *nickel nitrate-Alu C suspension* under different dispersion conditions. It can be seen that dispersions agitated mechanically for 10 minutes were not able to break agglomerates and aggregates effectively. However, with an additional ultrasonic treatment for 4 minutes and amplitude of 50 %, the PSD was reduced by about two orders of magnitude. Simply mixing a stable suspension with the required amount of hydrolyzed TEOS changed the stability of the suspension and created large agglomerations and a bimodal distribution (red curve). Fortunately, mixing TEOS before mechanical and ultrasound dispersions could solve the agglomeration problem so that after dispersion final PSD, which was measured for the mixture of suspension-binder system, was in the same range of particles sizes of the initial well-dispersed suspension (without binder).

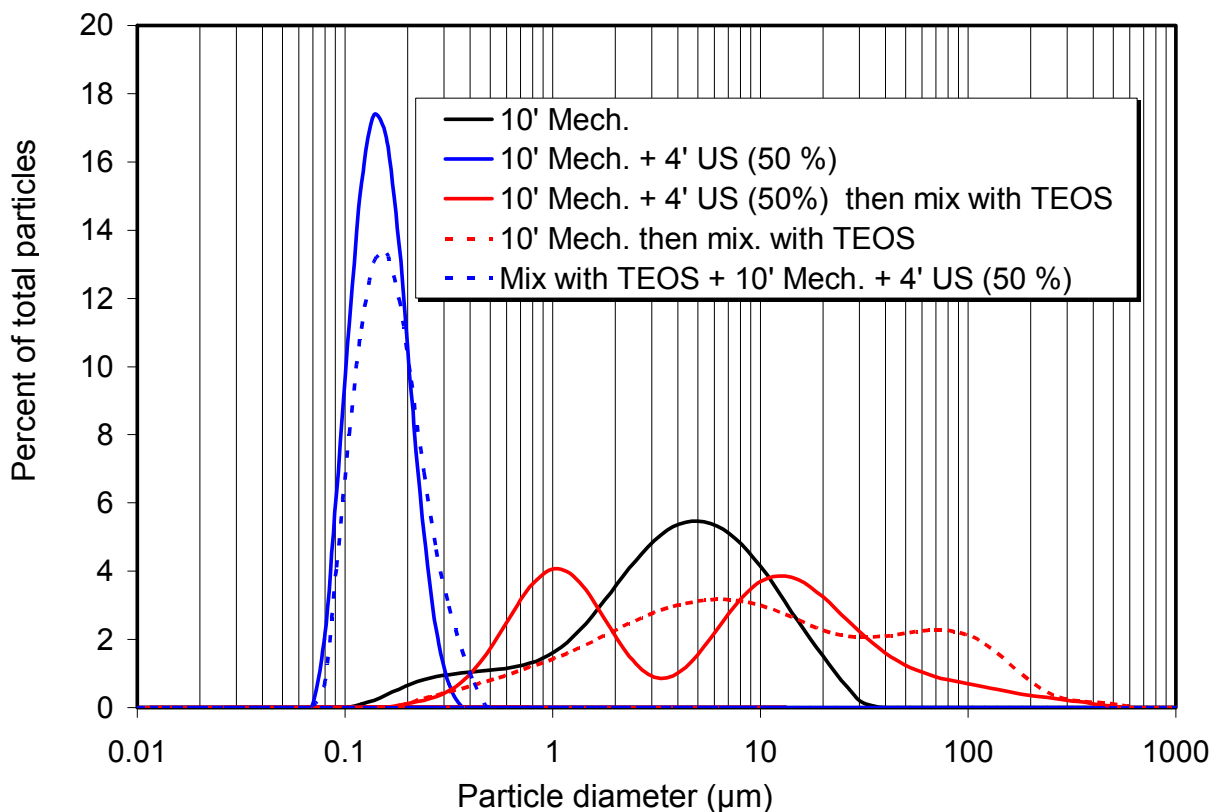


Fig. 6-34: Particle size distributions of non-aqueous *nickel nitrate-Alu C suspension* before and after addition of TEOS and under different dispersion conditions

Comparing Fig. 6-33 with Fig. 6-34 shows that Alu C has been dispersed in water and ethanol in a similar manner so that particle sizes of this powder in both mediums are distributed from 70 nm to 400 nm with an average particle size of around 150 nm.

#### 6D.2.4 ATR spectroscopy of *nickel nitrate-Alu C* suspension

Sedimentation behavior of the suspensions can be monitored using ATR (Attenuated Total Reflection) spectroscopy. Fig. 6-35 shows ATR transmission of aqueous *nickel nitrate-Alu C* suspension (with Alu C content of 4.3 wt. % and nickel nitrate of 13.51 wt. %) measured at different sedimentation times.

Broad absorption band of aluminum oxide is observed between wave numbers of 800 and 930  $\text{cm}^{-1}$ , which is in good agreement with symmetric stretch of  $\text{Al}_2\text{O}_3$  at  $850 \pm 80 \text{ cm}^{-1}$  reported in [115], [116].

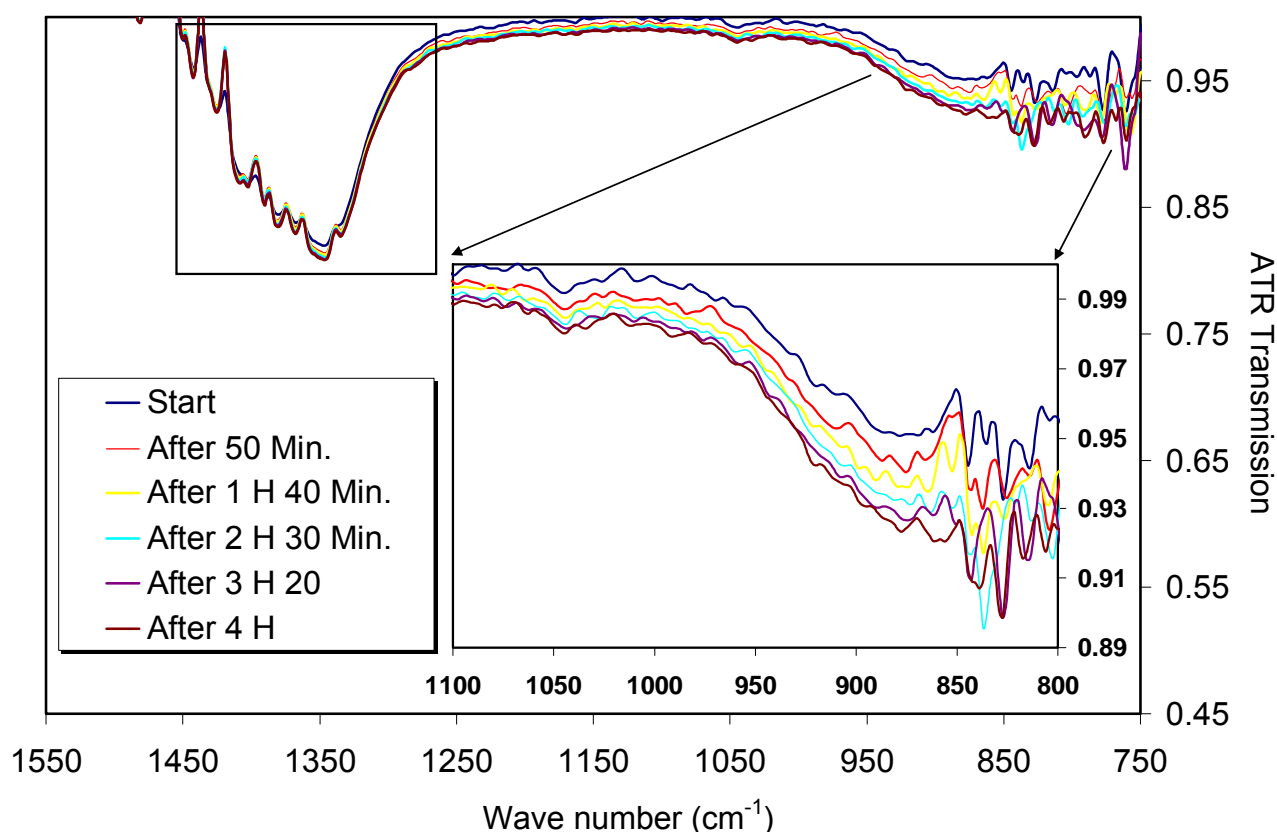


Fig- 6-35: ATR-Transmission of Alu C-nickel nitrate suspension with 4.3 wt. % solid content and after different sedimentation times

The left small box in Fig. 6-35 demonstrates absorption peaks, which belong to  $\text{NO}_3$  ( $1356.2 \text{ cm}^{-1}$ ),  $\text{N}=\text{O}$  ( $1433.3$  &  $1458.3 \text{ cm}^{-1}$ ) and  $\text{N}-\text{O}$   $1492.39 \text{ cm}^{-1}$  stretch bands [117].

After 4 hours, only 3 % decrease in ATR transmission due to the sedimentation is observed. It means that the prepared *nickel nitrate-Alu C* suspension was stable for that period and no significant aggregation and sedimentation occurred in the suspension. The same ATR measurement was done for ethanol based suspension and the same attenuation was observed. Ethanol based suspensions, which had been mixed with TEOS coupling agent, showed about 10 % reduction in transmission after 4 hours. This means that addition of TEOS bounded the particles and changed the interactions between the particles, resulting in a less stable suspension.

### **6D.2.5 Suspensions with different nickel contents**

To study the effect of different nickel volume fractions on optical properties of the Ni- $\text{Al}_2\text{O}_3$  cermet absorber, different suspensions (A to E) were prepared by dissolving different amounts of nickel nitrate into the solvent.

If we ideally consider that no voids would exist in the final cermet layer and all nickel ions are converted to pure nickel particles after deposition, drying and sintering in pure  $\text{H}_2$  atmosphere, then we can use the density of aluminum oxide powder and nickel to calculate the final nickel volume fraction of the sintered cermet layer. According to that, weight percentages of the suspension constituents were determined in a way that final cermet layers with nickel volume fractions of 0.2 to 0.6 can be obtained. In fact, assuming no porosity for a thin film derived from powders is not true. Therefore considered nickel volume fractions are used to entitle suspensions with their nickel volume percentages. It means a 20 % nickel suspension is a suspension, in which the volume percentage ratio of nickel to aluminum oxide is 20 to 80.

Weight percentages of solvent,  $\text{Al}_2\text{O}_3$  and nickel nitrate in a 100 g suspension have been calculated and listed in Table 6-8. Like before, first nickel nitrate was dissolved in distilled water or ethanol and then alumina powder was added to the solution gradually. Powders were dispersed mechanically for 15 minutes, then ultrasonic wave with amplitude of 50 % was applied and finally the ultrasonic treated suspension was re-dispersed mechanically for 15 minutes.

## 6. Results and discussion

Table 6-8: Weight percentages of the suspension constituents, nickel volume percentages and weight fractions of 5 different suspensions

Suspension	Al <sub>2</sub> O <sub>3</sub> (wt. %)	H <sub>2</sub> O or ethanol (wt. %)	nickel nitrate (wt. %)	Initial nickel (weight fraction)	nickel % - Al <sub>2</sub> O <sub>3</sub> % volume percentage in the suspension
A	4.32	82.16	13.51	0.38	20 %-80 %
B	3.98	75.66	20.35	0.50	30 %-70 %
C	3.56	67.80	28.62	0.61	40 %-60 %
D	3.12	59.30	37.57	0.70	50 %-50 %
E	2.62	49.93	47.44	0.78	60 %-40 %

In Fig. 6-36, prepared suspensions of A to E for deposition of cermet layers with different nickel contents are shown. Dissolving more nickel nitrate into the solvent led to suspensions with darker green color. The written percentages from now on refer to suspension volume percentages. A comparison between the real nickel weight fraction in the solid film and the suspension nickel weight fraction can be found in section 6D.4.



Fig. 6- 36: Prepared aqueous suspensions with different nickel contents for deposition of cermet layers

### 6D.2.6 pH and conductivity

pH and conductivity values of aqueous and non-aqueous suspensions, which described in the last section, were measured using pH meter and conductivity meter. The measured values are shown in Fig. 6-37 and 6-38. As pH is a measure of hydronium ions (H<sub>3</sub>O<sup>+</sup>) in the solution, measuring pH of alcohol-based suspensions would give no sense. Although in non-aqueous media, an operational pH scale (pH\*)

## 6. Results and discussion

---

with a  $pH^* = 7.15$  for pure ethanol and an isoelectric point can be defined for the specific solvent [118]. Usually, using a water-based reference electrode for measuring pH of an ethanol-based suspension may result in a sluggish response and the steady state will not be reached after a long time. In this study, pH values of non-aqueous suspensions were measured using a water-based reference electrode but steady pH values were obtained after 5-10 minutes. Existence of six water molecules around the nickel (II) center in the hydrated salt provided enough hydronium ions in the ethanol suspensions to measure a reliable pH value.

It can be seen from Fig. 6-37 that in both ethanol and water systems, dissolving more nickel nitrate decreased the pH value and made the suspension more acidic. Before addition of nickel nitrate only  $H_3O^+$  ions in connection with  $OH^-$  present on the surface of  $Al_2O_3$  but after addition of nickel nitrate, hydronium ions may be displaced with  $Ni^+$  ions and released into the solution (adsorption of  $Ni^+$  is raised with increasing  $Ni^+$  concentration). Such a release of hydronium ions may contribute to a decrease in pH value. Moreover, it is also likewise that different reactions on the particle surface change the balance of ions in the solvent and strong ion difference (SID) influences water dissociation. A decrease in SID will increase hydrogen ion liberation from water.

Since low-dielectric-constant media like ethanol have a low degree of electrolyte dissociation and consequently lower  $H^+$  ion concentration, lower conductivity and pH are measured for non-aqueous suspensions than aqueous suspensions. By calculating water content and hydronium ion concentration of A and E ethanol based-suspensions, a difference of 0.55 in their pH values is expected theoretically. Similar pH difference was measured experimentally for these two suspensions. This indicates that the measured pH values of non-aqueous suspensions are related to their water contents.

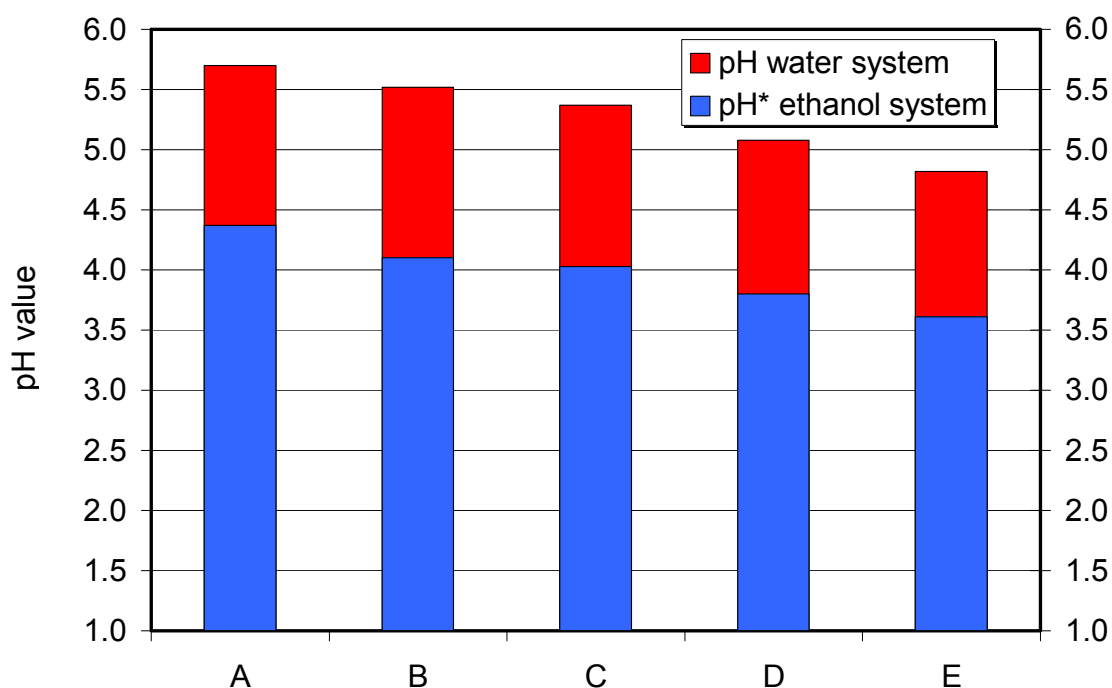


Fig. 6-37: pH values of suspensions A to E

As shown in Fig. 6-38, addition of nitrate and nickel ions has drastically increased the conductivity of both aqueous and non-aqueous suspensions, compared to that of water. It is also obvious that the higher the ion concentration, the higher is the conductivity.

Suspension A without any additives was the most stable suspension among the others and retained its original properties for few days. According to the zeta potential-pH dependency curve of Fig. 6-30, pH of aqueous suspension A is in its optimum value and no base or acid is needed to shift the pH to a position, where the zeta potential is maximum. For other aqueous suspension (B to E) no significant instability was observed for short terms and therefore their  $\zeta$ -pH curves were not measured. Experimentally it was observed that alcohol based suspensions are as stable as aqueous suspensions. Unfortunately, the Acoustosizer was not able to measure the zeta potential of alcoholic suspensions. In addition to ATR spectroscopy, the colloidal stability of ethanol suspensions was visually studied by letting them in a covered test tube at room temperatures and monitoring the sedimentation under different pH values.

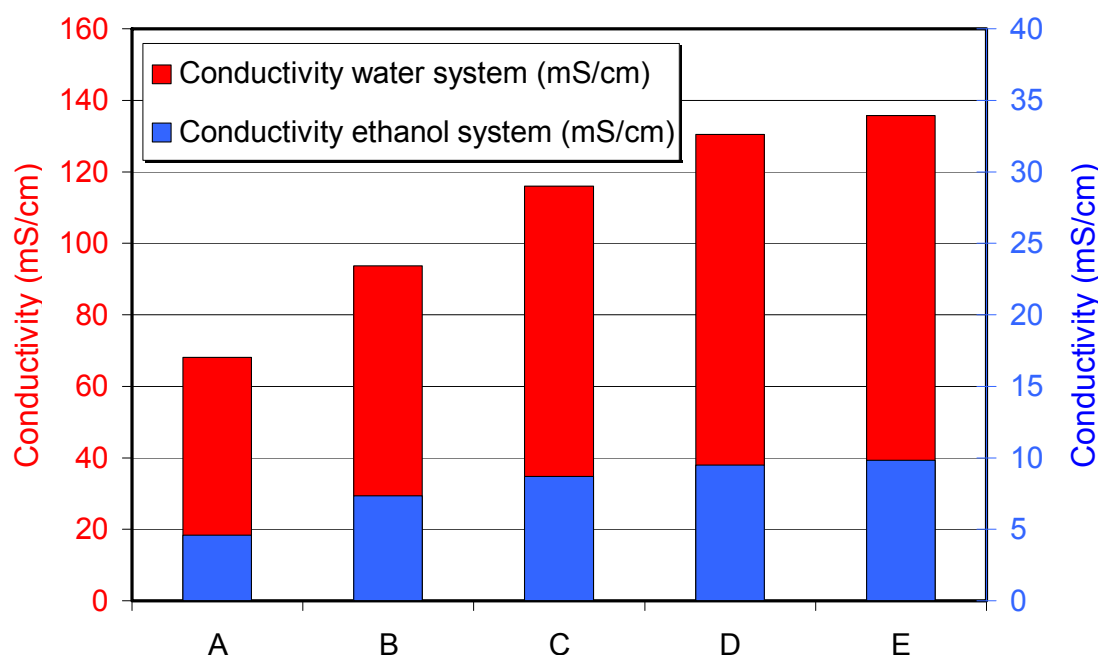


Fig. 6-38: Conductivity of suspension A to E

In comparison to aqueous suspensions, there is experimental evidence that a substantial surface charge density with the associated counterion layer also can be created in ethanol media [118]. In alcohol-based suspensions, due to low degree of electrolyte dissociation, very long-range double-layer is created resulting in a slowly decaying potential and much weaker repulsion between charged particles. The surface potential and the ionic strength in the solution are the two most important parameters controlling electrostatic stabilisation in aqueous as well as non-aqueous media. The ionic strength controls the range of the double-layer repulsion so that low ionic concentration in a non-aqueous suspension leads to enormous Debye lengths, resulting in weaker forces of repulsion than found in aqueous systems [119]. In this study ionic strength of the ethanol suspensions were significantly increased by dissolving nickel nitrate into the ethanol medium and because of that good colloidal stability obtained. ATR and sedimentation monitoring of solid particles confirmed having good colloidal stabilities for the most of non-aqueous suspensions. Only at very high nickel concentrations (like suspensions D and E), slight sedimentation was observed after few hours. This can be explained by less stability due to the reduced zeta potential of high acidic mediums and overlapping thick stern layers of the particles.



### 6D.2.7 Conclusions

- There was a large difference between the particle size distributions of nano Alu C powders measured by Mastersizer and Acoustosizer. The particle size distribution measured using Acoustosizer was narrower and closer to the real sizes measured by analyzing SEM images.
- By adjusting pH value of the *nickel nitrate-Alu C* suspension between 4 and 6, one can get a well-dispersed colloidal coating suspension (with nickel content of 20 %).
- Only suspensions with solid contents less than 10 wt. % and preferably less than 5 wt. % are suitable for deposition of high quality thin films. Aqueous and non-aqueous suspensions should have Newtonian behavior and viscosities less than 10 mPa·s.
- Comparing to mechanical dispersion, ultrasonic dispersion had a positive effect on dispersion of nano powders. Using ultrasonic treatment large aggregates were broken more effectively and suspensions with lower viscosity were obtained.
- In non-aqueous suspensions, water content of the hydrated nickel salt and high ion concentration of the electrolyte provided enough repulsive forces between the particles so that it became possible to stabilize ethanol-based suspensions electrostatically.
- In both aqueous and non-aqueous suspensions, increasing nickel nitrate decreased the pH value and increased the conductivity of the suspension.
- Addition of TEOS destabilized the dispersed suspension but after new dispersion of additive and initial suspension, stable coating suspension with narrow PSD and fine particles obtained.
- By measuring ATR transmission, no significant sedimentation occurred for *nickel nitrate-Alu C* suspension for a measuring period of 4 hours. In comparison, TEOS contained suspensions was less stable. ATR Spectroscopy, PSD measurement and visual observation confirmed that alcohol based suspensions were as stable as aqueous suspensions.

### 6D.3 Heat treatment in H<sub>2</sub> atmosphere

After drying and annealing the prepared thin films, nickel ions probably would be changed to nickel oxide. To achieve spectral selectivity, it is necessary to reduce all nickel oxides to pure metallic nickel crystals. For that purpose all the prepared samples were heat treated in a pure H<sub>2</sub> atmosphere after drying. Instead of forming

## 6. Results and discussion

---

gas ( $N_2+H_2$ ), pure  $H_2$  atmosphere was preferred to avoid any possible oxidations at higher temperatures.

Because of the need to a non-oxidizing environment during sample's annealing, heat treatment technique has to be carefully designed. Lower sintering temperatures and short dwelling time at peak temperature is favoured because it avoids growing large nickel crystallites, undesired oxidations and diffusion of substrate material into the film. According to the study of Rao on kinetics of nickel oxide reduction with hydrogen [120], a 53  $\mu m$  thick nickel oxide sample is completely reduced to nickel in 6 hours by tempering at 300 °C or in 10 minutes by tempering at 400 °C.

In this study two sintering profiles were used; 1) Sintering temperature: 450 °C, duration 1 hour, heating rate: 7.5 °C/min. 2) Sintering temperature: 700 °C, duration 30 minutes, heating rate: 7.5 °C/min. Profile 2 was used mostly for annealing thin films deposited on thick copper substrates. By annealing at peak temperature of 700 °C any copper oxide existing on the copper substrate is also reduced to copper. Fig. 6-39 shows a polished aluminium substrate coated through *nickel nitrate-Alu C* suspension, before and after reducing in  $H_2$  atmosphere at 450 °C. A significant colour change from white to dark colour is observable after nickel oxide reduction and sintering. The dark appearing of the final absorber resulted from the absorption effect of the nickel nano-crystals, which have been dispersed in aluminium oxide matrix.



Fig. 6-39: Selective  $Ni-Al_2O_3$  coating derived from an aqueous *nickel nitrate-Alu C* suspension (suspension A) before and after reducing in  $H_2$  atmosphere at 450 °C

### 6D.4 Non-optical characterization of the prepared samples

A cermet layer with a thickness of less than 1  $\mu\text{m}$ , comparable to Fig. 6-40, was deposited on the reflective copper and aluminum substrates. The prepared cermet selective coating was then characterized using XRD, SEM, and EDX analysis. The size of the aluminum oxide particles, size of the nickel crystallites and weight fraction of the nickel in the cermet layer are determined. The effect of annealing temperature on the particle size and reduction of nickel oxide were investigated.

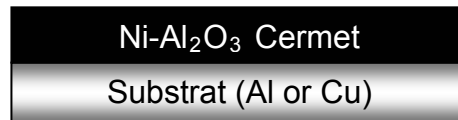


Fig. 6-40: layer configuration of the prepared Ni-Al<sub>2</sub>O<sub>3</sub> solar absorbers with single cermet structure

#### 6D.4.1 Phase identification and crystal size determination by XRD

Standard X-ray diffraction (XRD) characterization was performed for deposited composite thin film before and after reduction at 450 °C for 1 hour in hydrogen atmosphere. Thin film composition and nickel crystal sizes were determined by XRD measurement. For that, single crystalline silicon wafer was used as substrate and it was coated through *nickel nitrate-Alu C* suspension (Suspension A). As-deposited sample was dried and heat treated in air at 450 °C. Similar sample was annealed in the same condition but this time under flow of pure hydrogen. Fig. 6-41 shows the diffraction pattern of NiO-Al<sub>2</sub>O<sub>3</sub> thin film before and after annealing in H<sub>2</sub> atmosphere. °C. For comparison and better characterization, diffraction pattern of Alu C powder is shown in the background with a blue colour.

In X-ray diffraction pattern of NiO-Al<sub>2</sub>O<sub>3</sub>, pure nickel peaks also exist. This means that after heat treatment in air not all nickel ions have been converted to nickel oxide. XRD diffraction pattern of the reduced NiO-Al<sub>2</sub>O<sub>3</sub> coating (Ni-Al<sub>2</sub>O<sub>3</sub>) shows (111), (200) and (222) peaks for nickel, indicating that nickel crystals have not been grown in a preferred orientation. After reduction of NiO-Al<sub>2</sub>O<sub>3</sub> coating in hydrogen atmosphere, the largest NiO (012) peak has been disappeared. In addition, nickel oxide peaks with (202) and (006) planes are no longer observed at double diffraction

angles of 79.3 and 79.5 degrees. It means 1 hour annealing in H<sub>2</sub> atmosphere has effectively reduced the nickel oxide to pure nickel.

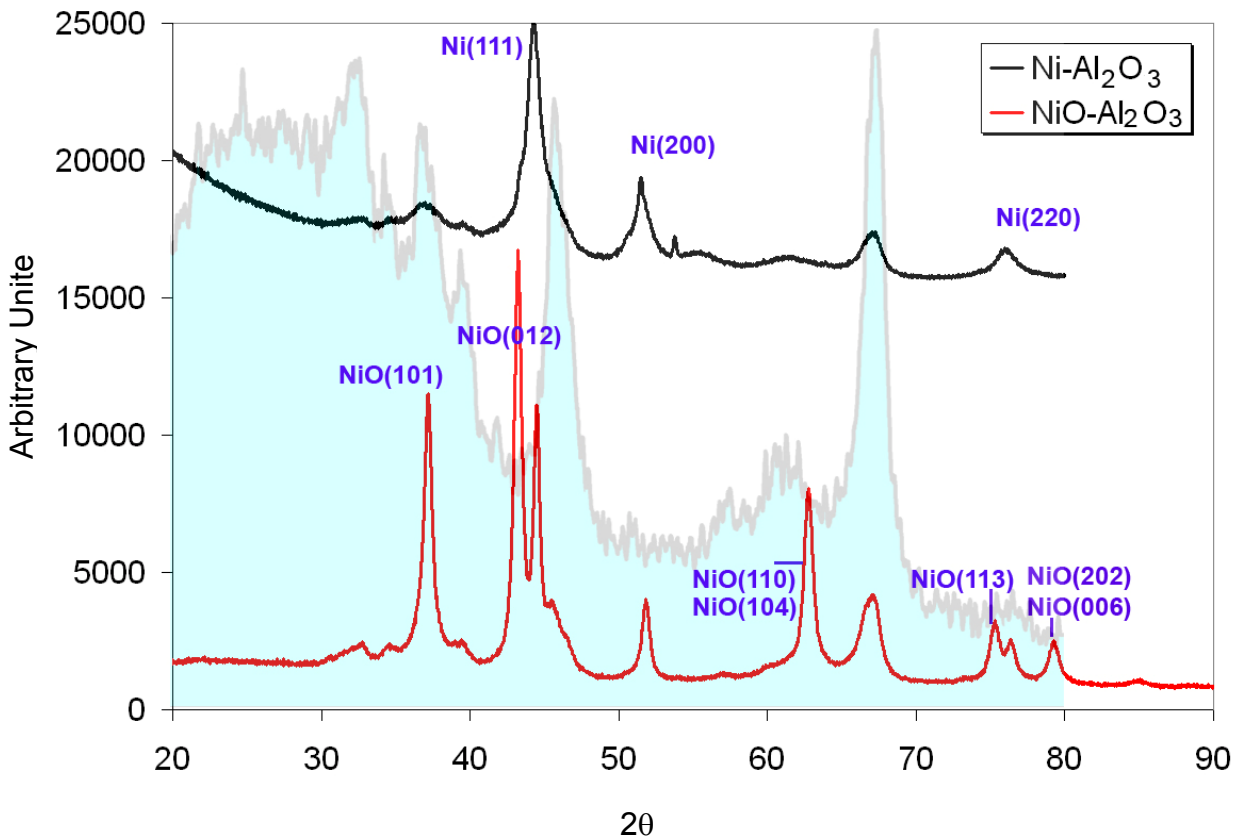


Fig.6-41: Measured X-ray diffraction patterns of NiO-Al<sub>2</sub>O<sub>3</sub> thin film before and after annealing in H<sub>2</sub> atmosphere. Background: Diffraction peaks of Alu C powder

The sizes of the nickel crystallites were calculated using TOPAS software and the Scherrer equation according to the broadening of three peaks of nickel. Peak analyzing by Gauss and Pseudo-Voigt functions both showed crystallite sizes of about 9 to 9.5 nm for the sample annealed at 450 °C. The same measurement for the sample, which was annealed at 700 °C, showed nickel crystallite sizes of about 20 to 28 nm depending on the considered diffraction peak.

#### 6D.4.2 SEM Characterization

##### Coatings derived from aqueous suspension

Surface and microstructure of Ni-Al<sub>2</sub>O<sub>3</sub> cermet selective coatings were characterized using SEM. Fig. 6-42 and 6-43 show SEM images of the cermet thin films prepared from aqueous suspension (suspension A) and annealed at 450 °C and 700 °C,

## 6. Results and discussion

---

respectively. As expected, the cermet layer consists of nano-particles having a regular spherical shape. Sizes of the particles are about 10 to 50 nm that is lower than particle sizes measured by Acoustosizer or Mastersizer. Growth of the particles with sintering temperature is clearly observed so that particles of the sample annealed at 700 °C are larger than those of the sample prepared at 450 °C.

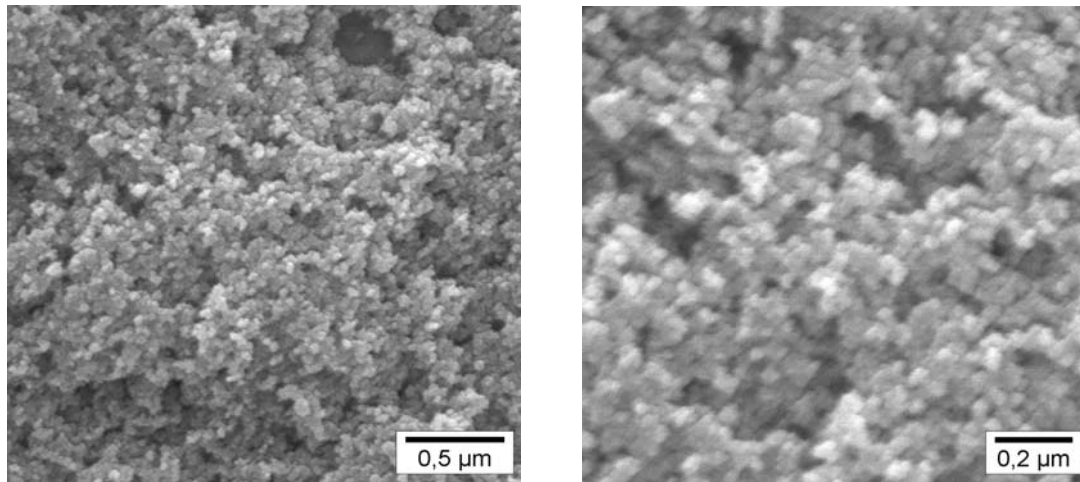


Fig. 6-42: Surface of Ni-Al<sub>2</sub>O<sub>3</sub>/Cu absorber annealed at 450 °C for 1 hour in H<sub>2</sub> atmosphere

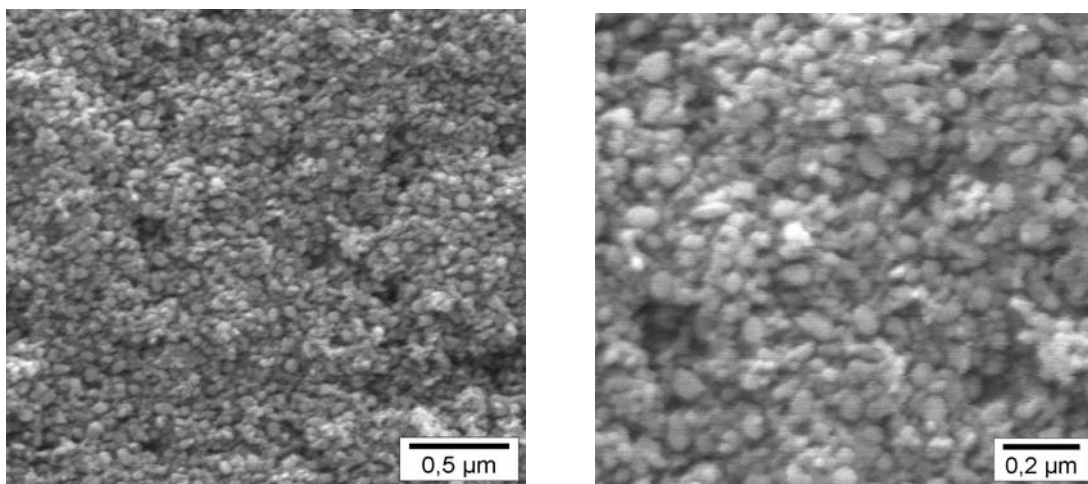


Fig. 6-43: Surface of Ni-Al<sub>2</sub>O<sub>3</sub>/Cu absorber annealed at 700 °C for 30 minutes in H<sub>2</sub> atmosphere

Fig. 6-44 shows cross sectional view of the Ni-Al<sub>2</sub>O<sub>3</sub> absorber coating, prepared at 450 °C. Thicker coating was deposited on the substrate to get a better substrate-thin

film contrast. It can be concluded that the film is not very porous and almost a homogenous dense layer can be derived through this fabrication technique.

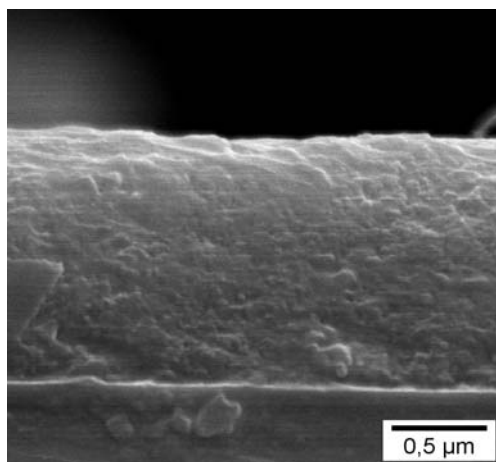


Fig. 6-44: Surface of Ni-Al<sub>2</sub>O<sub>3</sub>/Cu absorber annealed in H<sub>2</sub> atmosphere at 450 °C for 1 hour

### Coatings derived from non-aqueous suspension

Suspension A and B were prepared but this time ethanol was used as dispersing medium. The deposited thin films were dried and then annealed in hydrogen at 450 °C for 1 hour. As shown in Fig. 6-45, the prepared Ni-Al<sub>2</sub>O<sub>3</sub> selective absorbers have particles with the sizes ranging from 10 to 30 nm. This shows that the dispersion and stability of the ethanol suspension was good enough to avoid formation of large agglomerations. It is not possible to distinguish nickel crystallites among aluminium oxide particles.

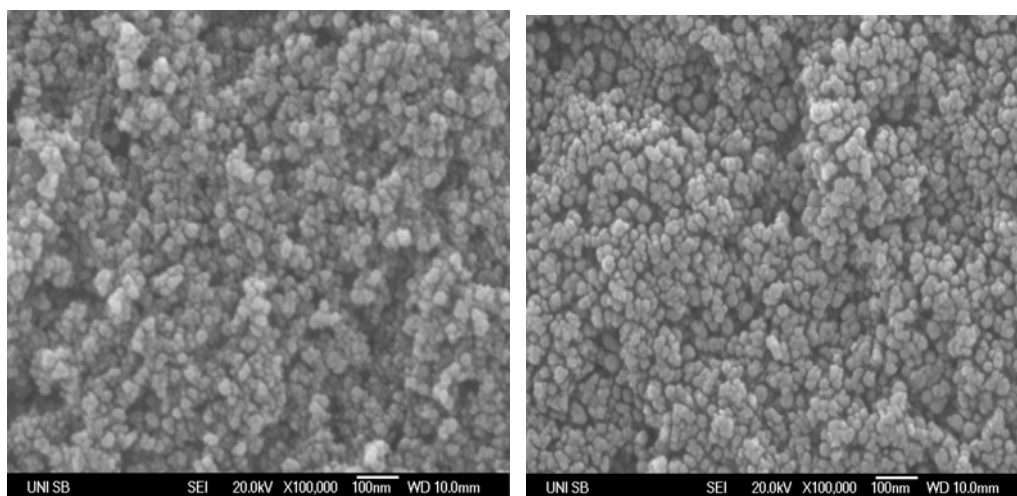


Fig. 6-45: Surface image of Ni-Al<sub>2</sub>O<sub>3</sub>/Cu absorber derived from ethanol-based suspensions A (left) and B (right)

Particle sizes of the sample prepared from suspension B are slightly higher than the particle sizes of the sample prepared from suspension A.

### 6D.4.3 EDX analysis

Energy dispersive X-ray analysis (EDX) was used for the characterization of the compositions and ratio of the nickel/ $\text{Al}_2\text{O}_3$  in the samples. Four different ethanol based suspensions (suspensions A, B, C and E) were prepared. Single crystal silicon wafer was used as substrate and thin film of cermet material deposited on it and processed like before. EDX spectra of the samples prepared from suspension B and E are shown in Fig. 6-46.

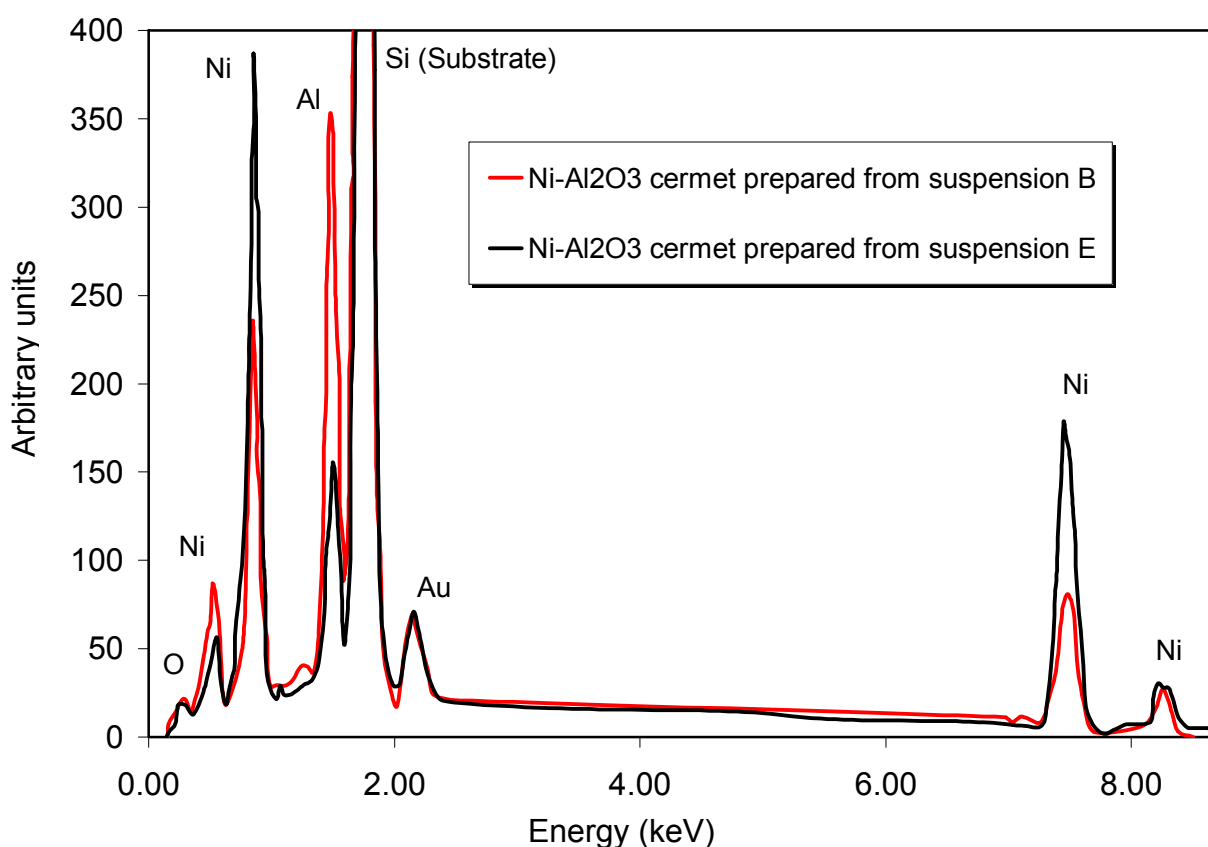


Fig. 6-46: EDX spectra for Ni- $\text{Al}_2\text{O}_3$  selective absorber prepared from non-aqueous suspensions B and E

The peak positions are specific to a particular element and intensity (height) is proportional to its relative abundance. Take-off angle for EDX measurement was  $35^\circ$  and accelerating voltage set on 20 KV. In addition to qualitative analysis, quantitative

## 6. Results and discussion

---

analysis was done on the cermet samples prepared from suspensions with different amounts of nickel. The silicon peak of the substrate was ignored and according to the peak intensity of each element, atom percentage and weight percentage of that element were calculated. In Table 6-9 measured weight percentages of the elements, which exist in the composition of cermet thin films, have been listed. Comparing these results with the weight fractions of the initial formulation (see Table 6-8) shows, that weight fraction of the nickel in the final cermet layer is approximately 10 to 20 % less than initial nickel weight fraction, which existed in the suspension. This deviation is still within the precision of the technique ( $\pm 20\%$ ). It is interesting that the measured values of the nickel weight fractions are very close to the volume percentages of nickel in the suspension.

Table 6-9: Summary of EDX elemental analysis of cermet thin films prepared from suspensions with different amounts of nickel

	element wt. % suspension A	element wt. % suspension B	element wt. % Suspension C	element wt. % suspension E
Aluminum	35.32	32.5	8.52	18.13
Nickel	21.68	27.01	48.21	57.87
Oxygen	42.99	40.49	43.27	24
Substrate	Si	Si	Si	Si

### 6D.4.4 Adhesion test

The mechanical properties of pure Ni-Al<sub>2</sub>O<sub>3</sub> cermet layer are poor as the layers are easily removed after tape test (See Fig. 6-47). To improve the adhesion of cermet thin films to the substrate, an inorganic coupling agent, which can tolerate high temperatures, is needed. Silane based coupling agents are interesting candidates because after decomposition of their organic part, only pure amorphous SiO<sub>2</sub> would remain between aluminum oxide particles and at the substrate/ film interface. Fortunately, existence of such SiO<sub>2</sub> network in the cermet layer will not destroy the spectral selectivity of the Ni-Al<sub>2</sub>O<sub>3</sub> cermet layer. It can even improve that by reducing the normalized refractive index of the cermet layer.

Al-Daoudi could improve the adhesion of his powder-derived ITO layers by using TEOS, GPTS and MPTS coupling agents [121]. Silanes are very effective at improving adhesion between two otherwise incompatible materials. As adhesion



## 6. Results and discussion

---

promoters, silanes bind the coating chemically to the substrate through a silane bridge [122]. This is therefore attributed to the building of a silica network (Si-O-Si) during the polymerization and condensation of the functionalized silanes. It is possible that the functional groups on the substrate surface also react with the silanol functional group (SiOH) to create strong bond.

In this study, TEOS (tetraethyl orthosilicate) was used as the coupling agent. Addition of TEOS silane modifier to the coating suspension provided excellent bonding to the substrate (see Fig. 6-47). All coatings showed an excellent adhesion to the substrate in agreement with the tape test procedure (DIN 58196-K2). TEOS could improve also the scratch resistance of the films, so that only slight scratches were observed for these coatings.

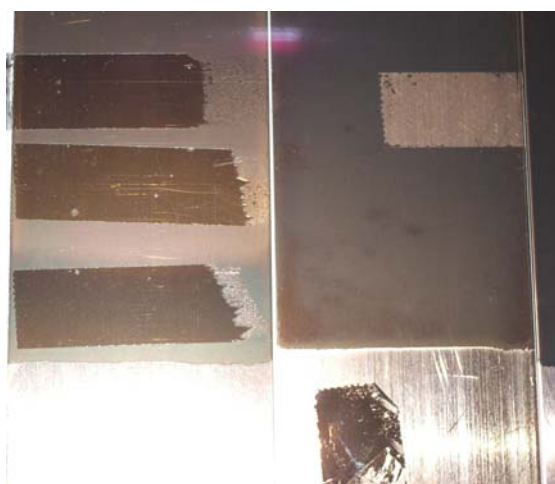


Fig. 6-47: Scotch adhesion test on the samples, prepared with or without TEOS coupling agent

TEOS must be hydrolyzed before use. The reaction proceeds via a series of condensation reactions that convert the TEOS molecule into a mineral-like solid via the formation of Si-O-Si linkages. Rates of this conversion are sensitive to the presence of acids and bases, because both serve as catalysts. In this study one mole TEOS was hydrolyzed using 4 moles 0.1 molar HCl-water solution and 4.6 moles 1-propanol. It is particularly noteworthy to notice that only a relatively small amount of this coupling agent is sufficient to enhance the mechanical properties of the Ni-Al<sub>2</sub>O<sub>3</sub> films. Better mechanical properties are obtained when the amount of silane is increased.

### 6D.4.5 Conclusions

- Annealing wet thin films in H<sub>2</sub> atmosphere at 450 °C reduced nickel oxides to pure nickel. It even changed the colour of the samples from white to dark black-brown.
- Analysis of diffraction peaks showed crystallite sizes of about 9 to 9.5 nm for the sample annealed at 450 °C and 20 to 28 nm for the sample annealed at 700 °C.
- SEM micrographs approved that cermet layer consists of spherical nano-particles with sizes ranging from 10 to 50 nm. The porosity of the prepared cermet layer was not high and cross section view of the deposited layer showed homogenous and dense layer.
- According to the EDX measurements, weight fraction of nickel in the final cermet layer was approximately 10 to 20 % less than initial nickel weight fraction, which existed in the suspension.
- Addition of TEOS silane coupling agent to the coating suspension provided excellent adhesion of the cermet thin film to the substrate.

### 6D.5 Optical characterization of the prepared samples

Aqueous suspensions were used along of this study for developing the method and verifying the possibility of using nano-powder suspensions for making cermet thin films. Nevertheless, for final optical characterization and optimization, cermet layers derived from ethanol suspensions were preferred due to their better thin film quality. In comparison to the water, evaporation point of ethanol is lower and the resulted wet film is dried quicker. In addition, ethanol has higher surface wettability and wets the substrate surface better. Due to these advantages, it was preferred to conduct cermet optimization and absorber durability tests also on ethanol-derived absorbers. Hydration possibility of aluminum oxide powders in adjacent to the water was another reason, which persuaded us to use ethanol as disperse medium.

### 6D.5.1 Effect of nickel volume fraction on spectral selectivity

#### 6D.5.1.1 Aqueous suspensions

Many copper substrates were coated using aqueous coating suspensions and spin coating deposition method. In spin coating, only a small piece of polished copper was enough to conduct the deposition. Therefore, small copper substrates were prepared and polished. A cermet layer was then deposited on the substrate at a given rotational speed. The higher the speed the thinner is the thickness of the cermet layer.

To see the effect of nickel content on the optical property of the sintered cermet layer, different aqueous suspensions of B to E were prepared. It was supposed ideally that thin films of suspension B to E would have nickel volume percentages of 30 to 60 % (see Table 6-8). These nickel percentages are used for presenting the effect of nickel content on the optical properties of the cermet.

The prepared copper substrates were deposited at a constant revolution speed of 12000 rpm using suspensions B to E. This enabled us to investigate the effect of different nickel contents on the optical property of a cermet layer with a given thickness. As the difference in viscosities of the suspensions B to E was not large, the thicknesses of the deposited layers at speed of 1200 rpm were considered equal. As shown in Fig. 6-48, increasing the nickel in the cermet layer significantly decreased spectral reflectance of the absorber layer for wavelengths between 1.7 to 10  $\mu\text{m}$ . At 60 % nickel, a broader absorption peak of aluminium oxide is observed. This can be due to the less stability of the suspension E and slightly higher thickness of the film. To have a semi-ideal selectivity, the reflection at transition wavelength of 2.5  $\mu\text{m}$  should be around 0.5. In this case, high solar absorption and high infrared reflection can be obtained simultaneously. Having a cut-off wavelength (transition wavelength from low to high reflectivity regions) higher or lower than 2.5  $\mu\text{m}$  would lead to a higher solar absorptance and thermal emittance or lower solar absorptance and thermal emittance, respectively.

According to the reflectance curves of Fig. 6-48, it is seen that the cermet layer prepared from aqueous suspension C shows the best spectral selectivity. Therefore it can be concluded that 40 % is the optimum nickel content for a Ni-Al<sub>2</sub>O<sub>3</sub> cermet layer derived from an aqueous suspension. Suitable ascending slope from low reflectivity

region to high reflectivity region, cut-off wavelength of around 2.5  $\mu\text{m}$  and high far-infrared reflectivity of this cermet proposes that nickel/ $\text{Al}_2\text{O}_3$  ratio of the suspension C would lead to a cermet with a promising selectivity.

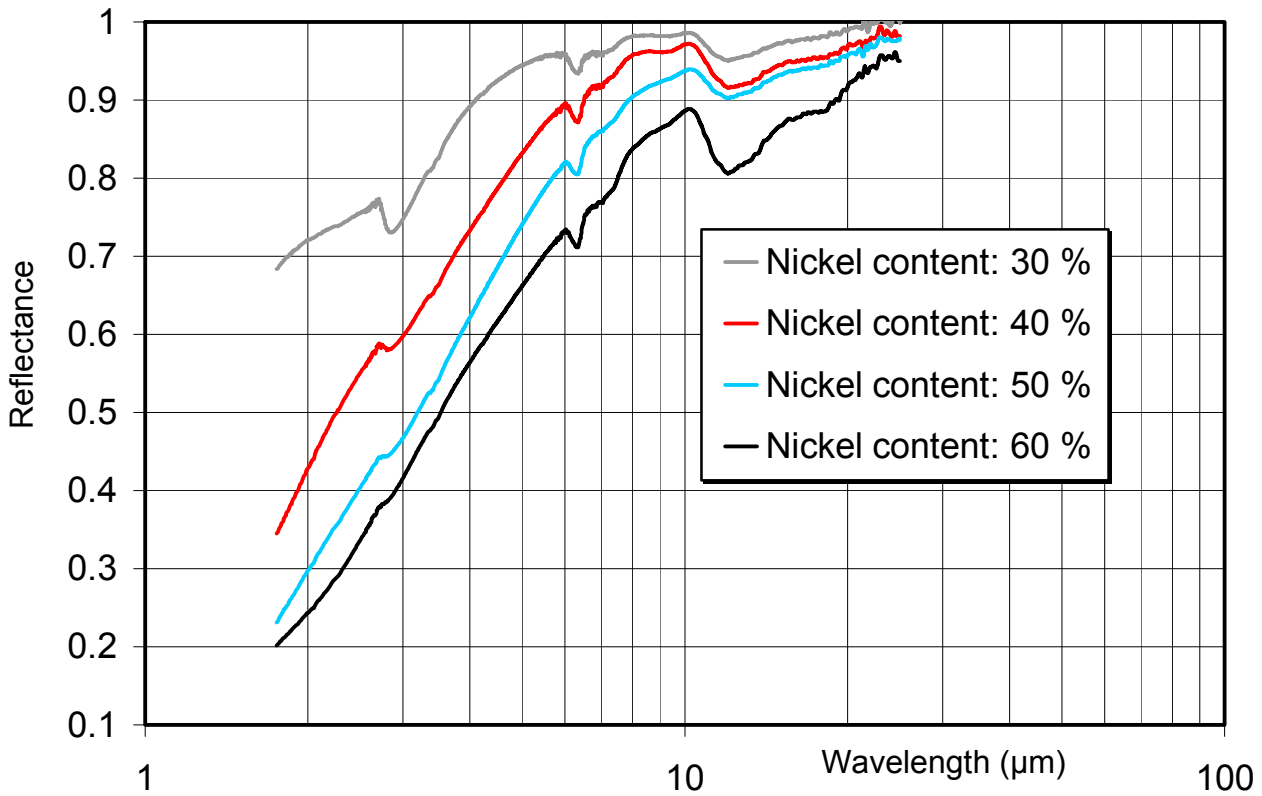


Fig. 6-48: Effect of nickel content on spectral reflectance of a Ni- $\text{Al}_2\text{O}_3$  cermet absorber layer

#### 6D.5.1.2 Non-aqueous suspensions

In this section, similar to the previous section, the effects of the nickel content and cermet thickness on spectral selectivity of the samples derived from non-aqueous suspensions are investigated. Moreover, changes in spectral selectivity due to the addition of TEOS binder are studied and discussed.

Commercially polished aluminum substrates were dipped into the non-aqueous suspensions of A, B, C, D with given nickel contents and withdrawn at different withdrawal speed of 0.5, 1, 1.5, 2 and 3 mm/s. The deposited samples were dried and annealed at 450  $^{\circ}\text{C}$  for 1 hour in a tube furnace as described before. Comparing to the spin coating technique, dip-coating method enabled deposition of cermet coatings of high quality on larger substrates.

All the results, which are presented here and in the following sections, belong to the cermet layers, which were deposited from ethanol-based suspensions by dip-coating technique. Like before, nickel percentage of the suspension is used for presenting the effect of nickel content on the optical properties of the cermet. The real nickel contents of the cermet layers were measured using EDX and are listed in Table 6-9. Reflectance measurements were carried out in order to investigate the spectral selectivity of the prepared samples. In Table 6-10, measured solar absorptance and thermal emittance values of all the samples have been listed.

### **Nickel content: 20 %**

Fig. 6-49 shows the effect of different substrate withdrawal speeds on the reflectance curves of Ni-Al<sub>2</sub>O<sub>3</sub> cermets prepared from suspension A. Suspension A had been formulated so that ratio of nickel to aluminum oxide was 20:80.

It can be seen from Fig. 6-49 and Table 6-10 that for a given nickel content of 20 %, increasing the thickness has increased both the solar absorptance and to some extent the thermal emittance values. Here, increasing the withdrawal speed from 1 mm/s to 3 mm/s, increased the solar absorptance value about 9 % and thermal emittance value about 6 %. Maximum solar absorptance of about 0.7 was achievable with this suspension. The cut-off wavelength has been located around 1 μm. The higher the withdrawal speed, the thicker cermet layer will be obtained and because of that, a dipper aluminum oxide absorption band around 11 to 14 μm is observed. Few interference peaks are also observed only for the thickest sample deposited with substrate withdrawal speed of 3 mm/s.

Diluted hydrolyzed TEOS binder was added to the suspension A in a ratio of 2:9. Adding TEOS to the system changed the selectivity in an interesting manner, so that higher solar absorptivity and better selectivity obtained. Solar absorptance of 0.87 and thermal emittance of 0.08 obtained for the modified Ni-Al<sub>2</sub>O<sub>3</sub> selective absorber. Compared to the non-modified cermet, increase in solar absorptivity was about 25 %. When the substrate is heated in the furnace, the organic silicon compounds form silicon dioxide, e.g. according to the following equation:



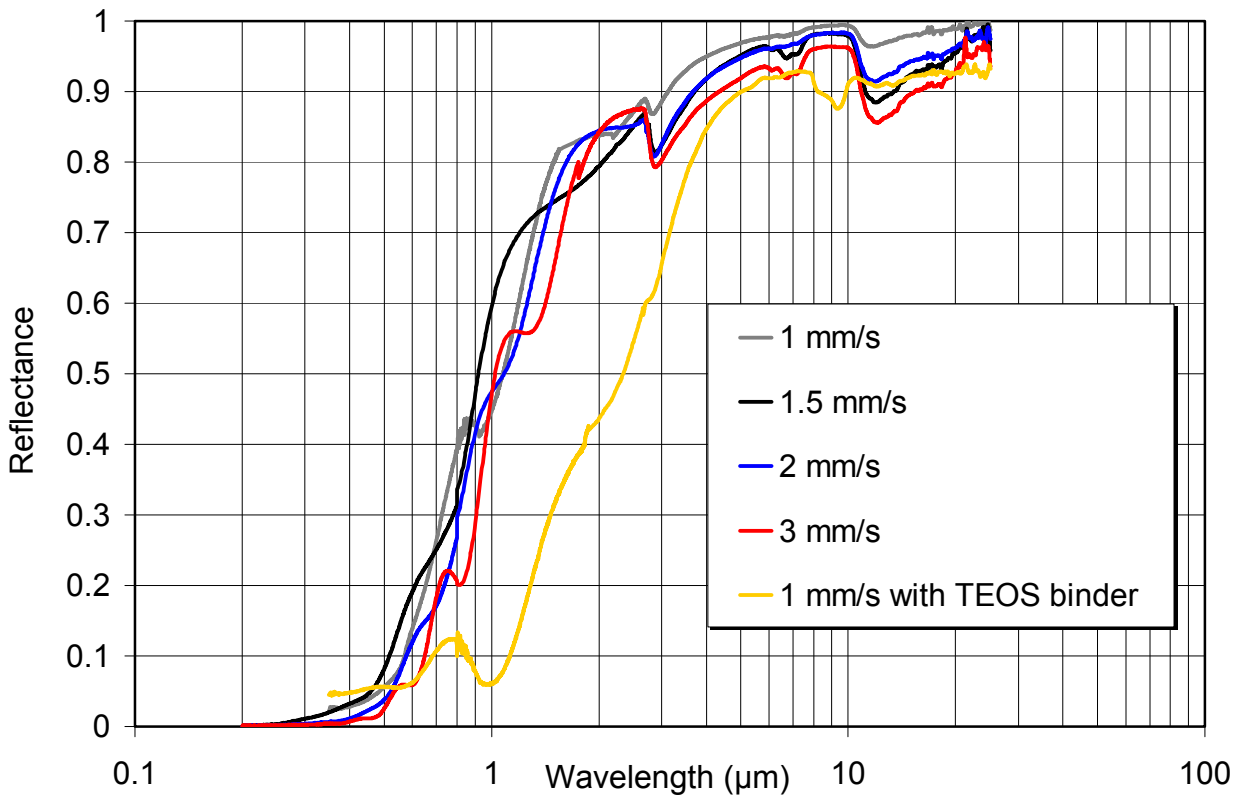


Fig. 6-49: Reflectance curves of Ni-Al<sub>2</sub>O<sub>3</sub> cermet prepared at different substrate withdrawal speeds from suspension A (Nickel content: 20 %)

The developed SiO<sub>2</sub> network would decrease the total refractive index of the cermet layer that is now composed of three components: nickel, Al<sub>2</sub>O<sub>3</sub> and SiO<sub>2</sub>. Compared to Al<sub>2</sub>O<sub>3</sub>, the lower refractive index of SiO<sub>2</sub> decreases the total refractive index of the cermet layer. Because of that, reflection of air/cermet interface for the incoming solar wavelengths would be lower and a higher absorptivity was obtained for the Ni-Al<sub>2</sub>O<sub>3</sub> cermet layer modified with SiO<sub>2</sub>. Now, adjacent to the aluminum oxide absorption band, an additional absorption peak is observed around wavelength of 9.5 μm, which belongs to the SiO<sub>2</sub> and is in good agreement with the active bond-stretching vibration of Si-O group at about 1050 cm<sup>-1</sup>[123]. Addition of diluted TEOS has lowered the viscosity and the overall solid contents of the suspension so that for the modified Ni-Al<sub>2</sub>O<sub>3</sub> cermet smaller absorption band of aluminum oxide is observed. Moreover, due to the dilution of the suspension, absorption band of aluminum hydroxide at 3 μm has been almost disappeared.

**Nickel content: 30 %**

Four single cermet absorbers were prepared with the ethanol-based suspension B. Substrate withdrawal speed varied from 0.5 to 3 mm/s. Suspension B had been formulated so that the ratio of nickel to aluminum oxide was 30:70.

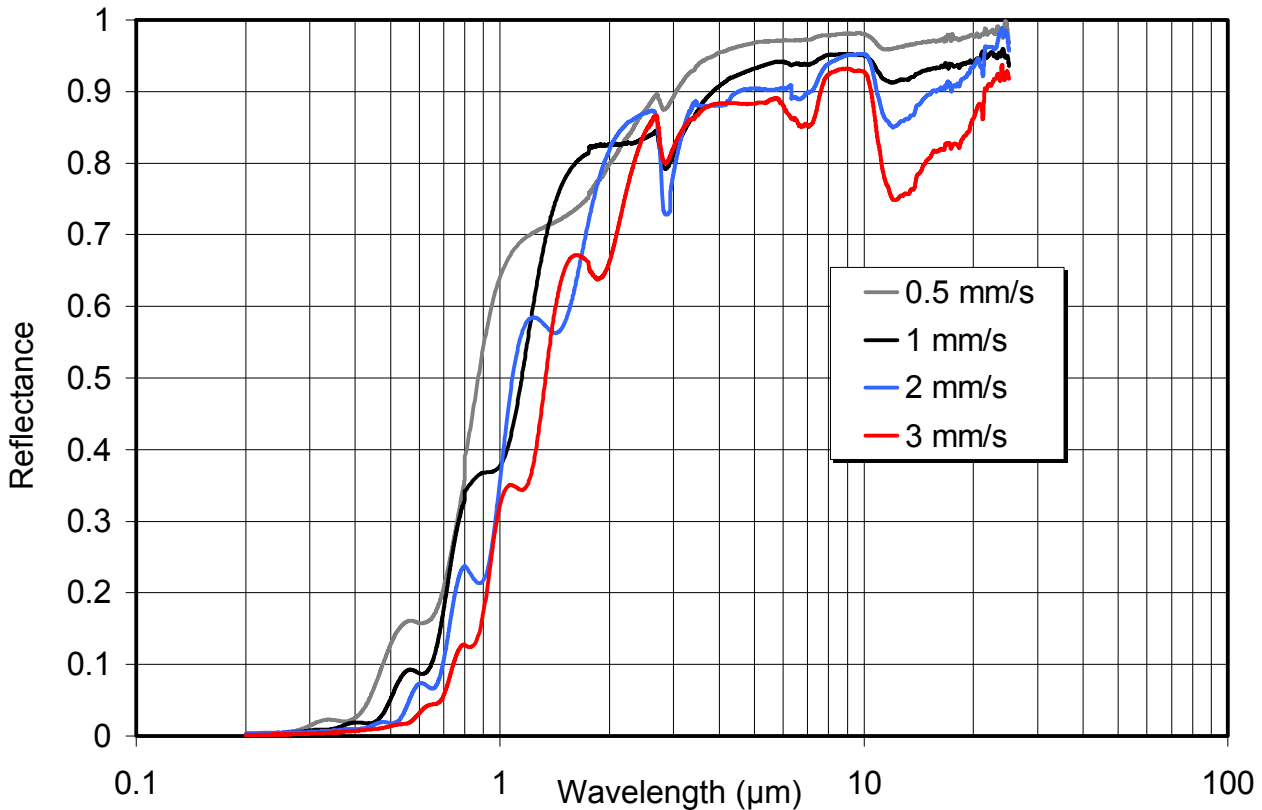


Fig. 6-50: Reflectance curves of Ni-Al<sub>2</sub>O<sub>3</sub> cermets prepared at different substrate withdrawal speeds from suspension B (Nickel content: 30 %)

Fig. 6-50 shows typical reflectance curves of these samples. Cut-off wavelengths of thin samples (with withdrawal speed of 1 or 2 mm/s) are around 1.2 μm but for a thicker cermet, slight shift towards higher wavelengths because of the higher absorption is observed. For example, at 3 mm/s withdrawal speed, the cut-off wavelength is around 1.4 μm.

Depending on the film thickness, solar absorptance values of 0.6-0.78 and thermal emittance of 0.03 to 0.15 were obtained (see Table 6-10). Comparing to the cermet layers with 20 % nickel and similar thicknesses, better selectivity has been obtained. Few interference peaks for the wavelengths between 1 to 3 μm are observed for thick samples (deposited with withdrawal speed of 2 and 3 mm/s).

**Nickel content: 40 %**

Fig. 6-51 shows the effect of different substrate withdrawal speeds on reflectance curves of Ni-Al<sub>2</sub>O<sub>3</sub> cermets prepared from suspension C. Suspension C had been formulated so that the ratio of nickel to aluminum oxide was 40:60.

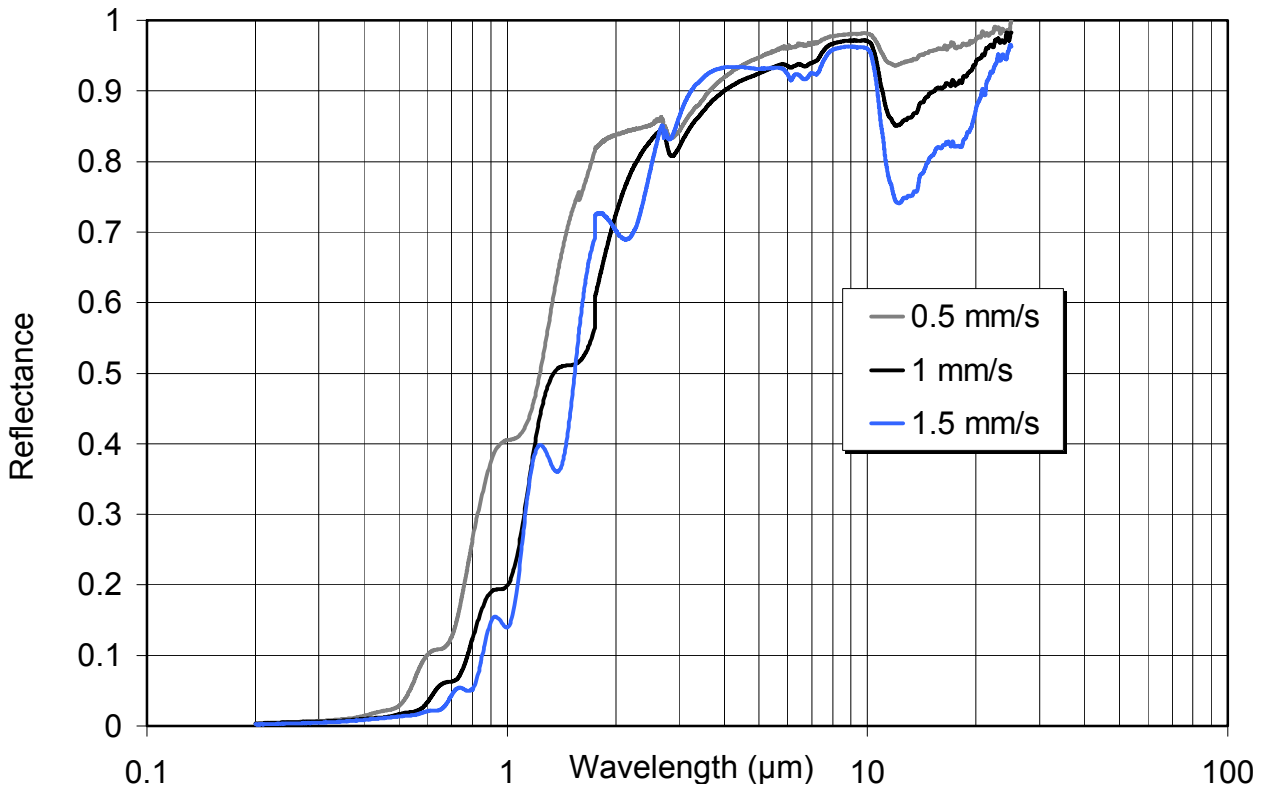


Fig. 6-51: Reflectance curves of Ni-Al<sub>2</sub>O<sub>3</sub> cermets prepared at different substrate withdrawal speeds from suspension C (Nickel content: 40 %)

Three cermet layers with withdrawal speeds of 0.5, 1 and 1.5 mm/s were dip-coated on aluminum substrates. Comparing to the cermets obtained from suspensions A and B, cermets deposited from suspension C show higher solar absorptance due to the lower refractive index and higher extinction coefficient. Solar absorptance values of about 0.80-0.82 and emittance values of 0.07-0.13 were obtained. Transition from low to high reflectance regions occurs now at higher wavelength (around 1.6 μm).

**Nickel content: 50 %**

Using suspension D, only one sample was prepared and for withdrawal speed of 1 mm/s, solar absorptance of about 0.92 and thermal emittance of 0.21 obtained.



## 6. Results and discussion

---

Thicker cermet layers were not investigated because this would lead to higher thermal emittance, which was not desired.

Table 6-10: Effect of nickel content and cermet thickness on the optical properties of Ni-Al<sub>2</sub>O<sub>3</sub> cermet absorbers

Nickel (%)	Suspension	Withdrawal speed (mm/s)	Solar absorptance	Thermal emittance
20 %	A	1	0.624	0.017
20 %	A	1.5	0.602	0.056
20 %	A	2	0.661	0.044
20 %	A	3	0.693	0.081
20 %	A + TEOS binder	1	0.87	0.08
30 %	B	0.5	0.593	0.026
30 %	B	1	0.670	0.063
30 %	B	2	0.722	0.087
30 %	B	3	0.779	0.148
40 %	C	0.5	0.695	0.036
40 %	C	1	0.798	0.075
40 %	C	1.5	0.822	0.13
50 %	D	1	0.917	0.241

### 6D.5.2 Thickness of the deposited cermets

In Fig. 6-52, final Ni-Al<sub>2</sub>O<sub>3</sub> selective absorbers are shown. A cermet layer derived from coating solution A has been dip coated on different substrates like glass, aluminum and copper, at different withdrawal speeds. It can be concluded that by varying substrate withdrawal speed, submicron to micron coatings can be deposited onto different kinds of substrates.

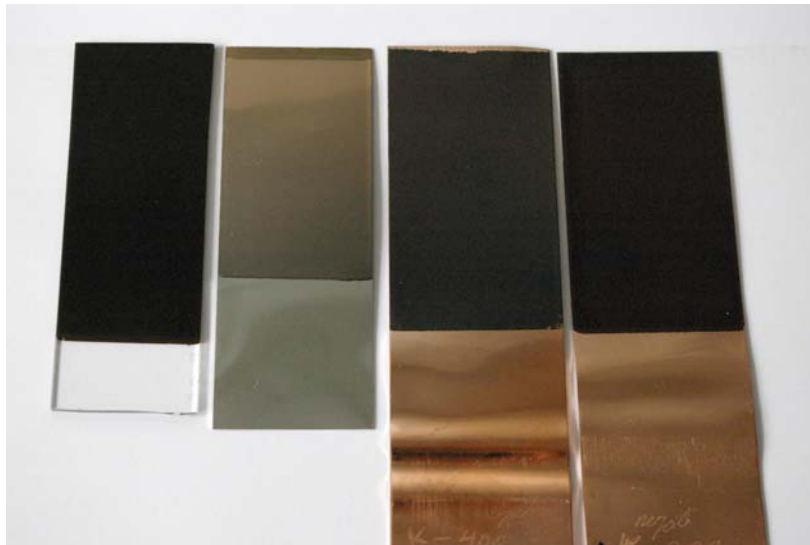


Fig. 6-52: From left to right; glass, aluminum and copper substrates coated with single Ni-Al<sub>2</sub>O<sub>3</sub> cermet layer with different thicknesses

Using stylus profilometer, thicknesses of the dip-coated cermet layers on glass substrates at different withdrawal speeds were measured. Suspension A was used as the coating suspension. As shown in Fig. 6-53 cermet thickness is increased almost linearly by increasing the substrate speed. Lower thicknesses could be achieved by dilution of the suspension or by reducing the substrate speed.

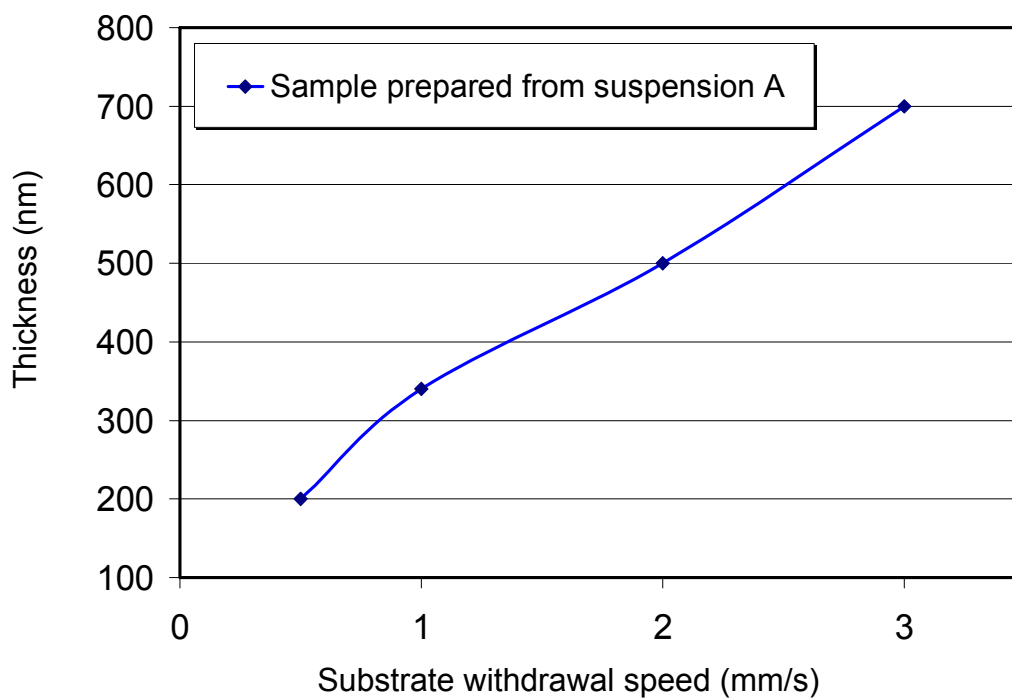


Fig. 6-53: Thickness of the cermet layer deposited on glass substrates which withdrawn from suspension A at different speeds

### 6D.5.3 Conclusions and discussions

- It was shown experimentally that cermet absorption peaks move to lower frequencies with increasing metal volume fraction in dielectric material. This is the same conclusion obtained in [3] according to the theory of the dielectric function of composite materials .
- 40 % was the optimum nickel content in the suspension. Suitable ascending slope from low to high reflectivity regions, cut-off wavelength of around 2.5  $\mu\text{m}$  and high far-infrared reflectivity of the resulted cermet proposes that nickel/ $\text{Al}_2\text{O}_3$  ratio of the suspension C would lead to a cermet with a promising selectivity. The resulted solar selective absorber showed solar absorptance of 0.8 and thermal emittance of about 0.07. For thinner cermet (prepared with low substrate withdrawal speed of 0.5 mm/s), 10 % lower solar absorptance and 4 % lower thermal emittance obtained. Single ungraded cermet layers with homogeneous volume fractions deposited on metal reflectors and coated with an anti-reflection layer show normal solar absorptance of 0.8 [49]. Therefore, the optical properties of developed Ni- $\text{Al}_2\text{O}_3$  selective absorbers in this study are the same as state of the art of cermet absorbers, which are usually produced by sputtering technique.
- By varying substrate withdrawal speed, cermet coatings with submicron to micron thicknesses obtained.
- Addition of diluted TEOS lowered the viscosity and the overall solid contents of the suspension. Moreover, TEOS changed the selectivity of the Ni- $\text{Al}_2\text{O}_3$  absorber in an interesting manner, so that higher solar absorptivity and better selectivity obtained. Solar absorptance and thermal emittance of the modified Ni- $\text{Al}_2\text{O}_3$  selective absorber were 0.87 and 0.08, respectively. Compared to non-modified cermet, increase in solar absorptivity was about 25 %.

### 6D.6 Stability Test

Eight samples were prepared and considered for aging tests. Among them, four samples with the name of 300B, 300D, 300E, 200A were subjected to the high humidity test and samples 300H, 300A, 400A and 400C aged at high temperature. Humidity test carried out in the climate chamber under temperature of 60 °C and humidity of 60 % for 144 hours and thermal aging test was performed on the selected samples for 200 hours at 300 °C.

## 6. Results and discussion

---

First, the optical property of a single cermet layer was measured. Then an anti-reflective coating ( $\text{SiO}_2$  layer) was deposited on the cermet layer and the optical property was measured again. At the end, the anti-reflective coated sample was subjected to the stability tests and the effect of durability tests on its optical properties was investigated. Fig. 6-53 shows schematically the layer orders of the prepared samples for aging tests. In Table 6-11 and 6-12, the parameters  $\alpha$ ,  $\varepsilon_{therm}$  and PC for all samples before and after adding anti-reflective coating and after aging test can be found

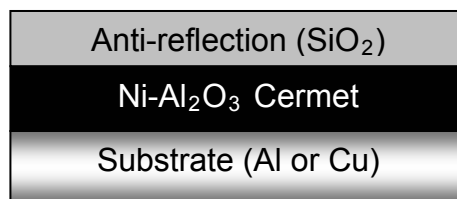


Fig 6-54: Configuration of the Ni- $\text{Al}_2\text{O}_3$  absorber, which was used for durability test

Before applying anti-reflective coating ( $\text{SiO}_2$ ), a base cermet layer made of 40 % nickel suspension deposited first onto all aluminum. The only exceptions were samples 300A and 300E. The aluminum substrates of these two samples, prior to deposition of absorber layer were coated with a silica layer with withdrawal speed of 1 and 2 mm/s, respectively. The used coating solution contained TEOS as coupling agent. Due to that, a strong infrared absorption peak of  $\text{SiO}_2$  is observed around 9  $\mu\text{m}$  (see Fig. 6-55 to 6-62). Adding silica anti-reflection (protective) layer aggravated this absorption peak.

All similar samples like 300H, 300B, 300D, which had a cermet layer deposited by dip coating technique and substrate withdrawal speed of 1.5 mm/s, showed similar selectivity and solar absorptance of about 0.89-0.9 and thermal emittance of about 0.08-0.1. As these samples prepared from suspension, which were manufactured at different times, it can be concluded that through this technique reproducible optical selectivity can be obtained. It should be remarked here that for all samples, fresh hydrolyzed TEOS was used as coupling agent and also as precursor for  $\text{SiO}_2$  anti-reflection or anti-diffusion layer, except for 300E and 300B samples. For these two samples, two days aged hydrolyzed TEOS solution was used which probably more condensation and cross-links of Si-O chains over time changed the slope of the

reflectance curve for wavelengths higher than 3  $\mu\text{m}$ . Applying thin  $\text{SiO}_2$  layer between substrate and cermet layer of samples 300E and 300B, declined the selectivity of these samples.

Comparing to 300 series samples, sample 400A had a thicker cermet layer and showed higher solar absorptance of 0.926 and thermal emittance of 0.133. Oppositely, sample 400C, which had a thinner cermet layer, resulted a lower solar absorptance of 0.843 and thermal emittance of 0.058.

### **6D.6.1 Effect of anti-reflection (protective) $\text{SiO}_2$ layer**

By comparing selectivity of similar samples like 300D, 300G and 300H before and after adding anti-reflective coating, it can be concluded that adding an anti-reflection layer increased the solar absorptance 3 to 8 % and to the same extent the thermal emittance. Such increase in normal thermal emittance value was due to strong absorption band of Si-O in far-infrared region. The highest increase in emittance belongs to the sample 300D that has the thickest anti-reflective coating (deposited with substrate withdrawal speed of 15 mm/s). The most effective anti-reflective coating belongs to the sample 200A that improved solar absorptance of about 0.08 and thermal emittance of about only 0.03.

In fact, the most effectiveness of an anti-reflection is to increase the solar absorptivity by lowering the front surface reflection or by eliminating or shifting the undesired interference peaks located on the high energetic solar wavelengths. Since the prepared  $\text{Ni-Al}_2\text{O}_3$  cermet layers without anti-reflective coatings show very high absorptivity and almost no interference peaks in solar region, no antireflection was necessary. In this study  $\text{SiO}_2$  layer was used to protect the underlay cermet layer against degradations. Small increase in thermal emittance due to the addition of  $\text{SiO}_2$  layer can be tolerated, if such a coating avoid or reduce operational and atmospheric degradations.

### **6D.6.2 Effect of humidity test on the optical properties**

The silica-coated absorbers aged under high humidity atmosphere for 144 hours appeared to be positively affected so that humidity test enhanced the selectivity of the absorbers. The solar absorptance values of the most samples remained unchanged but their thermal emittance values were decreased. In Table 6-11 optical

## 6. Results and discussion

properties of 4 samples (300B, 300D, 300E and 200A), which prepared for humidity test, as well as changes in optical property after addition of SiO<sub>2</sub> protective coating and humidity test are listed. In Fig. 6-55 to 6-58, the related reflectance curves of the samples are shown.

Table 6-11: Optical properties of Ni-Al<sub>2</sub>O<sub>3</sub> cermet absorbers with and without SiO<sub>2</sub> protective coating and after humidity test

Sample Name	Treatment	Withdraw speed for cermet layer (mm/s)	Withdraw speed for SiO <sub>2</sub> layer (mm/s)	$\alpha$	$\varepsilon$
300B	Substrate/Cermet	1.5	--	0.90	0.10
300B	" + SiO <sub>2</sub> protective layer	1.5	1	0.930	0.177
300B	Humidity test	1.5	1	0.930	0.130
300B			PC	$\Delta\alpha$	$\Delta\varepsilon$
300B			-0.0235	0	-0.047
300D	Substrate/Cermet	1.5	--	0.896	0.109
300D	" + SiO <sub>2</sub> protective layer	1.5	15	0.945	0.200
300D	Humidity test	1.5	15	0.940	0.127
300D			PC	$\Delta\alpha$	$\Delta\varepsilon$
300D			-0.0315	-0.005	-0.073
300E	Substrate/SiO <sub>2</sub> (2 mm/s)/Cermet	1.5	1	0.895	0.155
300E	" + SiO <sub>2</sub> protective layer	1.5	3	0.917	0.204
300E	Humidity test	1.5	3	0.925	0.164
300E			PC	$\Delta\alpha$	$\Delta\varepsilon$
300E			-0.0280	0.008	-0.04
200A	Substrate/Cermet	1	--	0.862	0.086
200A	" + SiO <sub>2</sub> protective layer	1	8	0.936	0.115
200A	Humidity test	1	8	0.94	0.11
200A			PC	$\Delta\alpha$	$\Delta\varepsilon$
200A			-0.0065	0.004	-0.005

After performing the humidity test, selectivity curves of samples 300B, 300D and 300E (Fig. 6-55 to 6-57) show almost unchanged reflectance for wavelengths less than 10  $\mu\text{m}$  but higher reflectance for wavelengths larger than 10  $\mu\text{m}$ . Typically after aging tests the emittance value is either increased or remains unaffected. Nevertheless, humidity aging did not raise the thermal emittance value but even decreased that significantly about 0.04 to 0.07. This was discussed with Dipl.-Ing. M. Köhl who is specialist in solar collector aging procedures and standards in

Fraunhofer institute of solar energy,. The reason seems to be related to the used hydrolyzed-TEOS solution. It is possible that the annealed  $\text{SiO}_2$  layers were not in their equilibrium circumstances or a part of their organic component still remained in the film. In addition to that, porosity of the cermet layer and long heat treatment may lead to shrinkage in thickness of  $\text{SiO}_2$  layer. The lower the thickness, the lower emittance value is obtained. Sample 200A was an exception so that in spite of its thick  $\text{SiO}_2$  coating, increase of its thermal emittance after addition of anti-reflective coating was not as high as other samples and remained unchanged after aging test. The only difference of this sample was the usage of fresh and slightly diluted hydrolyzed TEOS solution as precursor of  $\text{SiO}_2$  layer. This confirms that the way of TEOS hydrolyzation and the time of usage can affect the property of  $\text{SiO}_2$  coating. It is evident for all samples that spectral reflectance in the solar wavelength range was almost unaffected after humidity aging test and consequently solar absorptance values remained unchanged.

After performing humidity test, the performance criterion of all samples became negative which means humidity test improved the selectivity of the absorbers. Finally, it can be fairly concluded that the prepared  $\text{Ni-Al}_2\text{O}_3$  samples experienced no degradation at high humidity atmosphere.

As reported by Carlsson et al. [124], one of the main degradation mechanism of  $\text{Ni-Al}_2\text{O}_3$  cermet absorbers at high humidity is hydration of aluminum oxide to boehmite. An indication of hydration is strong absorption bands that appear at  $3\ \mu\text{m}$ , between  $6$  and  $7\ \mu\text{m}$  and at around  $9\ \mu\text{m}$ , suggestion the formation of pseudoboehmite [18]. In the reflectance curves of the non-treated samples, small absorption peak around  $3\ \mu\text{m}$  and very tiny peaks between wavelengths  $6$  to  $7\ \mu\text{m}$  is observed. Distinguishing absorption peak of pseudoboehmite around  $9\ \mu\text{m}$  due to the strong absorption of Si-O-Si bands is very difficult. In comparison to the samples derived from ethanol-based suspensions, higher absorption peak between  $6$  to  $7\ \mu\text{m}$  is seen in reflectance curve of the samples prepared from aqueous suspensions (See Fig. 6-49). This means, due to the higher amount of water, more aluminum oxide was participated in reaction with water and transformed into boehmite. After the humidity test no sign of further hydration was detected either by visual inspection of the samples or in the spectral reflectance.

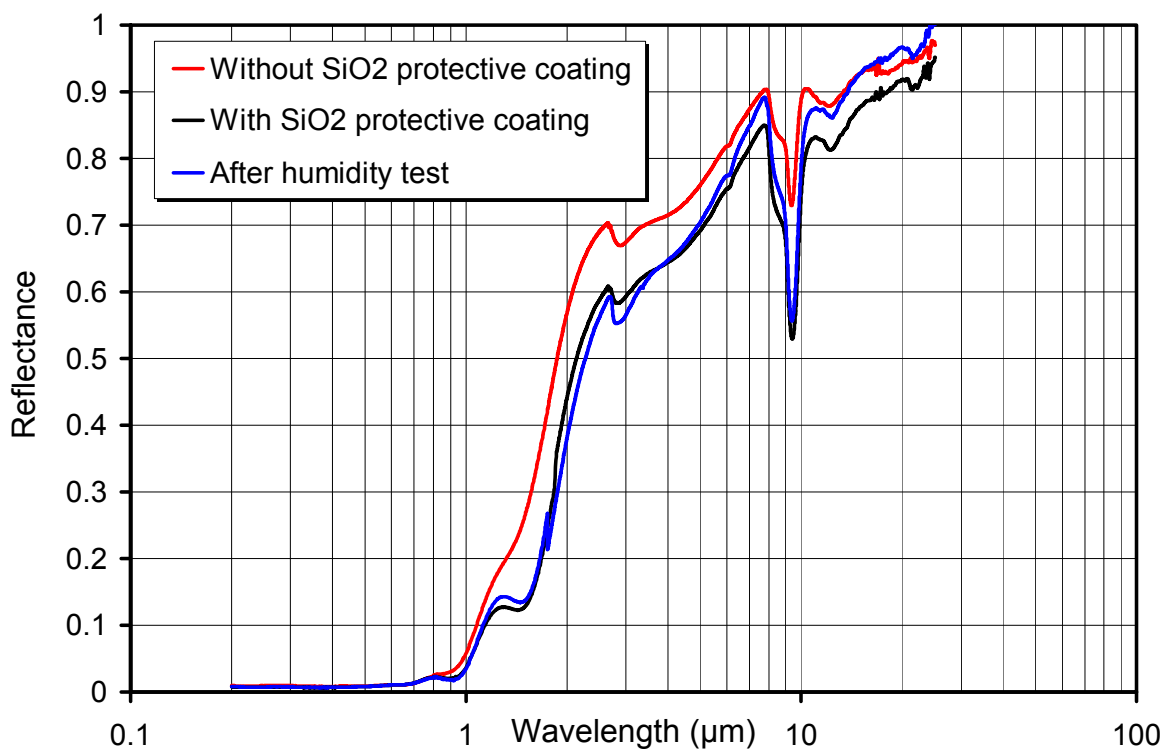


Fig. 6-55: Effect of SiO<sub>2</sub> protective coating and humidity test on the reflectance curve of sample 300B

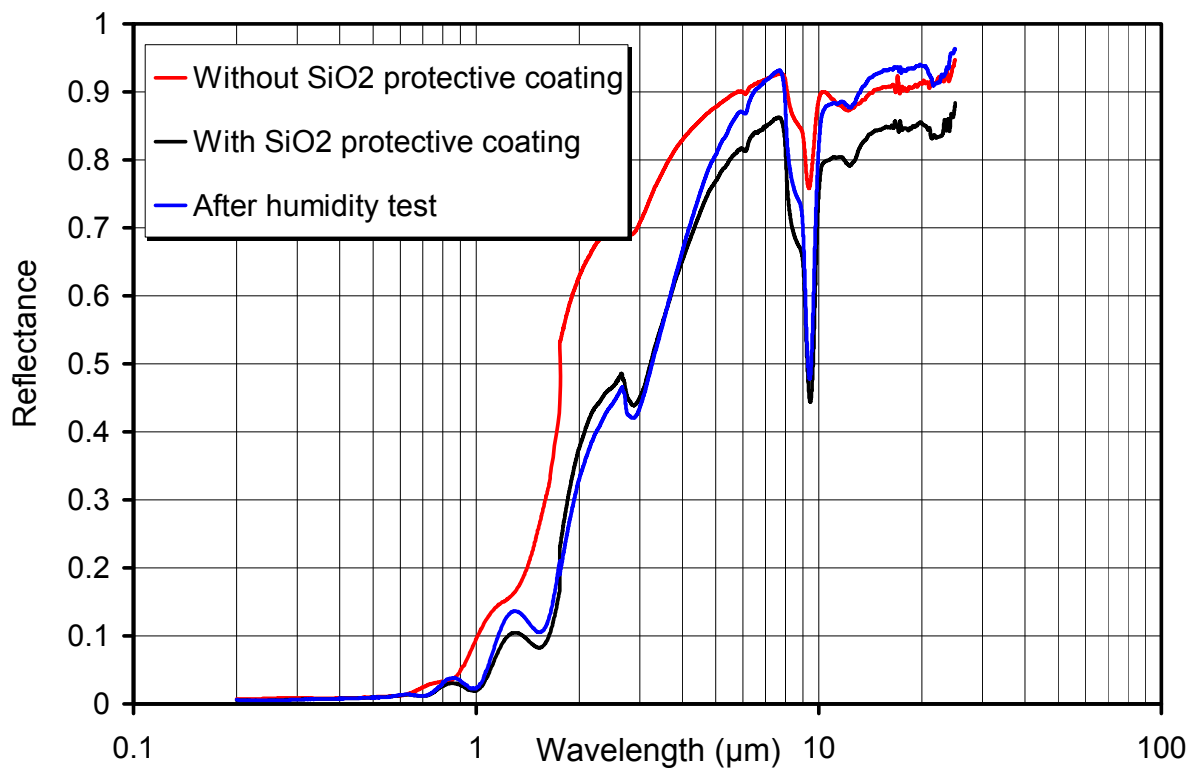


Fig. 6-56: Effect of SiO<sub>2</sub> protective coating and humidity test on the reflectance curve of sample 300D



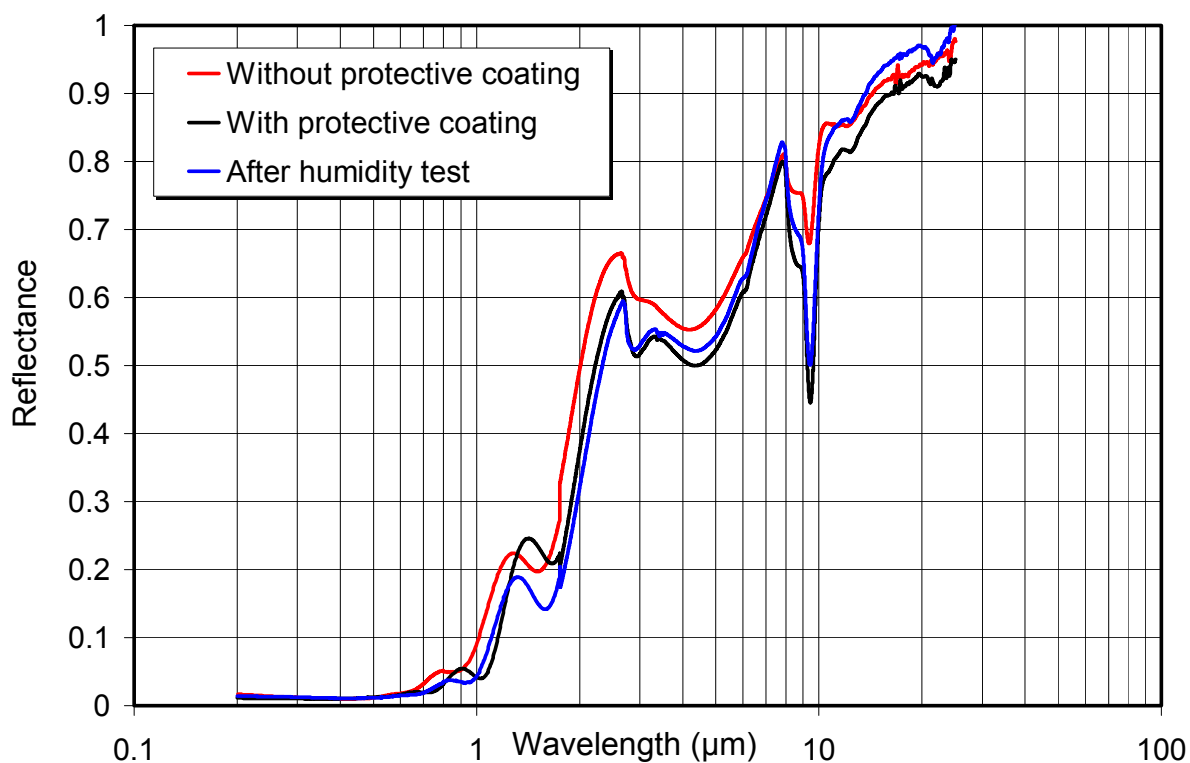


Fig. 6-57: Effect of SiO<sub>2</sub> protective coating and humidity test on the reflectance curve of sample 300E

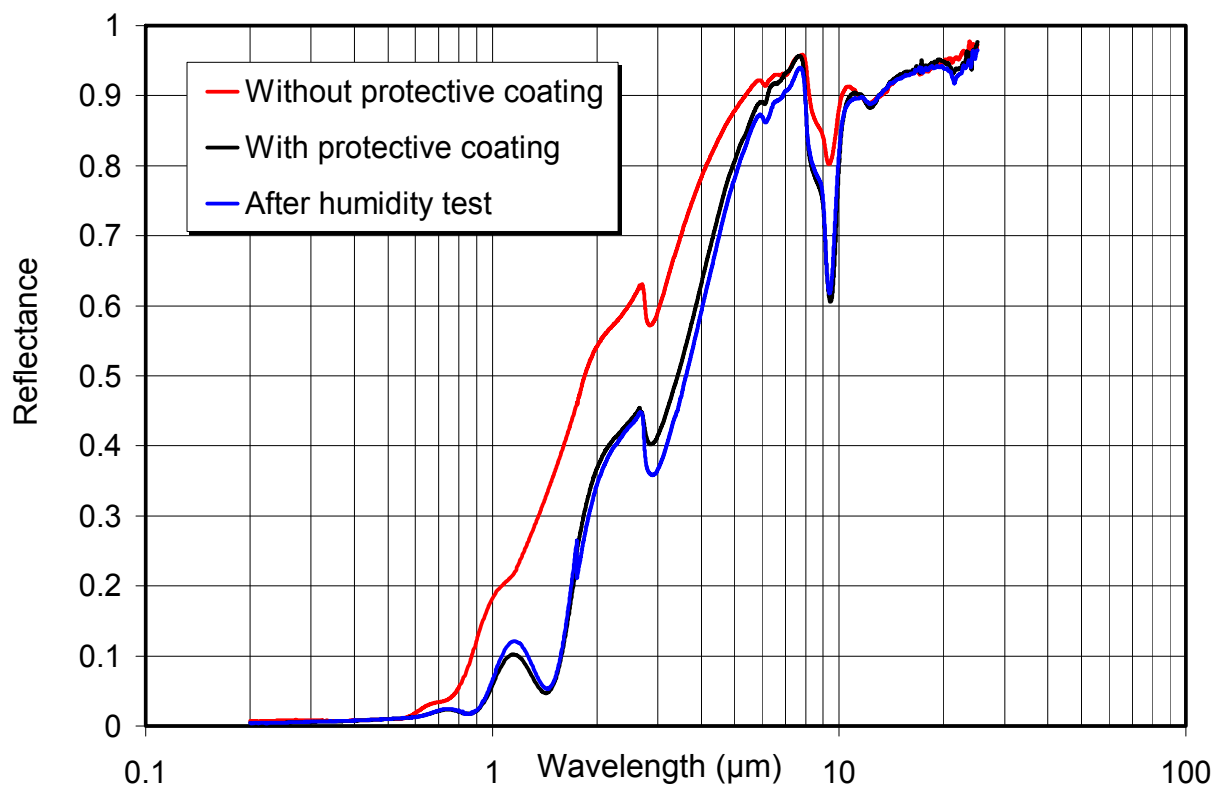


Fig. 6-58: Effect of SiO<sub>2</sub> protective coating and humidity test on the reflectance curve of sample 200A

## 6. Results and discussion

### 6D.6.3 Effect of thermal aging test on the optical properties

Optical properties of four different Ni-Al<sub>2</sub>O<sub>3</sub> cermet absorbers with and without anti-reflection (protective) layer and after thermal aging test are shown in Fig. 6-59 to Fig. 6-62. Their measured selectivity parameters have been also listed in Table 6-12.

Table 6-12: Optical properties of Ni-Al<sub>2</sub>O<sub>3</sub> cermet absorbers with and without SiO<sub>2</sub> protective coating and after thermal aging test

Sample Name	Treatment	Withdraw speed for cermet layer (mm/s)	Withdraw speed for SiO <sub>2</sub> layer (mm/s)	$\alpha$	$\varepsilon$
300H	Substrate/Cermet	1.5	--	0.899	0.078
300H	" + SiO <sub>2</sub> Protective layer	1.5	4	0.942	0.113
300H	300 °C 300 Hours@ air	1.5	4	0.908	0.115
300H			PC	$\Delta\alpha$	$\Delta\varepsilon$
300H			0.035	-0.034	0.002
300A	Substrate/SiO <sub>2</sub> (1mm/s)/Cermet	1.5	--	0.847	0.077
300A	" + SiO <sub>2</sub> Protective layer	1.5	4	0.919	0.147
300A	300 °C 300 Hours@ air	1.5	4	0.864	0.115
300A			PC	$\Delta\alpha$	$\Delta\varepsilon$
300A			0.039	-0.055	-0.032
400A	Substrate/Cermet	2	--	0.926	0.133
400A	" + SiO <sub>2</sub> Protective layer	2	6	0.953	0.19
400A	300 °C 300 Hours@ air	2	6	0.919	0.151
400A			PC	$\Delta\alpha$	$\Delta\varepsilon$
400A			0.014	-0.034	-0.039
400C	Substrate/Cermet	1	--	0.843	0.058
400C	" + SiO <sub>2</sub> Protective layer	1	10	0.903	0.11
400C	300 °C 300 Hours@ air	1	10	0.868	0.125
400C			PC	$\Delta\alpha$	$\Delta\varepsilon$
400C			0.042	-0.035	0.015

Similar to humidity tests, thermal emittance values of some samples like 300H and 400C remained almost unaffected after thermal aging test while those of other samples like 300A and 400A were decreased significantly. In addition to the reasons mentioned in the last section, another possible reason for different behavior of different samples can be the inhomogeneity of temperature along tube furnace. All four samples were annealed together, therefore it is possible that samples were

exposed to different temperatures during annealing and some of them did not receive enough heat for fully evaporation of the organic parts.

Contrary to humidity test, thermal aging test declined the solar absorptance values of the most samples about 3 %. The highest reduction (about 5 %) belongs to sample 300A which had an anti-diffusion layer and the thinnest protective coating. At high temperatures, oxidation of metallic nickel to nickel oxide may take place and result in a decrease in the solar absorptance of coatings [125].

After performing the thermal aging test, PC values from 0.01 to 0.04 obtained. The lowest PC belongs to the sample 400A which had the thickest cermet layer and protected with a thick SiO<sub>2</sub> coating. As all PC values are under 0.05 and heat-treated absorbers passed the adhesion test, an absorber can be qualified only when PC value is less than 0.015 (see appendix B). This is true for sample 400A that showed performance criterion value of about 0.0145.

Thermal aging test revealed that the developed cermet absorbers are stable under elevated temperature for a long time. Comparing to standard qualification test, the performed thermal aging test was more rigorous. In this study, the samples were aged thermally for 200 hours at 300 °C instead of 250 °C.

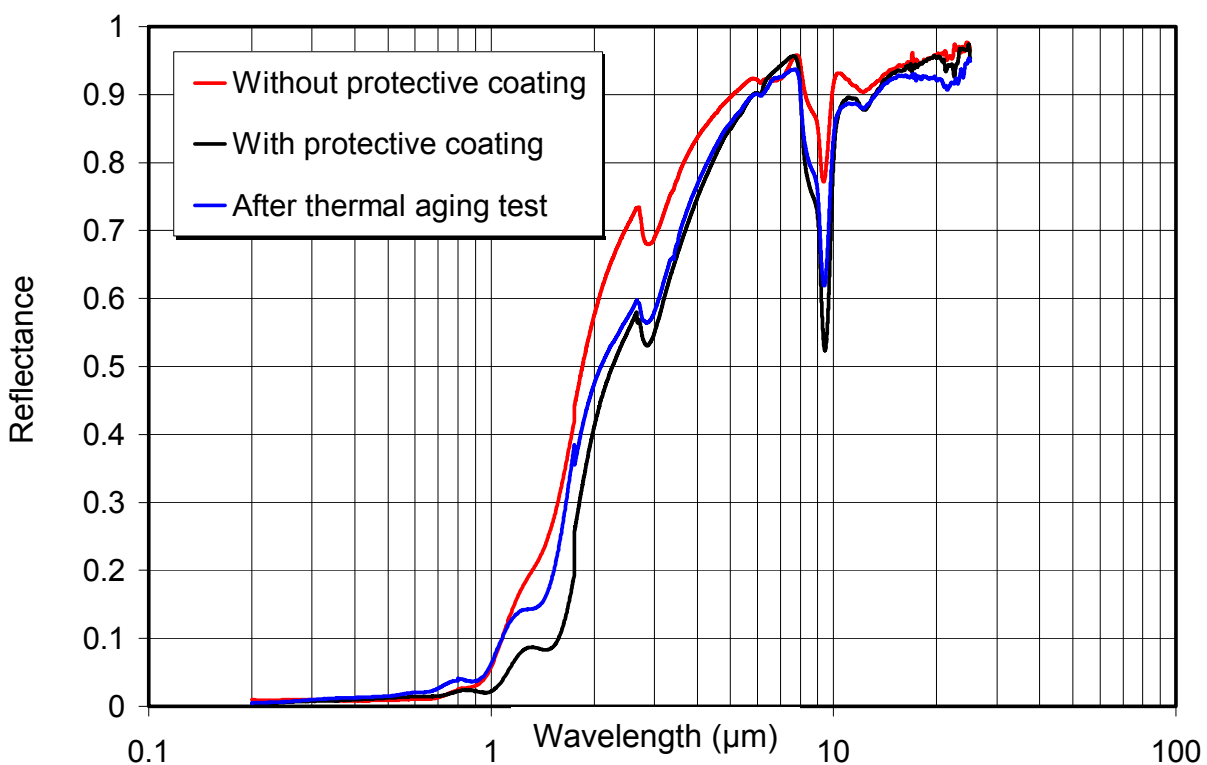


Fig. 6-59: Effect of SiO<sub>2</sub> protective coating and thermal aging test on the reflectance curve of sample 300H

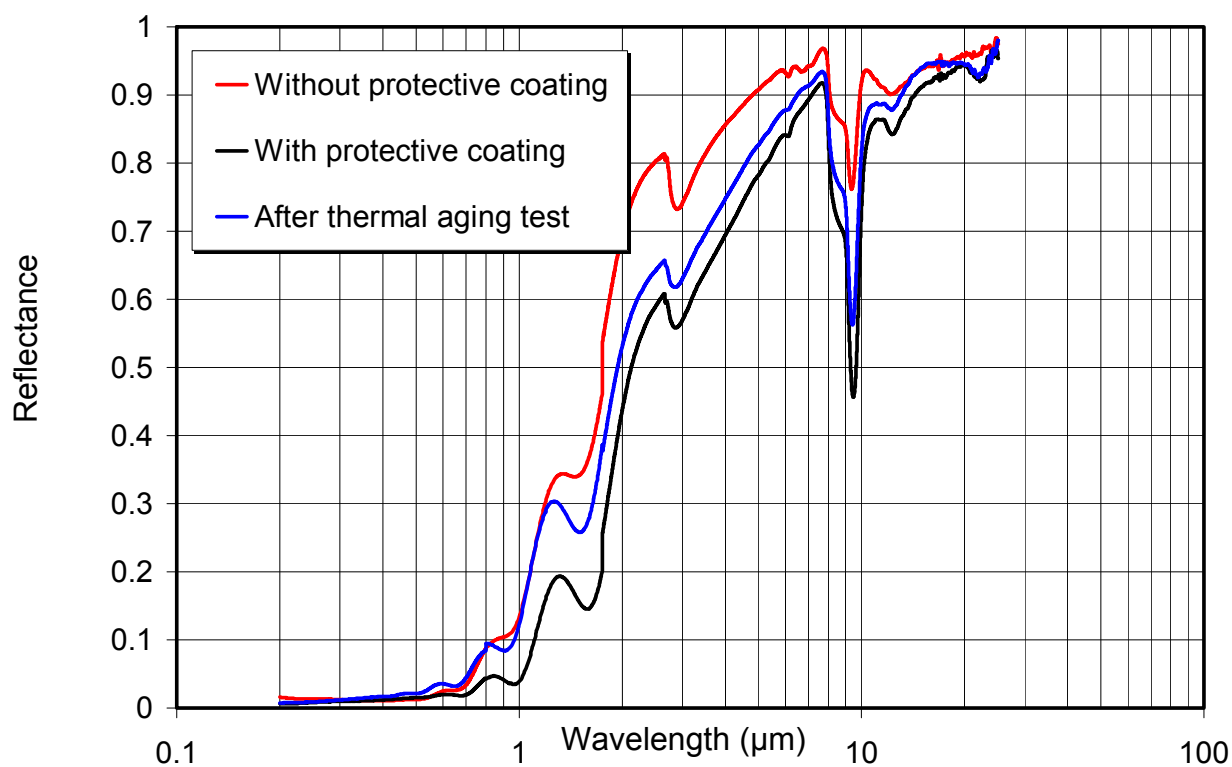


Fig. 6-60: Effect of SiO<sub>2</sub> protective coating and thermal aging test on the reflectance curve of sample 300A

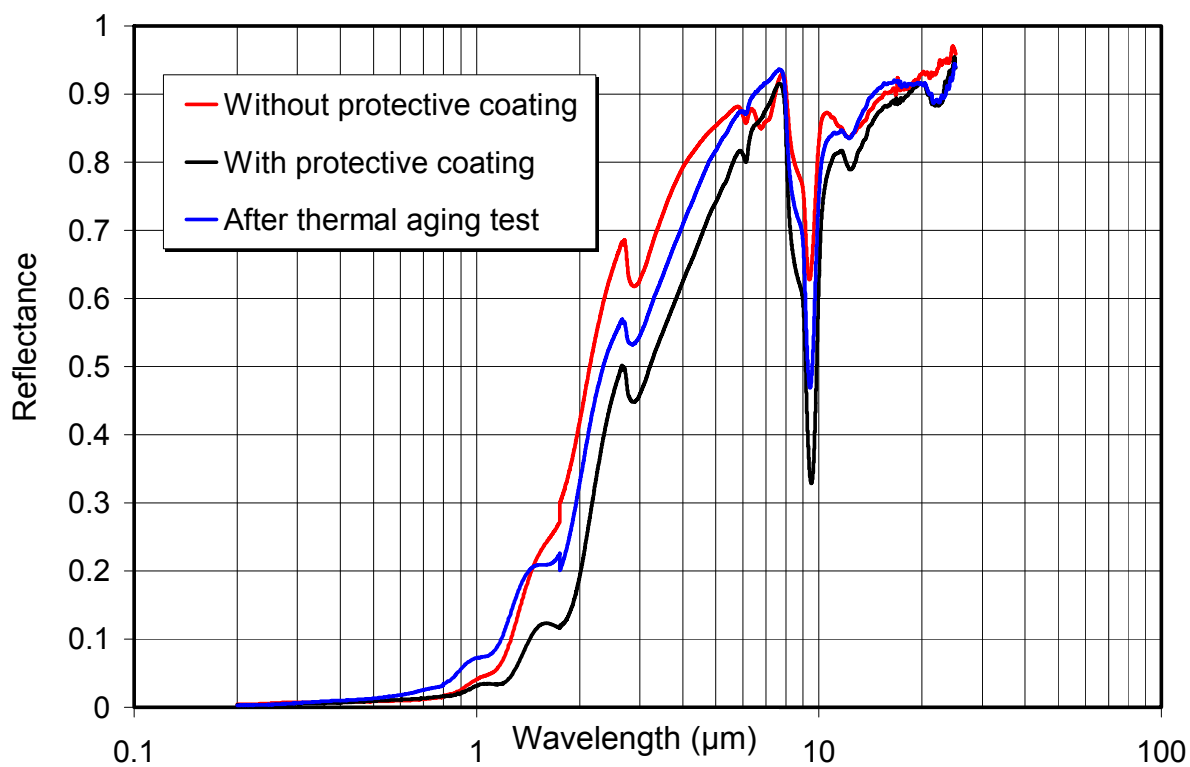


Fig. 6-61: Effect of SiO<sub>2</sub> protective coating and humidity test on the reflectance curve of sample 400A

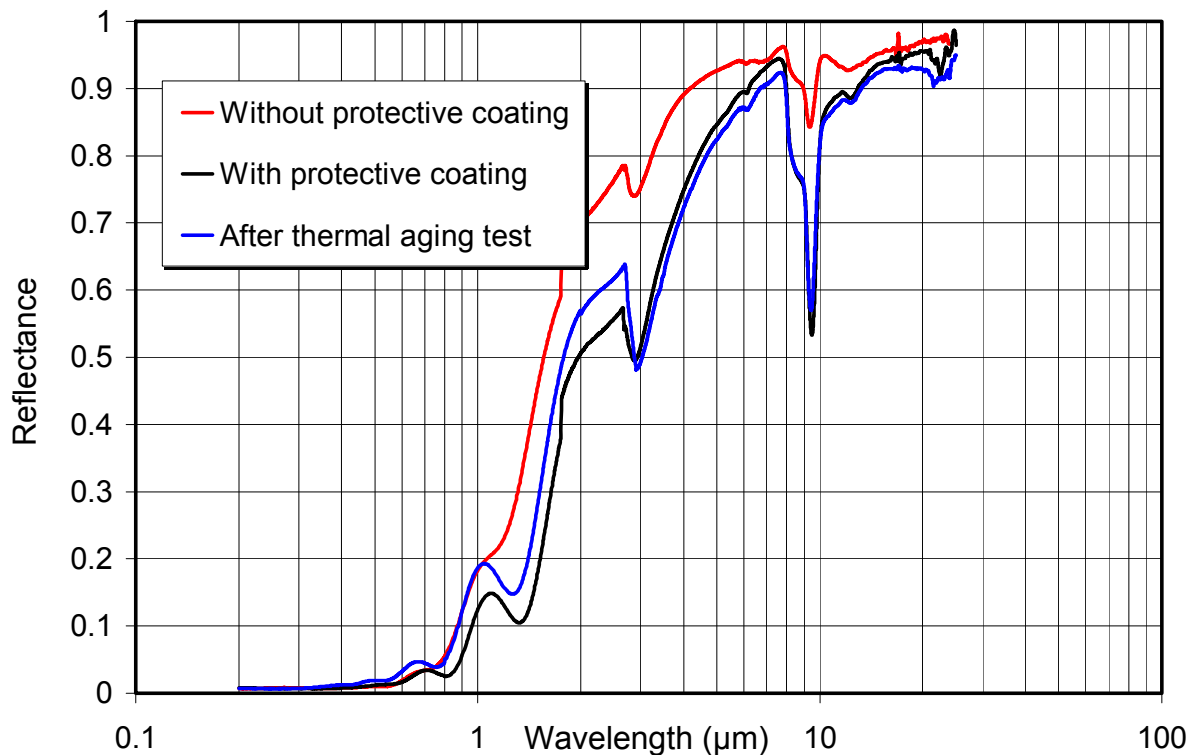


Fig. 6-62: Effect of SiO<sub>2</sub> protective coating and humidity test on the reflectance curve of sample 400C

### 6D.6.4 Conclusions and discussion

- Samples prepared with similar deposition parameters showed reproducible optical properties. For example, solar absorptance of about 0.89-0.9 and thermal emittance of about 0.08-0.1 obtained for similar samples, which all had a cermet layer deposited by dip coating technique and substrate withdrawal speed of 1.5 mm/s.
- Applying thin anti-diffusion SiO<sub>2</sub> layer between substrate and cermet layer declined the selectivity of the samples.
- Adding an anti-reflection (protective) layer increased the solar absorptance 3 to 8 % and to the same extent the thermal emittance. The highest increase in emittance belonged to the sample that had the thickest SiO<sub>2</sub> protective coating. Increase in thermal emittance was due to the strong absorption band of Si-O in far-infrared region.
- Sathiaray and co-workers [126] reported a solar absorptance of 0.87 with normal emittance of 0.07 for a Ni-Al<sub>2</sub>O<sub>3</sub> cermet layer of 70 nm with 0.21 nickel metal volume fraction, deposited on a molybdenum reflector with a 60 nm SiO<sub>2</sub> anti-reflection layer.

## 6. Results and discussion

---

In this study, similar selectivity obtained for single cermet structure without protective coating.

- The best obtained selectivity belonged to the sample 300H and 200A with solar absorptance value of about 0.94 and thermal emittance value of about 0.11.
- Humidity aging test did not raise the thermal emittance value of silica-coated absorbers but even decreased that significantly about 0.04 to 0.07. It is possible that annealed SiO<sub>2</sub> layer was not in its equilibrium circumstance or a part of its organic components still remained in the film and only longer heat treatment (during aging test) provided the equilibrium conditions. In addition to that, shrinkage of SiO<sub>2</sub> layer due to the porosity of the cermet layer or inhomogeneity of temperature along tube furnace would be other reasons, which can explain drop of the emittance values.
- After humidity aging test spectral reflectance in the solar wavelength range was almost unaffected and consequently solar absorptance values remained unchanged.
- After performing humidity test, negative PC values obtained for all samples. It means that the humidity test even improved the selectivity of the absorbers. Finally, it can be fairly concluded that the prepared Ni-Al<sub>2</sub>O<sub>3</sub> samples experienced no degradation at high humidity atmosphere.
- Similar to humidity test, after thermal aging test, thermal emittance values of the samples either remained unchanged or decreased significantly. However, contrary to humidity test, thermal aging test declined the solar absorptance values of the most samples about 3 % and consequently higher PC values from 0.01 to 0.04 obtained.
- T. Boström has shown in his thesis [127] that the temperature increase rate strongly influences performance. The higher the temperature increase rate, the better the absorber performed in the accelerated ageing test. Investigation of this effect on stability of the developed absorbers of this study is recommended.
- It was evident from reflectance curves of all samples that small portion of aluminum oxide has been hydrated to boehmite. An indication of hydration was small absorption bands that appeared at 3 μm and between 6 and 7 μm. Compared to ethanol suspensions, stronger absorption bands of samples derived from aqueous suspensions show that more aluminum oxide was undergone in reaction with water and transformed to boehmite.
- Generally, after thermal and humidity aging tests, PC values lower than 0.05 obtained. As the performed thermal aging test was more rigorous than standard

## 6. Results and discussion

---

procedure and samples passed the adhesion test, it can be concluded that the developed cermet absorbers are stable under elevated temperature and high humidity atmosphere for a long time. For comparison, Ni-Al<sub>2</sub>O<sub>3</sub> films prepared using RF sputtering and deposited on molybdenum coated stainless steel substrates started to degrade rapidly above 350 °C when heated in air [53]. Finally it can be concluded that the new cermet based absorbers can be qualified for low- to mid-temperature thermal collectors.

### **7. Conclusion remarks and summary**

The main effort of this thesis was made to further increase the spectral selectivity of cermet based selective absorbers by inducing surface roughness on the surface of the cermet layer or by micro-structuring the metallic substrates before deposition of the absorber coating. Moreover along of this study, a novel and cost-effective technique for fabrication of cermet selective absorbers was developed. Compared to present technologies like electroplating or sputtering, the composite cermet absorbers were prepared in an easier, cheaper and environmental friendly manner. The properties of the prepared absorber were investigated by means of SEM, EDX, XRD, WLI, AFM and spectrophotometers.

The optical properties of the absorber surfaces essentially depend on the microstructure and roughness of the surface. Compared to smooth multilayer absorbers, optical properties of the absorbers with rough surfaces are less thickness-sensitive. Generally, any small changes in the thickness of the smooth layers of a multiplayer absorber will change interference absorptions and can descend the spectral selectivity drastically, whereas a rough interface decreases the interference effect and allows more light to come into the underlay layers by reducing the surface reflection.

Along of this study, using a roughening technique (deposition on hot substrates) and two structuring techniques (laser and imprint micro-structuring), suitable surface roughness and structures were obtained and the effect of surface textures on enhancement of the solar absorption was investigated, theoretically and experimentally.

It was shown that heating the substrate during deposition of Cu-Al<sub>2</sub>O<sub>3</sub> cermet absorber changes morphology of the cermet and anti-reflection layers. For better light absorption through multiple reflections-absorptions (light trapping phenomena), surface features with high depths and high aspect ratios were needed. Increasing the thickness of the rough cermet layer to obtain deeper structures was not the solution because it led to high thermal emittance. Finally, by keeping the thickness of the cermet layer as low as what simulation program proposed and using a roughness template layer (here Al<sub>2</sub>O<sub>3</sub>) under the IR-reflector layer, a new efficient structure was created. The thickness of the rough template layer can be as high as desired because it will not affect the thermal emittance value. Compared to the graded,



## 7. Conclusion remarks and summary

---

double or triple cermet structures, which are highly sensitive to the layer thickness and deposition parameters, fabrication of such simple configuration is easier and it can reduce the fabrication costs. Due to the effective surface roughness of the new structure, excellent and near to ideal selectivity was obtained. The new developed structure increased the solar absorptance ( $\alpha$ ) of the smooth Cu-Al<sub>2</sub>O<sub>3</sub> from 0.840 to 0.965, while the emittance value was kept as close as that of copper substrate (0.028). The developed Cu-Al<sub>2</sub>O<sub>3</sub> absorber in this study would be a highly efficient absorber candidate for evacuated solar tube collectors.

As a result of this thesis, the effect of surface micro-structuring of the metallic substrates on improving the spectral selectivity of low emittance metals is now better understood. It was shown theoretically, that both structure shape and structure aspect ratio have large influence on the spectral selectivity of pure low emittance metals like copper and tungsten. According to the results of optical simulation, deep sinusoidal structure is the most effective surface profile among of lamellar, sinusoidal and triangular profiles that can enhance the solar absorptivity of copper and tungsten significantly. Whereas optical properties of lamellar structures were not sensitive to different structure aspect ratios and no significant increase in selectivity was observed.

Through direct laser structuring, copper and stainless steel plates were structured. Structuring parameters like structure period or depth could be modified easily by changing the interference parameters, laser intensity and number of laser pulses. It was found that the larger the aspect ratio, the better the solar absorptance. Solar absorptance of 0.508 and thermal emittance of 0.096 were obtained for a structured copper sample with structure aspect ratio of 0.36 and period of 4  $\mu\text{m}$ . It means due to the structuring, solar absorptance of a smooth copper sample was enhance about 36 %. Measured total reflectance of samples was in good agreement with that of predicted by PCGrate simulation program. Compared to unstructured stainless steel sample, structuring increased the absorptivity of the stainless steel substrate about 10 % while increase in emittance was only 1 %.

For structuring a glass or metallic substrate prior to thin film deposition, embossing (imprint) structuring method was also employed. In this method, surface profile of a metallic master was transferred to a flexible silicon rubber. Then, special sol was spread on a glass substrate and was structured with the prepared silicon stamp. The

## 7. Conclusion remarks and summary

---

substrate and the structured sol-gel layer were tempered at high temperature. After tempering, shrinkage of the structure parameters was only 10-15 %. The tempered sol-gel layer was thermally stable at elevated temperatures. Finally, for studying the optical effect of the structuring, a tungsten thin film with a thickness of about 200 nm was deposited on the structured sol-gel layer. Tungsten thin film replicated very well the structuring profile of the sol-gel layer at its interface with air. Compared to unstructured tungsten thin film, an increase of 15 % in solar absorptance was observed.

Direct laser structuring was a robust and simple patterning technique with least processing steps. There was no need to any mask, photo-resist and etching solutions. For mass production and structuring of large surfaces, the studied direct laser and imprint structuring technologies are more suitable than the other techniques like optical or e-beam lithography. Embossing can rapidly pattern large areas with feature sizes that are more costly and time consuming with electron-beam or ion-beam patterning.

All three investigated structuring and roughening techniques improved the optical properties of coated and uncoated substrates. Solar absorber manufacturers can employ one or two of the presented techniques to boost the selectivity only by addition of one extra step to the production lines.

In addition to selectivity improvement techniques, this thesis covers new preparation technique, optical and non-optical investigations and durability tests of Ni-Al<sub>2</sub>O<sub>3</sub> cermet selective absorbers. For making thin films of a cermet composite like Ni-Al<sub>2</sub>O<sub>3</sub>, special powder suspensions were developed and stabilized. This was achieved by dispersing nano powder of aluminum oxide in ethanol or distilled water, in which nitrate salt of nickel already solved.

Effect of different powder dispersion techniques and suspension parameters (like pH, solid content, additives) on particle size distribution and stability of the suspensions were investigated. It was found that cermet coatings prepared from a coating suspension, in which volume percentage of nickel to aluminum oxide is 40:60 would show a promising selectivity. The resulted cermet absorber with a thickness of about 200 nm had solar absorptance of 0.8 and thermal emittance of about 0.07. According to the state of the art of solar absorbers, single ungraded cermet layers with homogeneous volume fractions, deposited on metal reflectors and coated with an

## 7. Conclusion remarks and summary

---

anti-reflection layer show normal solar absorptance of 0.8. Therefore, the optical performance of the wet-chemically manufactured Ni-Al<sub>2</sub>O<sub>3</sub> absorber surface is comparable to that of commercial selective absorbers, which are normally produced with sputtering technique.

Through addition of a coupling agent like TEOS, adhesion and scratch resistance of the thin film were improved significantly. Fortunately, the developed silica network enhanced the solar absorption of cermet layer by lowering the effective refractive index of the cermet. Solar absorptance and thermal emittance of the modified Ni-Al<sub>2</sub>O<sub>3</sub> selective absorber were 0.87 and 0.08, respectively. Compared to non-modified cermet, increase in solar absorption was about 25 %. These values obtained from Ni-Al<sub>2</sub>O<sub>3</sub> samples, which were prepared from a stable suspension with nickel content of 20 %.

To protect cermet coating against of atmospheric degradations, surface of the cermet layer was coated with a SiO<sub>2</sub> coating prepared from hydrolyzed TEOS. The effect of this anti-reflection (protective) coating on optical performance and stability of the prepared absorbers was investigated. Depending on different thicknesses of cermet and protective layers, different spectral selectivities obtained. The best sample showed solar absorptance value of about 0.94 and thermal emittance value of about 0.11.

Degradation of the prepared absorbers was also studied in this work. The Ni-Al<sub>2</sub>O<sub>3</sub> absorber surface passed accelerated high temperature and high humidity tests. Based on accelerated aging test results, the Ni-Al<sub>2</sub>O<sub>3</sub> absorber surface is estimated to be suitable for glazed applications like solar heating system, operating at low to medium temperatures. Due to the promising optical performance and good thermal and humidity stability, the developed cermet absorbers can compete economically and optically with high quality (e.g. sputtered) absorbers.

The material costs for coating itself are negligible compared to the cost of the substrate. For example for a double layer absorber the material costs are less than 20 cents per square meter. As a comparison, the material cost for sputtered spectrally selective absorber is about 5 to 10 Euros per square meter (through communication with suppliers). The production and equipment costs cannot be estimated exactly now. It depends on many parameters like production capacity or chosen equipment. But since industrial ovens and deposition facilities are already in

## 7. Conclusion remarks and summary

---

use within the industry it should not be too expensive to construct or adapted the existing process and equipment to the one which is suitable for production of powder derived cermet absorbers. Dip coating process that was used in this study is very suitable for coating large surfaces and of practical interest for large-scale production in industry. Spraying the coating suspension on large substrates is also proposed but its feasibility should be verified for the first time.

### **8. Future outlooks**

To confirm the highly positive effect of the roughness template layer and substrate heating on selectivity enhancement of the most sputtered solar absorbers, other metal-dielectric combinations and higher substrate temperatures should be tested. Instead of aluminium oxide as roughness template layer, cermet or other simple or composite materials with suitable microstructure can be used.

In direct laser structuring of metallic substrates, other metals than those who were tested (Cu and SS) can be structured and studied. For example metals like molybdenum or tungsten, which have low thermal emittance, are good candidates. As molybdenum or tungsten has higher melting points than copper, it is expected that more regular structures with less deformation can be obtained. The structuring parameters can be further optimized to get deeper structures without damaging the shape of the pattern.

In this study using the only available metallic master, feasibility of the embossing technique in surface structuring and enhancement of the optical absorption of a metallic substrate was investigated. Using this technique, sharp structures with high aspect ratio obtained quickly. For achieving the highest possible light absorption through the surface geometrical effect, optimized structuring profile and parameters are needed. It is recommended that new metallic masters with optimized surface profiles and structure parameters be designed and employed for increasing solar absorption of the real absorber coatings. For that aim, simulation results of chapter 4 can be used.

The procedure of making cermet based selective absorber using developed powder technique was patented. Of course developing the whole process from the beginning to the final product was out of the scope of this study. The main focus of this study was on designing, constructing and roughly optimization of the chemically derived absorbers.

Further selectivity improvement using double or multiple cermet structures, optimized anti-reflection or protective coatings and thinner layers are recommended. In order to obtain a denser cermet layer with less porosity, it is recommended to fabricate the cermet layer by multiple depositions of very thin cermet layers. For doing that, diluted suspensions with lower solid contents than what was employed in this study should

## 8. Future outlooks

---

be used. Such stack of thinner cermet coatings can be fabricated by repeating the coating process (dip-coating, drying, densification).

Using this technique various cermet thin films like Ag-Al<sub>2</sub>O<sub>3</sub>, Ni-AlN, Cu-SiO<sub>2</sub>...can be prepared and studied. Only metals that their oxide forms are reduced at temperatures lower than melting or softening temperature of the substrate can be selected as the metallic component of the cermet layer.

Non-aqueous suspensions with high ion concentrations can be further sterically stabilized. Effect of different wetting, rheology and dispersing agents on the particle size and stability of the suspension can be investigated.

For fully qualification of the developed Ni-Al<sub>2</sub>O<sub>3</sub> cermet absorber as a commercial product, more accurate and additional durability tests should be carried out.

**9. References**

- [1] W. Weiss and M. Rommel, *Solar Heat for Industrial Processes*, AEE INTEC, May.
- [2] O. T. Inal and A. Scherer, *Review: Optimization and microstructural analysis of electrochemically deposited selective solar absorber coatings*. *J. Mater. Sci* 21 (1986) 729-736.
- [3] Q. C. Zhang and D. R. Mills, *High solar performance selective surface using bi-sublayer cermet film structures*. *Sol. Energy Mater. Sol. Cells* 27 (1992) 273-290.
- [4] M. Farooq and M. G. Hutchins, *A novel design in composites of various materials for solar selective coatings*. *Sol. Energy Mater. Sol. Cells* 71 (2002) 523-535.
- [5] I. T. Ritchie and B. Window, *Application of thin graded-index films to solar absorbers*. *Applied Optics* 16 (1977) 1977.
- [6] G. L. Harding, B. Window, D. R. McKenzie, A. R. Collins and C. M. Horwitz, *Cylindrical magnetron sputtering systems for coating solar selective surfaces onto batches of tubes*. *J. Vac. Sci. Technol.* 16 (1979) 2105-2108.
- [7] B. Lee, *The progress and prospect of middle/high temperature evacuated tubular solar collector*. *Renew. Energ.* 24 (2001) 539-544.
- [8] Q. C. Zhang, *Stainless-steel-AlN cermet selective surfaces deposited by direct current magnetron sputtering technology*. *Sol. Energy Mater. Sol. Cells* 52 (1998) 95-106.
- [9] Q. C. Zhang, K. Zhao, B. C. Zhang, L. F. Wang, Z. L. Shen, D. Q. Lu, D. L. Xie and B. F. Li, *High performance Al-N cermet solar coatings deposited by a cylindrical direct current magnetron sputter coater*. *J. Vac. Sci. Technol.* 17 (1999) 2885-2890.
- [10] M. Lazarov, P. Raths, H. Metzger and W. Spirkl, *Optical constants and film density of TiNxOy solar selective absorbers*. *J. Appl. Phys.* 77 (1995) 2133-2137.
- [11] H. Schellinger, M. Lazarov, W. Assmann, B. Bauer and C. Steinhausen, *Improved selective properties of SiO<sub>2</sub>/TiNxOy-Al tandem absorbers effected by tempering*. *SPIE* 2255 (1992) 172-181.
- [12] L. Kalulza, A. Surca-Vuc and B. Orel, *Structural and IR spectroscopic analysis of sol-gel processed CuFeMnO<sub>4</sub> Spinel and CuFeMnO<sub>4</sub>/Silica films for solar absorbers*. *Journal of sol-gel Science and Technology* 20 (2001) 61-83.
- [13] Z. C. Orel and G. M. K., *Spectrally selective paint coatings preparation and characterization*. *Sol. Energy Mater. Sol. Cells* 68 (2001) 337-353.

## 9. References

---

- [14] Z. C. Orel, *Characterization of high-temperature-resistant spectrally selective paints for solar absorbers*. Sol. Energy Mater. Sol. Cells 57 (1999) 291-301.
- [15] W. F. Bogaerts and C. Lampert, *Review Materials for photothermal solar energy conversion*. Journal of material science 18 (1983) 2847-2875.
- [16] P. Konttinen, P. D. Lund and R. J. Kilpi, *Mechanically manufactured selective solar absorber surfaces*. Sol. Energy Mater. Sol. Cells 79 (2003) 273-283.
- [17] P. Konttinen and P. D. Lund, *Characterization of selective absorbers prepared through a mechanical treatment*. Proceedings of the World Renewable Energy Congress VII, ed. E. Science. (2002), Cologne, Germany.
- [18] P. Konttinen and P. D. Lund, *Thermal stability and moisture resistance of C/Al<sub>2</sub>O<sub>3</sub>/Al absorber surfaces*. Sol. Energy Mater. Sol. Cells 82 (2004) 361-373.
- [19] M. R. Nejati, V. Fathollahi and M. K. Asadi, *Computer simulation of the optical properties of high-temperature cermet solar selective coatings*. Solar Energy 78 (2005) 235-241.
- [20] B. O. Seraphin, *Thin films in photothermal solar energy conversion*. Thin solid films 90 (1982) 395-403.
- [21] P. Konttinen, *Characterization and aging studies of selective solar C/Al<sub>2</sub>O<sub>3</sub>/Al absorber surfaces*, Helsinki university of technology, (2004).
- [22] H. Sai, H. Yugami, Y. Kanamori and K. Hane, *Solar selective absorbers based on two-dimensional W surface gratings with submicron periods for high-temperature photothermal conversion*. Sol. Energy Mater. 79 (2003) 35-49.
- [23] Q. C. Zhang, K. Zhao, B. C. Zhang, L. F. Wang, Z. L. Shen, Z. J. Zhou, D. Q. Lu, D. L. Xie and B. F. Li, *New cermet solar coatings for solar thermal electricity applications*. Solar Energy 64 (1998) 109-114.
- [24] C. G. Granqvist and V. Wittwer, *Materials for solar energy conversion: An overview*. Sol. Energy Mater. Sol. Cells 54 (1998) 39-48.
- [25] C. E. Kennedy, *Review of Mid-to High-temperature solar selective absorber materials*, NREL (National Renewable Energy Laboratory),
- [26] J. Spitz, *Selective surfaces for high temperature solar photothermal conversion*. Thin solid films 45 (1977) 31-41.
- [27] J. A. Thornton, A. S. Penfold and J. L. Lamb, *Sputter-deposited Al<sub>2</sub>O<sub>3</sub>/Mo/Al<sub>2</sub>O<sub>3</sub> selective absorber coatings*. Thin solid films 72 (1980) 101-109.



## 9. References

---

- [28] A. B. Meinel and M. P. Meinel, *Applied Solar Energy : an Introduction*. (1976), Addison-Wesley.
- [29] U. Kreibig and M. Vollmer, *Optical properties of metal clusters*. ed. P. U. Gonser. (1995), Springer.
- [30] R. Messier, S. V. Krishnaswamy, L. R. Gilbert and P. Swab, *Black a-Si solar selective absorber surfaces*. J. Appl. Phys. 51 (2006) 1611-1614.
- [31] L. R. Gilbert, R. Messier and R. Roy, *Black germanium solar selective absorber surfaces*. Thin solid films 54 (1978) 149-157.
- [32] G. B. Reddy, D. K. Pandya and K. L. Chopra, *Chemically deposited PbS-Antireflection layer selective absorbers*. Sol. Energ. Mater. 15 (1987) 153-162.
- [33] R. B. Pettit and R. R. Sowell, *Solar absorptance and emittance properties of several solar coatings*. J. Vac. Sci. Technol. 13 (1975) 596-602.
- [34] R. F. Bunshah, *Handbook of deposition technologies for films and coatings*. 2nd. ed. (1994), New Jersey: Noyes Publications.
- [35] H. Schmidt and M. Mennig, *Wet Coating Technologies for Glass*. (2000), Saarbrücken.
- [36] G. V. Franks and L. Meagher, *The isoelectric points of sapphire crystals and alpha-alumina powder*. Colloids Surf. A 214 (2003) 99-110.
- [37] F. Mucklich and A. Lasagni, *Art and science of micro-patterning*. Revista SAM journal 1 (2005) 1-17.
- [38] M. A. McCord and M. J. Rooks, *SPIE Handbook of Microlithography, Micromachining and Microfabrication*. ed. P. Rai-Choudhury. (2000).
- [39] A. F. Lasagni, *Advanced design of periodical structures by Laser Interference Metallurgy in the micro/nano scale on macroscopic areas*, Saarland University, Saarbrücken (2006).
- [40] M. von Allmen and A. Blatter, *Laser-Beam Interactions with Materials*. 2nd. ed. (1995), Berlin: Springer.
- [41] B. Sepeur-Zeitz, *Mikrostrukturierung organisch-anorganischer Kompositmaterialien über Prägeverfahren*, University of Saarland, Saarbrücken (1999).

## 9. References

---

- [42] M. Mennig, A. Gier and H. Schmidt, *Preparation of micropatterns with profile heights up to 30 microns from silica sols*, vol. 3136 "Sol-gel Optics IV". Proc. SPIE, ed. J. D. Mackenzie. Vol. 3136. (1997), San Diego. 480-485.
- [43] J. A. Duffie and W. A. Beckmann, *Solar engineering of thermal processes*. 2nd ed ed. (1980), New York: John Wiley and Sons.
- [44] B. Carlsson, *Recommended qualification test procedure for solar absorber surface durability*, Swedish national testing and research institute,
- [45] B. Carlsson, K. Möller, M. Köhl, U. Frei and S. Brunold, *Qualification test procedure for solar absorber surface durability*. Sol. Energy Mater. Sol. Cells 61 (2000b) 255-275.
- [46] M. Köhl, M. Heck, S. Brunold, U. Frei, B. Carlsson and K. Möller, *Advanced procedure for the assessment of the lifetime of solar absorber coatings*. Sol. Energy Mater. Sol. Cells 84 (2004) 275-289.
- [47] H. Z. Tabor, *Receiver for solar energy collectors*, Israel 2917817, 1959
- [48] C. A. Arancibia-Bulnes, C. A. Estrada and J. C. Ruiz-Suarez, *Solar absorptance and thermal emittance of cermets with large particles*. J.Phys. D: Appl. Phys. 33 (2000) 2489-2496.
- [49] Q. C. Zhang and D. R. Mills, *Very low-emittance solar selective surfaces using new film structures*. J. Appl. Phys. 72 (1992) 3013-3021.
- [50] G. E. McDonald, *Spectral reflectance properties of black chrome for use as a solar selective coating*. Solar Energy 17 (1975) 119-122.
- [51] A. Andersson, O. Hunderi and C. G. Granqvist, *Nickel pigmented anodic aluminum oxide for selective absorption of solar energy*. J. Appl. Phys. 51 (1980) 754-764.
- [52] C. G. Granqvist, *Materials science for solar energy conversion systems*. (1991), Oxford: Pergamon press.
- [53] T. Sathiaraj, R. Thangaraj, H. Al Sharabaty, M. Bhatnagar and O. P. Agnihotri, *Ni-Al<sub>2</sub>O<sub>3</sub> selective cermet coatings for photothermal conversion up to 500 °C*. Thin solid films 190 (1990) 241-254.
- [54] J. Salmi, J.-P. Bonino and R. S. Bes, *Nickel pigmented anodized aluminium as solar selective absorbers*. J. Mater. Sci. 35 (2000) 1347-1351.

## 9. References

---

- [55] H. G. Craighead and R. A. Buhrman, *Optical properties of selectively absorbing metal/insulator composite films*. J. Vac. Sci. Technol. 15 (1978) 269-271.
- [56] E. Wäckelgard and G. Hultmark, *Industrially sputtered solar absorber surface*. Sol. Ener. Mat. Sol. Cells 54 (1998) 165-170.
- [57] C. M. Lampert, *International development and advances in solar selective absorbers*. SPIE 3138 134-145.
- [58] D. R. McKenzie, *Gold, silver, chromium, and copper cermet selective surfaces for evacuated solar collectors*. Appl. Phys. Lett. 34 (1979) 25-27.
- [59] M. Mast and K. Gindele, *Ni/MgF<sub>2</sub> cermet films as selective solar absorbers*. Thin solid films 126 (1985) 37-42.
- [60] M. Lanxner and Z. Elgat, *Solar selective absorber coating for high service temperatures, produced by plasma sputtering*. SPIE 1272 (1990) 240.
- [61] K. Gelin, *Preparation and characterization of sputter deposited spectrally selective solar absorber*, Uppsala university, Uppsala (2004).
- [62] J. C. Fan, *Sputtered films for wavelength-selective applications*. Thin solid films 80 (1981) 125-136.
- [63] M. Lazarov, A. Brunotte, T. Eisenhammer and R. Sizmann, *Effect of roughness on TiN<sub>x</sub>O<sub>y</sub>-Cu selective absorber*. SPIE 1727 (1992)
- [64] J. H. Schön, G. Binder and E. Bucher, *Performance and stability of some new high-temperature selective absorber systems based on metal/dielectric multilayers*. Sol. Energy Mater. Sol. Cells 33 (33) 403-416.
- [65] S. Craig and G. L. Harding, *composition, optical properties and degradation modes of Cu/(Graded Metal-carbon) solar selective surfaces*. Thin solid films 101 (1983) 97-113.
- [66] Q. C. Zhang and D. R. Mills, *New cermet film structure with much improved selectivity for solar thermal applications*. Appl. Phys. Letter 60 (1992) 545-547.
- [67] Q. C. Zhang, *Recent progress in high temperature solar selective coatings*. Sol. Energy Mater. Sol. Cells 62 (2000) 63-74.
- [68] Y. Yin and R. E. Collins, *Optimization and analysis of solar selective surfaces with continuous and multilayer profiles*. J. Appl. Phys. 77 (1995) 6485-6491.

## 9. References

---

- [69] Q. C. Zhang, Y. Yin and D. R. Mills, *High efficiency Mo-Al<sub>2</sub>O<sub>3</sub> cermet selective surfaces for high-temperature applications*. Sol. Energy Mater. Sol. Cells 40 (1996) 43-53.
- [70] C. Nunes, V. Teixeira, M. L. Prates, N. P. Barradas and A. D. Sequeira, *Graded selective coating based on Chromium and titanium oxynitride*. Thin solid films 442 (2003) 173-178.
- [71] G. A. Niklasson and C. H.G., *Selective solar absorption of chemically aluminum-silicon films*. J. Appl. Phys. 54 (1983) 54885490.
- [72] H. G. Craighead, R. E. Howard and D. M. Tennant, *Textured thin-film Si solar selective absorber using reactive ion etching*. Appl. Phys. Lett. 37 (1980) 653.
- [73] G. A. Nyberg, H. G. Craighead and R. A. Buhrman, *Surface roughness and thermal stability of graded cermet photothermal absorber coatings with very high absorptivities*. Thin solid films 96 (1982) 185-190.
- [74] G. A. Nyberg and R. A. Buhrman, *Macroscopic surface roughness in metal-dielectric composite films: Photothermal absorber applications*. Appl. Phys. Lett. 40 (1981) 129-131.
- [75] P. M. Curmi and G. L. Harding, *Surface texturing of copper by sputter etching with application for solar selective absorbing surfaces*. J. Vac. Sci. Technol. 17 (1980) 1320.
- [76] V. Chang and P. Bolsaitis, *A study of two binary eutectic aluminum alloys as selective absorbers for solar photothermal conversion*. Solar Energy Materials 4 (1980) 89-100.
- [77] G. D. Pettit, J. J. Cuomo, T. H. DiStefano and J. M. Woodall, *Solar absorbing surfaces of anodized dendritic tungsten*. IBM J. Res. Develop. 22 (1978) 372377.
- [78] R. T. Kivaisi and L. Stensland, *Spectral selectivity of nickel and chromium rough surfaces*. Appl. Phys. A 27 (1982) 233-238.
- [79] T. Sekino and K. Niihara, *Microstructural characteristics and mechanical properties for Al<sub>2</sub>O<sub>3</sub>/Metal nanocomposites*. Nanostructured Materials 6 (1995) 663-666.
- [80] T. Sekino, A. Nakahira and K. Niihara, *Relationship between microstructure and high temperature mechanical properties for Al<sub>2</sub>O<sub>3</sub>/W nanocomposites*. Transactions of the materials research society of Japan 16B (1994) 1513-1516.
- [81] T. Sekino, A. Nakahira, M. Nawa and K. Niihara, *Fabrication of Al<sub>2</sub>O<sub>3</sub>/W Nanocomposite*. J. Japan Soc. of Powd. and Powd. Metall 38 (1991) 326-330.

## 9. References

---

- [82] T. Sekino, T. Nakajima, S. Ueda and K. Niihara, *Reduction and sintering of a Nickel-dispersed-alumina composite and its properties*. J. Am. Ceram. Soc. 80 (1997) 1139-1148.
- [83] T. Sekino, T. Nakajima and K. Niihara, *Mechanical and magnetic properties of Nickel dispersed alumina-based nanocomposite*. Mater. Lett. 29 (1996) 165-169.
- [84] T. Eisenhammer, L. Miladin and S. Helmut, *Verfahren zur Herstellung selektiver Absorber*, Germany DE 19620645 C2, Schlüßer, A., 1995
- [85] T. Eisenhammer, H. Schellinger and M. Lazarov, *Process for producing selective absorbers*, USA 5912045, Pinalto, B., 1999
- [86] T. K. Boström, E. Wäckelgard and G. Westin, *Anti-reflection coatings for solution-chemically derived nickel-alumina solar absorbers*. Sol. Energy Mater. Sol. Cells 84 (2004) 183-191.
- [87] G. Katumba, J. Lu, L. Olumekor, G. Westin and E. Wäckelgard, *Low cost selective solar absorber coatings: characteristics of carbon-in-silica synthesized with sol-gel technique*. J. Sol-gel Sci. Techn. 36 (2005) 33-43.
- [88] T. Boström, E. Wäckelgard and G. Westin, *Solution-chemical derived nickel-alumina coatings for thermal solar absorbers*. Solar energy 74 (2003) 497-503.
- [89] T. Boström and E. Wäckelgard, *Optical properties of solution-chemically derived thin film Ni-Al<sub>2</sub>O<sub>3</sub> composite and Si, Al, and Si-Ti oxides*. J. Phys.: Condens. Matter. 18 (2006) 7737-7750.
- [90] C. J. Brinker and A. J. Hurd, *Fundamentals of sol-gel dip-coating*. J. Physics. III France 4 (1994) 1231-1242.
- [91] J. R. Reitz, F. J. Milford and R. W. Christy, *Foundations of Electromagnetic Theory*. 3rd Edition ed. (1979), New York: Addison-Wesley Inc.
- [92] T. Tesfamichael, *Characterization of selective solar absorbers, Experimental and theoretical modeling*, Uppsala university, Uppsala (2000).
- [93] H. C. van de Hulst, *Light scattering by small particles*. (1981), New York: Dover publications, Inc.
- [94] T. C. Choy, *Effective Medium Theory*. (1999), New York: Oxford university press Inc. 183.
- [95] G. A. Niklasson and C. G. Granqvist, *Optical properties and solar selectivity of coevaporated Co-Al<sub>2</sub>O<sub>3</sub> composite films*. J. Appl. Phys. 55 (1984) 3382-3409.

## 9. References

---

- [96] M. Neviere and E. Popov, *Light propagation in periodic media: differential theory and design*. (2003), New York: Marcel Dekker Inc.
- [97] *Green's function*, [http://en.wikipedia.org/wiki/Green's\\_function](http://en.wikipedia.org/wiki/Green's_function). Wikipedia, the free encyclopedia:
- [98] *Integral Method*, <http://www.pcgrate.com/etestlab/calculat>. International Intellectual Group, Inc:
- [99] E. G. Loewen and E. Popov, *Diffraction gratings and applications*. (1997), Marcel Dekker, Inc.
- [100] S. H. Cho, S. Lee, D. Y. Ku, T. S. Lee, B. Cheong, W. M. Kim and K. S. Lee, *Growth behavior and optical properties of metal-nanoparticle dispersed dielectric thin films formed by alternating sputtering*. *Thin solid films* 447-448 (2004) 68-73.
- [101] D. W. Lynch and W. R. Hunter, *Handbook of Optical Constants of Solids*. ed. E. D. Palik. (1985), New York: Academic Press.
- [102] T. Tesfamichael and A. Roos, *Treatment of antireflection on tin oxide coated anodized aluminum selective absorber surface*. *Sol. Energ. Mater.* 54 (1998) 213-221.
- [103] G. Zhou and J. C. Yang, *Self-assembly of metal-oxide nanostructures: Oxidation of Cu Films by In-situ UHV-TEM*. *Materials at high temperatures* 3 (2003) 247-252.
- [104] T. W. A. Njeh, H. Fuess, 2002. *Surf. Interface Anal.* 33 (Reflectometry studies of the oxidation kinetics of thin copper films) 626 - 628.
- [105] V. F. Drobny and L. Pulfrey, *Properties of reactively-sputtered copper oxide thin films*. *Thin Solid Films* 11 (1979) 89-98.
- [106] G. Papadimitropoulos, N. Vourdas, V. Em Vamvakas and D. Davazoglou, *Deposition and characterization of copper oxide thin films*. *Journal of Physics: Conference Series* 10 (2005) 182-185.
- [107] W. F. Bogaerts and C. M. Lampert, *Materials for photothermal solar energy conversion*. *J. Mater. Sci.* 18 (1983) 2847-2875.
- [108] F. M. A. Lasagni, *Study of the multilayer metallic films topography modified by laser interference irradiation*. *Applied Surface Science* 240 (2005) 214-221.

## 9. References

---

- [109] A. Lasagni, M. Seyler, C. Holzapfel, W. Maier and F. Mücklich, *Periodical Gratings in Mixed Oxide Films by Laser Interference Irradiation*. *Adv. Mat.* **17** (2005) 2228-2232.
- [110] S. J. Wilson and M. C. Hutley, *The optical properties of moth eye antireflection surfaces*. *Opt. Acta* **29** (1982) 993-1009.
- [111] I. Lopez, *Study of the optical properties of copper, steel and tungsten modified by laser interference microstructuring*, Saarland University, Saarbrücken (2006).
- [112] A. Braun, *Transparent polycrystalline alumina ceramic by means of electrophoretic deposition for optical applications*, University of Saarland, Saarbrücken (2005).
- [113] P. Somasundaran, *Encyclopedia of Surface and Colloid Science*. ed. A. Hubbard. Vol. 8. (2006), Taylor & Francis.
- [114] A. S. Dukhin and P. J. Goetz, *Acoustic and electroacoustic spectroscopy for characterizing concentrated dispersions and emulsions*. *Adv. Colloid Interface Sci.* **92** (2001) 73-132.
- [115] S. R. Desai, H. Wu, C. M. Rohlifing and L.-S. Wang, *A Study of the Structure and Bonding of Small Aluminum Oxide Clusters by Photoelectron Spectroscopy: Al<sub>x</sub>O<sub>y</sub>- (x=1-2, y=1-5)*. *J. Chem. Phys.* **106** (1997) 1309.
- [116] L. Andrews, T. R. Burkholder and J. T. Yustein, *Reactions of pulsed-laser evaporated aluminum atoms with oxygen. Infrared spectra of the reaction products in solid argon*. *J. Phys. Chem.* **96** (1992)
- [117] *NIST Standard Reference Database*, <http://webbook.nist.gov/chemistry/>.
- [118] J. Widegren and L. Bergström, *The effect of acids and bases on the dispersion and stabilisation of ceramic particles in ethanol*. *J. Eu. Ceram. Soc.* **20** (2000) 659-665.
- [119] F. M. Fowkes, H. Jinnai and M. A. Mostafa, *Mechanism of electric charging of particles in nonaqueous liquids*. *J. Am. Ceram. Soc.* **15** (1982)
- [120] Y. K. Rao and A. H. Rashed, *Kinetics of reduction of nickel oxide with helium-hydrogen gas mixtures in the range 300-400 °C*. *Trans. Instn Min. Metall.* **110** (2001) C1-C6.
- [121] N. Al-Dahoudi, *Wet chemical deposition of transparent conducting coatings made of redispersable crystalline ITO nanoparticles on glass and polymeric substrates*, University of Saarland, Saarbrücken (2003).

## 9. References

---

- [122] *Adhesion Promoter*; <http://www.specialchem4coatings.com/tc/silanes>.
- [123] Y. Shacham-Diamand, E. Finkman and Y. Pinkas and N. Moriya, *Study of the changes in the infrared transmission of SiO<sub>2</sub> spin-on-glass due to ion implantation*. Appl. Phys. Lett. 59 (1991) 2953-2955.
- [124] K. Möller, B. Carlsson, U. Frei, S. Brunold and M. Köhl, *Comparison between predicted and actually observed in-service degradation of a nickel pigmented anodized aluminium absorber coating for solar DHW systems*. Sol. Ener. Mat. Sol. Cells 61 (2000)
- [125] B. Carlsson, K. Möller, U. Frei and M. Köhl, *Accelerated life testing of solar absorber coating*. SPIE 2255 79-90.
- [126] T. Sathiaraj, R. Thangaraj and O. P. Agnihotri, *High absorptance and low emittance AR-coated Ni-Al<sub>2</sub>O<sub>3</sub> absorbers*. J. Phys. D: Appl. Phys. 23 (1990) 250-254.
- [127] T. Boström *Solution-chemically derived spectrally selective solar absorbers*, Uppsala university, Uppsala (2006).



## 10. Appendix A

### Visual Basic code of the selectivity calculator

```
Public fname As String
Public maxl As Integer
Sub form_load()
With ms1
.ColWidth(0) = 300
.ColWidth(1) = 700
.ColWidth(2) = 700
.Rows = 4
.Cols = 3
.TextMatrix(0, 1) = "W-lenght"
.TextMatrix(0, 2) = " Ref."
End With
End Sub
```

---

```
Private Sub readf_Click()
Dim wlen(1 To 40000) As Double
Dim reflect(1 To 40000) As Double
cmdialog1.ShowOpen
fname = cmdialog1.FileName
readfile wlen(), reflect(), maxl
End Sub
```

---

```
Sub readfile(ByRef wlen() As Double, ByRef reflect() As Double, ByRef maxl As Integer)
If fname = "" Then Exit Sub
Open fname For Input As #1
Do
n = n + 1
Input #1, x, y
wlen(n) = x
reflect(n) = y
Loop Until EOF(1)
Close
maxl = n
With ms1
.Rows = maxl + 1
.Cols = 3
.ColWidth(0) = 500
For i = 1 To 2
.ColWidth(i) = 700
Next
.Width = 2300
If n >= 5 Then .Height = 1700
If n <= 5 Then .Height = n * 300
For i = 1 To maxl
.TextMatrix(i, 0) = i
```

## 10. Appendix

---

---

```
.TextMatrix(i, 1) = wlen(i)
.TextMatrix(i, 2) = reflect(i)
.TextMatrix(0, 1) = "W-lenght"
.TextMatrix(0, 2) = " Ref."
Next
End With
End Sub
```

---

```
Private Sub cal_Click()
Dim af As Double
Dim ep As Double
Dim tem As Double
Dim wlen(1 To 40000) As Double
Dim reflect(1 To 40000) As Double
Form1.pic1.Refresh
Form1.pic2.Refresh
lbl4 = ""
lbl5 = ""
If flname = "" Then
er = MsgBox("the data file dose not selected", vbOKOnly, "Error")
Exit Sub
End If
readfile wlen(), reflect(), maxl
tem = Val(txt4)
calculate af, ep, maxl, tem
End Sub
```

---

```
Private Sub ms1_DblClick()
txt1.SetFocus
With ms1
txt1 = .TextMatrix(.Row, .Col)
lbl1.Caption = "cell(" + Str(.Row) + "," + Str(.Col) + ")="
End With
End Sub
```

---

```
Private Sub savef_Click()
If flname = "" Then
er = MsgBox("the path is not known", vbOKOnly, "Warning")
Exit Sub
End If
Open flname For Output As #1
For i = 1 To maxl
a = ms1.TextMatrix(i, 1)
b = ms1.TextMatrix(i, 2)
Print #1, a, b
Next
Close
End Sub
```

---

## 10. Appendix

---

```
Private Sub txt1_Change()  
With ms1  
.TextMatrix(.Row, .Col) = Val(txt1)  
End With  
End Sub
```

---

```
Sub calculate(ByRef af As Double, ByRef ep As Double, maxl As Integer, tem As  
Double)  
Dim ref(1 To 20) As Double  
Dim alfa As Double  
Dim eps As Double  
Dim strdata As String  
sw = CLng(maxl) * 50 * 2  
Form1.pic1.ScaleWidth = sw  
Form1.pic2.ScaleWidth = sw  
strdata =  
"0.402,0.458,0.498,0.537,0.576,0.614,0.652,0.690,0.730,0.775,0.820,0.869,0.923,1.  
003,1.064,1.170,1.258,1.532,1.689,2.292"  
t = 1  
refdata strdata, t, ref()  
answer ref(), alfa  
For i = 1 To sw  
Form1.pic1.Line (i, 0)-(i, 250), vbRed  
Next  
  
strdata =  
"1660,2050,2320,2560,2790,3010,3230,3460,3710,3970,4250,4570,4930,5350,5850  
,6480,7310,8510,10600,16300"  
t = tem  
refdata strdata, t, ref()  
answer ref(), eps  
For i = 1 To sw Step 5  
Form1.pic2.Line (i, 0)-(i, 250), vbRed  
Next  
lbl4.Caption = Format(alfa, "0.000")  
If tem = 0 Then  
lbl5.Caption = "not available"  
Else  
lbl5.Caption = Format(eps, "0.000")  
End If  
End Sub
```

---

```
Sub refdata(ByRef strdata As String, t, ref() As Double)  
If t = 0 Then  
er = MsgBox("Enter the teprature in K", vbOKOnly, "Warning")  
Exit Sub  
End If  
posp = 1  
For i = 1 To 19
```

## 10. Appendix

---

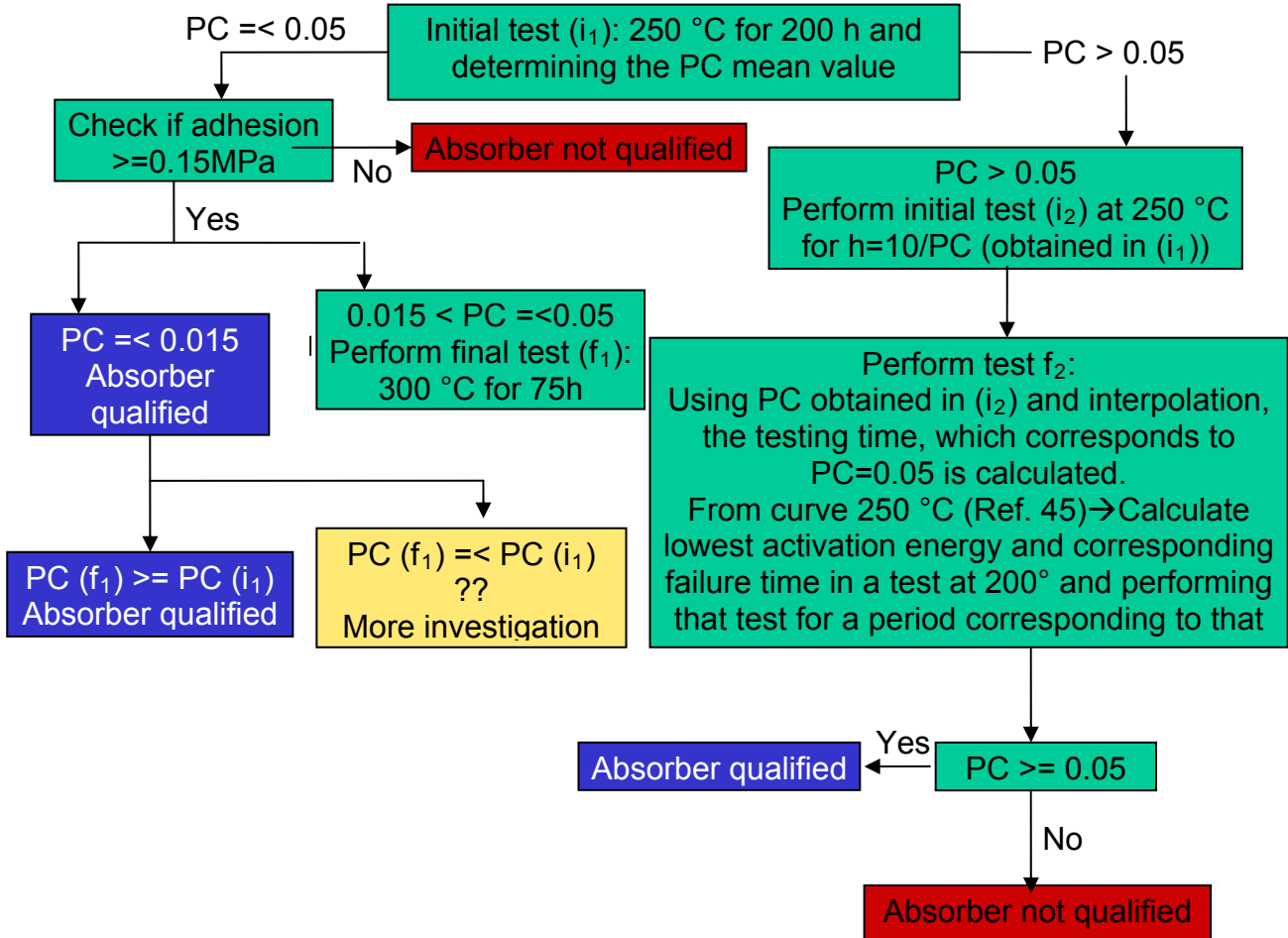
```
pos = InStr(posp, strdata, ",")
ref(i) = Val(Mid(strdata, posp, pos)) / t
posp = pos + 1
Next i
ref(20) = Val(Mid(strdata, posp, Len(strdata))) / t
End Sub
```

---

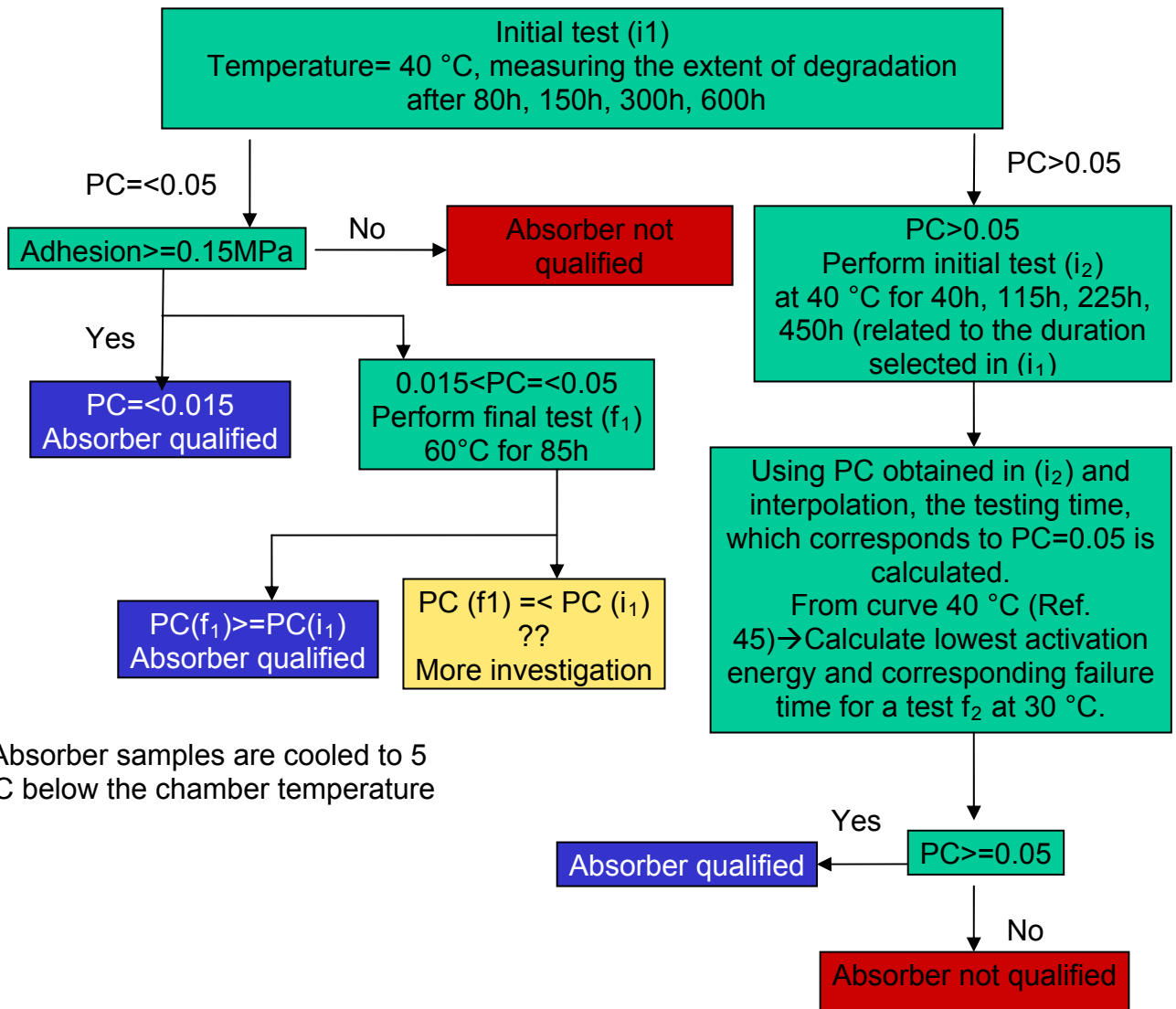
```
Sub answer(ByRef ref() As Double, ans As Double)
Dim ch(1 To 20) As Double
Dim va(1 To 20) As Double
Dim po(1 To 20) As Double
Dim dif(1 To 20) As Double
Dim flag As Boolean
For i = 1 To 10
dif(i) = 0.001 * i
Next
For i = 1 To 10
dif(i + 10) = 0.015 * i
Next
With ms1
p = 1
For i = 1 To 20
flag = False
For j = 1 To 20
For k = p To maxl
If Abs(Val(.TextMatrix(k, 1)) - ref(i)) <= dif(j) Then
Sum = Sum + Val(.TextMatrix(k, 2))
num = num + 1
po(num) = k
ch(num) = dif(j)
va(num) = Val(.TextMatrix(k, 2))
flag = True
p = p + 1
Exit For
End If
Next k
If flag = True Then Exit For
Next j
Next i
End With
If num = 0 Then Exit Sub
ans = 1 - Sum / num
End Sub
```

**10. Appendix B**

**Accelerated aging test: thermal test**



**Accelerated aging test: humidity test**



Absorber samples are cooled to 5 °C below the chamber temperature